

This item was submitted to Loughborough's Institutional Repository (<https://dspace.lboro.ac.uk/>) by the author and is made available under the following Creative Commons Licence conditions.



CC creative commons
COMMONS DEED

Attribution-NonCommercial-NoDerivs 2.5

You are free:

- to copy, distribute, display, and perform the work

Under the following conditions:

 **Attribution.** You must attribute the work in the manner specified by the author or licensor.

 **Noncommercial.** You may not use this work for commercial purposes.

 **No Derivative Works.** You may not alter, transform, or build upon this work.

- For any reuse or distribution, you must make clear to others the license terms of this work.
- Any of these conditions can be waived if you get permission from the copyright holder.

Your fair use and other rights are in no way affected by the above.

This is a human-readable summary of the [Legal Code \(the full license\)](#).

[Disclaimer](#) 

For the full text of this licence, please go to:
<http://creativecommons.org/licenses/by-nc-nd/2.5/>

Carbon Nanotubes Developed on Ceramic Constituents through Chemical Vapour Deposition

by
Jingjing Liu

A doctoral thesis submitted in partial fulfilment of the requirements for the award
of degree of Doctor of Philosophy of Loughborough University

Project Supervisor : Dr. Houzheng Wu

Date : 20 March 2012

ABSTRACT

Carbon nanotubes (CNTs) were successfully grown on the surface of carbon fibre reinforcements in carbon fibre architecture through in-situ catalytic chemical vapour deposition (CCVD). Success was also implemented on powders of oxides and non-oxides, including Y-TZP powder, ball milled alumina powder, alumina grits, silicon carbide powder. Preliminary results have been achieved to demonstrate the feasibility of making ceramic composites consisting of CNTs reinforcements.

Some common features of the CNTs were observed on the surface of different ceramic constituents. Firstly, tip-growth was the dominant growing pattern of CNTs, while catalyst particles were lifted up from the surface of substrates. Secondly, the diameter of CNTs was distributed in the range between 10 and 30nm, and varies with different processing conditions of CCVD. The length of CNTs was also varied from 100nm to 3µm. Thirdly, under the same processing condition of CCVD, the growth of CNTs was able to be applied on all the substrates mentioned above. For an optimised deposition of CNTs, a CVD condition was set to crack methane at 650°C at ambient pressure.

A model was proposed for understanding of the mechanism of catalytic growth of CNTs through microstructural analysis. The model was based on the first law of thermodynamics and could explain the relationship between the size of catalyst particles and initiation of the growth of CNTs.

CNTs/CF reinforced carbon composite and CNTs/Al₂O₃ ceramics were manufactured in the laboratory scale, and can be scaled-up for industrial processing and commercial applications. Two steps were involved: first is the integration of CNTs onto substrates that are subsequently used as the constituents of composites, and second is the introducing of matrix materials into the composite preforms. For the former one, chemical vapour infiltration (CVI) was used to introduce carbon matrix into the CNTs/CFs hybrid preform through cracking methane. While for the alumina ceramics, a chemical method was used to produce a chemically bonded ceramic nanocomposite that sintered at extremely low temperature of 150°C. Microstructural analysis suggested that CNTs were well preserved during densification process.

KEYWORDS

In-situ growth, catalytic Chemical vapour deposition (CVD), Carbon nanotubes (CNTs), ceramic matrix composites (CMC), carbon fibre, alumina, zirconia, silicon carbide.

ACKNOWLEDGEMENTS

I would like to take this opportunity to thank my project supervisor, Dr Houzheng Wu for his guidance throughout my project. I would also like to thank all group members in Dr. Wu's research group for their assistance.

Thanks to the staff of Materials Department at Loughborough University, especially to Mr. Raymond Owens, Mr. Andy Woolley, Mr. John Bates and Dr. Zhaoxia Zhou for their assistance and technical support, without which much of this project wouldn't be possible.

The most importantly, I deeply appreciate my family members for their full support and encouragement.

CONTENTS

| | |
|--|-----|
| List of Abbreviations | I |
| List of Tables | II |
| List of Figures | III |
| | |
| CHAPTER 1 Introduction | |
| | |
| 1.1 Introduction | 1 |
| 1.2 Aims of project | 4 |
| | |
| CHAPTER 2 Literature Survey | |
| | |
| 2.1 Basics of carbon nanotubes | 6 |
| 2.1.1 Discovery of carbon nanotubes | 6 |
| 2.1.2 Structure of CNTs and its physical and mechanical properties | 6 |
| 2.2 Synthesis of CNTs | 9 |
| 2.2.1 Development of CNT's synthetic methods | 9 |
| 2.2.2 Hypothesis of catalytic growth mechanism for CNTs | 9 |
| 2.2.3 Arc discharging | 16 |
| 2.2.4 Laser ablation | 19 |
| 2.2.5 Chemical vapour deposition (CVD) | 22 |
| 2.2.5.1 Preparation of catalysts | 22 |
| 2.2.5.2 Designs of apparatus | 25 |
| 2.2.5.3 Gas composition and decomposition temperatures | 28 |
| 2.3 Ex-situ usages of CNTs in composites | 30 |
| 2.3.1 Ex-situ manufacture of CNTs/polymer composites. | 30 |
| 2.3.2 Ex-situ manufacture of CNTs/metal and ceramic composites. | 32 |
| 2.4 In-situ catalytic chemical vapour deposition of CNTs | 36 |
| 2.4.1 In-situ CCVD of CNTs on surface of carbon fibres | 36 |
| 2.4.1.1 Surface pre-treatment of CF and catalysts preparation | 37 |
| 2.4.1.2 CVD apparatus design | 42 |
| 2.4.1.3 Processing conditions | 46 |

| | | |
|-------|--|----|
| 2.4.2 | In-situ CCVD of CNTs on ceramic powders | 48 |
| 2.5 | Fabrication techniques for CF and ceramic based composites | 51 |
| 2.5.1 | Fabrication of CF composites | 51 |
| 2.5.2 | Fabrication of ceramic composites | 54 |
| 2.6 | Summary | 56 |

CHAPTER 3 Experimental Methods

| | | |
|-------|--|----|
| 3.1 | Catalyst selection and preparation | 58 |
| 3.1.1 | Catalyst precursors | 58 |
| 3.1.2 | Impregnation of catalyst precursor onto carbon fibres | 60 |
| 3.2 | In-situ catalytic chemical vapour deposition (CCVD) | 60 |
| 3.2.1 | Equipment set up | 60 |
| 3.2.2 | In-situ deposition process | 62 |
| 3.3 | In-situ growth CNTs on carbon fibre surface | 63 |
| 3.3.1 | Carbon fibre source | 63 |
| 3.3.2 | Pre-treatment of as-received carbon fibres | 65 |
| 3.3.3 | Optimising processing condition of CVD for growth of CNTs on surface of CFs. | 67 |
| 3.4 | In-situ growth of CNTs on SiC powder | 69 |
| 3.4.1 | Attrition milling | 70 |
| 3.4.2 | Surface pre-treatment and coating of catalyst precursor | 71 |
| 3.5 | In-situ growth of CNTs on Al ₂ O ₃ powder | 72 |
| 3.6 | In-situ growth of CNTs on Y-TZP powder | 74 |
| 3.7 | Manufacture of CNTs reinforced composites | 74 |
| 3.7.1 | Preparation of CNTs/CF reinforced carbon composite | 74 |
| 3.7.2 | CNTs reinforced phosphate bonded Al ₂ O ₃ ceramics | 76 |
| 3.8 | Microstructure characterisation | 80 |
| 3.8.1 | Scanning electron microscopy (SEM) | 80 |
| 3.8.2 | Transmission electron microscopy (TEM) | 81 |
| 3.8.3 | SEM image analysis by imaging softwares | 84 |

CHAPTER 4 CNTs In-situ Growth on Surface of CFs

| | | |
|---------|---|-----|
| 4.1 | Effect of surface pre-treatment of PAN-based CFs | 86 |
| 4.2 | Effect of selection of catalyst precursors | 88 |
| 4.3 | Optimisation of In-situ growth of CNTs on surface of CFs | 92 |
| 4.3.1 | Concentration of catalyst precursor | 92 |
| 4.3.2 | Optimisation of CVD temperature for the growth of CNTs | 98 |
| 4.3.3 | CNTs growing on PANOX CF block | 108 |
| 4.3.4 | Microstructural analysis of catalyst particles and growth of CNTs | 112 |
| 4.3.4.1 | Analysis of the size of catalyst particles | 112 |
| 4.3.4.2 | TEM analysis of catalyst particles and growth of CNTs | 118 |

CHAPTER 5 CNTs In-situ Growth on Ceramic Particles

| | | |
|-----|--|-----|
| 5.1 | In-situ growth of CNTs on surface of SiC | 126 |
| 5.2 | In-situ growth of CNTs on surface of Al ₂ O ₃ | 130 |
| 5.3 | In-situ growth of CNTs on Y-TZP powder | 135 |
| 5.4 | TEM analysis of catalytic growth of CNTs on Al ₂ O ₃ particles | 138 |

CHAPTER 6 Preliminary Work in Manufacture of CNT Reinforced Composites

| | | |
|-----|---|-----|
| 6.1 | Manufacture of CNTs/CFs reinforced carbon composite | 142 |
| 6.2 | Manufacture of chemically bonded CNTs/Al ₂ O ₃ composites | 148 |

CHAPTER 7 Growth mechanism of CNTs

| | | |
|---------|--|-----|
| 7.1 | Surface chemistry and roughness of CFs | 153 |
| 7.2 | Thermal dynamic study of in-situ formation of catalyst particles | 155 |
| 7.3 | Understanding of CNTs growth mechanism | 161 |
| 7.3.1 | Carbon absorption and diffusion | 161 |
| 7.3.2 | Theory of carbon diffusion and growth of CNTs | 163 |
| 7.3.2.1 | Contact of Co–substrate interface and theory of carbon | |

| | |
|--|-----|
| diffusion | 163 |
| 7.3.2.2 Initiation of the growth of CNTs | 166 |

CHAPTER 8 Conclusions and Further work

| | |
|------------------|-----|
| 8.1 Conclusions | 173 |
| 8.2 Further work | 177 |

CHAPTER 9 References

LIST OF ABBREVIATIONS

| | |
|---|---|
| CNTs | Carbon nanotubes |
| CVD | Chemical vapour deposition |
| CCVD | Catalytic chemical vapour deposition |
| CVI | Chemical vapour infiltration |
| °C | Degree Celsius |
| µm | micrometer |
| nm | nanometer |
| GPa | Gigapascal |
| MPa | Megapascal |
| mol/l | mole per liter |
| % | Percentage |
| ΔH | Enthalpy |
| ΔS | Entropy |
| Δ _r G° | Standard Gibbs free energy of reaction |
| Δ _f G° | Standard Gibbs free energy of formation |
| Δ _r G | Gibbs free energy of reaction |
| Δ _f G | Gibbs free energy of formation |
| E | Young's modulus |
| Co(NO ₃) ₂ | Cobalt nitride |
| Co ₃ O ₄ | Cobalt (III) oxide |
| CoO | Cobalt (II) oxide |
| Fe(NO ₃) ₃ | Iron (III) nitride |
| Fe(C ₅ H ₅) ₂ | Ferrocene |
| Ni(NO ₃) ₂ | Nickel nitride |
| FeCl ₃ | Iron (III) chloride |

LIST OF TABLES

Table 2.1 – Averaged diameter of CNTs in relation with the size of catalysts

Table 3.1 – Catalyst precursors and their concentrations used.

Table 3.2 – In-situ deposition process

Table 3.3 – Processing parameters for in-situ CCVD growing CNTs on CF

Table 3.4 – Three types of Al₂O₃ powders prepared for growth of CNTs

Table 4.1 – Summary of measurements on catalyst particles and CNTs in
Fig.4.3~4.5.

Table 4.2 – Summary of measurements on catalyst particles and CNTs in
Fig.4.7~4.12.

Table 7.1 – Standard thermodynamic quantities for selected substances.

Table 7.2 – Calculated $\Delta_r H^\circ$ and $\Delta_r G^\circ$ for reactions (1) ~ (3).

LIST OF FIGURES

- Figure 2.1 – Formation of a single-wall CNT through rolling a graphene layer by defined Chiral Vector of $\vec{C}_h = n\vec{a}_1 + m\vec{a}_2$, where a_1 and a_2 are lattice vectors
- Figure 2.2 – Tip-growth model
- Figure 2.3 – Possible carbon nanotube growth modes
- Figure 2.4 – Distribution of diameter of CNTs prepared by different concentration of iron particles, a) 0.75 at% Fe:C and b) 0.075 at% Fe:C ratios
- Figure 2.5 – First arc discharging apparatus
- Figure 2.6 – Schematic apparatus of modified arc discharge with electrodes in liquid nitrogen
- Figure 2.7 – Schematic apparatus of laser ablation
- Figure 2.8 – SWCNTs from laser ablation
- Figure 2.9 – Magnetron sputtering of stainless steel film on graphite substrate and reduced by hydrogen. Left ones: catalyst particles reduced from SS films with the thickness of 2 and 50 nm, respectively. Right ones: as-produced CNTs from the catalysts prepared on the left, the diameters of which were 2 and 15 nm, respectively
- Figure 2.10 – Two-beam excimer laser ablation with bombard targets covered with metallic diaphragms
- Figure 2.11 – Design of thermal CVD apparatus based on hydrocarbon gas flow
- Figure 2.12 – Design of floating method of CVD setup
- Figure 2.13 – Design of PE-CVD experimental setup
- Figure 2.14 – Vertically grown CNTs achieved through CVD: A) without plasma and B) with plasma
- Figure 2.15 – CNTs yield varies with the content of H_2 in hydrocarbon gas
- Figure 2.16 – Averaged diameters of CNTs grown at different temperatures and dwelling time
- Figure 2.17 – Crack bridging in MWNT/polystyrene thin film induced by thermal stresses
- Figure 2.18 – Left: Uniformly dispersed 5vol% CNTs/Cu nanocomposites in the

centre region. Right: Stress-strain curve of CNTs/Cu composites with different amount of dispersion of CNTs

Figure 2.19 – MWCNTs/alumina composites. Left: general dispersion of CNTs within alumina matrix. Right: micro-crack bridging by MWCNTs

Figure 2.20 – Typical trend of CNTs toughening effect from both Ahmad and Yamamoto. Left: Alumina composites reinforced by CNTs and SiC as secondary phase reinforcement. Right: Alumina composites with both acid-treated and non-treated CNTs

Figure 2.21 – In-situ grown CNTs on surface of a CF

Figure 2.22 – Surface morphologies of CFs accommodation of catalysts. A) and B) are surface morphologies before and after acid treatment. C) and D) are yield of CNTs respectively

Figure 2.23 – a) PLD deposition of Ni on one side of a CF paper b) in-situ formed Ni particles on CF after thermal annealing

Figure 2.24 – Growth of CNTs on surface of CFs by using Fe, Co and Ni as catalysts respectively

Figure 2.25 – CVD apparatus design for growth of CNTs on CF paper

Figure 2.26 – Typical microstructure of CNTs/CF paper by Ohmically heated apparatus

Figure 2.27 – Vertical floating CCVD reactor for CF substrate

Figure 2.28 – Horizontal floating CCVD apparatus design for different types of CF preforms

Figure 2.29 – Iron particles on surface of CFs. a) Ferrocene precursor coated on pre-treated surface of CF with 0.024vol% H₂S in carrier gas, b) same condition as a) but without H₂S

Figure 2.30 – CNTs-ceramic composite powder. (a) 5wt% Fe, 30%CH₄ on solid solution powder without attrition milling, (b) 10wt%Fe, 12%CH₄ on attrition milled solid solution powder

Figure 2.31 – Friction coefficient and wear loss as a function of CNT content in alumina. Top left: microstructure of 4.1wt% CNTs and top right: microstructure of 12.5wt% CNTs

Figure 2.32 – Schematic of a CVI tubular reactor

Figure 2.33 – A) Crack propagation and debonding at a fibre/matrix interface, and B) Modes of crack propagation

Figure 2.34 – Schematic hot press apparatus

Figure 3.1 – Flowchart of preparation of catalyst precursor solution

Figure 3.2 – Schematic processing apparatus design

Figure 3.3 – As received carbon fibres. a) PAN carbon fibre bundles in woven format; b) needled PANOX carbon fibre block derived from PANOX.

Figure 3.4 – Flowchart of surface pre-treatments of carbon fibres

Figure 3.5 – a) attrition milling machine and b) zirconia milling media

Figure 3.6 – Flowchart of sample preparation with ceramic powders

Figure 3.7 – Flowchart of possible CVI steps

Figure 3.8 – Schematic of fabricating AP bonded CNTs/ Al_2O_3 ceramic

Figure 3.9 – TEM sample preparation by FIB. a) Pt deposition on CNTs using electron beam, b) further Pt deposition using ion beam, c) prepared TEM sample for further thinning, and d) TEM sample lifted out.

Figure 4.1 – Surface morphology of carbon fibres before and after dip coating. (a) as-received carbon fibre; (b)-(c) after dip coating of as-received carbon fibre; (d) after acid treatment; (e)-(f) after dip coating of treated carbon fibre.

Figure 4.2 – SEM images of carbon fibres after CVD at 650°C for 30 minutes under different catalytic conditions: (a) Co derived from 0.1 mol/l $\text{Co}(\text{NO}_3)_2$ on as-received CF surface; (b) Co derived from 0.1 mol/l $\text{Co}(\text{NO}_3)_2$ on as-treated CF surface.

Figure 4.2 (Continued) – SEM images of carbon fibres after CVD at 650°C for 30 minutes under different catalytic conditions: (c) Fe derived from 0.1 mol/l $\text{Fe}(\text{NO}_3)_3$ on as-treated CF surface; (d) Fe derived from 0.1 mol/l Ferrocene on as-treated CF surface.

Figure 4.2 (Contiued) – SEM images of carbon fibres after CVD at 650°C for 30 minutes under different catalytic conditions: (e) Fe derived from 0.1 mol/l FeCl_3 on as-treated CF surface; (f) Ni derived from 0.1 mol/l $\text{Ni}(\text{NO}_3)_2$ on as-treated CF surface.

Figure 4.3 – Catalyst particles and CNTs developed on the surface of

PAN-CFs with acid surface treatment. $\text{Co}(\text{NO}_3)_2$ solution concentrations: 0.001 mol/l in (a) and 0.005 mol/l in (b), CVD at 600°C for 30 minutes.

Figure 4.4 – Catalyst particles and CNTs developed on the surface of PAN-CFs with acid surface treatment. $\text{Co}(\text{NO}_3)_2$ solution concentrations: 0.05 mol/l in (c) and 0.1 mol/l in (d), CVD at 600°C for 30 minutes. Image (e) showed magnified area in (d).

Figure 4.5 – Catalyst particles and CNTs developed on the surface of PAN-CFs with acid surface treatment. $\text{Co}(\text{NO}_3)_2$ solution concentration 0.3 mol/l, CVD at 600°C for 30 minutes.

Figure 4.6 – Diagram to show the measured diameter range of catalyst particles and the averaged diameter of CNTs with standard deviation included by using $\text{Co}(\text{NO}_3)_2$ solution with different concentrations.

Figure 4.7 – Surface morphology on carbon fibre, with CVD at 500°C for 30 minutes, $\text{Co}(\text{NO}_3)_2$ solution concentration: 0.3 mol/l.

Figure 4.8 – Surface morphology on carbon fibre, with CVD at 600°C for 30 minutes, $\text{Co}(\text{NO}_3)_2$ solution concentration: 0.3 mol/l.

Figure 4.9 – Surface morphology on carbon fibre, with CVD at 650°C for 30 minutes, $\text{Co}(\text{NO}_3)_2$ solution concentration: 0.3 mol/l.

Figure 4.10 – CNTs developed on carbon fibre, under high SEM magnification to observe the CF sample shown in figure 4.9.

Figure 4.11 – Catalyst particles developed on carbon fibre, under high SEM magnification to observe the CF sample shown in figure 4.9.

Figure 4.12 – Surface morphology on carbon fibre, with CVD at 650°C for 30 minutes, $\text{Co}(\text{NO}_3)_2$ solution concentration: 0.3 mol/l.

Figure 4.13 – Diagram to show the measured diameter range of catalyst particles and the averaged diameter of CNTs with standard deviation included by using various decomposing temperatures.

Figure 4.14 – Surface morphologies of CFs from CF block. Precursor solution: 0.05 mol/l $\text{Co}(\text{NO}_3)_2$. a) the raw CF surface; b) after impregnation of $\text{Co}(\text{NO}_3)_2$.

Figure 4.15 – Surface morphology on PANOX carbon fibre with CVD deposition for 60 minutes at 650°C, $\text{Co}(\text{NO}_3)_2$ solution with a concentration of

0.05 mol/l was used. a) overview of CNTs developed on surface of CF, b) appearance of CNT under high magnification, c) CNTs developed on fracture surface of CF.

Figure 4.16 – Surface morphology on PANOX carbon fibre, with CVD at 650°C for 60 minutes, and $\text{Co}(\text{NO}_3)_2$ solution concentration: 0.3 mol/l.

Figure 4.17 – Morphology of catalytic particles on the surface of carbon fibres and the histogram distribution of their size by using $\text{Co}(\text{NO}_3)_2$ solution with different concentrations: (a) 0.001 mol/l, and (b) 0.005 mol/l.

Figure 4.18 – Catalytic particles on the surface of carbon fibres and the histogram distribution of their size by using 0.05 mol/l $\text{Co}(\text{NO}_3)_2$ solution.

Figure 4.19 – Catalytic particles on the surface of carbon fibres and the histogram distribution of their size by using 0.1 mol/l $\text{Co}(\text{NO}_3)_2$ solution.

Figure 4.20 – Catalytic particles on the surface of PANOX-CF and the histogram distribution of their size by using 0.05 mol/l $\text{Co}(\text{NO}_3)_2$ solution: (a) on a hump, and (b) within grooves.

Figure 4.21 – TEM sample preparation and observation of CNTs/CF sample shown in figure 4.9. a) TEM sample preparation by FIB; b) bright field imaging of CNTs on surface of CF; c) and d) same particle imaged under STEM mode and HR-TEM, respectively; e) EDS spectrum of the particle shown in c) and d).

Figure 5.1 – a) An overview of the deposition of catalyst particles and the growth of CNTs on the surface of a SiC grit, concentration of $\text{Co}(\text{NO}_3)_2$ solution was 0.3 mol/l; b) and c) more details on the catalyst particles and CNTs under high magnifications.

Figure 5.2 – a) An overview deposition of catalyst particles and the growth of CNTs on the surface of attrition milled SiC grits, concentration of $\text{Co}(\text{NO}_3)_2$ solution was 0.6 mol/l; b) more details of CNTs under high magnification.

Figure 5.3 – Diagram to show the measured diameter range of catalyst particles and the averaged diameter of CNTs with standard

deviation included by using SiC particles with different size distributions and concentrations of catalyst precursor.

Figure 5.4 – CNTs grown on the surface of Al₂O₃. a) overview; b) zoom-in view.

Figure 5.5 – CNTs grown on the surface of Al₂O₃ processed with 0.3 mol/l Co(NO₃)₂ solution for 'AO-micron' alumina. a) overview b) and c) zoom-in view.

Figure 5.6 – CNTs grown on the surface of Al₂O₃ processed with 0.6 mol/l Co(NO₃)₂ solution. a) CNTs on 'AO-micron+nm' alumina grits, b) CNTs on 'AO-nm' alumina grits.

Figure 5.7 – (a) overview of CNTs grown in Y-TZP powder processed with 0.6 mol/l Co(NO₃)₂ solution, (b) zoom-in view.

Figure 5.8 – Histogram diagram of the measured averaged diameter of CNTs on surface of different ceramic grits.

Figure 5.9 – a) cross-sectional view of Al₂O₃ grit with CNTs grown on its surface; b) cross-sectional TEM foil of the Al₂O₃ grit shown in (a); c) cross-sectional view of the surface of Al₂O₃ in STEM.

Figure 5.10 – TEM EDS spectrums for both 'particle-1' and 'particle-2'.

Figure 5.11 – HRTEM images around the Co particles showing the laminated graphite structure. a) Co 'Particle-1'; b) Co 'Particle-2'.

Figure 6.1 – Pyrolytic carbon deposition on surface of CFs prepared without in-situ growth of CNTs. a) in-plane placed CFs, b) vertical placed CFs.

Figure 6.2 – Pyrolytic carbon deposition on surface of CFs prepared by in-situ growth of CNTs. a) in-plane placed CFs, b) vertical placed CFs.

Figure 6.3 – a) pyrolytic carbon deposition on surface of CFs without in-situ growth of CNTs. b) magnified interface area marked in a).

Figure 6.4 – a) pyrolytic carbon deposition on surface of CFs without in-situ growth of CNTs. b) magnified interface between surface of CF and pyrolytic carbon matrix.

Figure 6.5 – Aluminium phosphate bonded CNTs/alumina composite from as-prepared composite powder of 'AO-micron'.

Figure 6.6 – Aluminium phosphate bonded CNTs/alumina composite from as-prepared composite powder of 'AO-micron+nm'.

- Figure 6.7 – Aluminium phosphate bonded CNTs/alumina composite from as-prepared composite powder of ‘AO-micron+nm’.
- Figure 7.1 – Schematic drawing of surface chemistry and roughness of CFs on coating of catalyst precursor and formation of catalyst particles.
- Figure 7.2 – Calculated Δ_rG as increasing of temperatures for chemical reactions of (1), (2) and (3).
- Figure 7.3 – Simulated phase diagram of Co-C-O system at 650°C by using MTDATA.
- Figure 7.4 – Proposed interfacial contact between Co particles and surface of substrate and carbon diffusion within the bulk material of cobalt. a) flat surface with Co particles of different geometries, b) flat surface with agglomerated Co particles, and c) Co particles with spherical and reversed-pear geometries embedded in groove substrate.
- Figure 7.5 – Initiation of a growing CNT, and schematic drawing of the increased number of carbon atoms associated with volume expansion of the ideal gas.

CHAPTER 1 Introduction

1.1 Introduction

Since Iijima's clarification [1] of carbon nanotubes (CNTs) structure, there has been widespread interests in the development of CNTs and CNT-reinforced composites [2,3,4]. With the claimed superior properties [5,6], CNTs have become an important constituent of composites that can be used in construction [7], automotive [8] and aerospace [9] industry. The demand of CNTs is therefore growing rapidly in order to meet the large-scale manufacture of nano-composites [10].

CNTs can be produced through three types of techniques: arc-discharging [11], laser ablation [12] and chemical vapour deposition (CVD) [13]. Arc discharging is a simple technique that was widely used to produce C₆₀ fullerenes before CNT emerging, but purification is needed to separate catalyst particles and/or carbonaceous by-products [14]. Laser ablation employs laser source, instead of electrical arc, as energy source to produce single-wall carbon nanotubes (SWCNTs); it can produce CNT with high purity and high yield. For CVD technique, as opposed to the former two, there is no need of high energy source, and fewer technical constraints make it relatively easy to scale-up for industrial production [14]. However, CVD may produce relatively poorer quality of CNTs than arc discharging and laser ablation techniques. Due to its clear merits, researchers are developing various derivative techniques of CVD to improve the yield and quality of CNTs, as well as fit the specific needs.

Even though a number of successes have been achieved in the production of CNTs, the mechanism of the growth of CNTs is still under controversy. Several hypotheses have been proposed based on experimental observations. Most of the models are the following three processes or mechanisms: (i) tip/root growing process [15]; ii) solid-liquid-solid' reaction model [16]; (iii) diffusion and precipitation model [17]. It was also suggested various processing parameters were also involved in these models that were able to affect the growth of CNTs, including particle size of catalysts, atmosphere condition and temperatures and so on. This project is going to continue to investigate the effects of various processing conditions on the initiation and growth of CNTs. A model is also going to be proposed for the understanding of the growth mechanism of CNTs.

The dispersion of CNTs into matrix materials is facing challenges [18]. So far the improvement of mechanical properties is less than expected, mainly because the dispersing of CNTs homogeneously into the matrix of another material is extremely difficult. The CNTs/polymer is perhaps the first composite developed in year 2002 [2]. Since the raw polymer materials can dissolve in certain solvents, CNTs can be dispersed within polymers through solution-evaporation method to achieve relatively uniform distribution. However, in metal, ceramic matrices, CNTs tend to agglomerate at the early stage of powder processing, and may become unstable at the high temperature stage [2,3]. The most common method of dispersing CNTs into metals and ceramics is through long time mechanical agitation and/or ultrasonication. The main drawbacks include: 1) only limited level of dispersion of CNTs can be achieved; 2) longer processing time is needed; 3) The quality of CNTs could be

deteriorated.

Recently developed in-situ method has explored a possibility for homogeneous dispersion of CNTs into non-polymer based matrices [19,20,21], where CNTs can selectively grow on certain substrates that are directly used as constituents of the composites. Compared to ex-situ route, the in-situ CVD method does not require any dispersing techniques. Nano-sized metal particles, usually from transition metal group, are impregnated homogeneously onto substrates prior to catalytic growth of CNTs.

The in-situ catalytic CVD (CCVD) method is chosen as the technique to be studied in this research. Before now, there are a few studies on in-situ CCVD manufacture of CNTs. It was suggested that various processing parameters have influences on the yield and morphologies of CNTs, such as vacuum condition, composition of atmosphere, selection of catalysts, techniques of in-situ produce nano-sized catalyst particles and decomposition temperatures of hydrocarbon species. Some of the processing parameters are only capable to be controlled in laboratory scale, for example, the vacuum condition and in-situ formation of nano-catalyst particles. It is expected that through this research, these restrictions can be bypassed and a modified processing technology can be developed for more commercial and industrial applications.

In this thesis, in-situ CCVD will be used to grow CNTs/CFs on the surface of each carbon fibre filament, and on the surface of different types of ceramic particles. Through integration of CNTs into the architectures of CF, or

as-prepared ceramic powder, there may exist a prospect that ceramic composites consisting of CNT/F reinforcements can be manufactured without extra effort on the dispersion issue. As for CNTs/CFs preform, the homogeneous growth of CNTs on surface of CFs has provided a potential to modify the interface between CF and the matrix material for traditional CF reinforced composites. The surface area of CF can be tremendously increased with integration of CNTs into CF architecture. Therefore, the matrix material was not only bonded with CF surface, but also interacted within the forest of CNTs at the interface. When a crack propagates towards the surface of CF, more energy can be absorbed by deflecting the crack within the interface rather than propagating through. With the superior mechanical properties of CNTs, a high prospect of new generation of CF composites can be developed. The matrix material can be introduced through chemical vapour infiltration (CVI). At the same time, experimental evidences are expected to be achieved to understand the possible mechanisms of catalytic growth of CNTs.

1.2 Aims of project

The aims of this research include:

- 1) to develop a feasible processing technology to integrate CNTs into carbon fibre architectures, and as-prepared ceramic powders
- 2) to study the possible effects of processing parameters on catalytic growth of CNTs in order to optimise the yield of CNTs

3) to understand the mechanism of catalytic growth of CNTs in order to optimise the processing condition of CNTs.

4) Preliminary study on the fabrication of CNTs reinforced CF – carbon composite and chemically bonded CNTs/ Al_2O_3 composite.

CHAPTER 2 Literature Survey

2.1 Basics of carbon nanotubes

2.1.1 Discovery of carbon nanotubes

Since the first convincing report in 1991 [1], proper credit of discovery of carbon nanotubes (CNTs) was given to Iijima. However, the entire history of CNTs can be reversed back to the 1950s, when Roger Bacon (*Union Carbide*) observed a hollow tubular structure consisted of graphitic layers of carbon. This was thought an initial discovery which is possible the first CNTs that had been observed. In the 1970s, Endo [22] planned growth of these carbon filaments, which were thought to be the first synthesis of CNTs. But they did not characterise the products and thus was not considered as recognised invention. When detailed structural characterisation was revealed by Iijima, CNTs started to draw attention in scientific community. The discovery was completed after single walled carbon nanotubes, also known as buckytubes, was found by Iijima and Donald Bethune independently in 1993 [23,24]. Since then, the nanotube research has been developing dramatically as well as its potential applications.

2.1.2 Structure of CNTs and its physical and mechanical properties

Based on the history of discovery, CNTs can be generally divided into two categories, single walled nanotubes (SWNTs) and multi walled nanotubes (MWNTs). The SWNTs can be considered as wrapping a single graphene layer

at different chiralities. As shown in figure 2.1, SWNTs have three types of structures, zigzag, armchair and chiral structures. The MWNTs is consisted of multiple graphene layers rolled concentrically with different diameters. Within each layer or a wall of a CNT, C atoms are covalently bonded together by sp^2 bonds, while between walls of CNTs, only van der waals forces exist between C atoms. The size of CNTs is normally nanometres in diameter, and length from nanometres up to microns [1]

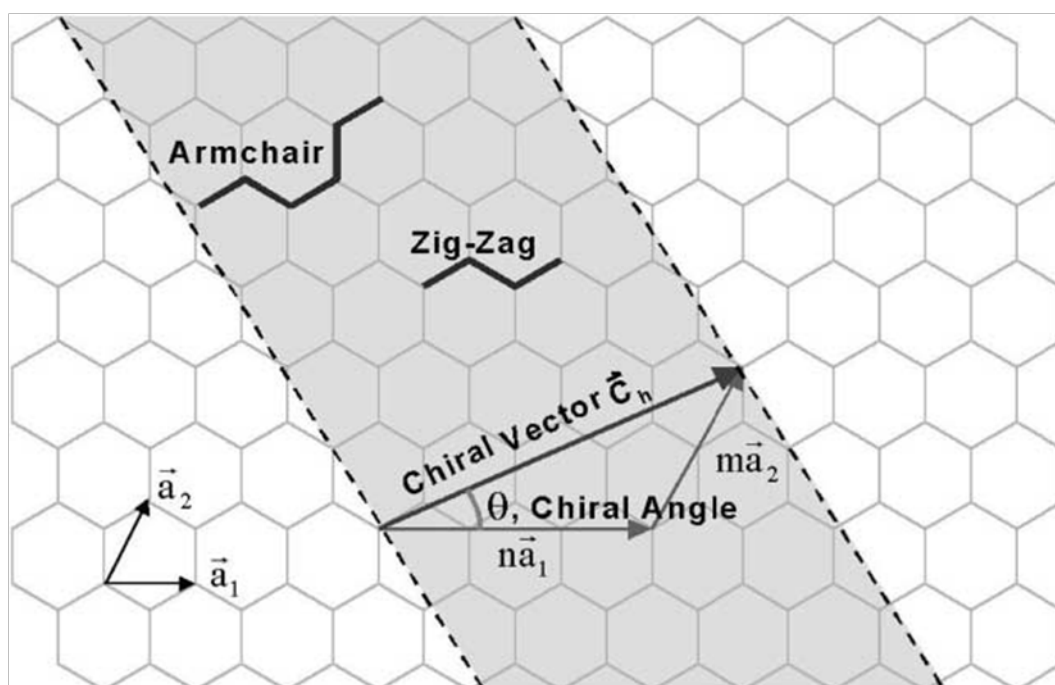


Figure 2.1 – Formation of a single-wall CNT through rolling a graphene layer by defined Chiral Vector of $\vec{C}_n = n\vec{a}_1 + m\vec{a}_2$, where a_1 and a_2 are lattice vectors[25]

There are exceptional strength and stiffness of carbon nanotubes in terms of tensile strength and Young's modulus respectively. The tensile strength of a MWCNT, tested in year 2000, is 63GPa [5], because of the covalent sp^2 bonds between each individual carbon atoms. Yong's modulus is even higher of up to

1 TPa [6] of SWCNT compared with general purpose stainless steel of only 0.2 TPa [26]. Besides, CNTs have low density of only 1.3 to 1.4 g/cm³, which gives a very high specific strength (*a material strength divided by its density*) of up to 48,000kN·m·kg⁻¹ [27]. It is so far the best known material, compared with only 154 kN·m·kg⁻¹ of high-carbon steel. However, CNTs cannot be used solo to bring out its potential of mechanical properties. One of the most important applications of CNTs is reinforcements in high strength, low weight and high performance composites.

Besides mechanical properties, CNTs also have some other physical properties. It has large specific surface area [28] (*total surface area per unit of mass*) of 1315 m²/g for single-walled CNTs [29], and also good electrical properties as metallic materials on certain types of CNTs [30]. It has potential to be used in energy devices, such as fuel cells and lithium batteries, to dramatically improve electrical efficiency. For semi-conducting CNTs, they can be used in manufacture of field-effect transistors for computer applications. CNTs are also flexible along axis because of the hollow structure and high aspect ratio (*length to diameter ratio*) of up to 50000 [31], therefore they can be used as nano-probes and sensors for STM and AFM instruments. Besides, in medical applications, they can also be used to carry drugs within their hollow structure and cure cancerous organisms because they are much smaller than blood cells [32].

2.2 Synthesis of CNTs

2.2.1 Development of CNT's synthetic methods

Generally three different processing methods have been developed for synthesis of CNTs. Initially based on Endo's method [16], small metal catalyst particles were used as seeds for fibrous materials to grow from. Carbon nanotube can be formed with the seed on tip and deposited carbon around its surface. This seeding method was considered the prototype of catalytic chemical vapour deposition (CCVD) method for producing CNTs. Arc discharging method was first used in CNT synthesis by Iijima in 1991. In 1995, Smalley's research group [33] from Rice University developed a laser ablation technique to synthesis CNTs using vaporised graphite target in 1200°C. Many researches so far have been focusing on CNT processing to enlarge the capability of production and lower cost for increasing demanding of using CNTs in various applications.

In this section, these three methods for fabrication of CNTs will be reviewed in details. CNTs growth mechanism will also be highlighted in advance for the understanding of the fundamentals in controlling the growth of CNTs.

2.2.2 Hypothesis of catalytic growth mechanism for CNTs

Most of the processing techniques so far are based on catalytic growth of CNTs. In order to control the growth, it is important to understand how the catalysts

triggered its formation and what factors were involved. However, the exact mechanism of catalytic growth of CNTs is still under controversy. It can be generally concluded from previous researches that three steps within CNTs catalytic growth: 1) initial stage of forming precursor of tubular graphene sheet as starting point of growth of CNTs, 2) continuous graphitisation of walls and 3) slowing down and termination of carbon graphitisation and eventually the growth of CNTs. For each step, people have argued how the graphene precursor initiates on catalyst particles, what is the driving force for continuous graphitisation and eventually how the growth of CNTs terminates.

Possibly the first speculation was made early in 1967 by Irving and Walker [34]. They proposed the initiation stage was C dissolved in metal particles and then metal carbide was formed, which was un-stable and then can be decomposed to metal and crystalline graphite structures. Derbyshire [35] based on the previous theory and concluded a carbon 'dissolution-precipitation' model and verified this on nickel, cobalt and iron particles respectively. The results showed reasonable support on nickel and cobalt, however, this model cannot be applied on iron since no precipitated graphite was found. Derbyshire explained that it may be caused by greater affinity of Fe for C results in stability of iron carbide. This model also does not answer the formation of tubular structure initiated on surface of catalyst particles.

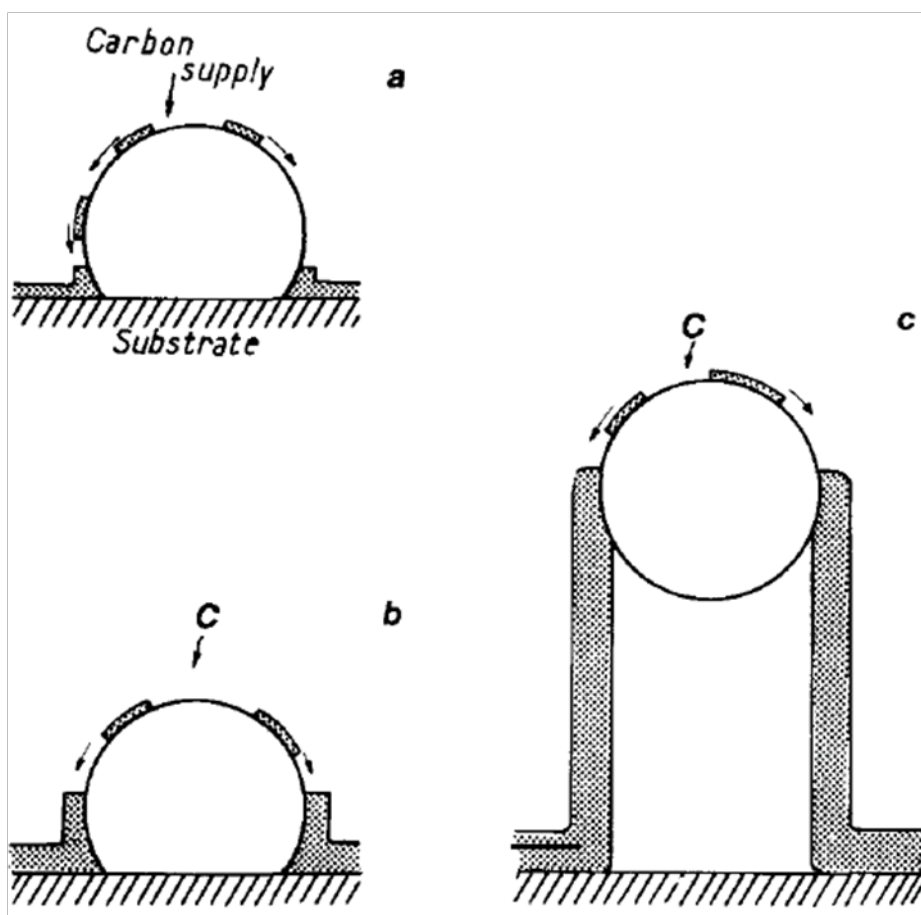


Figure 2.2 – Tip-growth model [16].

'Tip-growth model' was proposed by Endo [16] as shown in figure 2.2. They emphasized the growth of CNTs starts from a carbon shell formed at the bottom contact area between catalyst particle and the substrate. This carbon shell was diffused from the top surface and along the side portions of the catalyst particles. Continuous carbon supply from hydrocarbon species dissociates on the edge of the carbon shell and parallel to crystalline surface of the metal particles. Endo's tip-growth model did not take into account of the shape of catalysts and used spherical ones as a template for CNTs.

The tip-growth model has given people a lot of insights based on Endo's

observation. Baker and Harris [36] then summarised these thoughts in their book and also explained those particles are lifted by growth of CNTs, through 'extrusion' or 'root-growth'. As shown in figure 2.3, lateral grown graphitic layers also can be extruded from the carbon shell perpendicular upwards to the substrate, leaving the catalyst particles un-detached. Baker explained [37] a possible factor that may determine the mode of CNTs growth is the metal-support interactions. Weak interaction may results in easier lifting up following tip-growth mode, while strong interaction may lead to root-growth mode. However, Endo noted [38] that no matter which mode of the growth of CNTs is, catalyst particle is the point where continuous graphitization of CNTs starts from.

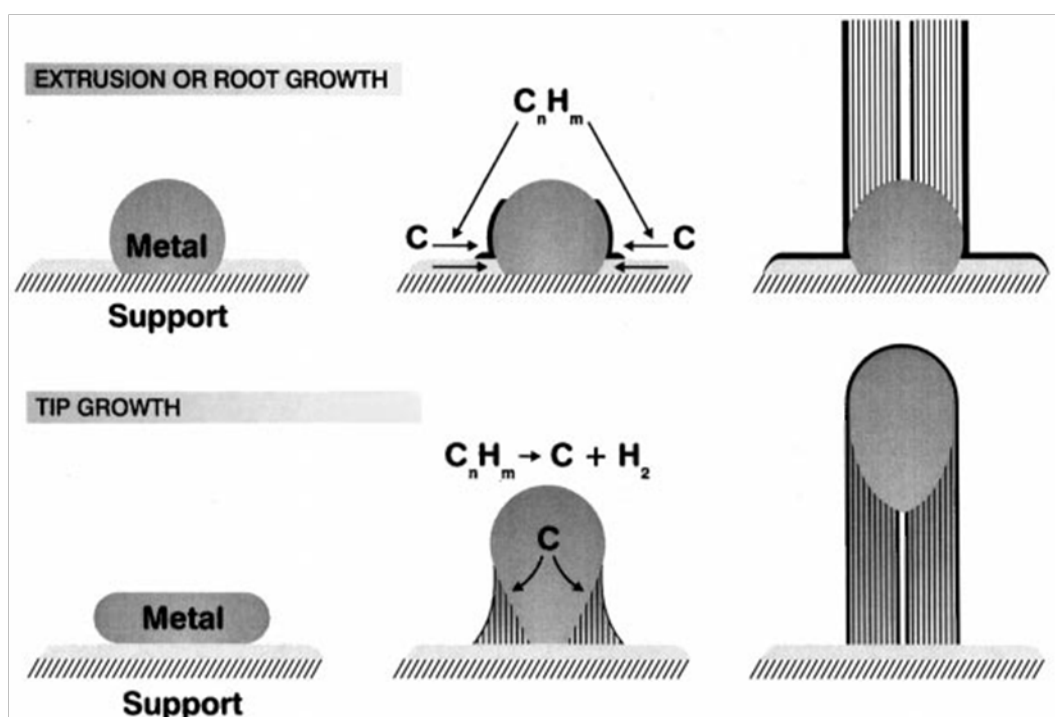


Figure 2.3 – Possible carbon nanotube growth modes [38].

Smalley [39] particularly proposed a yarmulke cap as the initiation graphene cap for growth of tubular filaments in their 'yarmulke mechanism'. They explained when the size of a metal particle is down to nano-scale, there will be tremendous surface energy which can only be diminished by chemisorbing the yarmulke graphene cap onto the surface of particles. This yarmulke cap, described by Dai *et al.* [41], has a special feature that it can prevent any type of open graphene edges during growth, which finally results in a carbon tube with no seams. Gorbunov *et al.* [17] have different thoughts about this graphene sheet in their solid-liquid-solid (SLS) model. They believe it is the defects from surface of the metal particle rather than the carbon shell itself that cause bulking of graphene sheet into tubular structure.

There were also some argues about driving force of continuous graphitisation. Baker [39] explained the driving force for continuous carbon diffusion through the particles is the temperature gradient, which is from the upper hotter leading surface to the cooler bottom. Sinnott [18] on the other hand, believed it is because of the concentration gradient of carbon dissolved in metal particles in their 'diffusion and precipitation' model. However, they are fundamentally the same, both temperature and concentration gradients refer to the direction from the upper part to bottom of the metal particles. Carbon atoms from continuous hydrocarbon species first deposit on top surface of catalysts, and then travel over the surface and through the bulk at the same time to the bottom of metal particles.

Sinnott also suggested the size of catalyst particles was an important factor that

could affect the diameter of CNTs, which was also agreed by Gorbunov [17]. They supposed that in tip-growth mode, the graphene layer of CNTs graphitise along the parallel direction to side portion of catalyst particles. Therefore the diameter of CNTs can be controlled by the size of catalysts. One can also use other processing parameters, e.g. temperature, substrates and concentrations of catalyst precursor to control the size distribution of metal catalysts, and eventually the diameter of CNTs. Sinnott [18] investigated the change of diameter distribution of CNTs as varying the ratio of catalyst precursor and hydrocarbon source as shown in figure 2.4. The results suggested that strong effect of the concentration of catalyst precursor on particle size distribution of catalysts. Table 2.1 confirmed the averaged diameter of CNTs matches well to that of iron particles. Gorbunov [17] further explained that the particle size of metal catalysts should also be in an optimum size range in order to form CNTs. Too small ones cannot transform enough amorphous carbon to CNT's structure before deactivation, while large ones will be in the solid state during decomposition of hydrocarbon species.

Table 2.1 – Averaged diameter of CNTs in relation with that of catalysts [18].

| Fe/C (at%) | Average nanotube inner diameter (nm) | Average nanotube outer diameter (nm) | Average Fe particle diameter (nm) |
|------------|--------------------------------------|--------------------------------------|-----------------------------------|
| 0.75 | 5.8 (3.0) | 33.6 (13.5) | 35.3 (12.6) |
| 0.075 | 4.3 (2.3) | 28.3 (9.9) | 28.2 (12.9) |

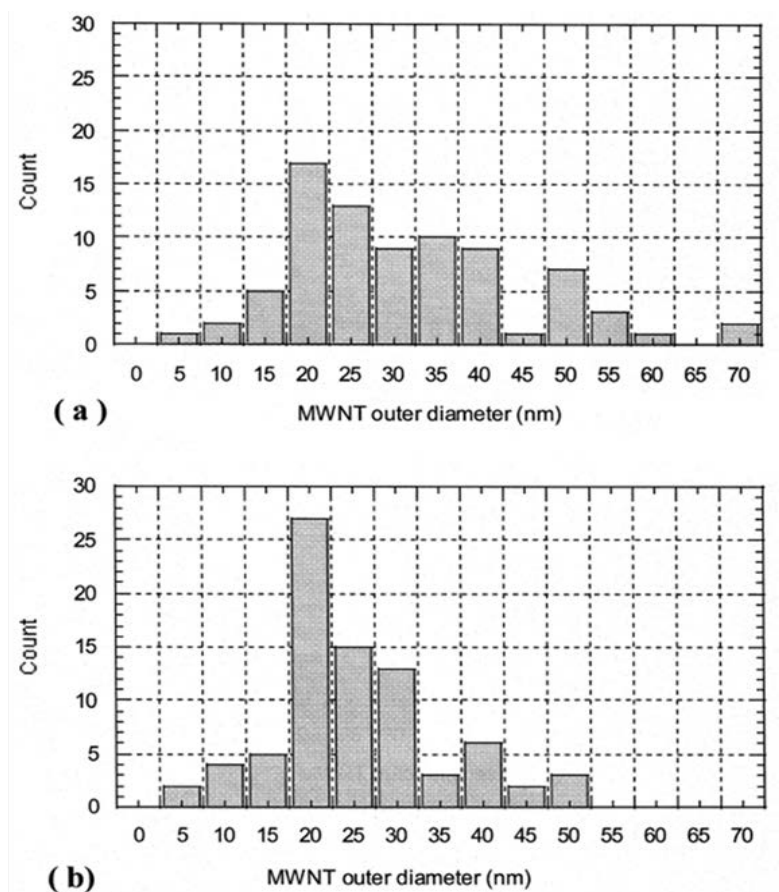


Figure 2.4 – Distribution of diameter of CNTs prepared by different concentration of iron particles, a) 0.75 at% Fe:C and b) 0.075 at% Fe:C ratios [18].

When Gorbunov *et al.* were explaining the size effect of catalyst particles on growth of CNTs, they were based on an assumption that metal particles were in the liquid state. Whether the metal particles are in solid or liquid state is still under debate, since the processing temperature for growth of CNTs is normally far below the melting point of metal catalysts or even metal-C alloys. However, there are indications that the metal particles can be liquidus. Helveg [40] employed in-situ TEM observation on dynamic formation of graphene layer at graphene-Ni interface, and series of images showed strong elongation has

occurred during lifting up of nickel particles by the growth of CNTs.

Lots of previous researchers, like Baker and Harris, generally believe catalyst particles can be in molten state because of supersaturated carbon dramatically reduced the melting point of metal particles when their size is down to nano-scale. This liquidus state of catalysts also can be beneficial for both initiation and continuous graphitisation of CNTs. Cao [41] explained the liquid droplet has a large accommodation coefficient (*a gas striking a solid/liquid surface*), which will attract the evaporated carbon to diffuse or dissolve into. This specific feature of liquid phase droplet makes it a preferential site for deposition of vapour source. When the continuous deposition meets a saturation threshold, the growth species will precipitate on the interface between liquid droplet and its substrate, first nucleation and then crystal growth in terms of lifting up the liquid droplet. It is another similar explanation as the 'tip growth' mechanism mentioned above but on more fundamental basis.

Researchers above seem all agreed that the eventual termination of growth of CNTs is because of an encapsulation of carbon on top surface of catalyst particles that prevent further deposition and diffusion of free carbon atoms. Therefore, the catalysts are deactivated.

2.2.3 Arc discharging

Arc discharging was cited [42] to be the most common and easiest way to produce CNTs since it is simple to undertake. Figure 2.5 shows the first arc

discharge apparatus produced originally to make fullerenes. Arc-vaporisation between two carbon rods was produced between two graphite electrodes placed closely up to 1mm. By filling helium or argon inert gas under low pressure in the chamber, rod-shaped nanotubes were formed from one of the vaporised graphite rod and deposited on the opposite one.

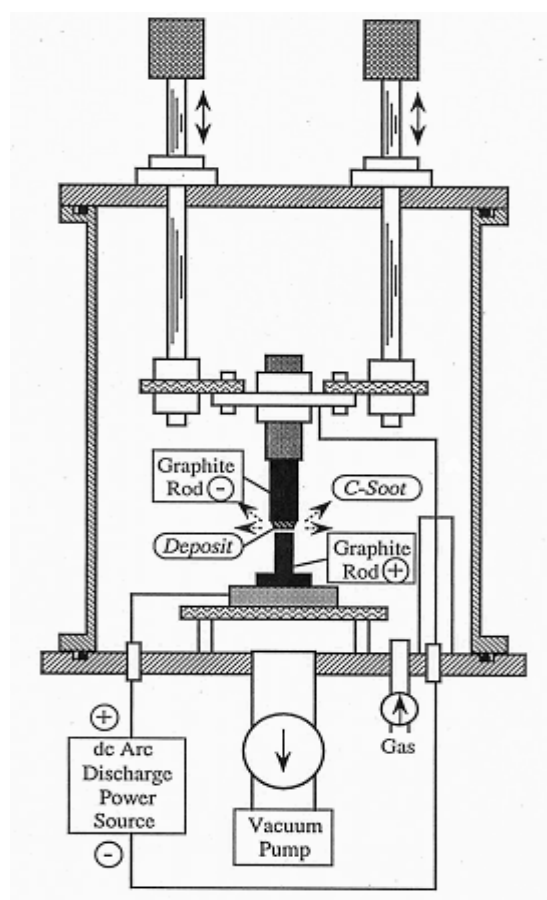


Figure 2.5 – First arc discharging apparatus [11]

It has been studied that [43] the morphologies of CNTs produced by arc discharging technique varies depending on different processing conditions. It can selectively produce SWCNTs by doping catalyst particles onto the anode graphite electrode, or MWCNTs through pure graphite electrodes. For

producing SWCNTs, The diameter distributions of SWCNTs can also be controlled by the gas mixture of helium and argon in the reaction chamber. Different diffusion coefficients and thermal conductivities from different mixture of helium and argon can affect the diffusion rate of carbon into metal catalyst particles and the diameters of SWCNTs grown on them [44]. Some other factors, such as temperature of carbon vapour and density of metal catalyst, were also claimed important by affecting nucleation of tubules and diameter distribution of SWCNTs. Journet and Bernier [45] even used Co and Mo in high concentration as catalysts to produce CNTs with diameters considerably smaller than 1.2-1.4 nm.

MWCNTs can also be produced through arc-discharging method if both electrodes are pure graphite. However, purification is necessary afterwards, since lots of by-products can also be formed, such as fullerenes and amorphous carbon. Without the existence of catalyst particles, some graphene sheets may also be formed.

Recent investigation [46] as shown in figure 2.6 has employed arc-discharging technique in liquid nitrogen to produce CNTs. This is the first economical route to produce highly crystalline MWCNTs, since neither low pressure nor expensive inert gases is needed. The yield of MWCNTs was high up to 70% of the reaction product, and SWCNTs were also produced under modified processing conditions.

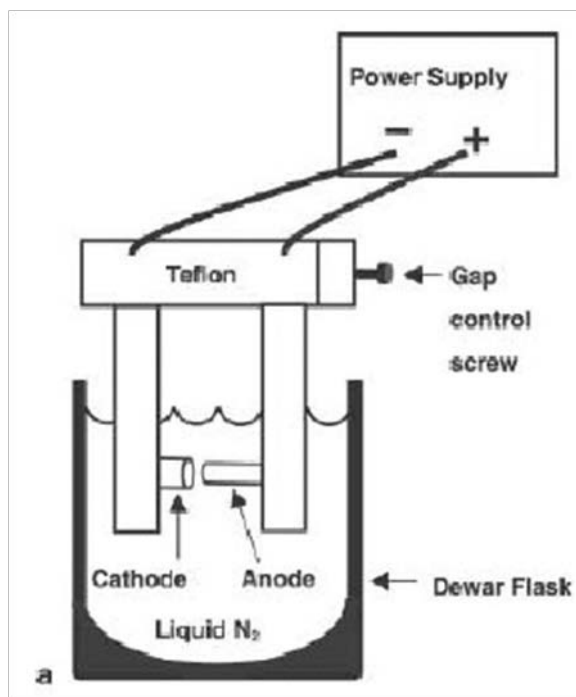


Figure 2.6 – Schematic apparatus of modified arc discharge with electrodes in liquid nitrogen [48].

2.2.4 Laser ablation

Smalley's group [12] developed a laser ablation technique at Rice University by using apparatus shown in figure 2.7. Laser ablation technique is similar to that of arc discharge since the mechanism for both of the apparatus design is the same. Laser ablation used laser power to vaporise graphite target. SWCNTs and MWCNTs can also be produced selectively depend on whether catalysts are doped onto graphite target.

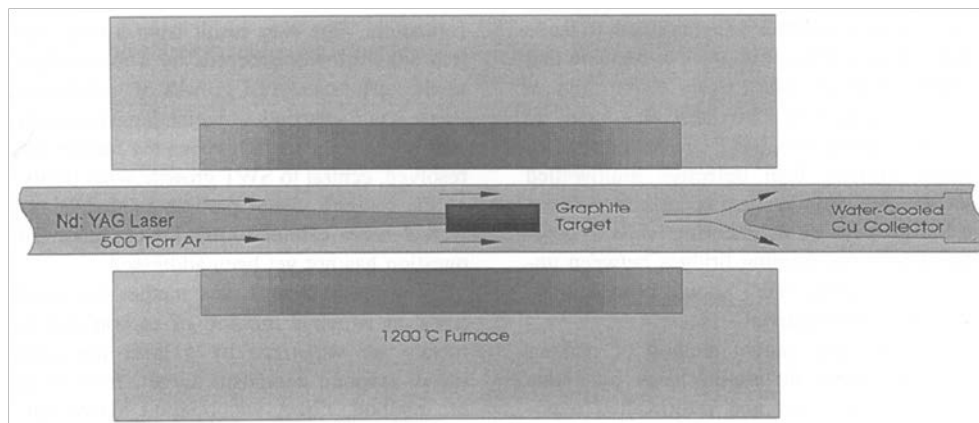


Figure 2.7 – Schematic apparatus of laser ablation [47].

Compared with arc discharging technique, laser vapourisation of carbon offers a higher yield and better properties of SWCNTs with narrow size distribution, when incorporating of graphite with Co, Ni, Fe, or Y nanoparticles. There are various catalysts, and it has been suggested [48] the best yield of catalyst mixture is Ni/Y (Ni/Y=4.2/1), by which up to 90% purity of nanotubes were obtained, as shown in figure 2.8. The averaged diameter of SWCNTs processed is 1.4 nm with 20-30% yield of reaction product. Since the optimum processing conditions between laser ablation and arc-discharging are almost the same, reactions taken place in both of the methods may undergo the similar mechanisms.

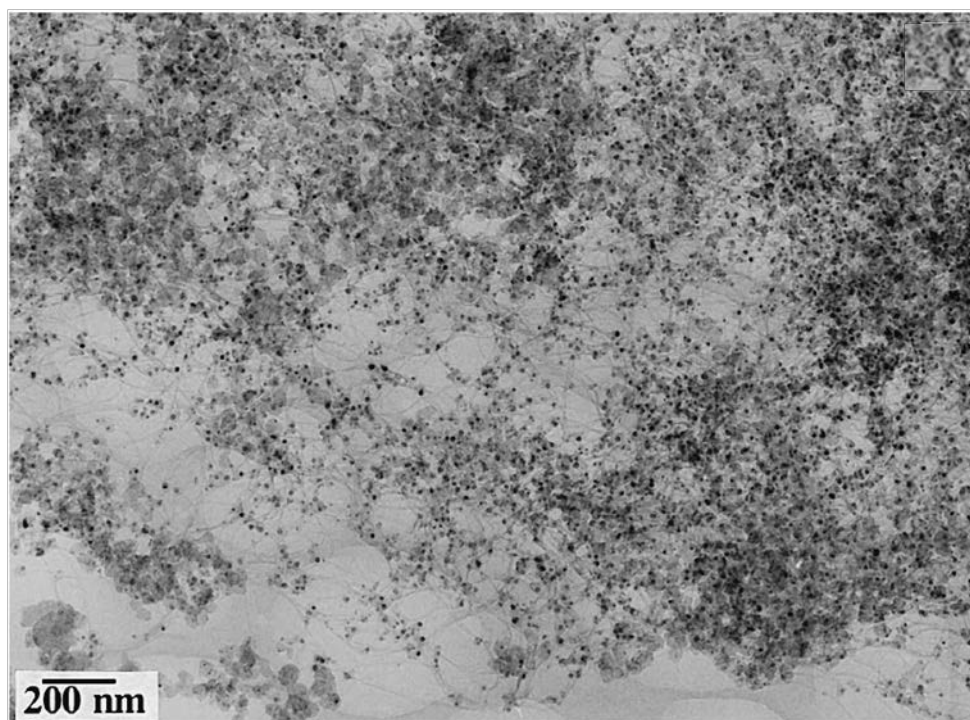


Figure 2.8 – SWCNTs from laser ablation [50].

Even though there are lots of comparisons of CNTs from arc discharge and laser ablation methods, they are both promising methods to produce SWCNTs. However, they are both suffering the same limitations. Firstly, they are still restricted to be scaled up for industrial applications. Based on the design of apparatus, only small amount of CNTs can be manufactured at one time. Secondly, the energy sources used to vaporise graphite electrodes for both of them require high cost. Thirdly, the CNTs produced from the two methods tend to be tangled together, as indicated in figure 2.8. It is difficult to align these CNTs for functional electronic devices. Finally, purification procedures are always necessary to get rid of other carbon by-products, especially for manufacturing MWCNTs. These limitations led to the development of catalytic chemical vapour deposition (CCVD) derived from Endo's seeding method.

2.2.5 Chemical vapour deposition (CVD)

Rather than vaporisation of graphite electrode, chemical vapour deposition (CVD) utilises gas phase of hydrocarbon species with an energy source on catalyst particles for growth of CNTs. The energy source is used to decompose hydrocarbon vapour into reactive carbon, which can be absorbed by catalyst particles on selected substrates. CVD method offers positional and directional control of the growth of CNTs and the potential to be scaled-up for industrial applications.

Generally there are two steps during CVD processing: 1) preparation of catalysts, and 2) actual synthesis of CNTs [49]. Within first step, catalyst particles can be prepared directly from its bulk material, or through impregnation of catalyst precursors. For the second step, gas composition and decomposition temperatures are the major factors to control the growth of CNTs.

During the last two decades, different techniques for synthesis of CNTs by CVD method have been developed. In the next section, details of CVD method, preparation of catalysts and processing condition will be introduced.

2.2.5.1 Preparation of catalysts

Since the size of catalyst particles plays an important role on the catalytic growth of CNTs, magnetron sputtering and pulsed laser deposition (PLD) were

mainly used to precisely control the size distribution of catalyst particles.

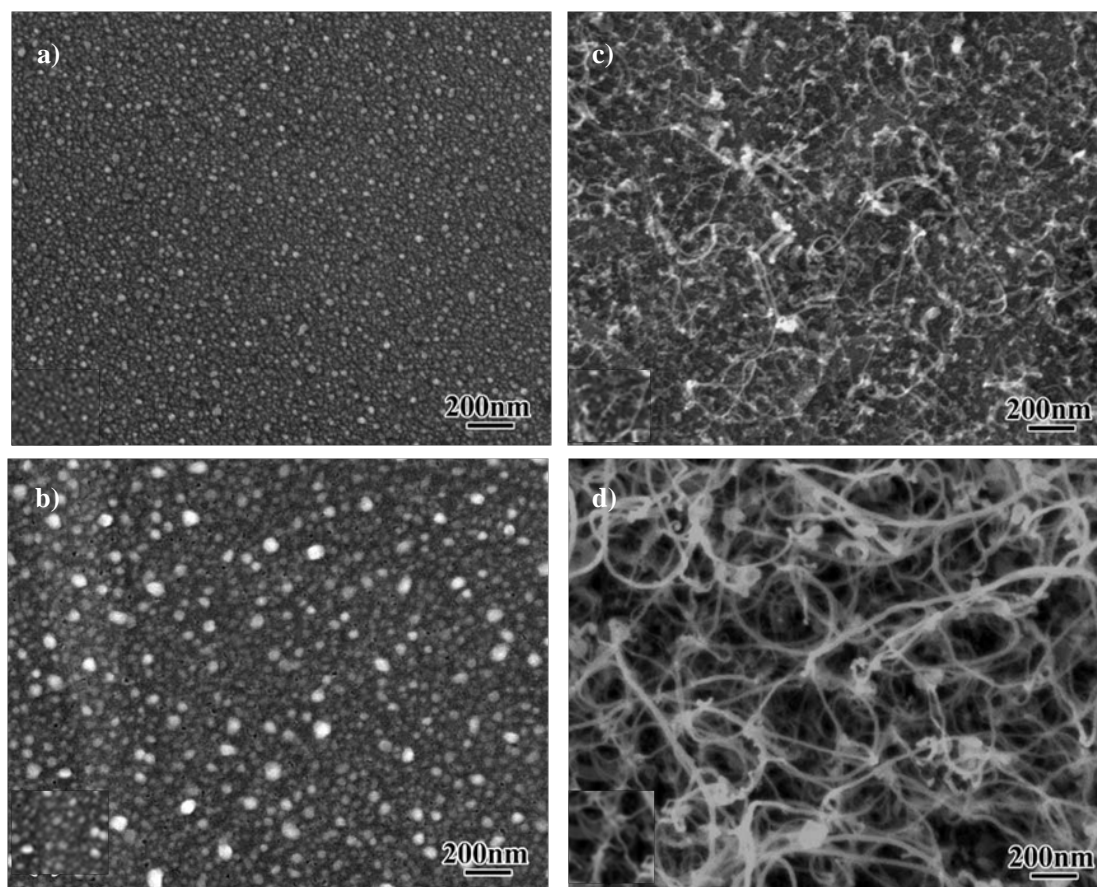


Figure 2.9 – Magnetron sputtering of stainless steel film on graphite substrate and reduced by hydrogen. a) & b): catalyst particles reduced from SS films with the thickness of 2 and 50 nm, respectively. c) & d): as-produced CNTs from the catalysts prepared on the left, the diameters of which were 2 and 15 nm, respectively [52].

Ren *et al.* [50] used magnetron sputtering to coat a stainless steel (SS) film onto graphite substrate. The nucleation of the combination of Fe, Co and Ni particles can be induced by thermal annealing in hydrogen. They also tried thermal method through etching SS film in ammonia, and then followed by annealing in hydrogen to induce nucleation of catalyst particles [51]. In either way, the size distribution of metal particles was controlled by the thickness of SS layer. Figure 2.9 shows as increasing of the thickness of SS film, size

distribution of catalyst particles varies, as well as the averaged diameter of CNTs.

Another technique that used to prepare catalyst particles was pulsed laser deposition (PLD), which was developed to produce high purity thin film from a wide range of materials [52]. Figure 2.10 demonstrates a typical PLD apparatus. It has metallic diaphragms that were used to cover bombard targets, which can prevent large droplets or particles that can deposit directly onto substrates [53]. During PLD, the targets were also rotating, so that a uniform ablation can be generated to produce particles with a narrow size distribution.

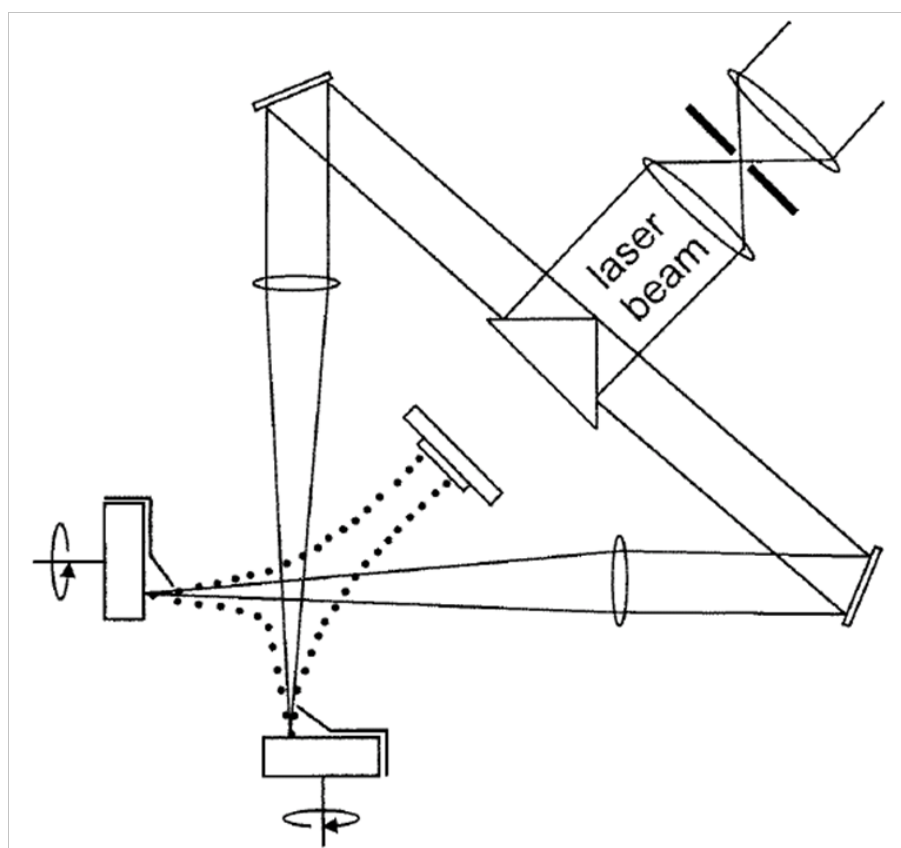


Figure 2.10 – Two-beam excimer laser ablation with bombard targets covered with metallic diaphragms [55].

2.2.5.2 Design of apparatus

Conventional CVD apparatus is based on thermal heat to 'crack' hydrocarbon vapour, normally through a tube furnace, as shown in figure 2.11. The specimen was impregnated with the material of catalysts, and put in the middle of the reaction tube. Prior to decomposition of hydrocarbon species, NH_3 or H_2 flow was applied on the specimen to produce catalyst particles through either chemical etching or thermal annealing as described above. Hydrocarbon gas flow was not turned on until target decomposition temperature was reached. An advantage of this technique was its convenience in controlling composition of gas flow.

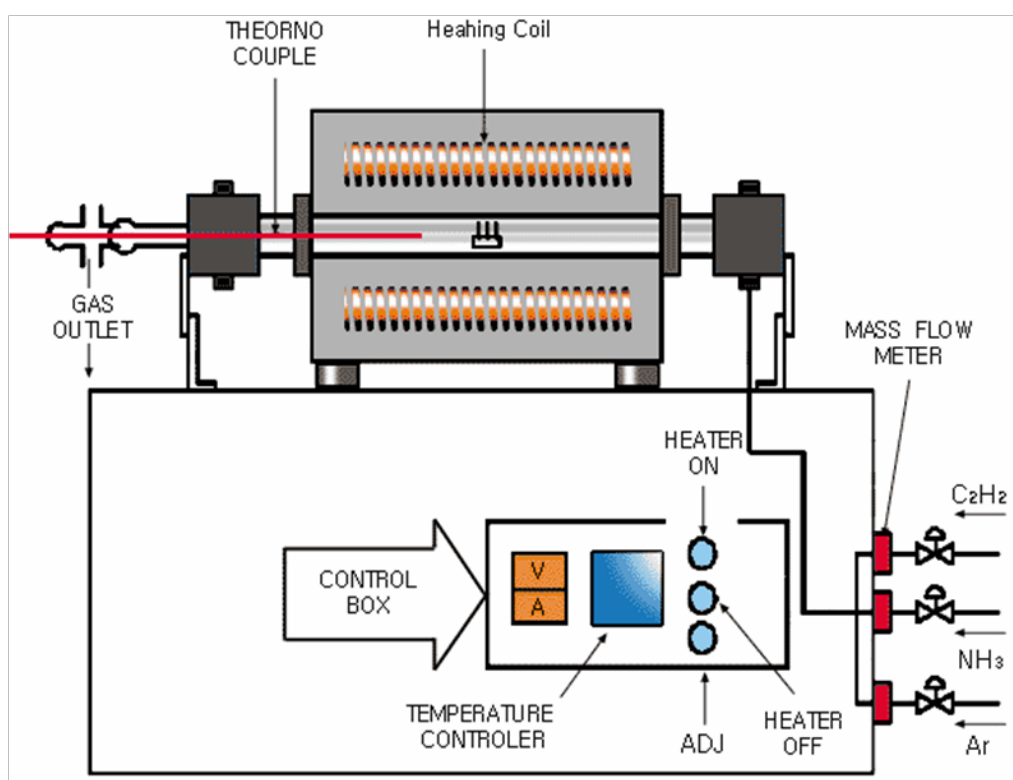


Figure 2.11 – Design of thermal CVD apparatus based on hydrocarbon gas flow [54].

A floating method was developed for continuous production of CNTs compared to previous non-continuous method. As shown in figure 2.12, hydrocarbon and catalysts were floating in a vertically placed furnace from the top end to the bottom. As floating of catalyst particles with hydrocarbon gas, CNTs can be produced and collected at the bottom end. The furnace can be also placed horizontally, by collecting CNTs in a tank connected to the outlet.

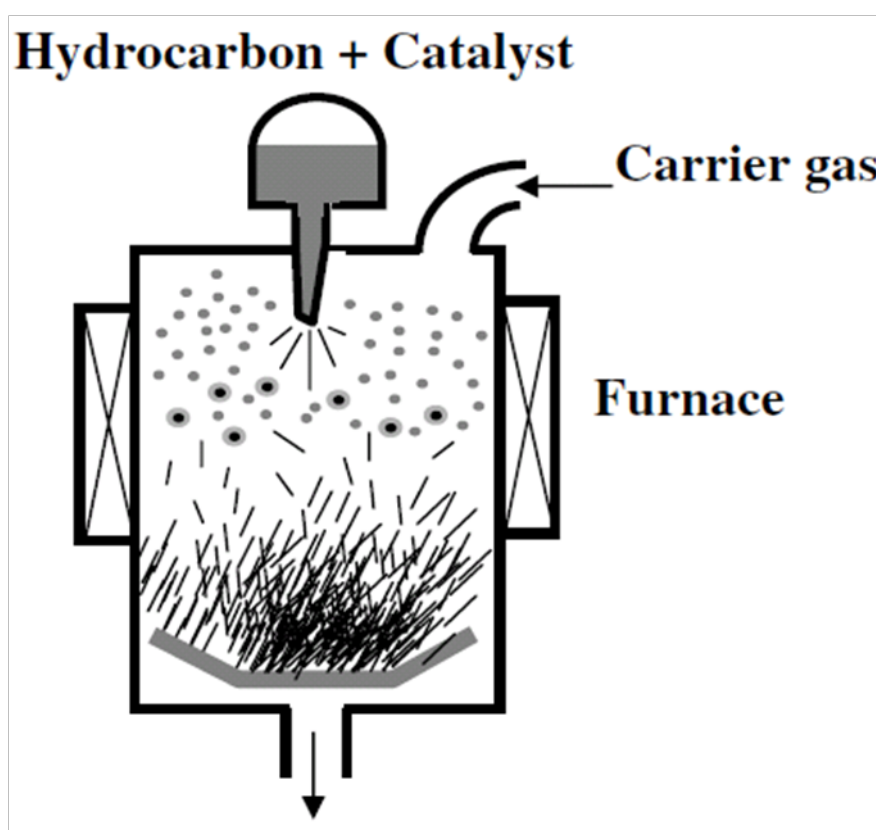


Figure 2.12 – Design of floating method of CVD setup [55].

Floating CVD technique offers a potential for scaled-up industrial applications. Volume production of CNTs is available by continuous floating hydrocarbon and catalyst mixture through the furnace [56].

Another CVD technique used for directional growth of CNTs on target substrate is called plasma enhanced CVD, which uses current flow generated by high frequency power to bombard the hydrocarbon gas during thermal CVD. Figure 2.13 shows additional parallel plate electrodes connected with external power source. During CVD, electric field will not only reduce activation energy for the growth of CNTs, but also cause alignment and prevent entanglement of CNTs [57].

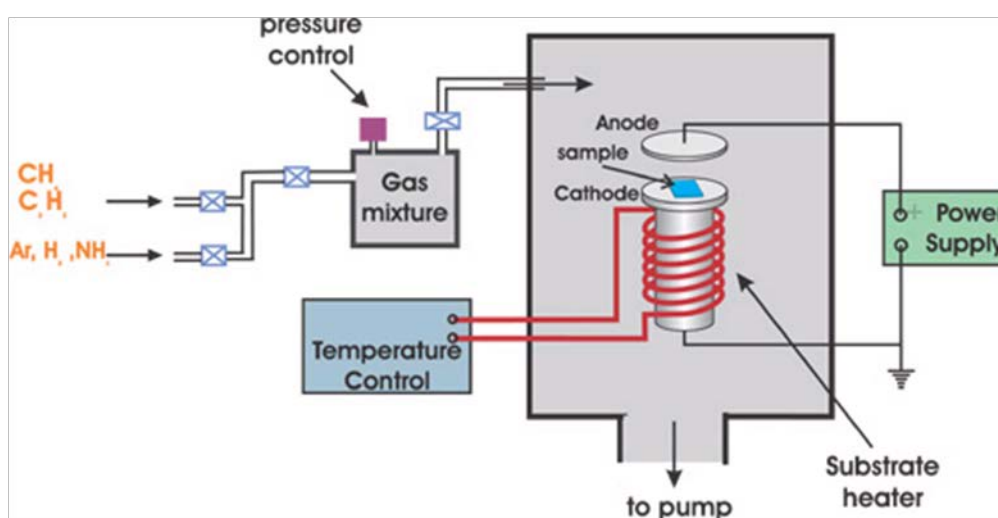


Figure 2.13 – Design of PE-CVD experimental setup [58].

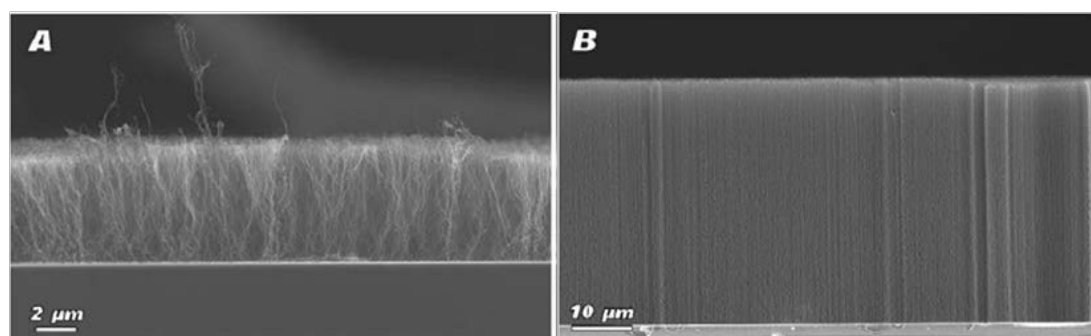


Figure 2.14 – vertically grown CNTs achieved through CVD: A) without plasma and B) with plasma [59].

Figure 2.14 suggests the effect of plasma on the alignment of CNTs growth, which can be used potential in electronic devices.

2.2.5.3 Gas composition and decomposition temperatures

During decomposition of hydrocarbon gas, a lot of researchers have suggested the importance of hydrogen on the growth of CNTs. Haubner [60] systematically investigated the effect of various H₂ concentration on the yield of CNTs as shown in figure 2.15, by using xylene decomposed at 750°C on iron particles. They suggested that the existence of hydrogen can increase the capability of catalyst particles transferring carbon atoms into nanotube structure, by preventing the formation of carbon supersaturation. Otsuka *et al.* [61] also indicated the hydrogen on both the initiation and final stages of CNTs growth can delay the deactivation of catalysts by carbon deposition layer, which can prevent further absorption of carbon atoms. Improvement of the yield of CNTs from figure 2.15 proved the positive effect of the growth of CNTs.

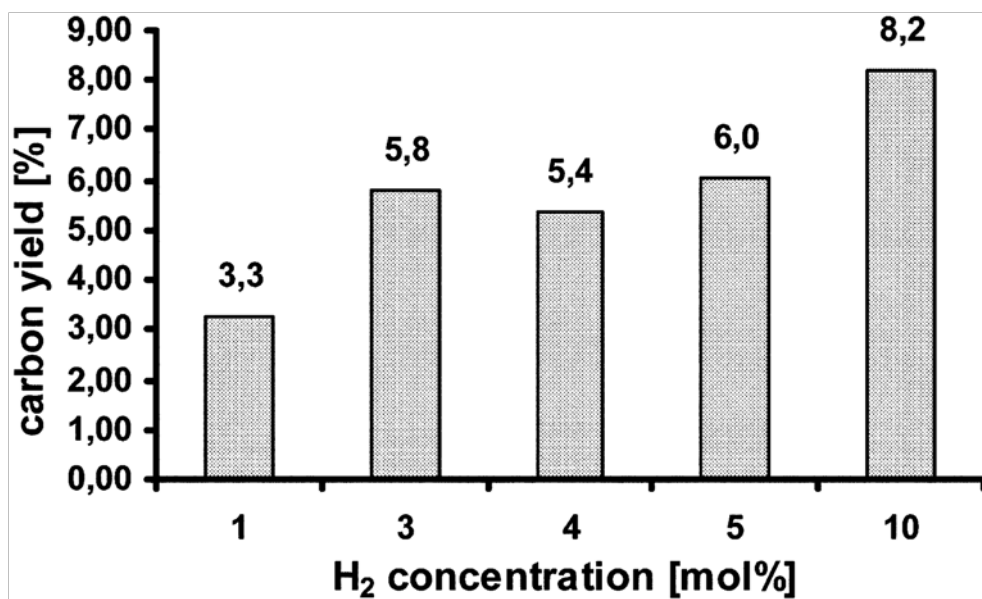


Figure 2.15 – CNTs yield varies with the content of H₂ in hydrocarbon gas [62].

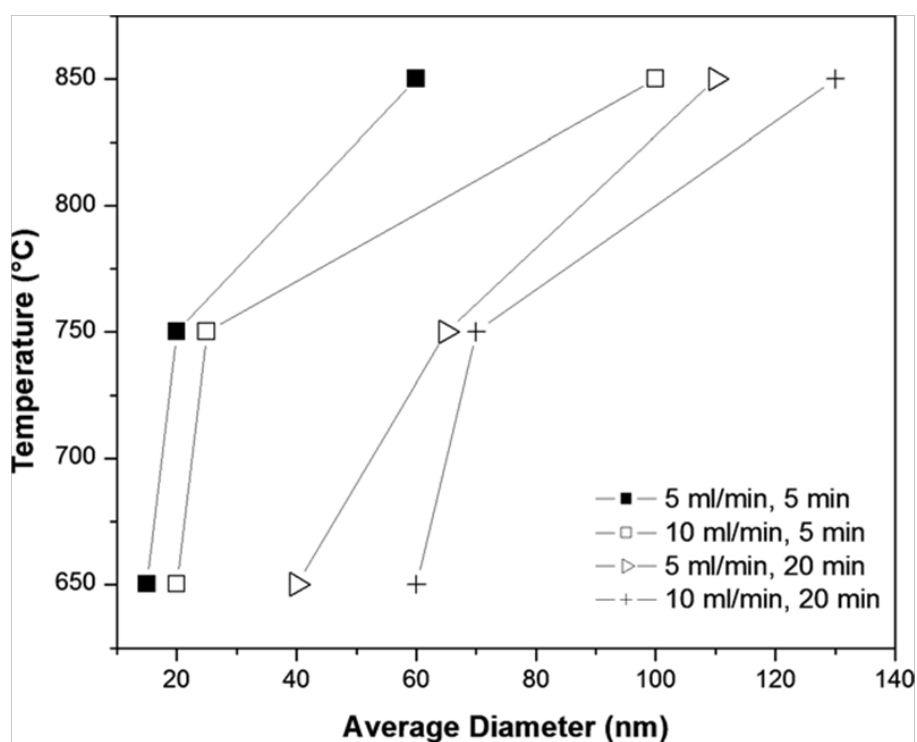


Figure 2.16 – Averaged diameters of CNTs grown at different temperatures and dwelling time [66]

Sulfur was also used by several researchers as a promoter for the growth of CNTs. The role of sulfur was ascribed to lowering the melting temperature of catalyst particles [63]. Martin-Gullon *et al.* [64] suggested that molten state of catalysts could increase their activity for the growth of CNTs and prevent the formation of amorphous carbon or soot.

The decomposition temperature is also vital for both the formation and size distribution of CNTs, as suggested by Karanikolos [65]. Figure 2.16 indicates the diameter of CNTs increases as the increasing of decomposition temperature of acetylene on Ni particles. Moisala [66] identified the highest efficiency for SWCNTs formation was between 700 and 900°C, when using iron as catalyst. They believed that variation of CNTs in diameter is dominated by the size of catalyst particles, which can be affected by decomposition temperatures.

2.3 Ex-situ usages of CNTs in composites

CNTs have been used as reinforcements in various matrices, such as polymers [2], metals [3] and ceramics [4]. Particularly in polymers, significant amount of researches have been done and certain achievement has been obtained.

2.3.1 Ex-situ manufacture of CNTs/polymer composites.

Shaffer and Windle [67] were the first to systematically study CNTs/polymer composites, and they tried to disperse CNTs into the stable gel-state polymers

during fabrication of CNTs/polymer composite films. Their work showed the importance of uniform distribution of CNTs within polymer matrices on the improvement of thermo-mechanical and electric properties of the composites. Their testing on CNTs/PVOH polymer film showed improvement in stiffness at elevated temperatures as well as electrical conductivity. Qian *et al.* [68] reported a 36-42% increase of elastic stiffness and 25% increase of tensile strength for a CNTs/PS polymeric composite dispersed with only 1 wt.% of CNTs. They used the solution-evaporation method to achieve relatively uniform dispersion and preserve integrity of CNTs. The purpose of their research was to improve toughness by load transfer through PS matrix-nanotube interface. In-situ TEM images indicated the bridging effect of the CNTs, the main toughening mechanism of which is shown in figure 2.17.

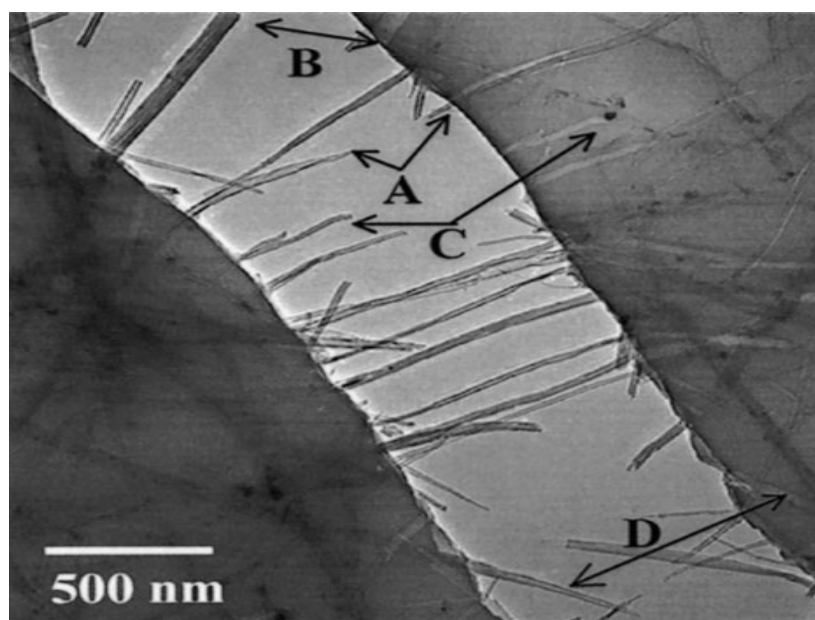


Figure 2.17 – Crack bridging in MWNT/polystyrene thin film [69]

2.3.2 Ex-situ manufacture of CNTs/metal and ceramic composites.

The manufacture of non-polymer based CNTs reinforced composites, such as metals and ceramics used as matrices, was mostly adapted in the powder based process. However, the uniform dispersion of CNTs in metal or ceramic powders is much more difficult than that in polymer matrices. Currently, the most common methods were mechanical stirring or ultrasonication to the powder-based matrices with addition of CNTs, and then followed by spark plasma sintering (SPS) or hot press during densification of the composite structure. The SPS technique can generate high temperature in short time period compared to thermal heat treatment, so that it can largely reduce the loss of CNTs. Kim *et al.* [70] tried 24-hour high energy ball milling of CNTs with Cu powder, which was reduced from copper nitrate. The CNTs and metal composite powder was sintered by SPS in vacuum conditions, followed by cold rolling and annealing at 650°C for 3 hours. Figure 2.18 shows relatively uniform dispersion of CNTs in some region within Cu matrix and strengthening effect of CNTs. Kim claimed a 60% improvement in tensile strength for CNTs/Cu composites compared to monolithic Cu. Kuzumaki *et al.* [71] further improved the processing technique by using aluminium as the matrix, through prolonged annealing of the composite in order to retain the strength of the matrix material.

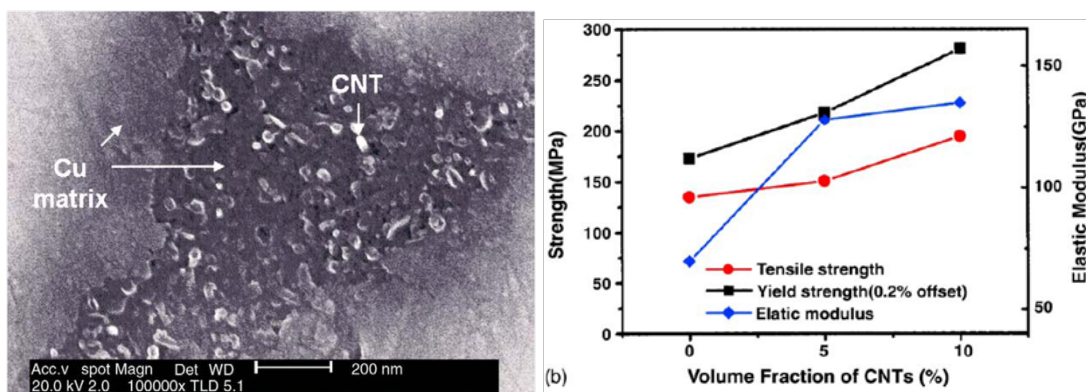


Figure 2.18 – Left: Uniformly dispersed 5vol% CNTs/Cu nanocomposites in the centre region. Right: Stress-strain curve of CNTs/Cu composites with different amount of CNTs [73].

The aim of introducing CNTs into ceramic matrix is to improve toughness. For ceramic powders, such as SiC and Al₂O₃, both ball milling and ultrasonic stir can be used to disperse CNTs into slurry of the powders. For the densification of the composites, both PS and hot press were tried. Ahmad and Pan [72] used SPS on long-time milled ball milled alumina powder for 24 hours, with the addition of SiC and CNTs as the second phase reinforcements. They claimed a 117% improvement in fracture toughness of the composite material, as well as maintaining the intrinsic hardness of alumina. Fan *et al.* [73] also tried hot press on alumina powder in inert gas atmosphere, with the addition of SWNTs through ultrasonication of SWNTs in PEG (*polyethylene glycol 2000*) solution. They claimed the fracture toughness of the as-produced composite was twice as that of the monolithic alumina, which they believed was likely caused by crack bridging and pullout of SWNTs.

Apart from mechanical methods of mixing CNTs with ceramic powders, people also developed solution methods in order to achieve a more uniform dispersion

of CNTs within the matrix materials. Yamamoto *et al.* [74] have dispersed 0.9vol% MWCNTs in aluminum-based solution precursor (*aluminum hydroxide and magnesium hydroxide*), and then the precursor solution was dehydrated at 600°C in argon atmosphere and followed by SPS sintering at 1500°C. The microstructural characterisation of the as-produced Al₂O₃/CNTs was shown in figure 2.19, where a relative uniform distribution of CNTs was observed.

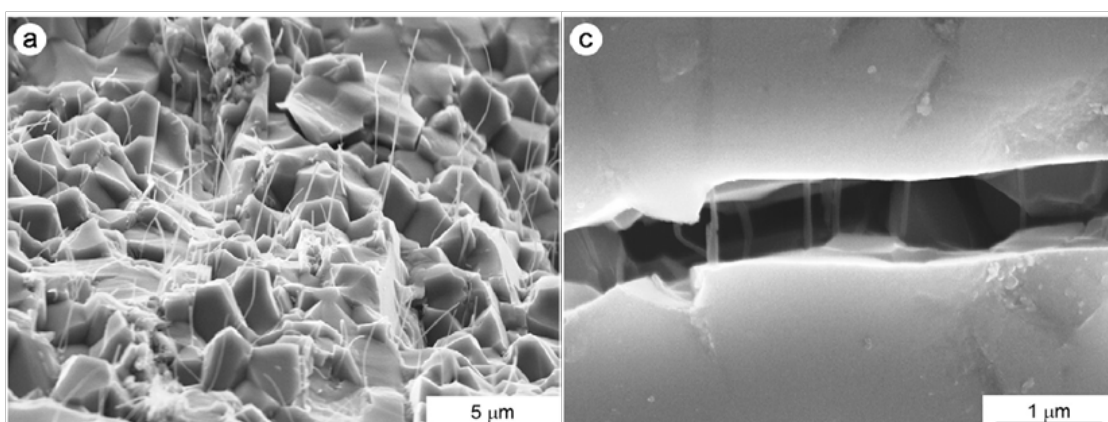


Figure 2.19 – MWCNTs/alumina composites. Left: general dispersion of CNTs within alumina matrix. Right: micro-crack bridging by MWCNTs [76].

The mechanical properties testing also showed that the improvement of fracture toughness of CNTs reinforced composites was significantly affected by the amount of CNTs. Previous researchers, such as Ahmad [74] and Yamamoto [76], were both tried to prepare series of Al₂O₃/CNTs composites. Figure 2.20 shows their results with similar trends of the change of fracture toughness as increasing of the amount of CNTs. The results indicated that the fracture toughness of CNTs reinforced composites can be increased as increasing the amount of CNTs, until a threshold was reached, beyond which the fracture toughness of the composite started to fall. Both Ahmad and Yamamoto

suggested the reason caused the decrease of fracture toughness was most likely because of the inhomogeneous dispersion and agglomeration of CNTs, when its amount exceeded a critical level.

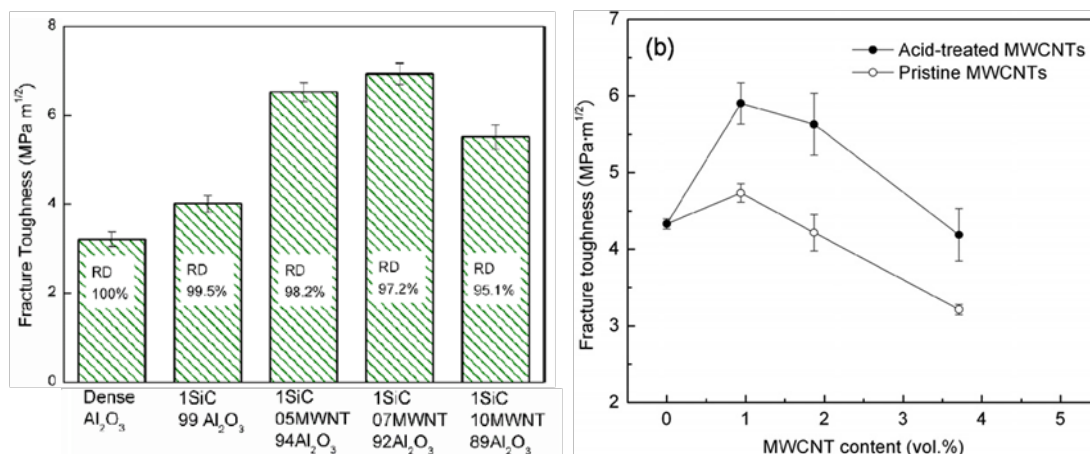


Figure 2.20 – Typical trend of CNTs toughening effect from both Ahmad and Yamamoto. Left: Alumina composites reinforced by CNTs and SiC as secondary phase reinforcement. Right: Alumina composites with both acid-treated and non-treated CNTs [74, 76].

No matter what matrix material was selected, previous researchers believed the importance of homogeneous dispersion of CNTs within the matrix leads to simultaneous increase of mechanical properties of the composite materials. However, it was also suggested that relatively uniform dispersion of CNTs through ex-situ methods was only valid when the amount of CNTs was low. Most of the results indicated that further increase the amount of CNTs would lead to decrease of mechanical properties, especially the fracture toughness as shown in figure 2.20.

2.4 In-situ CCVD of CNTs

Through in-situ method, CNTs are grown directly on surface of the target material, which will be densified for the manufacture of composites. The growth of CNTs is normally initiated on catalyst particles that are in-situ deposited on surface of the target material. Therefore, there will be no post-dispersing process required and therefore exists a possibility of achieving homogeneous dispersion of CNTs in composites. One of the typical examples is growth of CNTs on surface of CFs in order to prepare a carbon fibre preform for the manufacture of CNTs/CFs hybrid reinforced composites.

2.4.1 In-situ CCVD of CNTs on surface of CFs

In-situ growth of CNTs on surface of CFs through CCVD method follows all fundamentals of CVD principles described before. However, CNT/Fs in-situ growth on CFs is technically more difficult because of graphite nature of CFs: they absorb metal particles more easily and carbonaceous by-products may also form. Therefore, it should be taken more cautions when preparing CFs and catalysts to prevent rapid diffusion and promote suitable processing conditions for growth of CNTs.

Figure 2.21 gives an example of uniformly grown CNTs on CFs, prepared by Dodelet [75,76,77], who have done series of researches of CNTs/CFs hybrids. Within this section, details of processing procedures, including catalyst preparation, some specific CVD apparatus designs and processing conditions

will be reviewed.

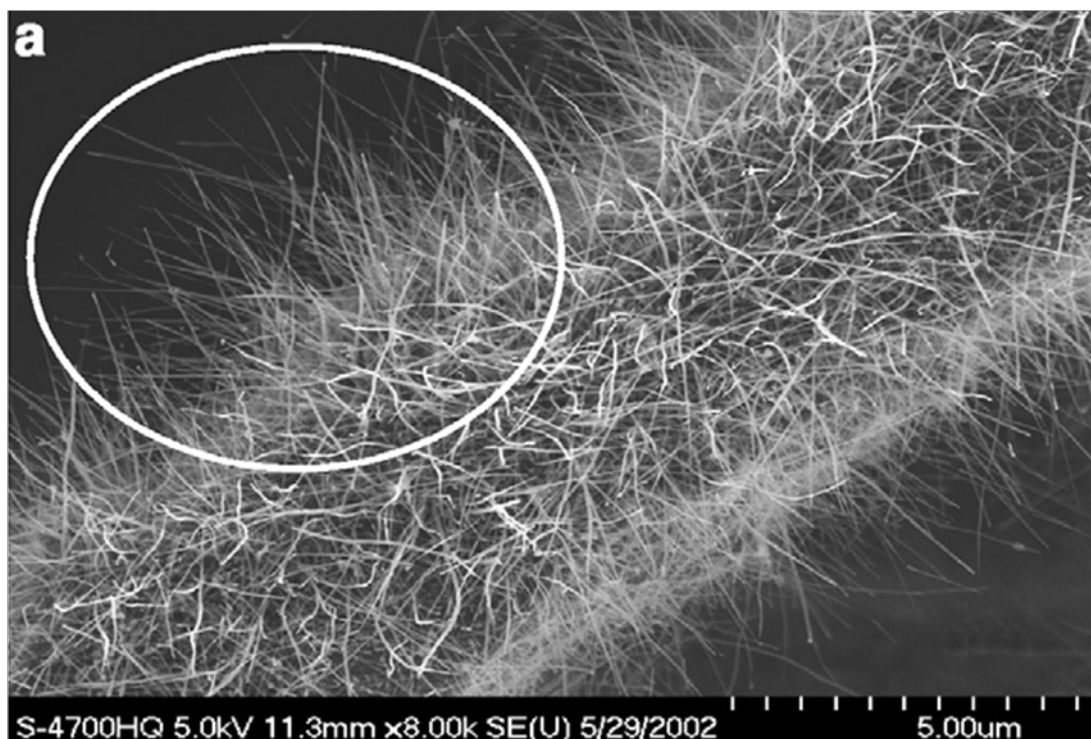


Figure 2.21 – In-situ grown CNTs on surface of a CF [78].

2.4.1.1 Surface pre-treatment of CF and catalysts preparation

Normally for CFs, certain surface pre-treatment is given to improve the surface morphologies for better accommodation of catalyst particles. Figure 2.22 shows the common feature of groove surface after washing in nitric acid, which can effectively accommodate more catalyst particles and homogeneous dispersion. Catalyst clusters can be effectively prevented compared to CFs without acid wash. A higher yield of CNTs is also found on treated CFs. Zhao *et al.* [78] also indicated that the longer CFs immersed in acid solution for oxidation, the deeper and possibly more uniform the CNTs could be in-situ grown on surface

of CFs. It is also called 'surface activation' of CFs somewhere else [79]. Luhrs *et al.* [80] suggested another surface activation method by burning CFs at 525°C in oxygen gas flow in order to remove sizing and activate CF surface. Based on their observations, no severe damage occurred except about 10% net weight loss of CF. They also claimed the surface of CF became rougher that was friendlier for loading of metal particles.

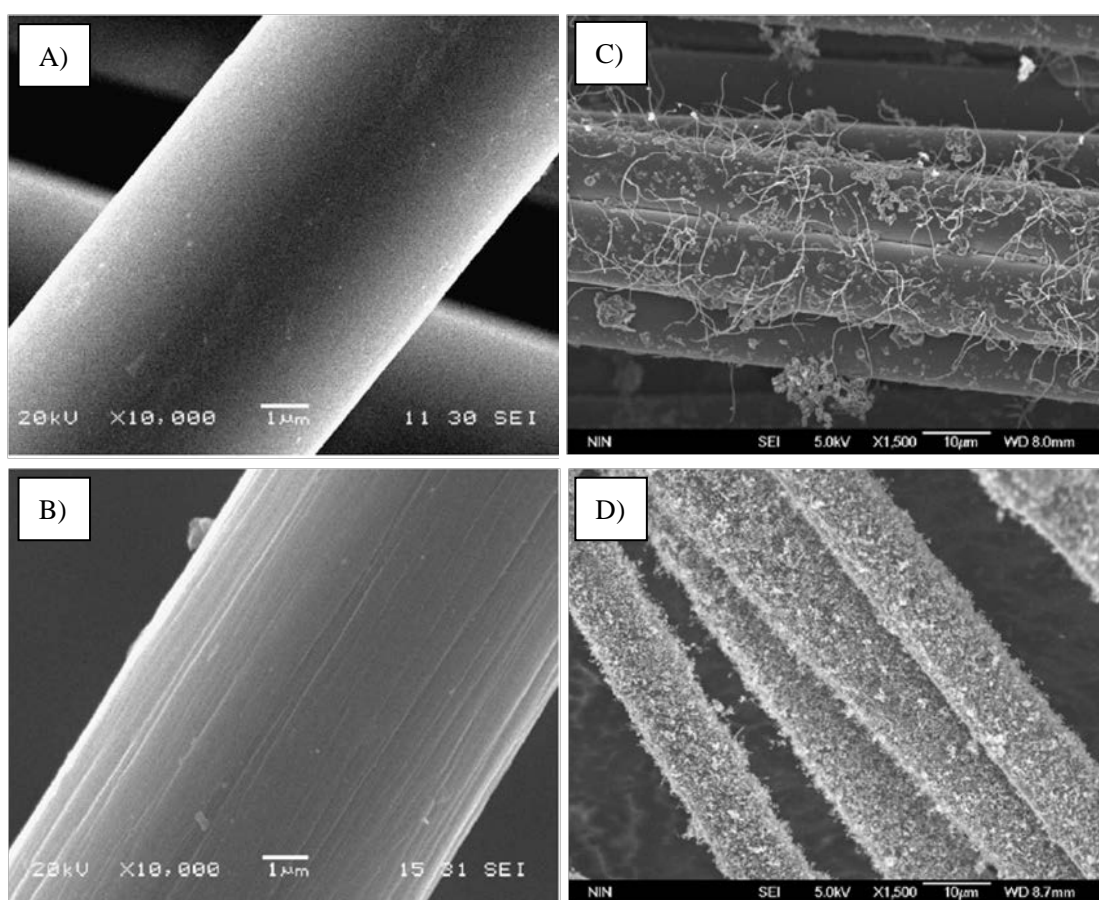


Figure 2.22 – Surface morphologies of CFs accommodation of catalysts. A) and B) are surface morphologies before and after acid treatment. C) and D) are yield of CNTs respectively [84].

Xia *et al.* [81] agreed the necessary and importance of activation of CF surfaces before in-situ CVD processing. They used ultrasonic stir of CFs in acetone and

ethanol respectively for 10 minutes in room temperature. CFs were then cleaned and boiled in sulfur acid and nitric acid mixture ($V_{H_2SO_4}:V_{HNO_3} = 1:3$) for 30 minutes before being cleaned in deionised water. Dodelet recommended the use of methanol during pre-treatment, which could improve the homogeneity of size and distribution of metal particles on the surface of CFs [77].

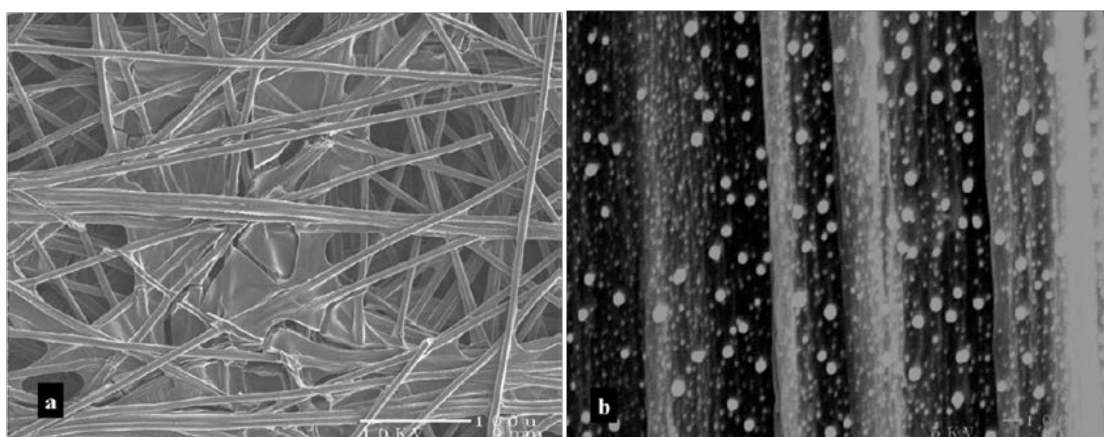


Figure 2.23 – a) PLD deposition of Ni on one side of a CF paper b) in-situ formed Ni particles on CF after thermal annealing [82].

There have been generally two ways of loading metal catalyst particles on surface of CFs: one is direct coating of metal catalysts by techniques described before, such as magnetron sputtering and PLD. Figure 2.23 demonstrates using PLD technique to coat a Ni film on one side of a carbon paper and then in-situ form Ni particles on surface of CFs after thermal annealing. The advantage of this technique is the size distribution of catalyst particles can be better controlled. However, the drawback is the limited penetration of the catalyst impregnation through the bulk material. As indicated from figure 2.23, only the top surface or one side of the bulk material was loaded with catalyst particles.

Another way of impregnation of catalysts is through solution method by using catalyst precursors. The general procedures are: firstly, dissolve metal salts into certain solvent to adjust precursor solution for various concentrations, and then the bulk material used as substrate is immersed in the as-prepared solution to load catalyst precursors. Previous researches have mainly focused on transition group metals and alloys, as shown in figure 2.24. Dodelet [77] suggested Ni-Co system by using their nitrates dissolved in silane-ethanol solution. The adjusted sulfonic acid-silicate through hydrolysis, which can give H^+ in exchange of Ni^{2+} and Co^{2+} from their nitrates. These ions then can be reduced to Ni-Co catalyst particles by hydrogen during CVD for the growth of CNTs. It was also suggested that electrochemical deposition (ELD) can be used to assist uniform coating of catalyst precursors [83].

Even though there are varieties of methods to prepare precursor solutions, it appears that Fe, Co and Ni were the three main catalysts used for the growth of CNTs on surface of CFs.

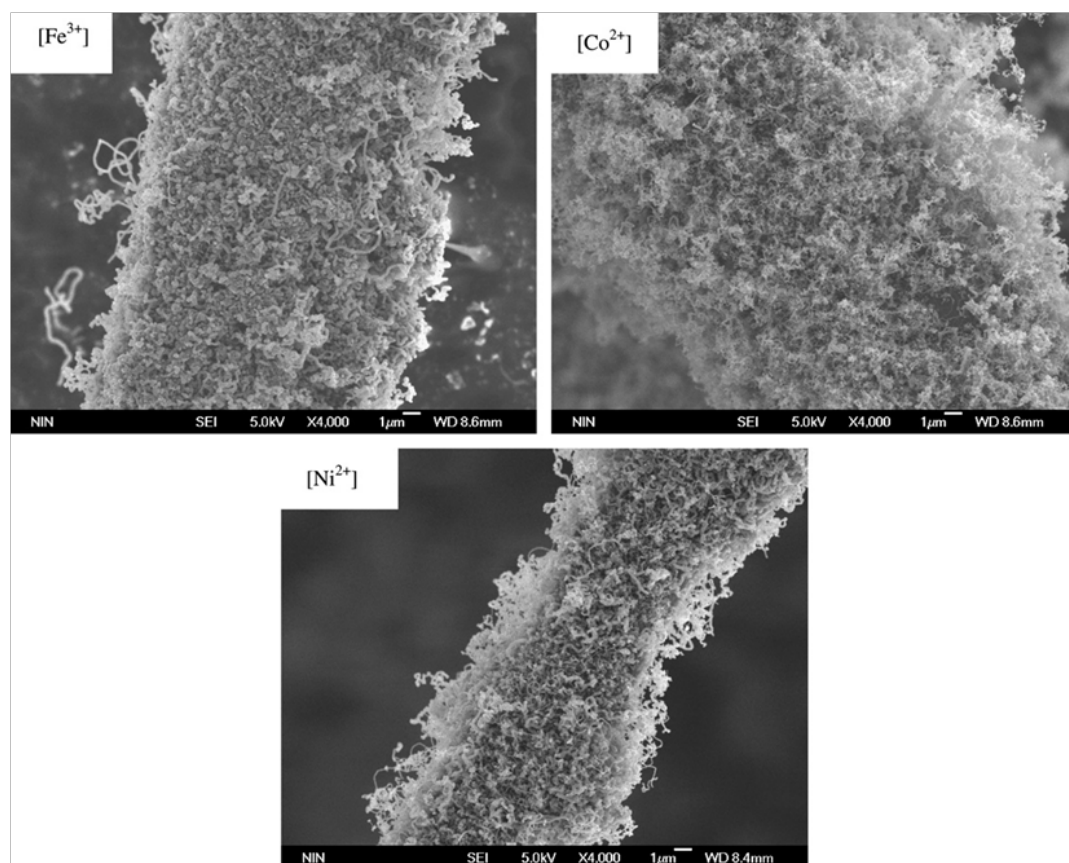


Figure 2.24 – Growth of CNTs on surface of CFs by Fe, Co and Ni as catalysts respectively [89].

The effects of Fe, Co and Ni particles for the growth of CNTs [78,84]. Among the three kinds of catalyst particles, Co has the best reducible capacity and can be easily reduced from oxides to nano-particles as required catalyst particles for CNT growth. Figure 2.24 shows when the rest of processing condition is the same, cobalt can give high yield and better quality of CNTs compared to iron and nickel, where amorphous carbon and by-products are easily formed. Cobalt ions are easier to loss electrons and absorb carbon, forming carbide. According to Manning *et al.* [85], who further interpreted that the decomposed carbon atom will form a metal carbide intermediate from graphite equilibrium at the metal-carbon interface, which will continuously provide free carbon and metal

nanoparticles for the in-situ growth of CNTs. As opposed to cobalt, the iron particle for example, has a fast diffusion rate into graphite surface, resulting formation of other carbon products [86]

In comparison, researches [87] based on these three catalysts on other systems showed nickel, on the other hand, offers better alignment of CNTs, higher growth rate and larger diameter of CNTs formed. Especially for the diameter of CNTs, similar trend was also observed on carbon substrate as shown in figure 2.24. O'Connell [88] concluded the effect of metal catalysts during CNTs growth, and recommended that the use of bimetallic or trimetallic mixtures of Fe, Co, and Ni with other elements as well, such as Y, Mo, Ru etc, for massive increase in the yield of CNTs. This suggestion has been taken into real production, and satisfactory results have been achieved by using Co-Ni system (Co/Ni = 1:1).

2.4.1.2 CVD apparatus design

So far, a few researches have been dedicated to develop CVD apparatus design for growth of CNTs on CFs. One technique based on the electric conductivity of CF has been proposed by Ohmic heating a 2 dimensional CF cloth placed vertically to the direction of hydrocarbon gas flow. As schematically showed in figure 2.25, carbon paper has the highest electric resistance so that can be heated up easily to 700°C within seconds [89,90]. Since the carbon paper is filtering all gas flows, the decomposition of hydrocarbon vapour takes place through the bulk substrate. Therefore, it is possible to have the growth of

CNTs through the whole green body, not just on the surface.

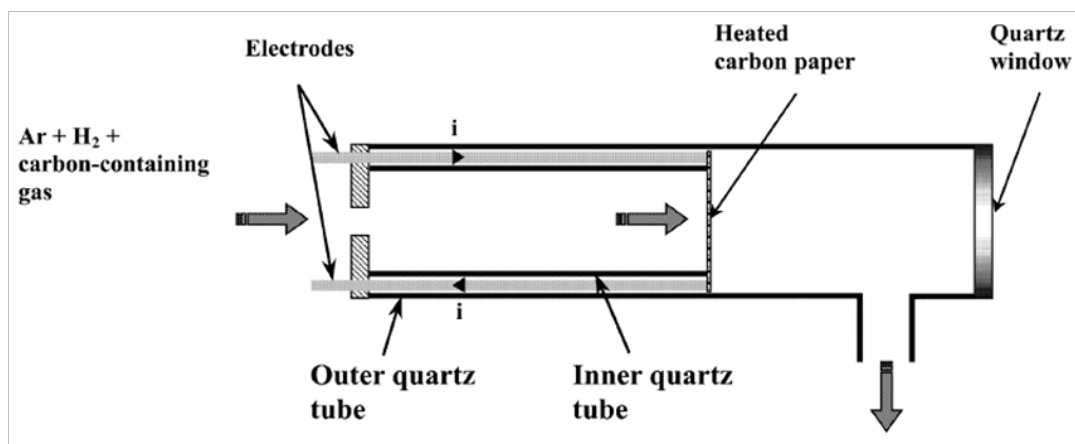


Figure 2.25 – CVD apparatus design for growth of CNTs on CF paper [95].

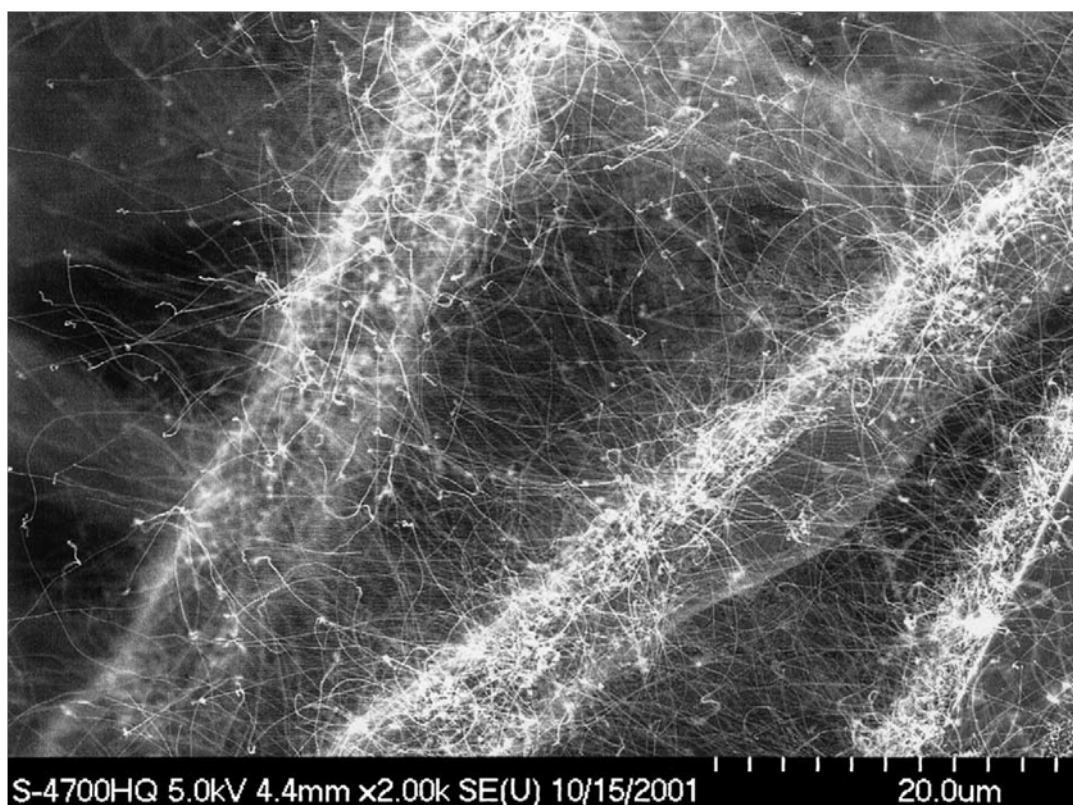


Figure 2.26 – Typical microstructure of CNTs/CF paper by Ohmically heated apparatus [90].

A typical microstructure of the hybrid CNTs/CFs paper produced by Ohmic heating method, as shown in figure 2.26. It indicates the decomposition of hydrocarbon has penetrated the preform, and the growth of CNTs has built up a network structure between adjacent CFs. If this network structure can be preserved well in composite end products, it may change the crack pattern of the whole structure and further toughen the materials.

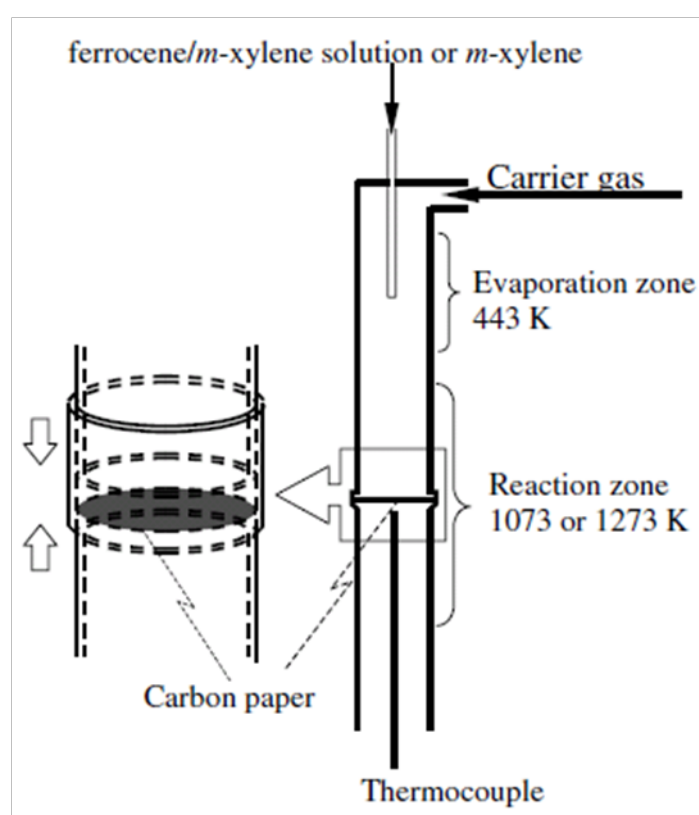


Figure 2.27 – Vertical floating CCVD reactor for CF substrate [91]

There are also variations of this apparatus design. For example, the electrical energy can be replaced by thermal energy, while tube furnace can also be placed vertically for floating of catalyst precursors through carbon paper substrate. Sonoyama *et al.* [91] employed this apparatus to successfully

synthesize similar type of CNTs/CFs hybrid preform by using iron as the catalyst, which was suggested not the best choice for CF substrate.

One distinct drawback for the above apparatus designs is the size and shape restriction of carbon preform. It has to be fitted into the tube furnace and its thickness should also be restrained within a range for penetration of gas flow. Normally 2 dimensional round shape of carbon paper or cloth can be applied. If complex shape of CF preform is required for structural CF composite, it has to be solved through other options. Mathur [92] recommended a possible solution by horizontal floating CCVD reactor, in the middle of which contains CF preforms with different shapes for manufacture of phenolic resin based CF-CNT composites, as shown in figure 2.28.

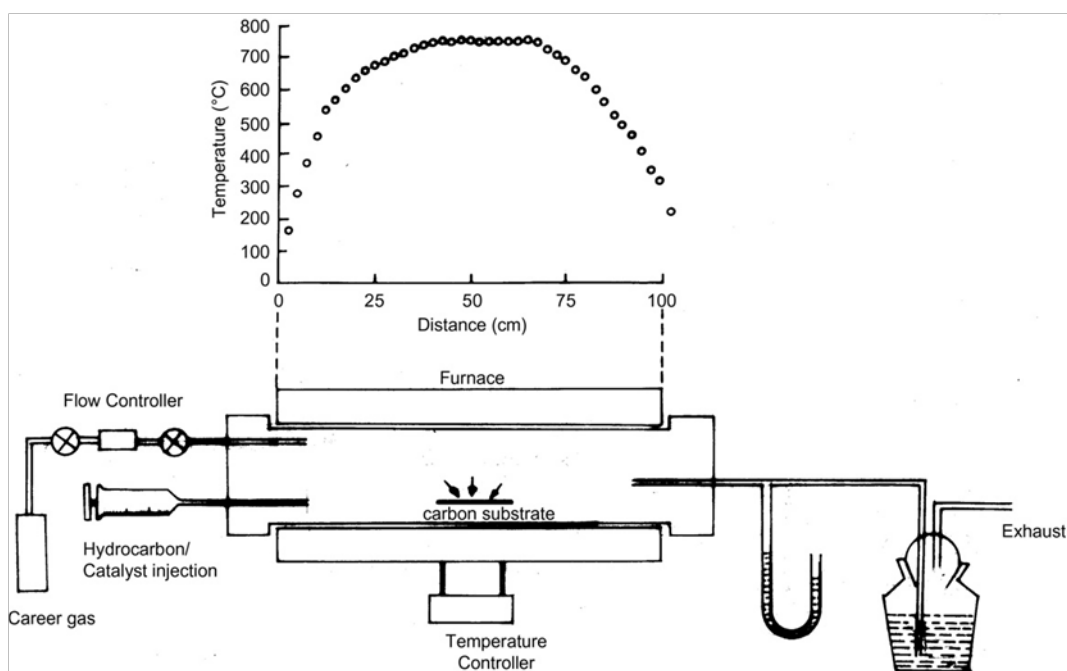


Figure 2.28 – Horizontal floating CCVD apparatus design for different types of CF preforms [92].

Different types of CF preform have been studied, for example, unidirectional CF tows, bi-directional and 3 directional carbon fibre cloth and felt. Results showed reasonable homogeneity of CNTs on CFs, however, the density of yield CNTs is far less, and the dispersion on surface of CFs is not as uniform as those prepared from former techniques. So far, there has been no research focusing on developing a suitable apparatus for flexible shapes of CF preforms available to produce high yield of CNTs with uniform distribution through the green body.

2.4.1.3 Processing conditions

The processing condition of in-situ CCVD growth of CNTs on CFs also follows the traditional CVD method for manufacture of CNTs, e.g. hydrogen content used to induce or reduce for the formation of catalyst particles and decomposition temperature on the growth rate of CNTs.

It was also found that for CF substrate, SWCNTs or MWCNTs can be selectively growing depending on hydrocarbon concentration. Zhu *et al.* [93] reported that SWCNTs were preferable at low methane concentration by using iron as catalyst, e.g. 10% within methane/hydrogen mixture. While increasing methane concentration, both SWCNTs and MWCNTs are expected.

They also suggested a processing temperature window for CNTs growth on surface of CF, which is between 650~800°C. They speculated the reasons again because of the fast diffusion rate as temperature beyond 800°C, especially for iron particles. They can diffuse into CF surface before

decomposition of hydrocarbon vapour, and therefore are not catalytic effective for growth of CNTs.

Several researchers particularly mentioned the importance of very small amount of H_2S within vapour flow on the formation of catalyst particles. Sonoyama *et al.* [94] employed 0.024vol% H_2S and found much more regular shape of iron particles formed on surface of CF compared to iron clusters and agglomerations appeared when not using H_2S . Based on Li's explanation [95], melting point of catalyst particles can be largely reduced from $1455^{\circ}C$ down to $797^{\circ}C$ by forming NiS or $645^{\circ}C$ for Ni+Ni₃S₂. Fragmentation could be induced to clusters or agglomerations of catalyst when the melting point was reduced, and nano-sized particles are expected for catalytic growth of CNTs [96].

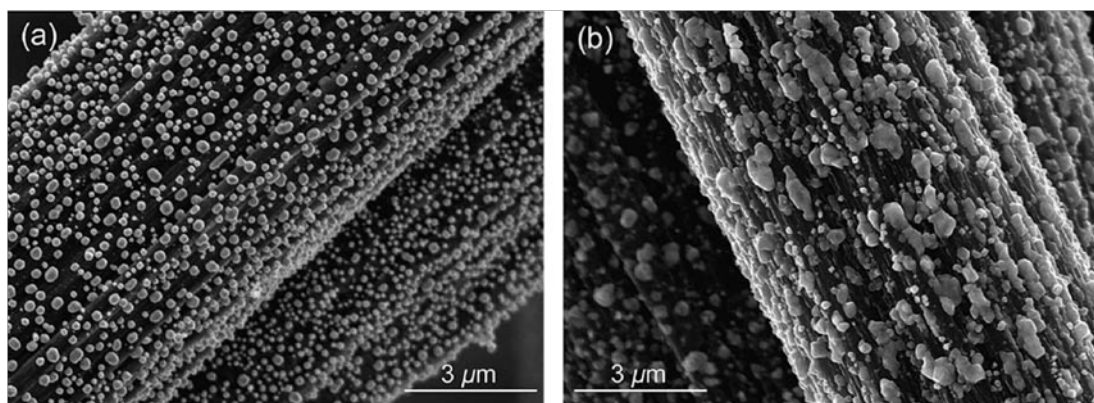


Figure 2.29 – Iron particles on surface of CFs. a) Ferrocene precursor coated on pre-treated surface of CF with 0.024vol% H_2S in carrier gas, b) same condition as a) but without H_2S [97]

2.4.2 In-situ CCVD of CNTs on ceramic powders

To manufacture CNTs reinforced ceramic composites, there are three technical problems to be addressed: 1) homogeneous dispersion of CNTs within ceramic matrix, 2) densification of the composites and 3) avoid possible damage of CNTs at high temperature that may lead to poor bonding of interfaces.

Peigney *et al.* [98,99] reported an original catalytic method for in-situ manufacture of CNTs reinforced ceramic composites. They prepared mixture of metal nitrates of Mg, Al, Fe, Co and Ni with urea dissolved in water. Certain amount of Mg in magnesium nitrate was substituted by transition metals of Fe, Co and Ni in the form of $Mg_{1-x}M_xAl_2O_4$ solid solution. The solution was dehydrated at 600°C and converted to oxide powder, which was heat treated in H_2-CH_4 mixture to produce CNTs-metal-ceramic spinel powder. They claimed a novel structure of the as-produced material as shown in figure 2.30. The composition of the spinel powder was Al_2O_3 , $MgAl_2O_4$ (*spinel*) and MgO, which was uniformly covered by network of carbon nanotube bundles. During the process, Peigney *et al.* also suggested attrition milling of the oxide powder before decomposition of methane would prevent agglomeration of powder particles and dispersion of CNTs.

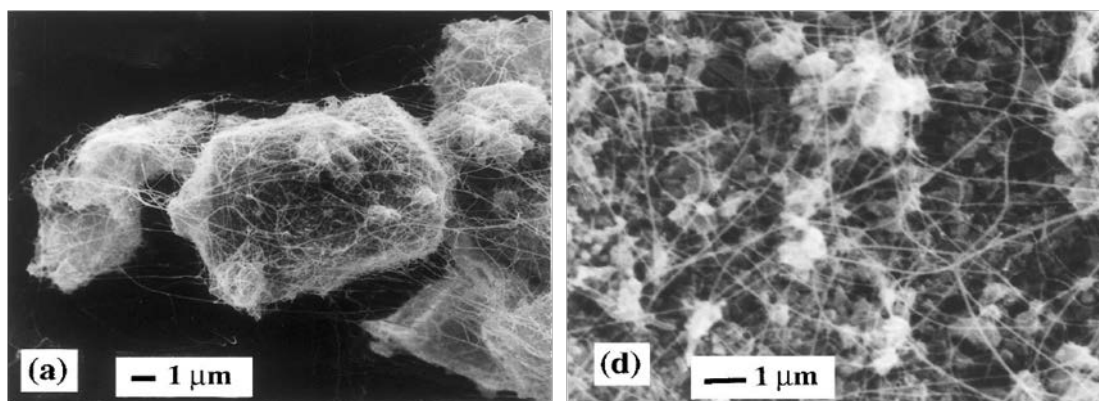


Figure 2.30 – CNTs-ceramic composite powder. (a) 5wt% Fe, 30%CH₄ on solid solution powder without attrition milling, (d) 10wt%Fe, 12%CH₄ on attrition milled solid solution powder [99].

The microstructural analysis shown in figure 2.30 also suggested the yield of CNTs was affected by processing parameters, including amount of catalysts, hydrocarbon content, and treatment of the substrate materials and so on. Reigney's researches above suggested that increasing the amount of catalysts and hydrocarbon content in a certain range can promote the yield of CNTs on surface of the target material. Akil *et al.* [100] also investigated the yield of CNTs on alumina particles by studying the decomposition temperature of hydrocarbon gas in the range from 700 to 1100°C. They suggested that the yield of CNTs on surface of alumina particles was optimised at 900°C, base on SEM observations. At both 700 to 1100°C, they claimed the processing temperatures were inactive for methane decomposition, and there were only small amount of carbon deposited suggested from XRD analysis. Peigney *et al.* [108] has quantified the yield of CNTs, and proposed the “quality of CNTs” calculated by the quantity of CNTs divided by total deposited carbon content.

The current research of CNTs dispersing in ceramic particles has explored a

wide range of applications for CNTs/ceramic composites. Lim *et al.* [101] studied CNTs-Fe- Al_2O_3 system to evaluate its friction performance. Figure 2.31 indicates that the addition of CNTs has almost no impact on friction coefficient, but up to 45% improvement in wear resistance compared to that with no CNTs added. This achievement can be applied to modern ceramic brakes to enhance their service time.

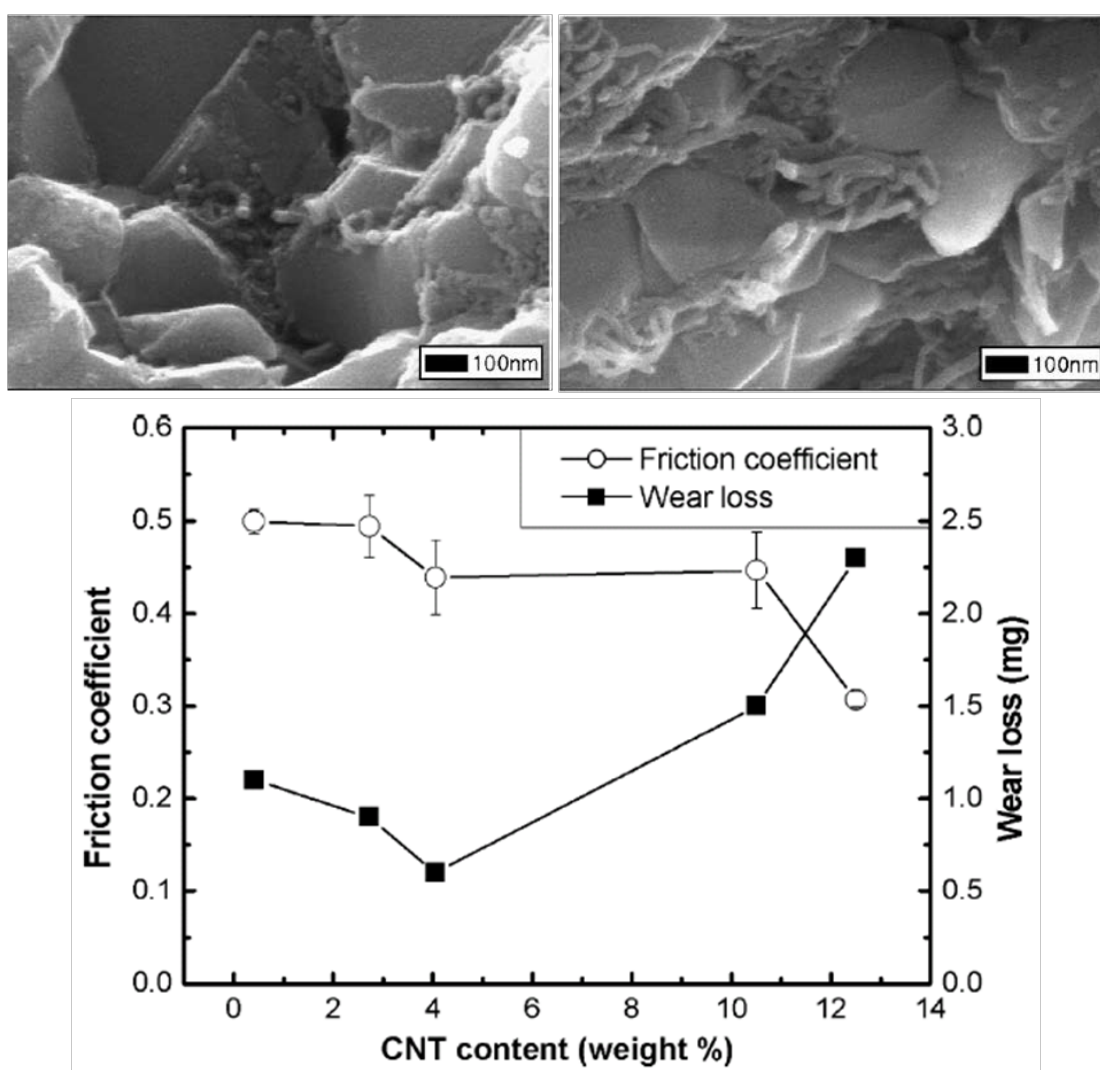


Figure 2.31 – Friction coefficient and wear loss as a function of CNT content in alumina. Top left: microstructure of 4.1wt% CNTs and top right: microstructure of 12.5wt% CNTs [101].

2.5 Fabrication techniques for CF and ceramic based composites

2.5.1 Fabrication of CF composites

For traditional CF reinforced composite there are generally two steps involved: preparation of CF preform and introduction of matrix materials. Especially for carbon or ceramic matrix, the material can be introduced through either polymer infiltration and pyrolysis (PIP) or chemical vapour infiltration (CVI) techniques.

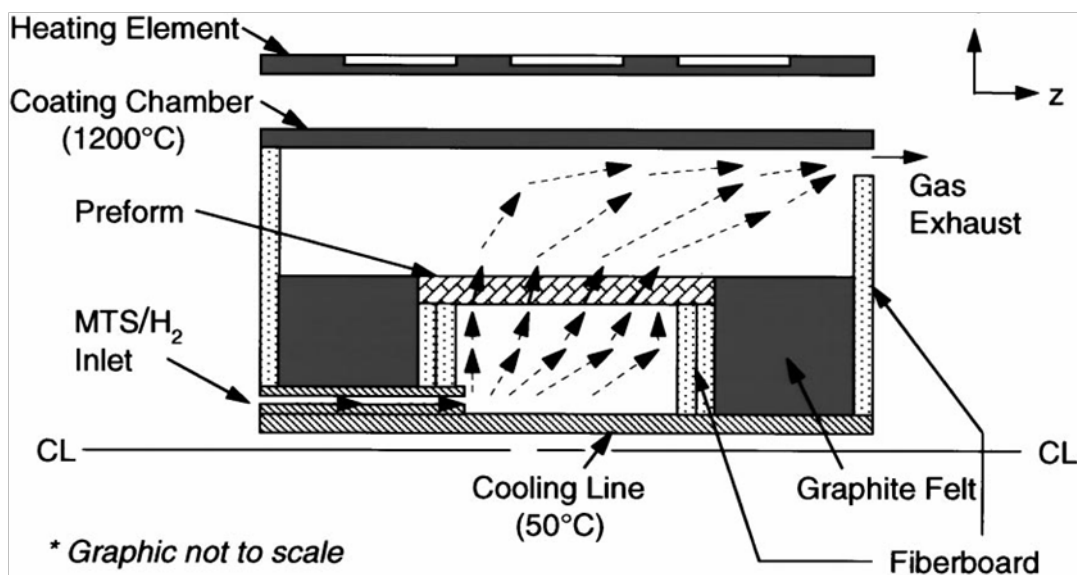


Figure 2.32 - Schematic of a CVI tubular reactor [102]

Both PIP and CVI techniques can be used to manufacture Carbon-Carbon (C-C) composites. As shown in figure 2.32, CVI technique involves continuous hydrocarbon gas flow such as methane infiltrating through porous CF preform at 1200°C. Deposition of pyrolytic carbon starts around surface of CF and eventually fills all space in the form of carbon matrix. However, the rate of deposition is slow, which results in large consumption of energy and resources.

PIP, on the other hand, includes impregnating polymeric carbon precursor, such as phenolic resin, which is decomposed into carbon at high temperature in inert atmosphere. The rate of carbon conversion is faster than that by CVI, but the density of the matrix is an issue, due to the loss of a large amount of volatile carbonaceous materials during pyrolysis, and cracking induced by shrinkage, which can lead to poorer densification and mechanical properties compared to those prepared through CVI technique [103].

CVI technique can also be used to manufacture CF reinforced ceramic composites. The most commonly used ceramic matrix is silicon carbide (SiC_4). Methyltrichlorosilane (MTS) is considered as precursor of SiC_4 via the following thermal decomposition:



However, the rate of the deposition is so fast that severe density gradient appears on finished products where a completely densified layer appears on the surface of the bulk, but porous in the interior region. Processing parameters such as decomposition temperatures and pressures were studied to maximise the homogeneity of densification [104].

In fibre reinforced ceramic matrix composites (CMCs), the interface between fibre and matrix plays an important role in both strengthening and toughening. Essentially toughening in CMC by CF reinforcements is achieved through interface debonding. Conventional mode I cracking that happens in a monolithic

brittle material can be switched to predominantly mode II shear cracking along a longitudinal CF surface [105], as shown in figure 2.33. The strength and the structure of the interface between fibre and matrix determine the load transfer mechanism of CF reinforced BMCs [106]. From mechanical property point of view, an optimised interface should be that debonding can be activated just before type I cracking starts and debonding area per volume can be maximised [107].

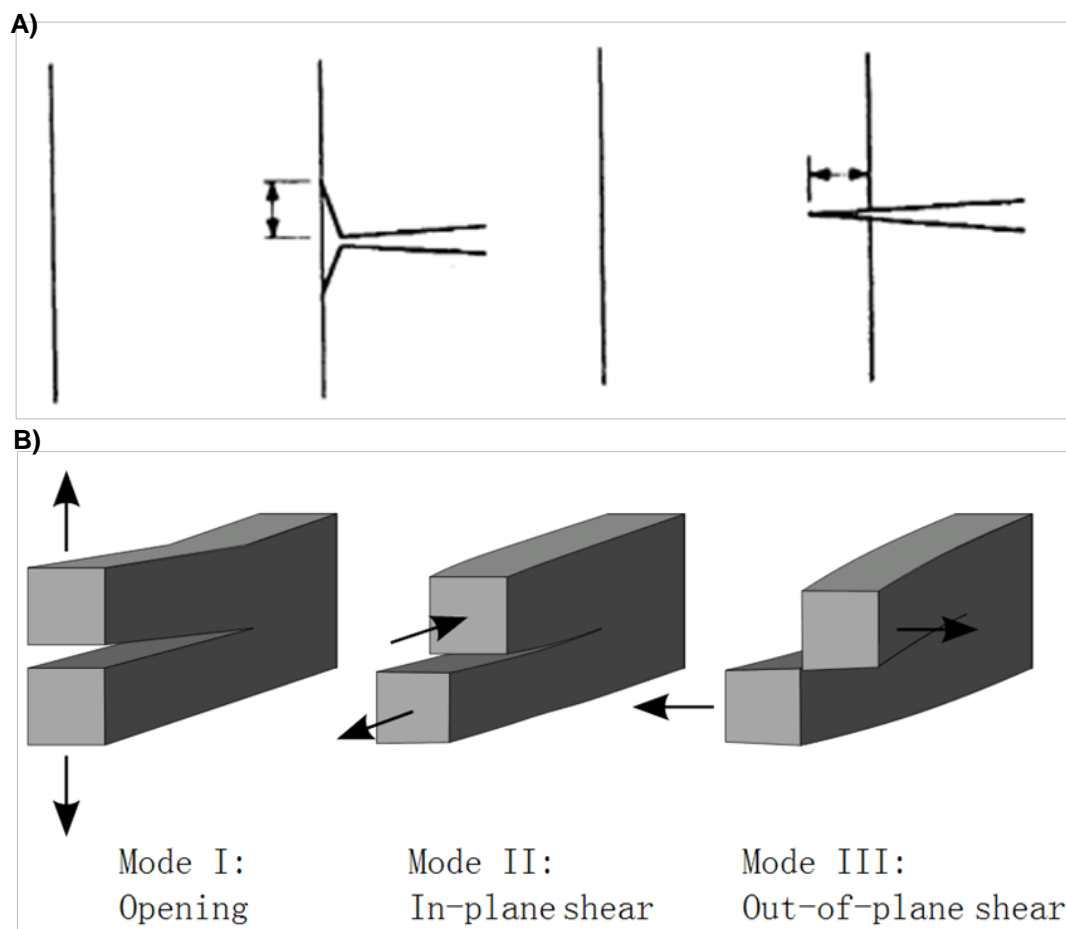


Figure 2.33 – A) Crack propagation and debonding at a fibre/matrix interface [108], and B) Modes of crack propagation [109].

2.5.2 Fabrication of ceramic composites

As described before, most used techniques for consolidating ceramic bodies with CNT reinforcements are hot press and spark plasma sintering (SPS). A typical hot press apparatus is shown in figure 2.34, and ceramic powders are pressed at certain pressure in a die and heated up to certain temperature at the same time. Graphite dies are used due to their high temperature resistance. For recently developed SPS-assisted HP technique, a pulsed DC power is applied to the upper and lower graphite punch to presumably accelerate heating rate in order to limit growth of matrix grains by shortening time at high temperatures.

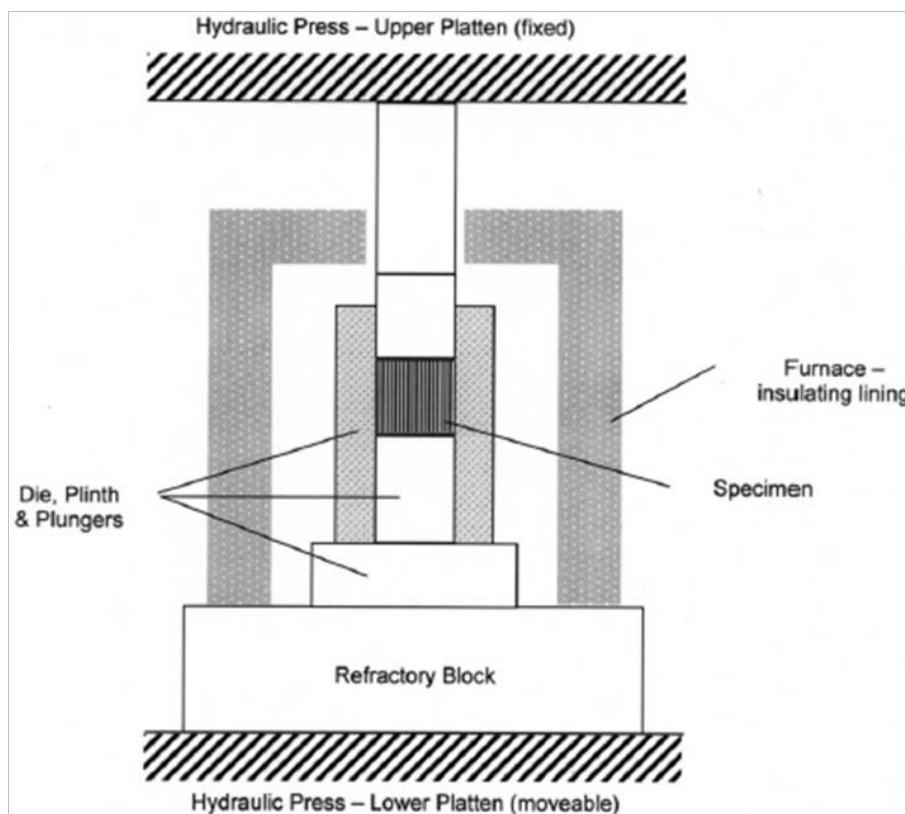


Figure 2.34 – Schematic hot press apparatus [110]

The preserved CNTs in ceramic matrix composites can not only provides improvement of mechanical properties such as fracture toughness, but also electrical and tribological properties [111,112]. However, it is difficult to preserve CNTs during high temperature processing, especially for manufacture of ceramic composites. Several researches have suggested the use of vacuum condition and inner gas to protect CNTs from high temperature damage [113,114].

Researchers started to develop alternative methods of manufacture ceramic composites reinforced by CNTs. Grobert *et al.* [115] proposed a spray pyrolysis method to produce CNTs/alumina flakes through spraying the slurry of catalyst precursor and alumina powder in hydrocarbon environment, where decomposition takes place for growth of CNTs on ceramic particles and densification of the composite powder at the same time. The microstructure observation showed homogeneous CNTs network among alumina particles. However, the largest drawback is the low density of the composite that could achieve. Grobert *et al.* suggested the use of smaller size ceramic powder with sintering agents at elevated decomposition temperature to achieve denser composite in their further work.

On the other hand, Wagh and Jeong [116,117,118] proposed series of researches about manufacture of chemically bonded phosphate ceramics (CBPCs) without hot press and SPS. It can be processed between 100~150°C for aluminium phosphate bonded alumina ceramics and even at room temperatures for magnesium oxide and hematite ceramics. They suggested a

sol-gel process, through which colloidal hydrophosphate sols were formed by dissolution of oxides in acid solution, and then converted into gel that connects surrounding un-reacted metal oxides. The gel can be pressed and cured at low temperature for the formation of berlinite-bonded ceramics.

In order to achieve the optimum microstructure, the authors also suggested that the ratio between metal oxides and phosphoric acid should be controlled carefully in order to form thin berlinite layer uniformly among metal oxide particles, and suitable pressure for better packing of ceramic powders. The mechanical properties have not been investigated, but, it can be a potential manufacturing route that some constituents may subject to deterioration at higher temperatures.

2.6 Summary

Since the discovery of CNTs, many researchers have been focusing on developing synthetic methods of CNTs for commercial applications. CVD method has drawn more and more attention because of its potential for scaled-up manufacture and directional growth of CNTs. Lots of processing parameters of CVD were investigated on the effects that influencing catalytic growth of CNTs.

CNTs have been used to fabricate nanocomposites, and are widely used as the reinforcement. A uniform distribution of CNTs within matrices was the key to simultaneous improvement of mechanical properties of the as-produced

composites. Currently CNTs are generally dispersed through ex-situ and in-situ methods. The amount of CNTs added into matrix materials through ex-situ methods was restrained to a low level (*the value varies depending on the type of matrix*), beyond which will lead to decrease of mechanical properties, especially fracture toughness of the composites. The main reason was likely because the current dispersing techniques in ex-situ method cannot avoid agglomeration of CNTs.

The researches on in-situ method have potentially explored the possibilities of homogeneous dispersing CNTs, especially on CFs and ceramic particles. Growth of CNTs is catalysed during CVD process and in-situ deposited on surface of target materials, which are used as the constituents of composites. The yield of CNTs can be affected by processing parameters during CVD. However, the main issue in in-situ catalytic CVD (CCVD) method was densification of the as-produced composites and prevent possible damage of CNTs during high temperature processing.

The effects of processing parameters on catalytic growth of CNTs have not been fully understood since the fundamental growth mechanism of CNTs is still under controversy. The understanding of the growth mechanism of CNTs is expected in this project, in order to optimise the yield of CNTs during in-situ CCVD process.

CHAPTER 3 Experimental Methods

3.1 Catalyst selection and preparation

Transition metals were selected for catalytic growth of CNTs, including Fe, Co and Ni. They were prepared by using their metal salts that were dissolved in acetone. Various substrates were impregnated by such solutions to achieve catalyst particles through further treatment at high temperatures.

3.1.1 Catalyst precursors

The following catalyst precursors had been investigated: Iron (III) chloride (*Acros Organics, UK*), iron (III) nitrate (98+% *SpeciFied, UK*), Ferrocene (98% *Acros Organics, UK*), cobalt (II) nitrate (98+% *SpeciFied, UK*) and nickel (II) nitrate (98+% *SpeciFied, UK*).

The concentration [M] of transition metal salts in acetone solvent was adjusted from 0.001 to 0.6 mol/l. By using cobalt nitrate as an example to show how the solutions were prepared. In order to prepare a 40ml of 0.1 mol/l $\text{Co}(\text{NO}_3)_2$ precursor solution, 40ml acetone (*Laboratory Reagent, $\geq 99.8\%$, Sigma-Aldrich, UK*) was measured by a 100ml-graduated glass-made cylinder. Then, 1.16g cobalt nitrate hydrate ($\text{Co}(\text{NO}_3)_2 \cdot 6\text{H}_2\text{O}$) was weighed in a glass beaker. The measured acetone was poured into the beaker and sealed by PTFE sealing film. The solution was magnetic stirred for 30 minutes, and the concentration of cobalt [Co] was adjusted to 0.1 mol/l. The flow chart of preparing solution of

catalyst precursor was shown in figure 3.1.

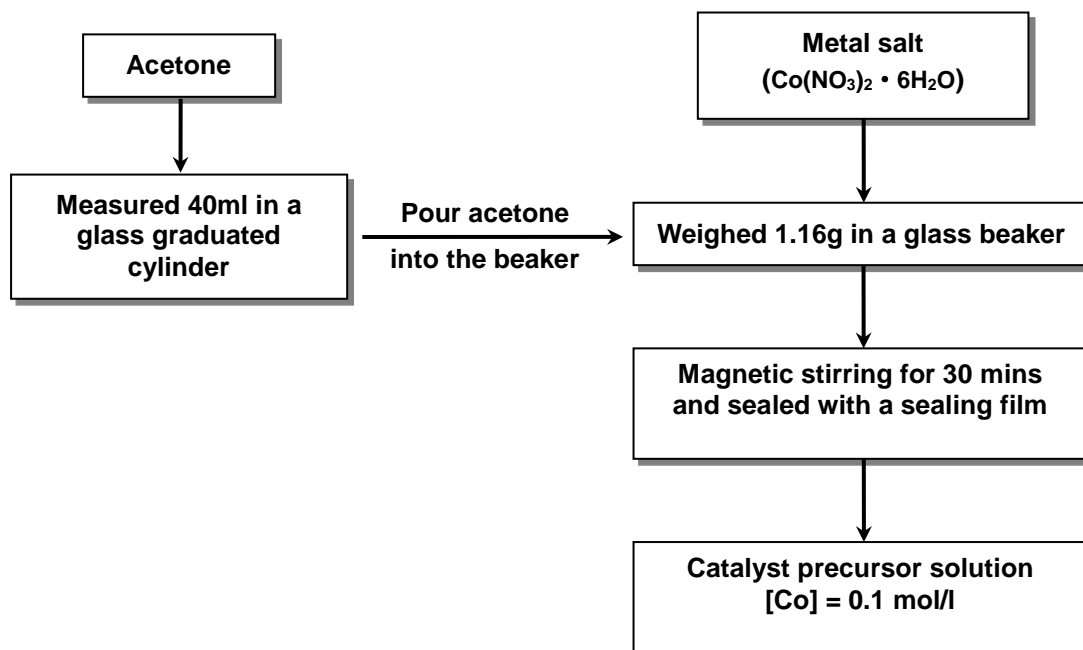


Figure 3.1 – Flowchart of preparation of catalyst precursor solution

Details of the catalyst precursors solution studied in this thesis were listed in table 3.1.

Table 3.1 – Catalyst precursors and their concentrations used.

| catalyst precursors concentrations [mol/l] | catalyst precursors | | | | |
|---|---------------------|-----------------------------------|---|-----------------------------------|-----------------------------------|
| | FeCl ₃ | Fe(NO ₃) ₃ | Fe(C ₅ H ₅) ₂ | Co(NO ₃) ₂ | Ni(NO ₃) ₂ |
| 0.001 | | | | √ | |
| 0.005 | | | | √ | |
| 0.05 | | | | √ | |
| 0.1 | √ | √ | √ | √ | √ |
| 0.3 | √ | √ | √ | √ | √ |
| 0.6 | | | | √ | |

√ catalyst precursor solutions prepared

3.1.2 Impregnation of catalyst precursor onto carbon fibres

Carbon fibres were used as substrates for in-situ catalytic growth of CNTs. Solutions of catalyst precursors were impregnated onto surface of carbon fibres through dip-coating method. Bundles of carbon fibres were immersed into the solution of catalyst precursor and then withdrawn from it. After drying in oven at 70°C for an hour, carbon fibre bundles were placed in a porcelain boat and positioned in the middle of a tube furnace. 3-dimensional carbon fibre block was also used for in-situ growth of CNTs. A piece of filter paper was placed under the CF block after it was withdrawn from the solution of catalyst precursor. The filter paper was used to suck the extra solution from inside the CF block before drying.

3.2 In-situ catalytic chemical vapour deposition (CCVD)

Thermal CVD was used for catalytic growth of CNTs through decomposition of methane at different cracking temperatures, from 500 to 700°C. A tube furnace was used to heat the samples placed in the middle of its working tube, while the hydrocarbon vapour and protection gas were flowing through.

3.2.1 Equipment set up

The CVD apparatus for CNTs growth is schematically shown in figure 3.2. A horizontal tube furnace (*LTF12/38/250, LENTON, UK*) was used, which had a working zone of 250mm in length and a maximum working temperature of

1150°C, and a maximum heating rate of 12.5°C/min. A separate working tube made of impervious aluminous porcelain (55% Al_2O_3 , LENTON, UK) was inserted through the working zone of the tube furnace. The working tube had a 25mm inner diameter and 700mm in length.

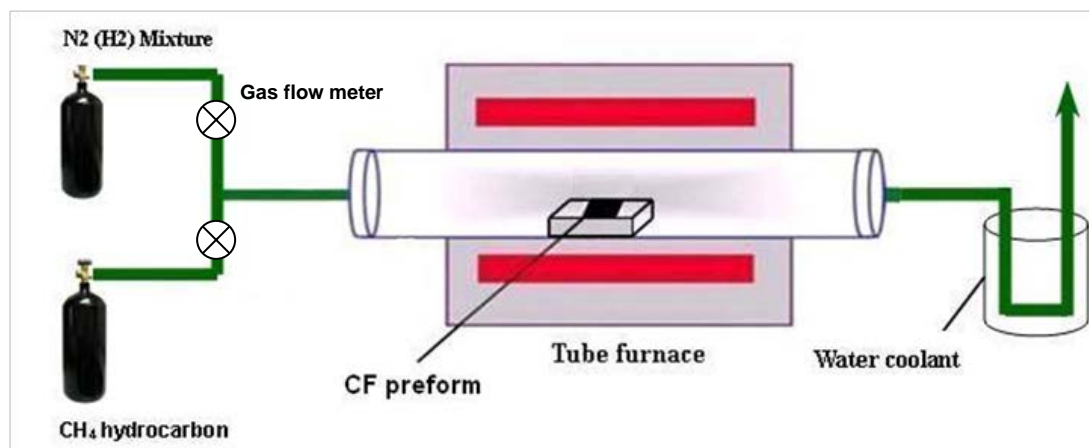


Figure 3.2 – Schematic of processing apparatus

Two types of gas were used, one of which is special gas (SG) mixture of nitrogen and hydrogen (3vol% hydrogen, BOC Special Gases, UK). The hydrogen was used to reduce catalyst precursor impregnated on the substrates into nano-sized transition metal particles. The nitrogen was used as carrying and protecting gas to maintain a low oxygen environment. Methane gas (CP grade N2.5, BOC Special Gases, UK) was used as hydrocarbon source. The methane molecular was cracked at the decomposition temperature into C atoms for growth of CNTs. The decomposition temperatures were between 600 to 700°C. Both types of gas were connected with flow meters before the inlet of the tube.

At the inlet of the tube furnace, all the gases were connected to a PVC tube with a bore diameter of 6 mm (*Fisher Scientific, UK*) through a hose nipple with an outer diameter of 6 mm (*Fisher Scientific, UK*) and sealed by a silicone rubber stopper with one-hole in the middle (*VWR-JENCONS, UK*). A U-shape copper tubing with an outer diameter of 6 mm was connected to the outlet of the tube furnace, and immersed in a beaker containing water to cool the tail gas. The cooled tail gas was then vent to outside atmosphere through a PVC tube. The outlet of the working tube was also sealed by the silicone rubber stopper.

3.2.2 In-situ deposition process

The heat treatment process was programmed by a controller installed in the tube furnace. Table 3.2 summarises the details of the deposition process.

Table 3.2 – In-situ deposition process.

| Steps | Programme details | Control of the gases [liter per minute (LPM)] |
|--|---|--|
| Ramp to 450°C | Heating rate 10°C/min | SG on at 0.8 LPM |
| Dwell at 450°C | 10 mins | SG increased to 3 LPM |
| Ramp from 450°C to cracking temperatures | Heating to 500°C, 600°C, 650°C, 700°C at a rate of 10°C/min | Maintain SG at 3 LPM Methane on at 2 LPM |
| Dwell at cracking temperature | 30 mins, or 60 mins | Maintain SG at 3 LPM Methane on at 2 LPM |
| Cool from cracking temperature to 25°C | Heating rate 10°C/min | Reduce SG to 0.8 LPM Methane gas off |
| At 25°C | Power off | SG off at 200°C |

SG is from the cylinder of nitrogen and hydrogen (3vol% hydrogen, *BOC Special Gases, UK*).

Three cracking temperatures were selected for decomposition of methane for either 30 or 60 minutes. When samples were positioned in the middle of the working tube and sealed by silicone rubber stopper, nitrogen and hydrogen gas mixture was turned on at a flowing rate of 0.8 liter per minute (LPM) and the working tube was heated up to 450°C at a rate of 10°C/min with a dwelling period of 10 minutes. The flowing rate of SG was increased from 0.8 to 3 LPM to reduce the metal oxide particles into metal ones. At the decomposition temperatures of methane, the flowing rate of methane gas was turned on at 2 LPM for 30 or 60 minutes.

3.3 In-situ growth CNTs on carbon fibre surface

There were two types of carbon fibres that were used as substrate for catalytic growth of CNTs. Before CCVD process, the surface of carbon fibres was pre-treated to improve catalyst precursor impregnation. Microstructural analysis on all the CF samples listed in table 3.3 was used to investigate the optimised processing conditions for the growth of CNTs on the surface of CF.

3.3.1 Carbon fibre source

Two sources of carbon fibre were used as substrates for catalytic growth of CNTs: PAN-based 3-dimensional woven carbon fibre cloth (*SGL Group, UK*) and 'PANOX' carbon fibre block (*Surface Transforms plc, UK*).

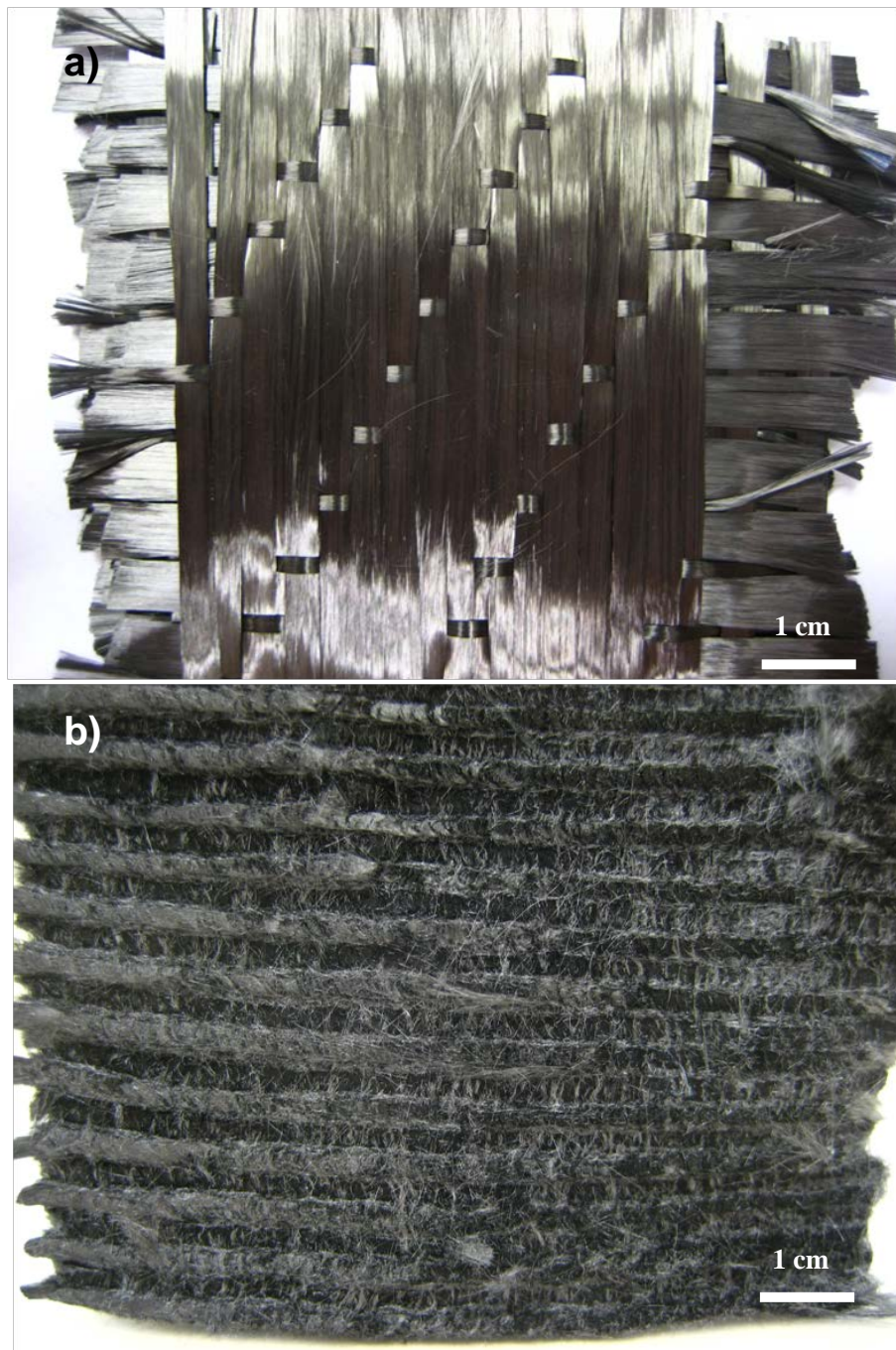


Figure 3.3 – As received carbon fibres. a) PAN carbon fibre bundles in woven format;
b) needled PANOX carbon fibre block derived from PANOX.

For the former type, manufacturers might have had certain surface treatment during manufacture to improve adhesion between fibre and the matrix material. For instance, surface oxidation is commonly used to modify fibres with the

surface functional groups to promote better interfacial bond characteristics [119,120]. Before weaving, fibre cloths are also normally coated with a layer of sizing materials in order to prevent any mechanical damage and improve compatibility with resins, as indicated in figure 3.3(a) where a shiny surface is seen for the CF bundle. The main content of the sizing materials was semi-cured epoxy resin [121]. The “sizing” layer had to be cleaned off before applying catalyst precursor. The PANOX fibre block was directly pyrolysed from PANOX fibres without any surface treatment followed. The format of PANOX fiber was needed block as shown in figure 3.3(b).

3.3.2 Pre-treatment of as-received carbon fibres

Acid solution was used to remove the sizing materials for PAN-based CFs. Acetone and nitric acid were chosen to remove the sizing layer. The woven PAN CF cloth was firstly ultrasonic stirred in acetone (*Laboratory Reagent, ≥99.8%, Sigma-Aldrich, UK*) for 10 minutes, the CF bundles in the woven structure was loosened by the ultrasonic stirring. Selected bundles of CF were then boiled in nitric acid (*>69.0%, Sigma-Aldrich, UK*) to dissolve the resin at a temperature of 60°C for 30 minutes. After withdrawing from nitric acid, the bundles of CF were rinsed in de-ionised water until pH indicator showed the rinsing water was in the neutral state. Finally, the washed bundles were ultrasonically stirred again in acetone before drying at room temperature. Needed PANOX CF block was manufactured without sizing materials.

Needed PANOX CF block was manufactured without sizing materials. Thus,

the PANOX CF block was ultrasonically stirred in acetone to remove impurities, such as ash, and then dried at room temperature before impregnation of catalyst precursor.

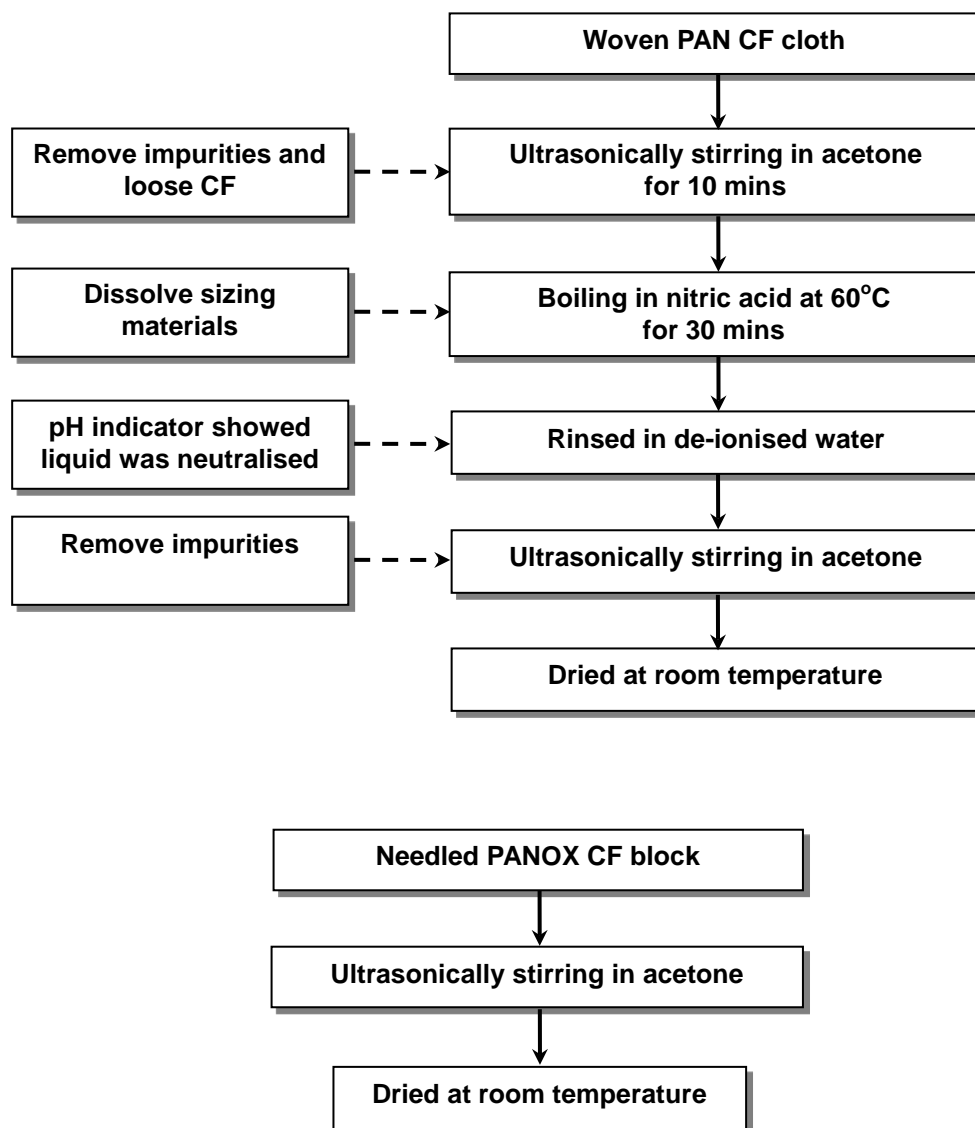


Figure 3.4 – Flowchart of surface pre-treatments of carbon fibres preforms.

3.3.3 Optimisation of processing conditions of CVD for the growth of CNTs on surface of CFs.

The optimised processing conditions of CVD for the growth of CNTs were studied through four aspects.

- First one was the effect of surface pre-treatment on CFs for impregnation of catalyst precursor. 0.1 mol/l $\text{Co}(\text{NO}_3)_2$ was prepared to impregnate onto two bundles of PAN-based CFs, one of which was surface pre-treated followed by method shown in figure 3.4, while the other one had no surface pre-treatment. The imaging software of “ImageJ 1.42q” was used to measure the area of coating materials on CFs before and after the surface pre-treatment. The percentage of coverage was calculated based on area of the coating materials divided by the typical regions selected on surface of CFs.
- Second one was catalyst precursors. Five different catalyst precursors were selected, including: FeCl_3 , Ferrocene, $\text{Fe}(\text{NO}_3)_3$, $\text{Co}(\text{NO}_3)_2$ and $\text{Ni}(\text{NO}_3)_2$ for comparative study. Solutions of the five catalyst precursors with a concentration of 0.1 mol/l were impregnated onto the surface of PAN-based CFs after surface pre-treatment. The as-impregnated samples were subjected to heat treatment in flowing methane up to a temperature of 650°C for 30 minutes. The SEM observation was used to assess the growth of CNT and to choose the best catalyst precursor for further study.
- Thirdly, after the selection of the most effective catalyst precursor, the

concentration of which was also adjusted to 0.001, 0.005, 0.05 and 0.3 mol/l. The imaging software of “UTHSCSA Image Tool[®] 3.0” was used to analyse size distribution of catalyst particles on surface of CFs while changing concentration of the catalyst precursor. The particle size was measured based on scale bars supplied in SEM images. The general method is to quantify the population of catalyst particles within selected regions, including those lifted by growth of CNTs.

Three steps were used to investigate the popularity of the growth of CNTs on catalyst particles based on previous SEM images. Firstly, a typical region was selected within a SEM image. Within this region, catalyst particles that were lifted up by growth of CNTs were marked and classified by diameter in an interval of 2.5 nm. By measuring the area of each enclosed particle region, the image tool was able to automatically convert the measurements into equivalent spheres. Diameters of the equivalent spheres were estimated based on the scale bar in the SEM images. Secondly, all particles within the selected region were marked, including those were marked before, and measured by the same way. A chart was created based on the value of percentage was expressed by the counts of catalyst particles in each interval divided by the overall number of catalyst particles in the selected region. The values of percentage were used to study the relationship between size of catalyst particles and growth of CNTs.

Finally, CNT growth at different decomposition temperatures of methane, as well as dwelling periods were investigated and evaluated, to improve the yield of CNTs. Cracking temperature of methane was adjusted from 500°C to 700°C,

and two dwelling periods, 30 and 60 minutes, were chosen. Details of the processing parameters were listed below in table 3.3 to study the optimised conditions for catalytic growth of CNTs on surface of CFs.

Table 3.3 – Processing parameters for in-situ CCVD growth of CNTs on CF.

| Peak temperature (°C) | Catalyst precursors | Dwelling time at the peak temperature (minutes) | Concentration of precursor solution (mol/l) |
|-----------------------|---|---|---|
| 500 | Co(NO ₃) ₂ | 30 | 0.3 |
| 600 | Co(NO ₃) ₂ | 30, 60 | 0.001, 0.005, 0.05, 0.1, 0.3 |
| 650 | FeCl ₃ | 30 | 0.1, 0.3 |
| | Fe(C ₅ H ₅) ₂ | 30 | 0.1, 0.3 |
| | Fe(NO ₃) ₃ | 30 | 0.1, 0.3 |
| | Co(NO ₃) ₂ | 30, 60 | 0.1, 0.3 |
| | Ni(NO ₃) ₂ | 30 | 0.1, 0.3 |
| 700 | Co(NO ₃) ₂ | 30 | 0.3 |

Besides CFs, ceramic powders were also investigated for catalytic growth of CNTs, including SiC, Al₂O₃ and yttria-stabilised tetragonal zirconia. CNTs/ceramic composite powders were manufactured by in-situ method, when Co(NO₃)₂ was used as the catalyst precursor.

3.4 In-situ growth of CNTs on SiC powder

SiC powder with an average grain size of 46 µm (320 grit, *Sigma-Aldrich, UK*) was chosen to study the in-situ growth of CNTs. Co(NO₃)₂ with a concentration of 0.3 and 0.6 mol/l in acetone were used as the catalyst precursor. The SiC powder was attrition milled before impregnation of catalyst precursor.

3.4.1 Attrition milling

In order to see the growth of CNTs on the finer SiC powder, an attrition mill (01-HD, 3mm YSZ milling balls, Union Process, US) was used, which is shown in figure 3.5. 20g of the SiC powder and 0.5 liters of acetone were poured into the milling vessel with zirconia (Y-TZP) spheres as milling media. The speed of the milling vessel with zirconia (Y-TZP) spheres as milling media. The speed of the arm was set at 300 rpm, and the total milling time was 4 hours. After milling, the SiC slurry was poured into a beaker and dried in oven at 70°C for an hour. The dried SiC slurry was meshed and milled back to powder with reduced particle size, compared with the original SiC powder.

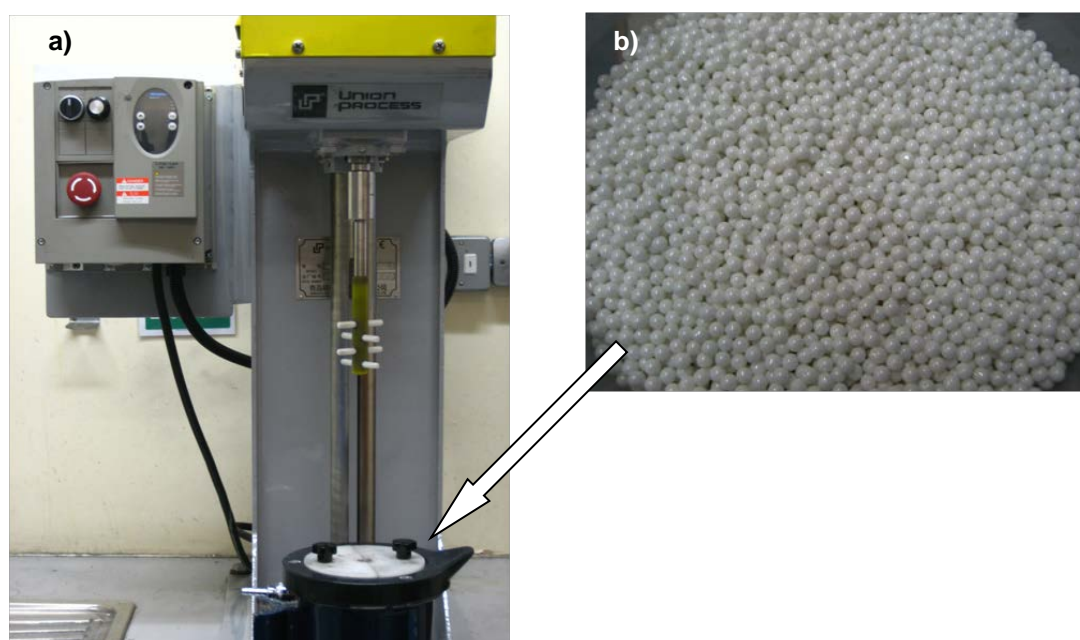


Figure 3.5 – a) attrition milling machine and b) zirconia milling media.

3.4.2 Surface pre-treatment and coating of catalyst precursor

SiC powder was immersed in hydrofluoric acid (HF) (48wt% in H_2O , $\geq 99.99\%$ trace metals basis, Sigma-Aldrich, UK) at room temperature for 30 minutes, in order to dissolve the SiO_2 layer on the surface of SiC particles. SiC powder was poured into 10wt% HF acid (diluted by de-ionised water) subjected to magnetic stirring for 30 minutes. The washed powder was collected with a filter paper after filtering the acid. Then the SiC powder was immersed in acetone with ultrasonication, in order to remove the residual HF acid. The as-treated SiC powder was kept in acetone in a sealed glass container to prevent further oxidation

Before CVD process, SiC and acetone slurry was taken from the container with a spoon, and discharged onto a piece of filter paper. The slurry was dried and the block was milled to powder state. The prepared solution of $Co(NO_3)_2$ was sucked by a burette and dropped onto the powder of SiC until the filter paper was over saturated. After impregnation of catalyst precursor, the slurry was placed in a $60^\circ C$ -oven and dried for 30 minutes. The dried block was milled to powder state and collected in a porcelain boat, which was positioned in the middle of the working tube of the CVD furnace. The procedures of surface pre-treatment and impregnation of catalyst precursor were shown in figure 3.6.

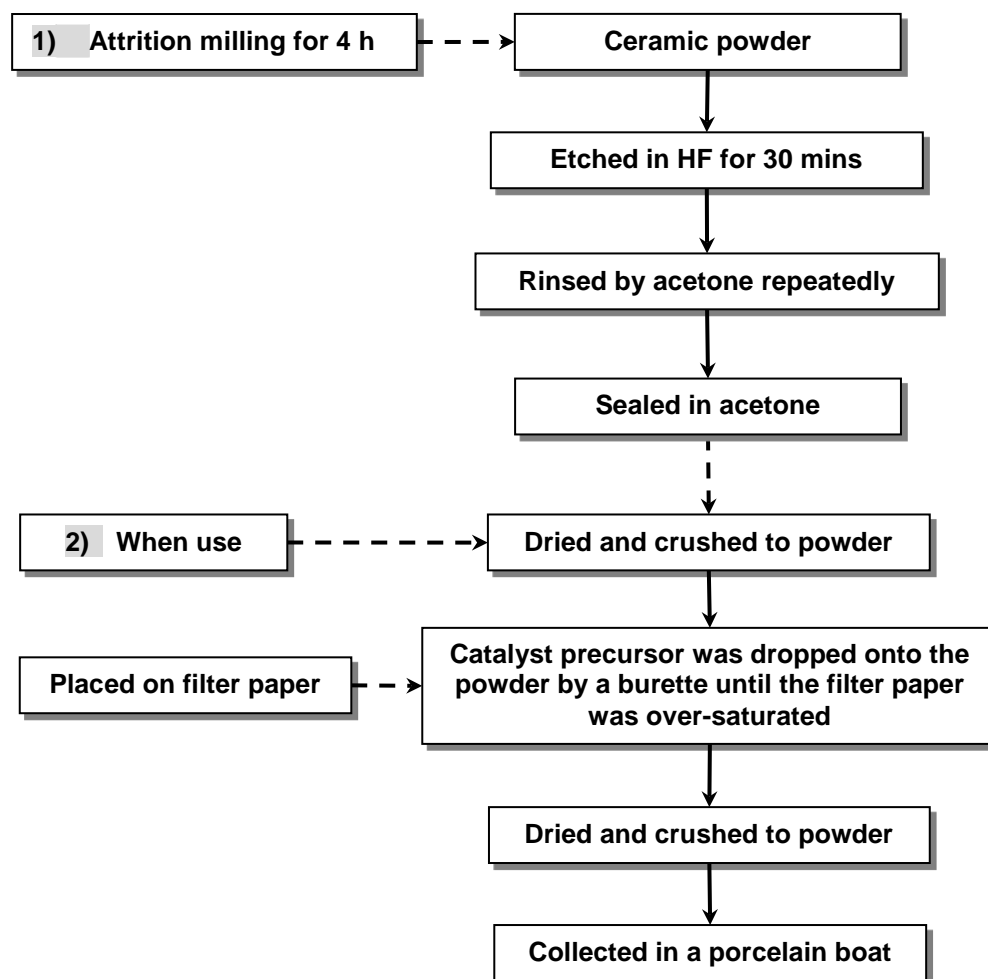


Figure 3.6 – flowchart of sample preparation with ceramic powders.

3.5 In-situ growth of CNTs on Al_2O_3 powder

Al_2O_3 powders were prepared through two sources: one is an as-purchased micron-scale Al_2O_3 powder (AO-micron) with a claimed particle size of 10 μm (Sigma-Aldrich, UK), the other is an as-purchased nano-scale Al_2O_3 powder (AO-nm) with a claimed particle size of 300 nm (Sigma-Aldrich, UK). The reason of choosing different Al_2O_3 powders was to study the possible effect of particle size on conducting the in-situ growth of CNTs. The micron-sized Al_2O_3 powder was attrition milled under 300 rpm for 5 hours, and then was mixed with

the nano-sized one based on the weight ratio of 1:1. The mixed Al_2O_3 powder was marked as 'AO-micron+nm'. The three types of Al_2O_3 powder was summarised in table 3.4, and used to fabricate $\text{Al}_2\text{O}_3/\text{CNTs}$ ceramic composite.

Table 3.4 – Three types of Al_2O_3 powders prepared for growth of CNTs.

| Types | AO-micron | AO-nm |
|--------------|--------------------------------|--------|
| AO-micron | 100wt% | 0wt% |
| AO-micron+nm | 50wt%, 5h attrition milling | 50wt% |
| AO-nm | 0wt% | 100wt% |

Before impregnation of the solution of catalyst precursor, the three types of Al_2O_3 powder were ultrasonicated in 10wt% diluted HF acid for 30 minutes at room temperature, and then rinsed and sealed in acetone as shown in figure 3.6.

$\text{Co}(\text{NO}_3)_2$ was selected as catalyst precursor for depositing catalyst particles on the surface Al_2O_3 particles and/or among the particles in the powder. The precursor solution was prepared with two concentrations: 0.3 and 0.6 mol/l. After impregnation with catalyst precursor as introduced in section 3.4.2 and figure 3.6, the powder samples were placed in porcelain boats and positioned in tube furnace for CCVD process. Methane flow was cracked at 650°C for 60 minutes.

3.6 In-situ growth of CNTs on Y-TZP powder

TZ-3Y powder (*TOSOH Chemicals, Japan*) was chosen for the CNT growth study. Specified by the manufacturer, this powder consists of agglomerates of primary zirconia particles with a size of ~50 nm, as estimated by TEM shown in section 4.3.3. The zirconia particles were delivered in granulated form for the ease of handling, the size of which is about 50 μm , measured by SEM.

In order to impregnate the catalyst precursor on surface of zirconia particles, 10g of TZ-3Y powder was firstly immersed in 40ml of acetone. The slurry was ultrasonically stirred for 15 minutes to break down the zirconia granules into particles. After ultrasonication, 0.6 mol/l $\text{Co}(\text{NO}_3)_2$ precursor solution was impregnated onto surface of zirconia particles as introduced in section 3.4.2 and figure 3.6. The powder sample was positioned in tube furnace of methane flow cracked at 650°C for 60 minutes.

3.7 Manufacture of CNTs reinforced composites

3.7.1 Preparation of CNTs/CF reinforced carbon composites

The manufacture route included two steps: 1) preparation of CNTs/CF hybrid preforms; 2) development of carbon matrix inside the preforms of carbon reinforcements.

- (i) CNTs/CF reinforcement preform

CF blocks with dimensions of 20mm x 10mm x 5mm were cut from a large piece of preform supplied by Surface Transforms Ltd, with a density of 1.38 g/cm³. The CF preform was derived from PANOX: the pyrolysing temperature was between 1200 and 1700°C, as advised by the supplier, but the exact temperature was not confirmed due to commercial interest reasons.

The CF preform was impregnated with catalyst precursor for CVD process to manufacture of CNTs/CF hybrid preform. For an example, in order to impregnate 0.3mol/l Co(NO₃)₂, the tailored CF preform was first placed on a piece of filter paper, then the Co(NO₃)₂ solution was sucked by a burette and dropped from the top surface of the CF block. When the bottom area of filter paper was over saturated, the CF preform was dried in oven at 60°C for 30 minutes. The dried CF preform was then positioned in tube furnace with methane flow cracked at 650°C for 60 minutes.

(ii) CNTs/CF reinforced carbon composite

After CVD process, the as-received CNTs/CF hybrid preform was delivered to industry. A CVI furnace was operated at vacuum condition with continuous methane flow infiltrating CNTs/CF preform. Methane was cracked into carbon at high temperature (>1000°C), and the porous preform was densified with carbon matrix deposited on the surface of CFs.

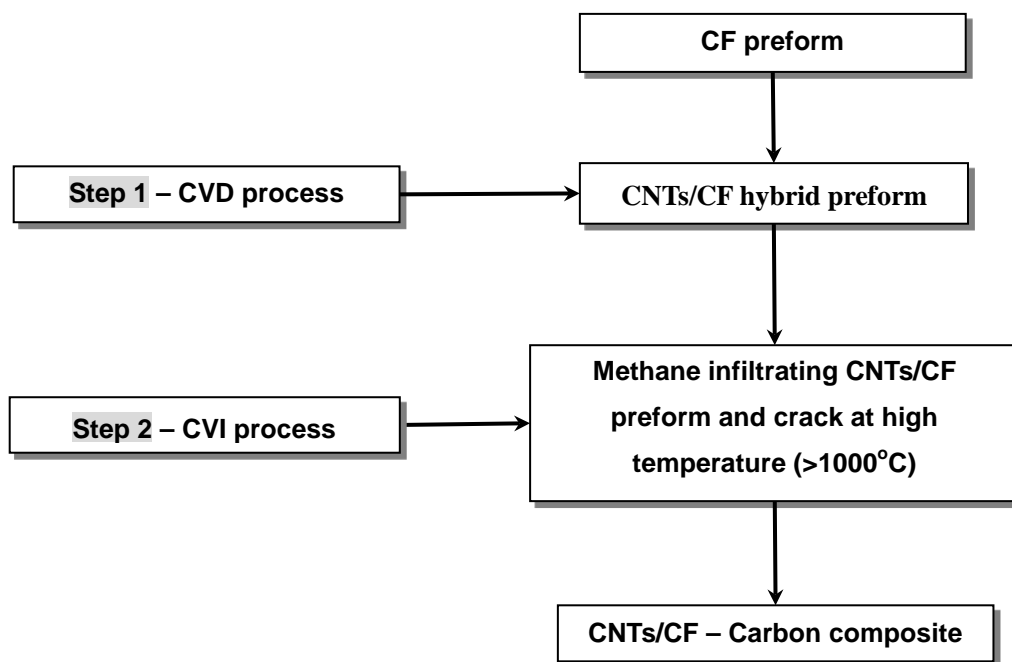


Figure 3.7 – flowchart of possible CVI steps.

Due to business confidential issue, some detailed processing parameters cannot be disclosed. Some possible steps were listed in figure 3.7. The process was required for a very long infiltration time up to weeks [122]. Slow pyrolytic carbon deposition was formed from the surface of CFs and generally built up perpendicularly upwards. When the preform was reached to required density, CVI process was stopped and the sample was cooled in an inert gas atmosphere. A reference CF preform without in-situ growth of CNTs was also used to produce CF reinforced carbon composite at the same processing condition.

3.7.2 CNTs reinforced phosphate bonded Al_2O_3 ceramics

The manufacture route for preparing phosphate bonded CNTs/ Al_2O_3 composite

also included two steps: 1) preparation of CNTs/ Al₂O₃ composite powder; 2) development of chemical binding inside the Al₂O₃ composite powder.

(i) CNTs/Al₂O₃ composite powder

CNTs/Al₂O₃ composite powder was produced through in-situ CVD method. Details of the processing route were introduced in section 3.4.2 and figure 3.6.

(ii) Chemically bonded CNTs/Al₂O₃ ceramic composite

Al(H₂PO₄)₃· $\frac{3}{2}$ H₂O was introduced into Al₂O₃ powder through chemical method, as a chemical bonding precursor, to produce aluminium phosphate (AP, AlPO₄) as a bonding agent. There were two methods of introducing mono-aluminium phosphate hydrate (Al(H₂PO₄)₃· $\frac{3}{2}$ H₂O) into the CNTs/Al₂O₃ composite powder.

(ii-a) method A and chemical reactions

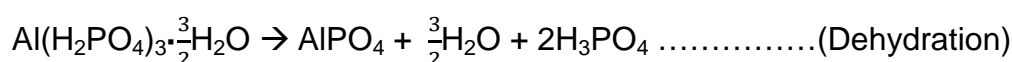
In method A, phosphoric acid (PA, H₃PO₄) (85wt.% in H₂O, Sigma-Aldrich, UK) was first diluted in deionised water and adjusted to a 50wt% in H₂O PA solution. 1ml of the PA solution was added into 3.0g of the CNTs/Al₂O₃ composite powder (AO-micron and AO-micron+nm), i.e. the mole ratio of AlPO₄:Al₂O₃ for the AP bonded Al₂O₃ ceramics is about 1:5. The slurry was agitated to a uniform gel state. The gel of 'AO-micron' was filled in a mould with the dimension of 10mm x 10mm x 5mm, while the gel 'AO-micron+nm' was coated onto a substrate (e.g. a carbon fibre reinforced carbon/silicon carbide (C_f/C-SiC) breaking disk) with the dimension of 10mm x 10mm before curing.

During the curing, series of the chemical reactions were taken place. First is the

dissolution of Al_2O_3 particles. When the PA solution was added in CNTs/ Al_2O_3 composite powder, part of the surface material of Al_2O_3 was dissolved in the solution through the reaction below:



The gel samples were sealed in an evaporating dish and dried in oven at 130°C for two days. Dehydration process of $\text{Al}(\text{H}_2\text{PO}_4)_3 \cdot \frac{3}{2}\text{H}_2\text{O}$ was taken place through the reaction below:



The reason of dehydrating $\text{Al}(\text{H}_2\text{PO}_4)_3 \cdot \frac{3}{2}\text{H}_2\text{O}$ in a sealed container is to reduce the evaporating rate of water content, by which to avoid porous structure within the Al_2O_3 ceramic. After two days of the slow dehydration, the lid of the evaporating dish was removed and the samples were dried at 150°C for two days. The latter step was to completely remove the water content and cure the samples. Therefore, combining the above two, gives the curing reaction as below:



(ii-b) method B

In method B, high pressure was used to compact the Al_2O_3 powder to desired

shape before adding PA solution. The pressing process was achieved through two steps: 1) 3.5g CNTs/ Al_2O_3 powder (AO-micron+nm) was die-pressed (1cm in diameter of the die) at room temperature with the pressure of $3.0 \times 10^7 \text{ Pa}$. The powder compact after die-press has a pellet shape with the diameter of 1cm. 2) the pellet was then sealed in a PVC bag for cold iso-static press (CIP) with the pressure of $8.0 \times 10^7 \text{ Pa}$. The thickness of the Al_2O_3 pellet after the two-step pressing was about 3mm, i.e. the density of the pellet was about 3.72 g/cm^3 .

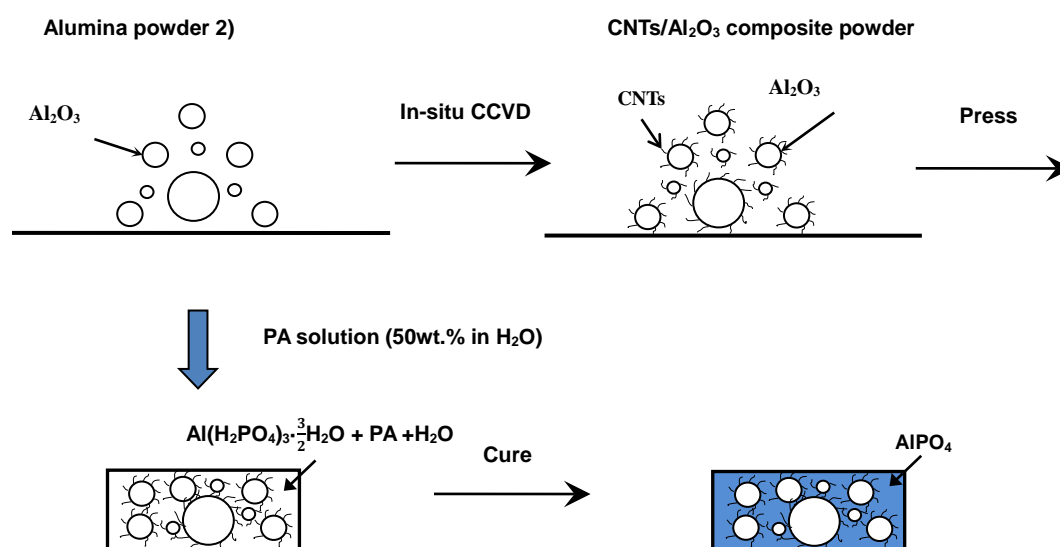


Figure 3.8 – Schematic of fabricating AP bonded CNTs/ Al_2O_3 ceramic.

After CIP, the 50wt% PA solution was added into the Al_2O_3 pellet. The Al_2O_3 pellet was placed on a piece of filter paper, while two drops, i.e. 0.1ml of the PA solution was dropped onto the surface of pellet. The as-prepared Al_2O_3 pellet was cured as introduced in (ii-a). Figure 3.8 schematically showed the general steps of method B of fabricating AP bonded CNTs/ Al_2O_3 ceramic.

3.8 Microstructural characterisations

3.8.1 Scanning electron microscopy (SEM)

Apart from examination of surface morphology of materials interested in this research, SEM was a key technique used to inspect and evaluate the growth of CNTs.

Field emission gun SEM (FEG-SEM) (*Carl Zeiss (Leo) 1530 VP, Carl Zeiss SMT AG Company, Germany*) was typically operated under an electron high tension (EHT) of 5kV. To inspect the CNT and catalyst particles, In-Len imaging mode was used to achieve better resolution. Whenever the length of the CNTs needs to be highlighted, a proper titling of the samples was used.

(1) CF samples

For all carbon-fibre samples, CF filaments were picked up randomly from CF bundles and placed on SEM sample stubs stuck with standard carbon adhesive disks. No further treatment before observation in the SEM.

(2) Ceramic powder samples

For ceramic powder samples, the powder samples were sprinkled on an SEM sample stub stuck with standard carbon adhesive disk. A thin layer of gold was sputtered to prevent any electric discharging.

3.8.2 Transmission electron microscopy (TEM)

TEM was used to examine the contact between substrates and catalyst particles, and the contact between substrates and CNTs. Details of sample preparation and TEM examination are given in the followings:

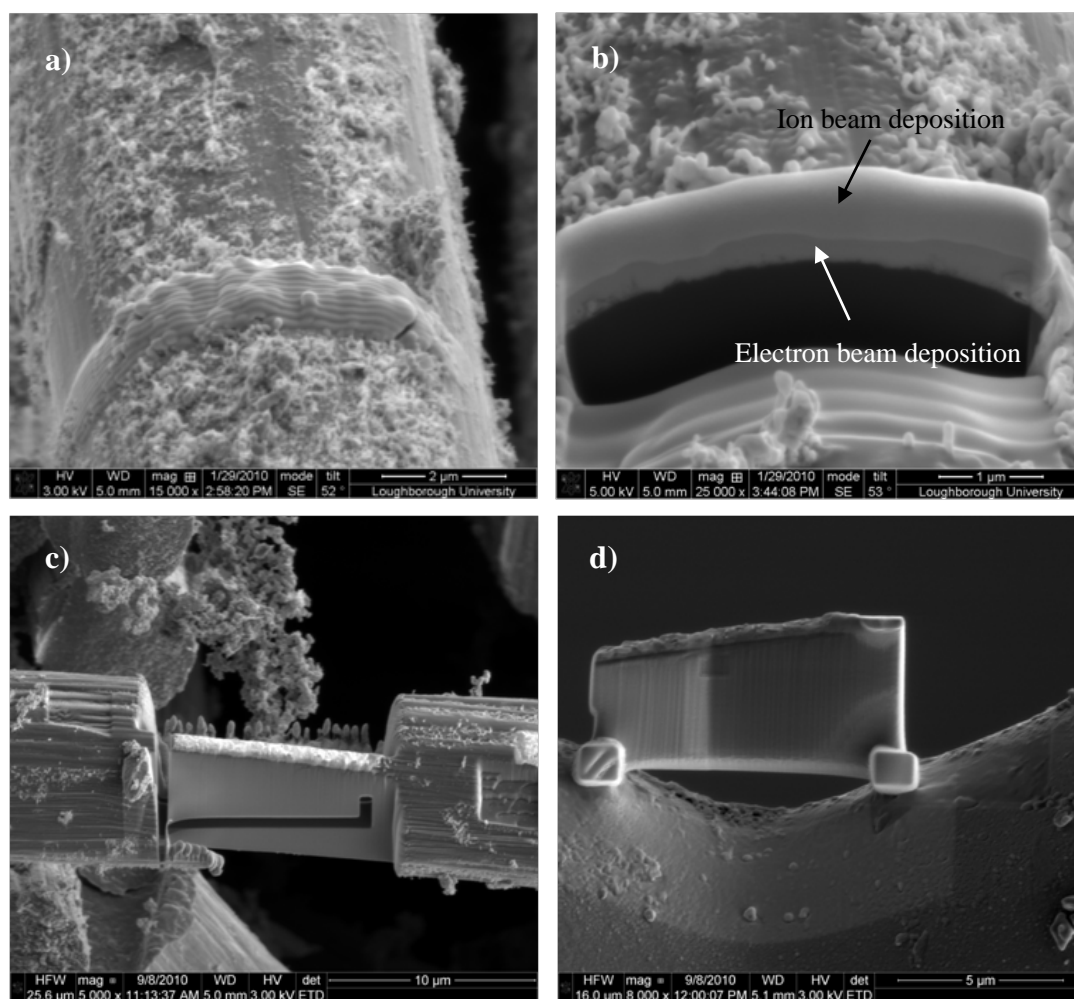


Figure 3.9 – TEM sample preparation by FIB. a) Pt deposition on CNTs using electron beam, b) further Pt deposition using ion beam, c) prepared TEM sample for further thinning, and d) TEM sample lifted out.

(1) TEM samples preparation

a. CNTs on CF substrate

The system of FEI Nova 600 Nanolab Dualbeam FIB/FEG-SEM was used for preparation of TEM samples. Take typical CNTs/CF preform as an example, on surface of a carbon fibre, a rectangle pattern ($10\ \mu\text{m} \times 1\ \mu\text{m}$) was selected on a typical region of CNTs and marked by Pt-electron deposition (*electron beam of 1.1 nA at 3kV*) as shown in figure 3.9(a). The Pt-electron deposition was applied to produce a layer protecting the CNTs. At the same position, Pt deposition was applied with 100pA ion beam at 5kV to finish the rectangular patterning as shown in figure 3.9(b).

Along two sides of the rectangular patterning, square holes ($10\ \mu\text{m} \times 5\ \mu\text{m} \times 5\ \mu\text{m}$ in depth) were dig with Ga ion beam of 20nA at 30kV, leaving a wall ($10\ \mu\text{m} \times 1\ \mu\text{m} \times 5\ \mu\text{m}$ in depth) in between as shown in figure 3.9(c). When the wall was thinned to about 200 nm in thickness by Pt ion beam with 3nA at 10kV, it was taken out by a micron probe and welded on a TEM copper grid.

b. CNTs on Al_2O_3 substrate

The procedures of preparing the TEM sample of CNTs on Al_2O_3 particles were the same as those introduced above.

(2) TEM examination

a. Analytic TEM

JEOL 2000FX TEM was used to investigate the contact between CNTs and the

substrates. It was operated at the bright field imaging mode, with the accelerating voltage of 200kV with the beam current of 40 μ A. Under this imaging mode, regions with higher atomic number, e.g. catalyst particles, will appear dark, while regions with lower atomic number, e.g. CNTs or no samples, will appear bright. The samples were enlarged by 200k and 400k, at which magnification morphologies of catalyst particles and their agglomerations were investigated.

b. HRTEM

A FEI Philips TECNAI F20 (with STEM and Oxford Isis EDS, University of Birmingham, UK) was used at three modes, with the accelerating voltage of 200kV with the beam current of 40 μ A:

- when a typical catalyst particle was selected, a high angle annular dark field (ADF) detector was used and the TEM was operated at STEM mode and the magnification of 450k. The images from STEM mode gave complementary contrast for the observation of interfacial contact between catalyst particles and substrates. Two kinds of catalyst particles were mainly investigated: one was those lifted up by growth of CNTs, and the other was those on substrates after CVD process.
- Secondly, with the same position and magnification of 450k under STEM mode, the catalyst particle was observed at bright-field (BF) imaging mode. EDX detector was applied to identify the chemical composition of the selected catalyst particles.

- The third mode was lattice imaging mode (high resolution TEM). The high resolution TEM (HRTEM) was particularly used to investigate interfacial contact between catalyst particles and substrates and graphene layers of CNTs, with a magnification of 1000k.

3.8.3 SEM image analysis by imaging softwares

The images from SEM observation were analysed by the image softwares, such as “UTHSCSA Image Tool[®] 3.0” and “Image J 1.42q”. The imaging tool was mainly used to quantify the size distribution of catalyst particles in typical areas, where growth of CNTs were selectively catalysed by cobalt particles. The general purpose was to study the popularities of catalytic growth of CNTs in associated with the diameter of catalyst particles. Details of the method were divided into three steps:

- Firstly, particles that have catalytic growth of CNTs were marked by circling their boundaries in the imaging tool, distinguished by different contrast. The image tool will then be able to count the number of pixels within the closed curves and automatically convert the circled area into equivalent spherical shape, the diameter of which can be calculated based on the scale bars in the SEM images.
- Secondly, all the particles in the selected region, as well as those have no catalytic growth of CNTs during CCVD process, were analysed by the same manner introduced in step one.

- Finally, a histogram diagram was generated to express the most popular size range of particles that for catalytic growth of CNTs. Details of the imaging analysis were shown in section 4.3.4.1.

“Image J 1.42q” was applied on quantitative measurements of the areas, such as the area of dried catalyst precursor solution attached on substrates. The target areas were first marked by circling their boundaries, and then the software was able to automatically count the number of pixels within the circulated areas. Based on the scale bars applied on the SEM images, the size of the area was able to be quantified. Details of the imaging analysis were shown in section 4.1.

Besides, “Image J 1.42q” was used to measure the density of catalyst particles and CNTs in SEM images. The number of catalyst particles or CNTs in the selected region was first counted, through distinguishing them by contrast. Then the size of the selected area was measured by the method introduced above. The density value was calculated through dividing the number of catalyst particles or CNTs by the size of the selected area.

CHAPTER 4 CNTs In-situ Growth on Surface of CFs

4.1 Effect of surface pre-treatment of PAN-based CFs

The surface morphology of CFs and their capability to have catalyst precursor solution attached were directly examined with SEM.

The as-received carbon fibres have a smooth surface, as shown in figure 4.1(a). After boiling in nitric acid at 60°C for 30 minutes, the surface of CFs became rougher, as shown in figure 4.1(b) where the characteristic features on the surface of as-manufactured carbon were revealed [84]. The comparison implies that the acid treatment had stripped off a layer from the surface of carbon fibre. Whilst the layer was not identified, from literature [83,131], this layer is suggested to be the sizing material, which is widely applied to protect the carbon fibre from any mechanical damage, and promote the compatibility of carbon fibre with matrix resin [130].

The capability of carbon fibres to attach the catalyst precursor solutions was tested and compared by immersing the fibres into $\text{Co}(\text{NO}_3)_2$ with a concentration of 0.1 mol/l, followed by drying at 60°C in oven. The dried surfaces were imaged with SEM, and the zones that had been wetted by precursor solution were highlighted by the patches with contrast different from those without precursor solution attached, as shown in figure 4.1(b) and (c). By using “image J 1.42q”, the measurements showed that about 8% area was occupied by dried precursor patches on surface of as-received carbon fibres,

while about 95% on the surface of the same carbon fibre but subjected to acid treatment.

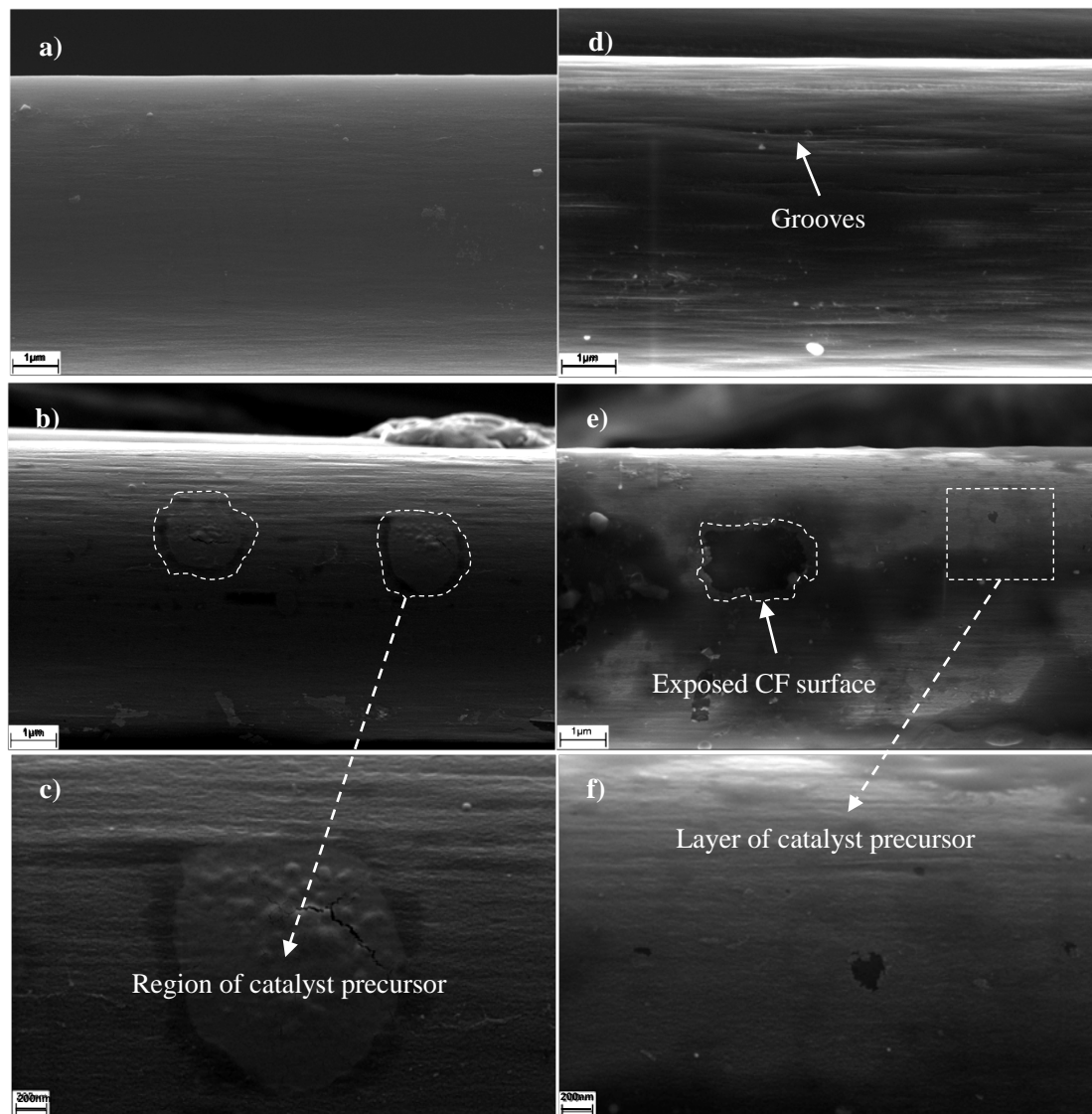


Figure 4.1 – Surface morphology of carbon fibres before and after dip coating. (a) as-received carbon fibre; (b)-(c) after dip coating of as-received carbon fibre; (d) after acid treatment; (e)-(f) after dip coating of treated carbon fibre.

The difference of the coverage of catalyst precursor indicated the improvement of wettability of PAN-based CF through acid treatment. Image f) showed the surface morphology of the coated layer was smoother than that on surface of

as-received CF.

4.2 Effect of selection of catalyst precursors

The selection of catalyst precursor was based on the visibility of CNTs on carbon fibre surface under the highest possible resolution of FEGSEM. Exemplary SEM images containing visible CNTs on the surface of CFs under the selected CVD conditions are shown in figure 4.2. Among particles derived from Fe, Co and Ni precursors, only particles derived from $\text{Co}(\text{NO}_3)_2$ demonstrated clear catalytic effect that the growth of CNTs were visible as shown in figure 4.2(b). Under the same processing condition, there were no visible CNTs on surface of CFs dipped with Fe and Ni precursors.

It was noticed that the acid pre-treatment had an impact on the growth of CNTs on surface of CFs. Figure 4.2(a) and (b) demonstrate the catalyst particles developed on an as-received surface and an as-treated surface of carbon fibre. For the former one, the equivalent diameter of catalyst particles derived from $\text{Co}(\text{NO}_3)_2$ were ranged from 6 to 35 nm, with an average value of 15.5 nm and a standard deviation of 7.6 nm; for the later one, the equivalent diameter are from 8 to 65 nm with an average value of 22.1 nm and a standard deviation of 16.9 nm. Under the same CVD conditions, however, there is no visible CNT on as-received CF, and clearly visible CNT on as-treated CF. Even though the equivalent diameter of catalyst particles have a clear overlap, but the catalytic effect was different.

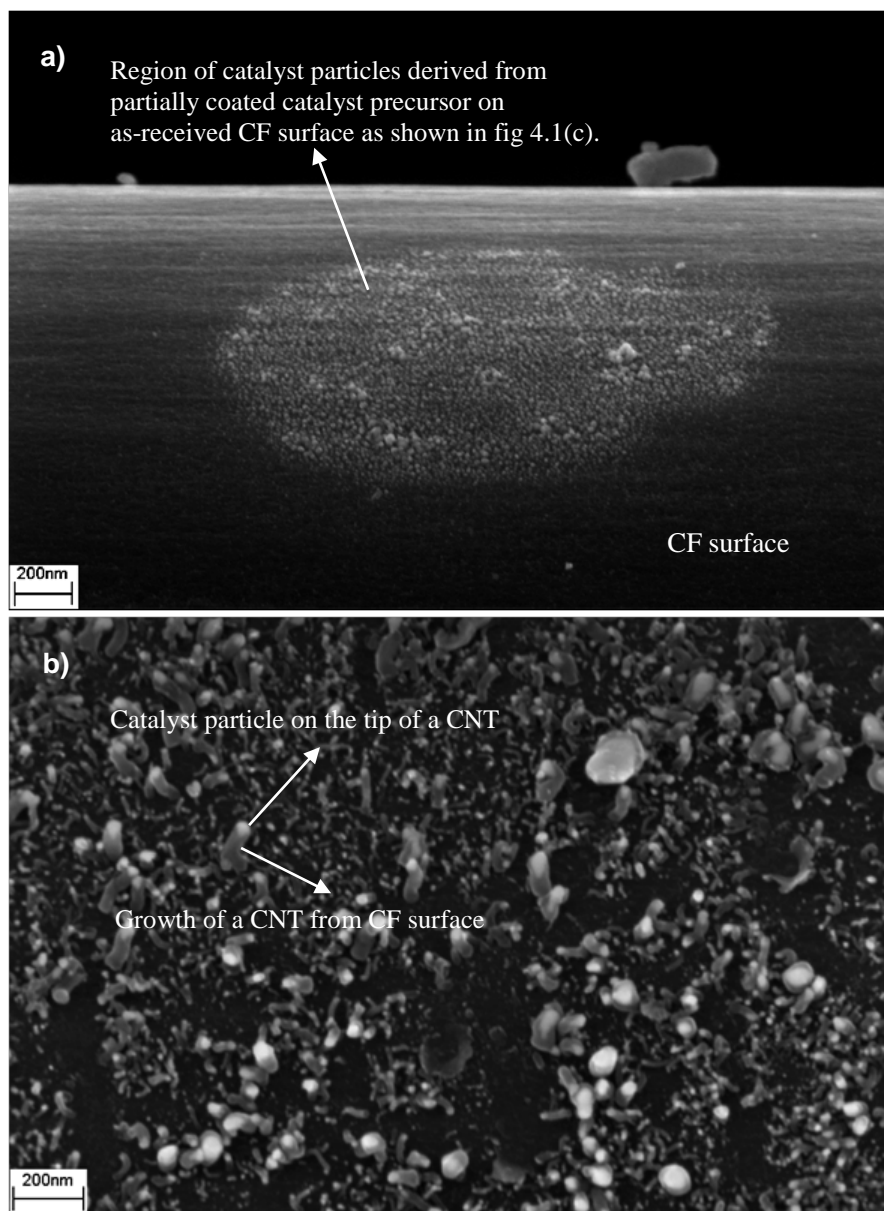


Figure 4.2 – SEM images of carbon fibres after CVD at 650°C for 30 minutes under different catalytic conditions: (a) Co derived from 0.1 mol/l $\text{Co}(\text{NO}_3)_2$ on as-received CF surface; (b) Co derived from 0.1 mol/l $\text{Co}(\text{NO}_3)_2$ on as-treated CF surface.

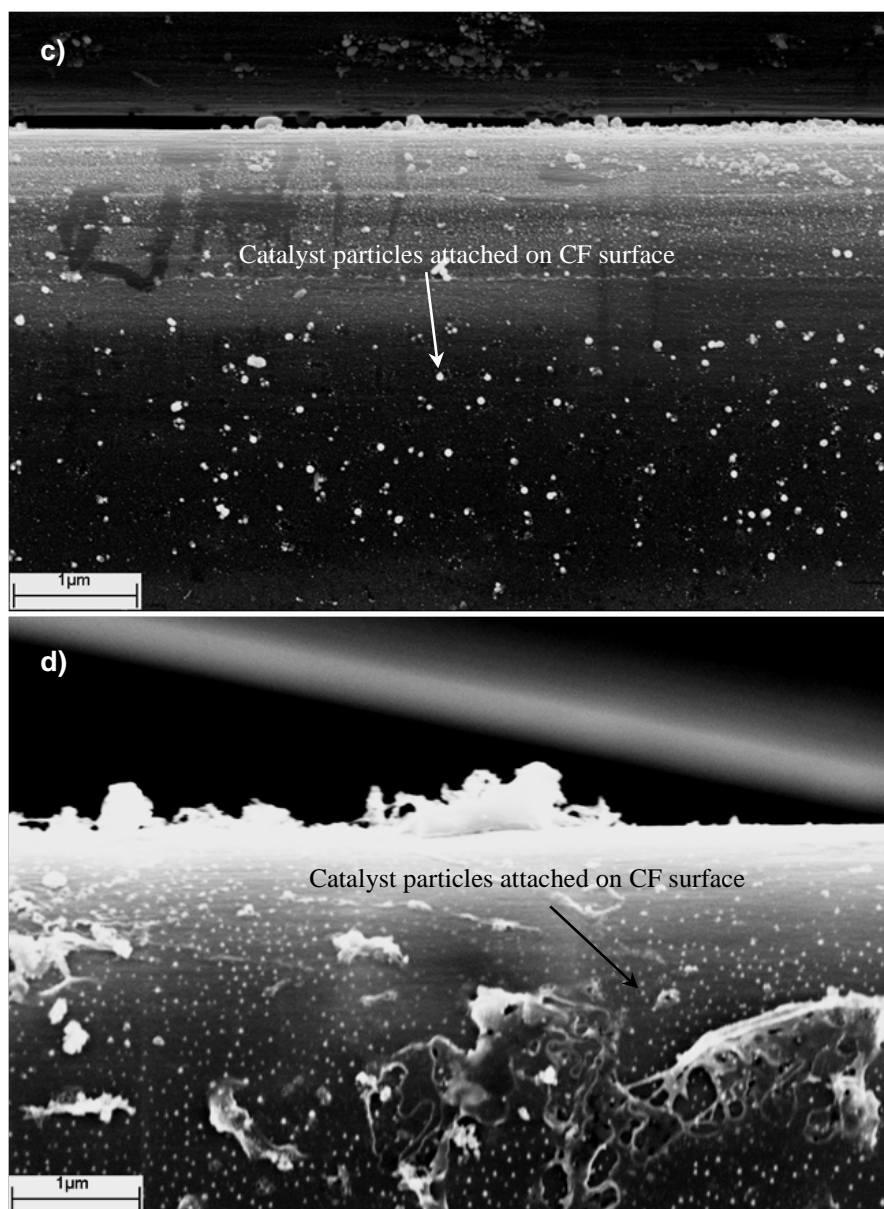


Figure 4.2 (continued) – SEM images of carbon fibres after CVD at 650°C for 30 minutes under different catalytic conditions: (c) Fe derived from 0.1 mol/l $\text{Fe}(\text{NO}_3)_3$ on as-treated CF surface; (d) Fe derived from 0.1 mol/l Ferrocene on as-treated CF surface.

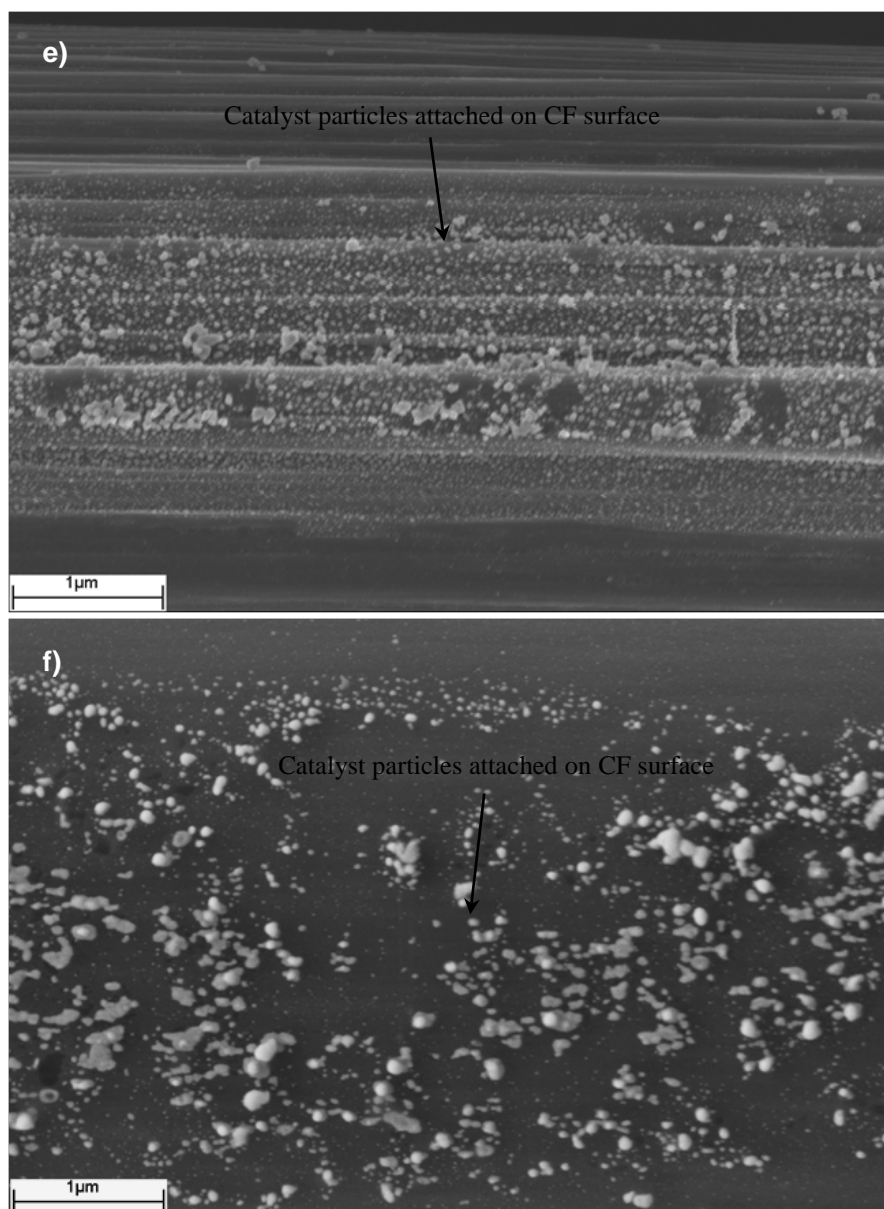


Figure 4.2 (Continued) – SEM images of carbon fibres after CVD at 650°C for 30 minutes under different catalytic conditions: (e) Fe derived from 0.1 mol/l FeCl_3 on as-treated CF surface; (f) Ni derived from 0.1 mol/l $\text{Ni}(\text{NO}_3)_2$ on as-treated CF surface.

More details on the as-treated surface shown in figure 4.2(b) were quantified: the yield (*No. of CNTs per area*) of CNTs was about 250 per $1 \mu\text{m}^2$, with the average equivalent diameter was $20 \text{ nm} \pm 10.5 \text{ nm}$. For each CNT, the outer diameter was governed by that of the catalyst particle on its tip, i.e. the

diameters of CNTs have the same size distribution as that of catalyst particles.

4.3 Optimisation of In-situ growth of CNTs on surface of CFs

To optimise the catalytic CVD conditions for the growth of CNTs when $\text{Co}(\text{NO}_3)_2$ was used as the catalyst precursor, three processing parameters were investigated: 1) concentration of catalyst precursor solution, 2) cracking temperature of methane, and 3) dwelling time at the cracking temperature.

4.3.1 Concentration of catalyst precursor

At the same CVD conditions, figure 4.3 ~ 4.5 represented typical regions of catalyst particles and growth of CNTs, while the concentration of $\text{Co}(\text{NO}_3)_2$ was increased from 0.001 to 0.3 mol/l.

The data from “ImageJ 1.42q” analysis suggested in figure 4.3(a), the average density (*No. of particles per area*) of catalyst particles was about 2500 per $1\mu\text{m}^2$, and the particle size was in the range from 3 to 25 nm, with an average equivalent diameter of 6.1 nm and a standard deviation of 1.3 nm. In figure 4.3(b), the average density of catalyst particles was about 3500 per $1\mu\text{m}^2$, and the equivalent diameter was in the range from 4 to 30 nm, with an average value of 8.8 nm and a standard deviation of 1.4 nm. Typical regions were also selected for catalyst particle size analysis in section 4.3.4.1.

Growth of CNTs was not visible in figure 4.3(a), while two CNTs were observed

in figure 4.3(b). The maximum length of the CNTs observed was about 100 nm, the averaged diameter of which was about $15 \text{ nm} \pm 1.1 \text{ nm}$.

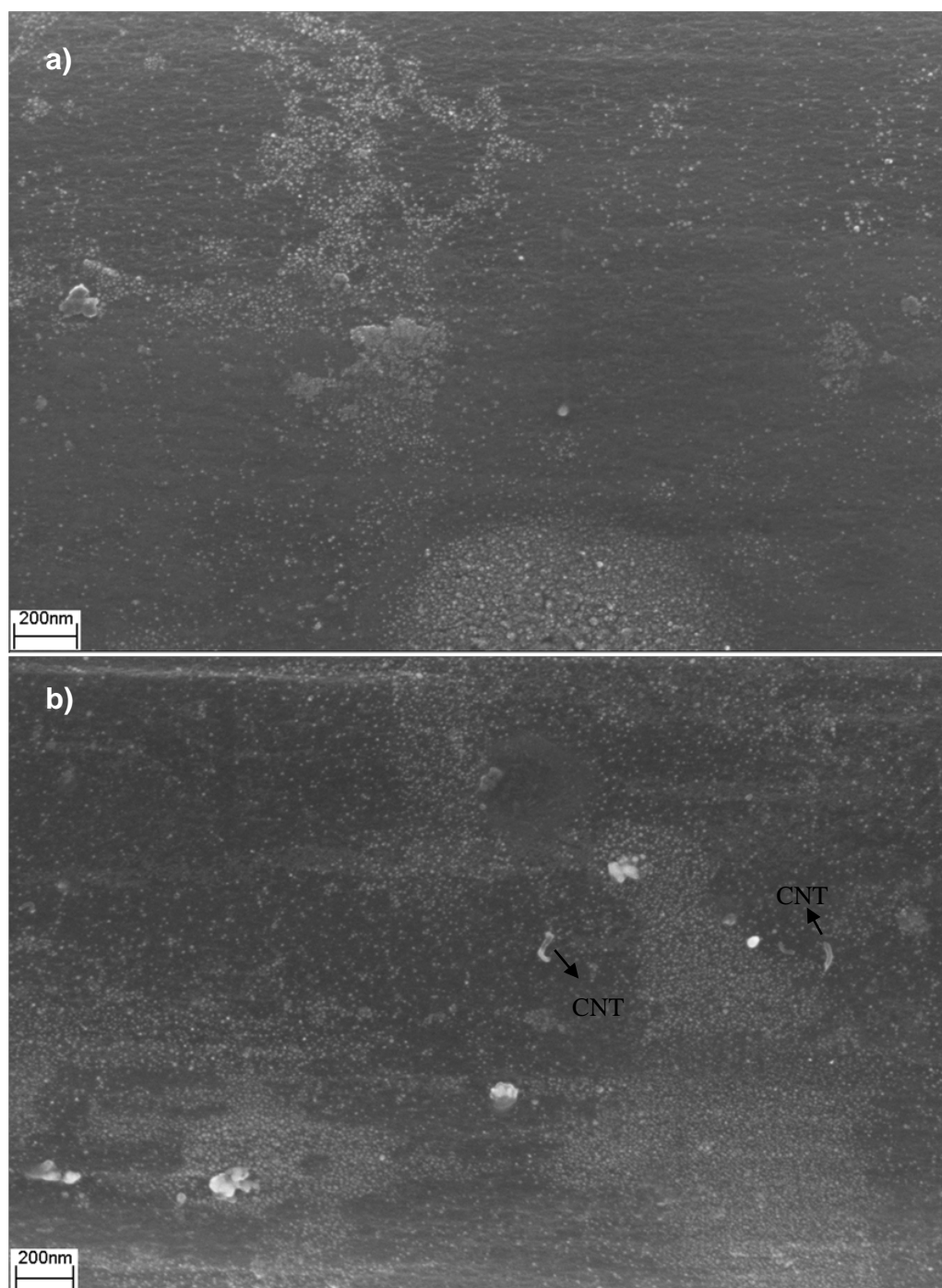


Figure 4.3 – Catalyst particles and CNTs developed on the surface of PAN-CFs with acid surface treatment. $\text{Co}(\text{NO}_3)_2$ solution concentrations: 0.001 mol/l in (a) and 0.005 mol/l in (b), CVD at 600°C for 30 minutes.

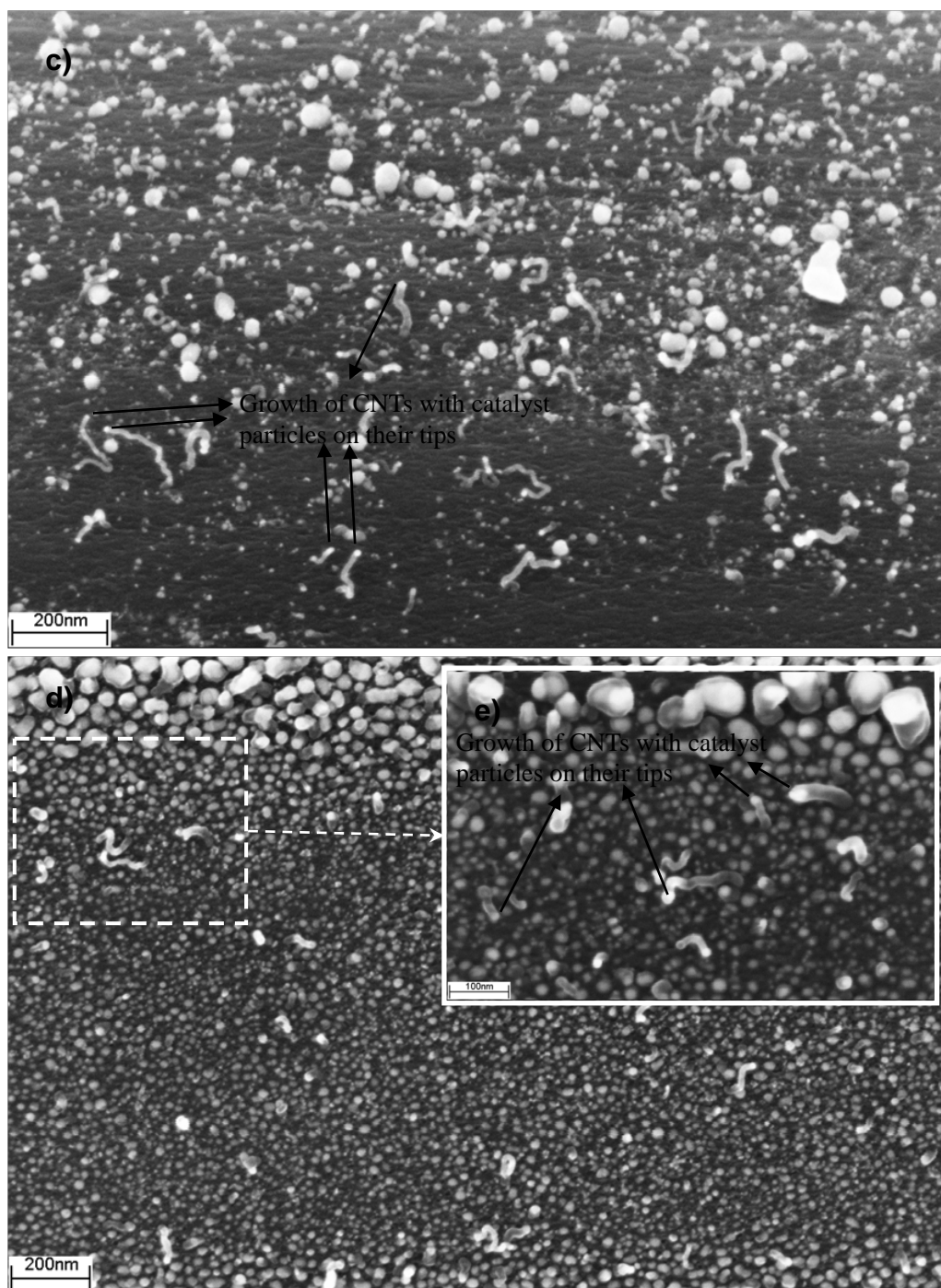


Figure 4.4 – Catalyst particles and CNTs developed on the surface of PAN-CFs with acid surface treatment. $\text{Co}(\text{NO}_3)_2$ solution concentrations: 0.05 mol/l in (c) and 0.1 mol/l in (d), CVD at 600°C for 30 minutes. Image (e) showed magnified area in (d).

In figure 4.4(c), growth of CNTs was clearly visible with catalyst particles on their tips. The maximum length of CNTs was about 250 nm, with the averaged diameter of which was $16.5 \text{ nm} \pm 3.5 \text{ nm}$. Compared to figure 4.3(a) & (b), the density of catalyst particles in figure 4.4(c) was reduced to about 760 per $1 \mu\text{m}^2$, but catalyst particles have a broadened particle equivalent diameter ranged from 5 to 50 nm, with an average value of 12.1 nm and a standard deviation of 9.6 nm.

The equivalent diameter of catalyst particles in figure 4.4(d) was ranged from 4 to 55 nm, with an average value of 18.2 nm and a standard deviation of 11.5 nm, which was similar to that in figure 4.4(c). However, the density of catalyst particles was increased to about 1323 per $1 \mu\text{m}^2$. It was also suggested in figure 4.4(d) that the growth of CNTs was based on tip-growing mode, the same as previously observed in figure 4.4(c). The averaged diameter of CNTs in figure 4.4(d) was $17.3 \text{ nm} \pm 4.5 \text{ nm}$. The yield of CNTs in both figure 4.4(c) & (d) was increased than that observed in figure 4.3(b).

In figure 4.5(e), the density of catalyst particles was about 3000 per $1 \mu\text{m}^2$ and yield of CNTs was significantly increased compared to images (b) ~ (d). The equivalent diameter of catalyst particles in figure 4.5(f) was ranged from 4 to 30 nm, with an average value of 15.5 nm and a standard deviation of 6.2 nm, while the averaged diameter of CNTs was $16.8 \pm 3.5 \text{ nm}$.

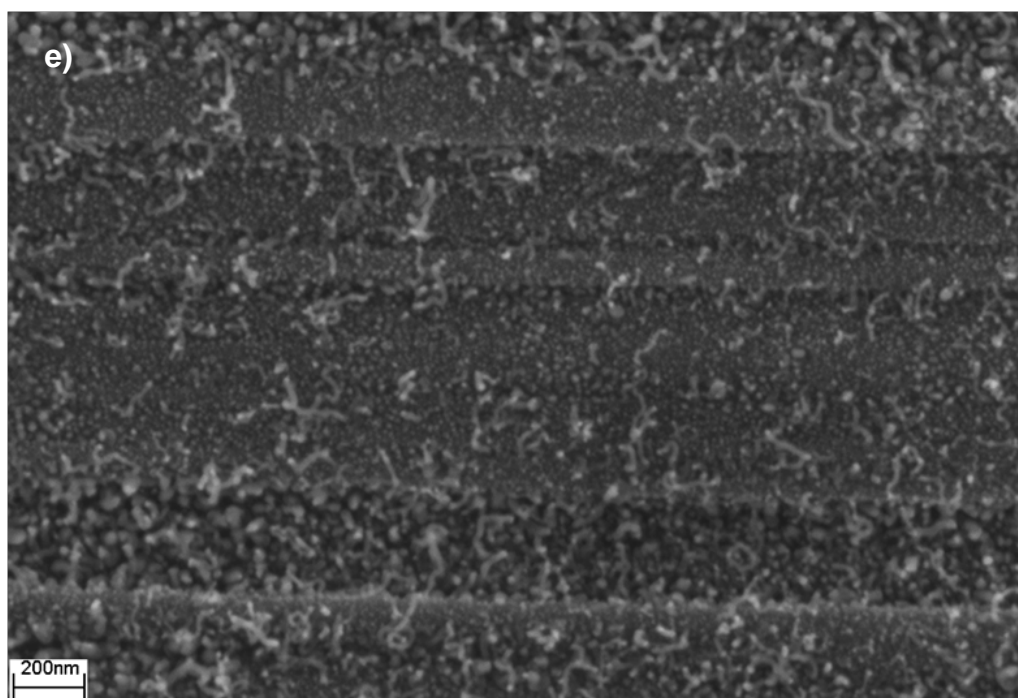


Figure 4.5 – Catalyst particles and CNTs developed on the surface of PAN-CFs with acid surface treatment. $\text{Co}(\text{NO}_3)_2$ solution concentration 0.3 mol/l, CVD at 600°C for 30 minutes.

Table 4.1 – Summary of measurements on catalyst particles and CNTs in Fig.4.3~4.5.

| Images | Concentrations (mol/l) | Diameter range of catalyst particles (nm) | Averaged diameter of catalyst particles (nm) | Density of catalyst particles (No./ μm^2) | Averaged diameter of CNTs (nm) | Max. length of CNTs (nm) |
|--------|------------------------|---|--|---|--------------------------------|--------------------------|
| (a) | 0.001 | 3 ~ 25 | 6.1 \pm 1.3 | 2500 | X | X |
| (b) | 0.005 | 4 ~ 30 | 8.8 \pm 1.4 | 3500 | 15.1 \pm 1.1 | 100 |
| (c) | 0.05 | 5 ~ 50 | 12.1 \pm 9.6 | 760 | 16.5 \pm 3.5 | 250 |
| (d) | 0.1 | 4 ~ 55 | 18.2 \pm 11.5 | 1323 | 17.3 \pm 4.5 | 150 |
| (e) | 0.3 | 4 ~ 30 | 15.5 \pm 6.2 | 3000 | 16.8 \pm 3.5 | 300 |

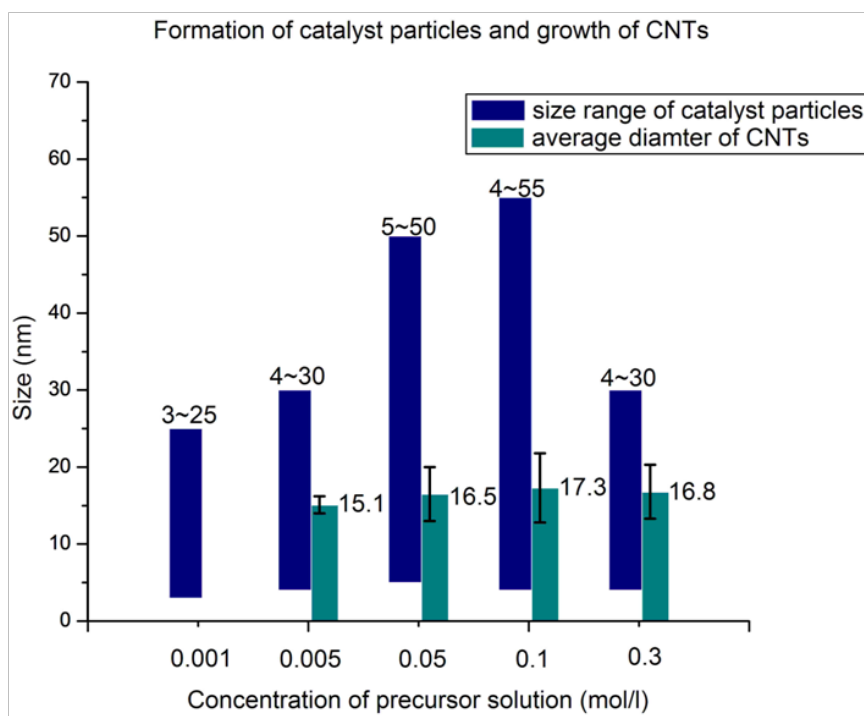


Figure 4.6 – Diagram to show the measured diameter range of catalyst particles and the averaged diameter of CNTs with standard deviation included by using $\text{Co}(\text{NO}_3)_2$ solution with different concentrations.

The experimental measurements in table 4.1 and figure 4.6 showed that from figure 4.3 to 4.5, increasing the concentration of precursor solution leads to a broader size distribution of catalyst particles. Figure 4.5(f) has the highest density of catalyst particles, and also the largest maximum length of CNTs. The growth of CNTs was visible in images (b) ~ (f). The diameter of CNTs under the same CVD conditions was popularly in the range of 10 ~ 25 nm, which was not notably affected by the variations of concentration of $\text{Co}(\text{NO}_3)_2$. However, not all catalyst particles had CNTs attached, even if their diameters were inside the same region as the diameter of CNTs.

4.3.2 Optimisation of CVD temperature for the growth of CNTs

The impact of CVD temperatures at 500°C, 600°C, 650°C and 700°C were investigated on the growth of CNTs developed on the surface of PAN-CFs with acid surface treatment, whilst the concentration of precursor solution of $\text{Co}(\text{NO}_3)_2$ was 0.3 mol/l.

(a) CVD accomplished at 500°C.

When CVD was accomplished at 500°C, no visible CNTs were available on the surface of carbon fibre, whilst the $\text{Co}(\text{NO}_3)_2$ coating was transformed into a layer of catalyst particles. The equivalent diameter of catalyst particles in figure 4.7 was in the range from 10 ~ 40 nm, with an average value of $18.9 \text{ nm} \pm 5.6 \text{ nm}$. A point was selected at the open edge area of this layer for EDX analysis, and the Co and oxygen peaks suggested that $\text{Co}(\text{NO}_3)_2$ was not fully reduced to Co particles, but in the form of cobalt oxides. The cobalt oxides may be either from thermo-decomposition and reduction of $\text{Co}(\text{NO}_3)_2$, or transformed from monolithic Co particles been oxidised again by the oxygen content in the working tube during CVD process.

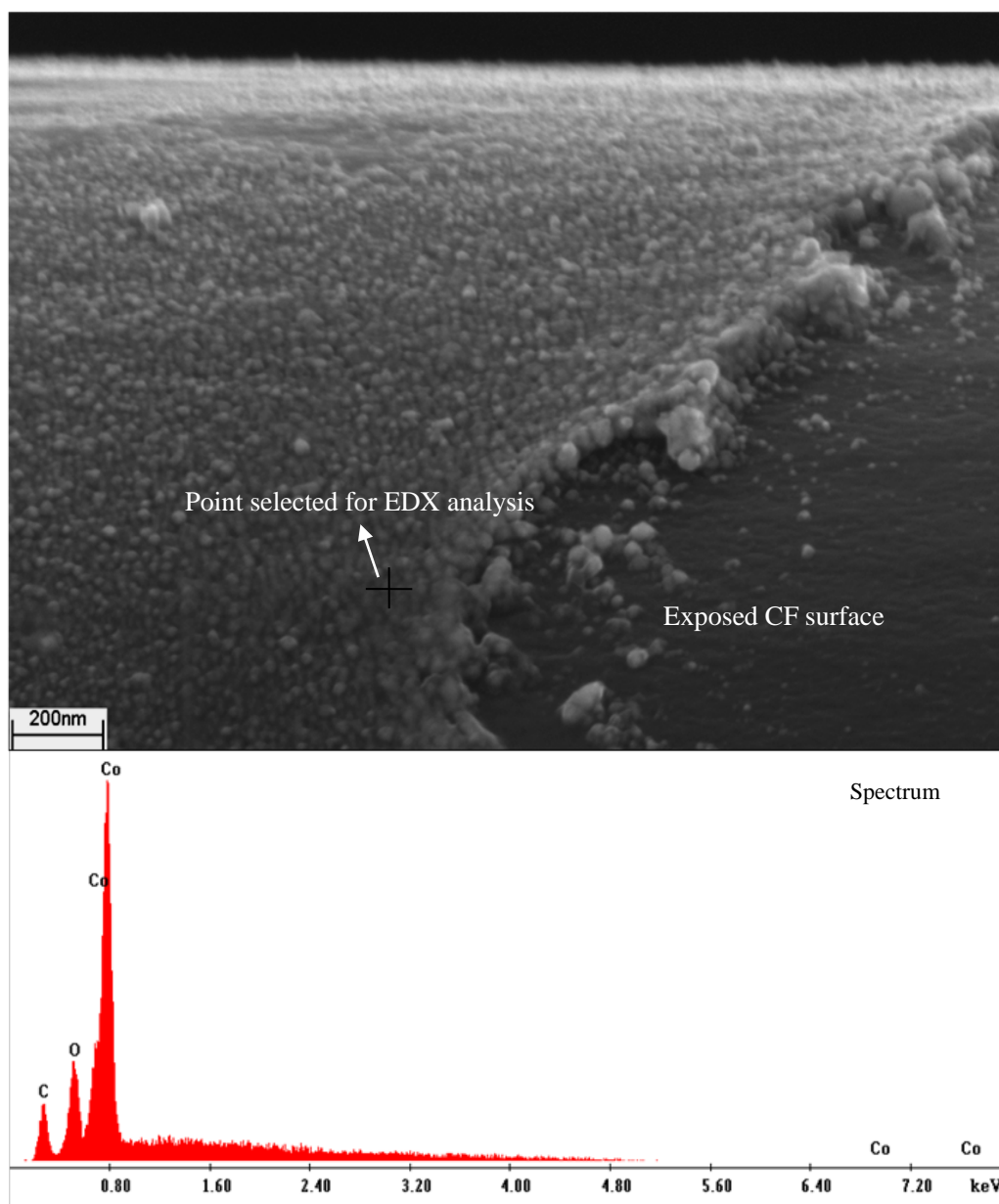


Figure 4.7 – Surface morphology on carbon fibre, with CVD at 500°C for 30 minutes, $\text{Co}(\text{NO}_3)_2$ solution concentration: 0.3 mol/l.

(b) CVD accomplished at 600°C.

When CVD was accomplished at 600°C, visible CNTs were available on surface of CFs. The surface morphology was similar to that introduced in figure 4.5 from section 4.3.1.

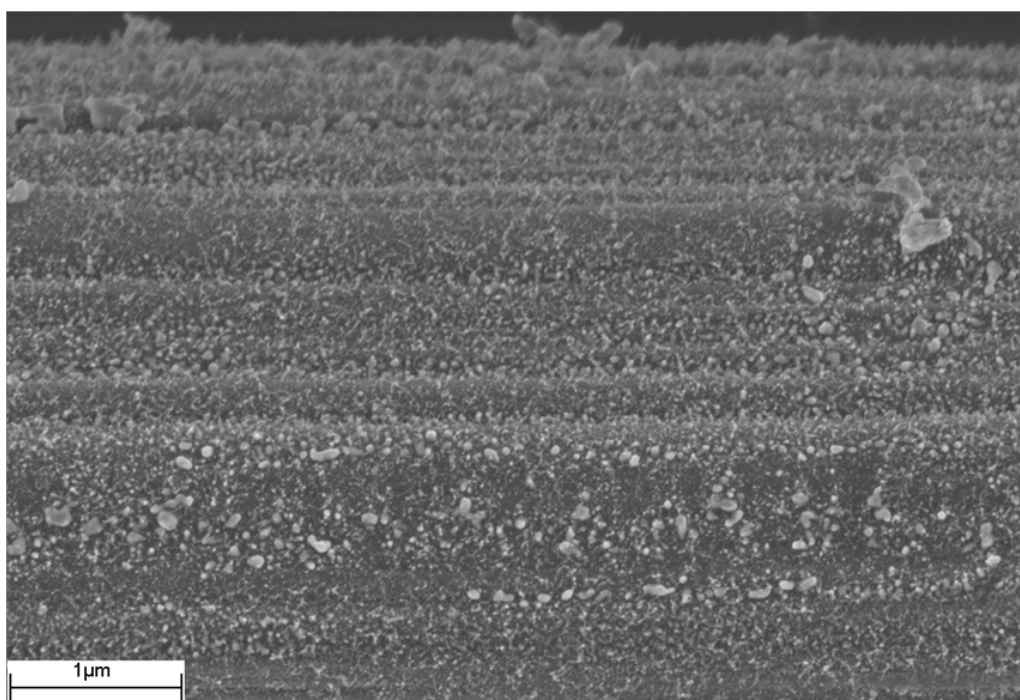


Figure 4.8 – Surface morphology on carbon fibre, with CVD at 600°C for 30 minutes, $\text{Co}(\text{NO}_3)_2$ solution concentration: 0.3 mol/l.

(c) CVD accomplished at 650°C.

When CVD was accomplished at 650°C, the yield of CNTs shown in figure 4.9 was further increased compared to that in figure 4.8. The surface of CF was covered by a forest of CNTs, the average equivalent diameter of which was $18.5 \text{ nm} \pm 4.1 \text{ nm}$. The maximum length of CNTs that can be observed in figure 4.9 was about 550 nm, indicating the rate of CNT growing was increased compared to that prepared at 600°C.

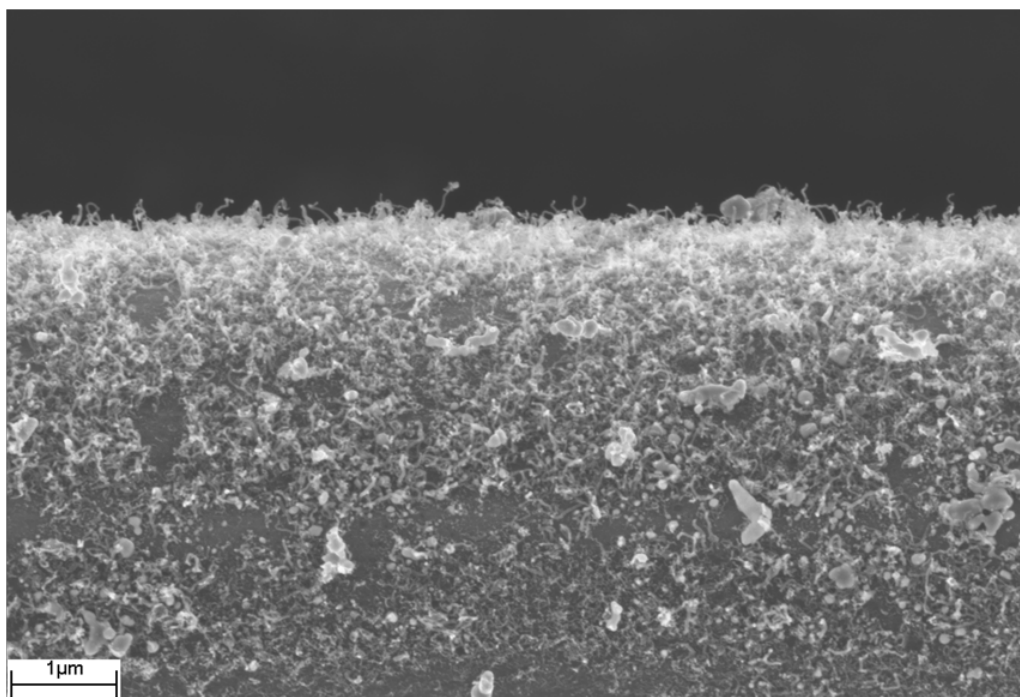


Figure 4.9 – Surface morphology on carbon fibre, with CVD at 650°C for 30 minutes, $\text{Co}(\text{NO}_3)_2$ solution concentration: 0.3 mol/l.

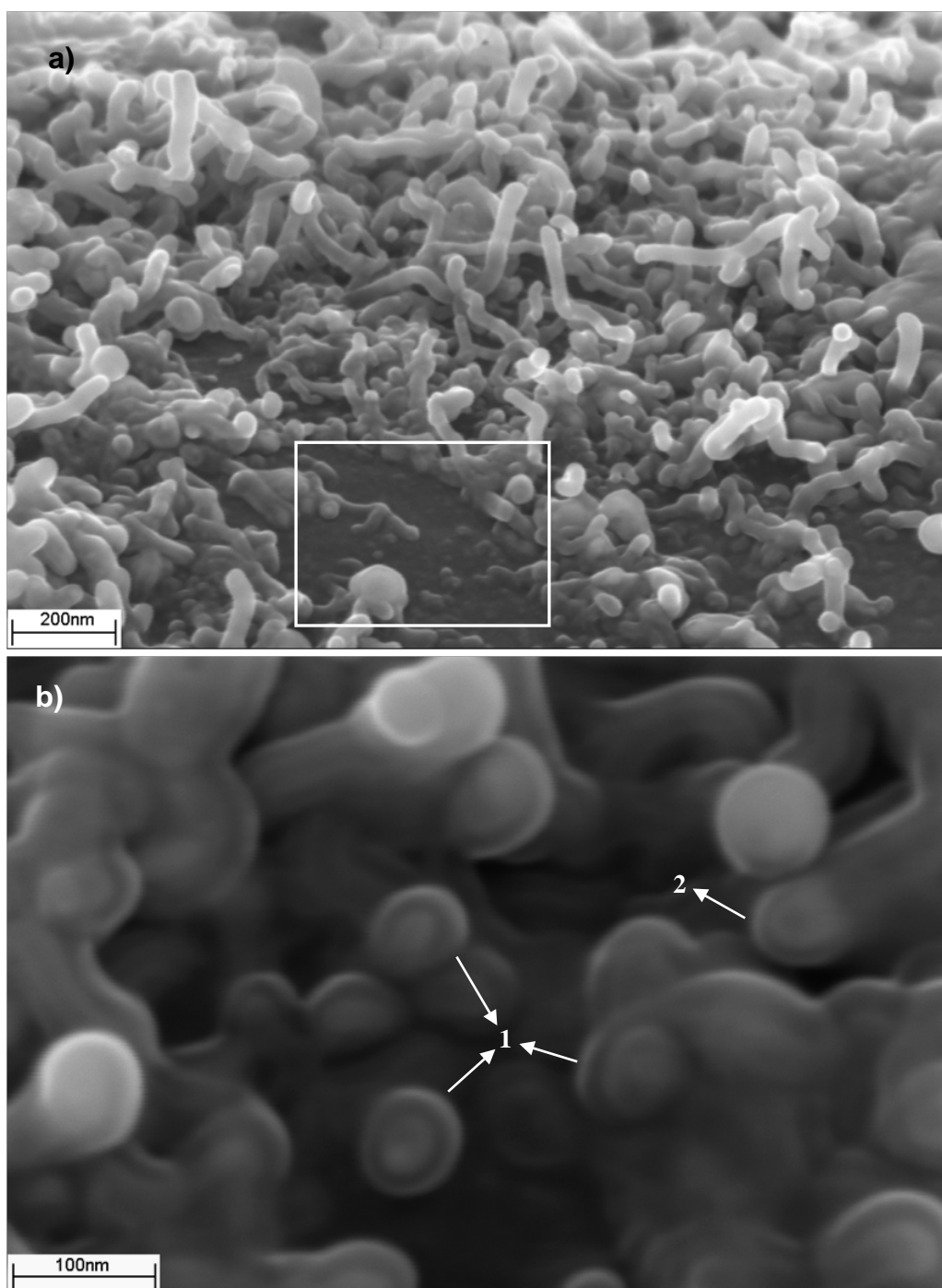


Figure 4.10 – CNTs developed on carbon fibre, under high SEM magnification to observe the CF sample shown in figure 4.9. a) overall view, and b) localised area.

Not all catalyst particles have CNTs attached, as the marked area shown in figure 4.10(a). The equivalent diameter of catalyst particles shown in figure 4.10(a), including those on tips of CNTs, was in the range from 8 ~ 32 nm, with an equivalent diameter of $24.6 \text{ nm} \pm 7.4 \text{ nm}$. It was suggested in figure 4.10(b) that the carbon deposition may result in encapsulation of catalyst particles, as the marked particles 1. No visible CNTs were observed on particles 1. Particle 2 has a CNT attached. Base on contrast of the SEM image, there may be carbon deposition on top surface of particle 2, which implies growth the CNT was terminated by the formation of an encapsulation of carbon deposition during CVD.

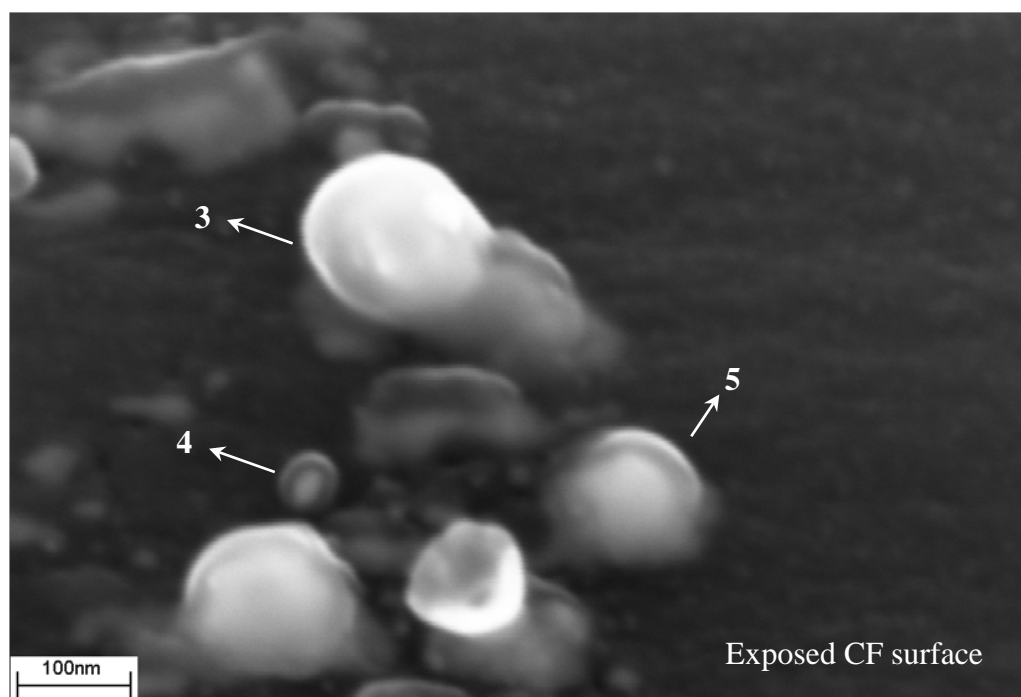


Figure 4.11 – Catalyst particles developed on carbon fibre, under high SEM magnification to observe the CF sample shown in figure 4.9.

A typical region was chosen to study initiation of the growth of CNTs on catalyst particles as shown in figure 4.11. The marked particle 3 was just lifted up from the surface of CF through growing up of a 'CNT root' from the substrate. It may imply that the carbon atoms could be absorbed on the top surface of the particle, and then diffused towards the interface between carbon and metal particle.

Particles 4 and 5 have no growth of CNTs attached. Based on contrast of the SEM image, both particle 4 and 5 were encapsulated in carbon deposition. The equivalent diameter of particle 4 was about 18 nm, which was in the size range as the diameter of CNTs. However, particle 4 was likely deactivated through rapid deposition of carbon, so free carbon atoms cannot be continuously absorbed due to the 'carbon shell'.

(d) CVD accomplished at 700°C.

When CVD was accomplished at 700°C, the size of catalyst particles in figure 4.12 was in the range from 8 ~ 65 nm, with an equivalent diameter of 28.2 nm, and a standard deviation of 18.2 nm. No visible CNTs were observed. Based on contrast of the SEM image, most of the catalyst particles were encapsulated by deposited carbon. The EDX analysis in the selected area also showed oxygen peak that implies the existence of cobalt oxides during crack of methane at 700°C.

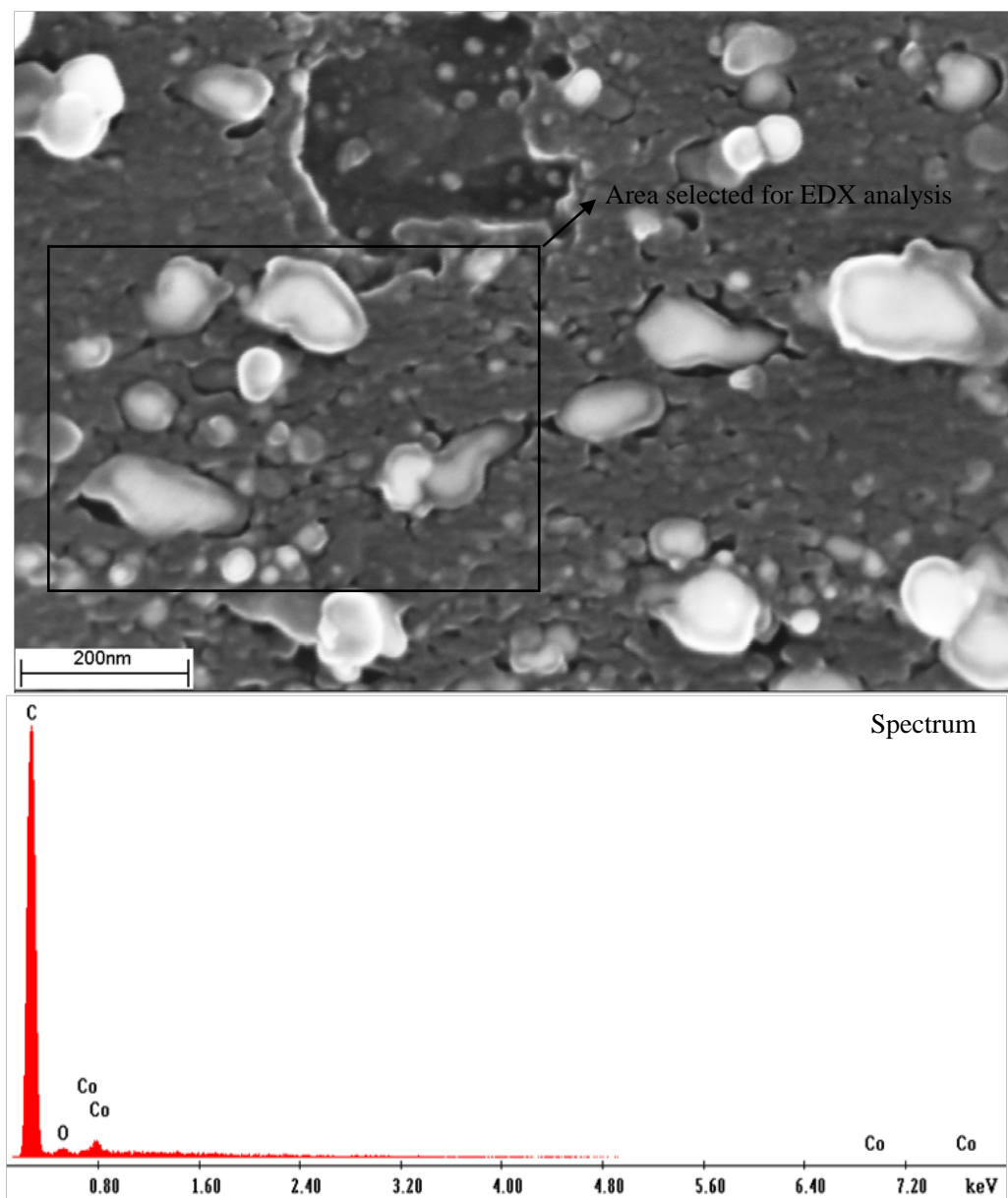


Figure 4.12 – Surface morphology on carbon fibre, with CVD at 700°C for 30 minutes, $\text{Co}(\text{NO}_3)_2$ solution concentration: 0.3 mol/l.

Table 4.2 – Summary of measurements on catalyst particles and CNTs in Fig.4.7~4.12.

| Images | CVD temperatures (°C) | Diameter range of catalyst particles (nm) | Averaged diameter of catalyst particles (nm) | Averaged diameter of CNTs (nm) | Max. length of CNTs (nm) |
|-----------|-----------------------|---|--|--------------------------------|--------------------------|
| Fig. 4.9 | 500 | 10 ~ 40 | 18.9±5.6 | X | X |
| Fig. 4.10 | 600 | 4 ~ 30 | 15.5±6.2 | 16.8±3.5 | 300 |
| Fig. 4.11 | 650 | 8 ~ 32 | 24.6±7.4 | 18.5±4.1 | 550 |
| Fig. 4.14 | 700 | 8 ~ 65 | 28.2±18.2 | X | X |

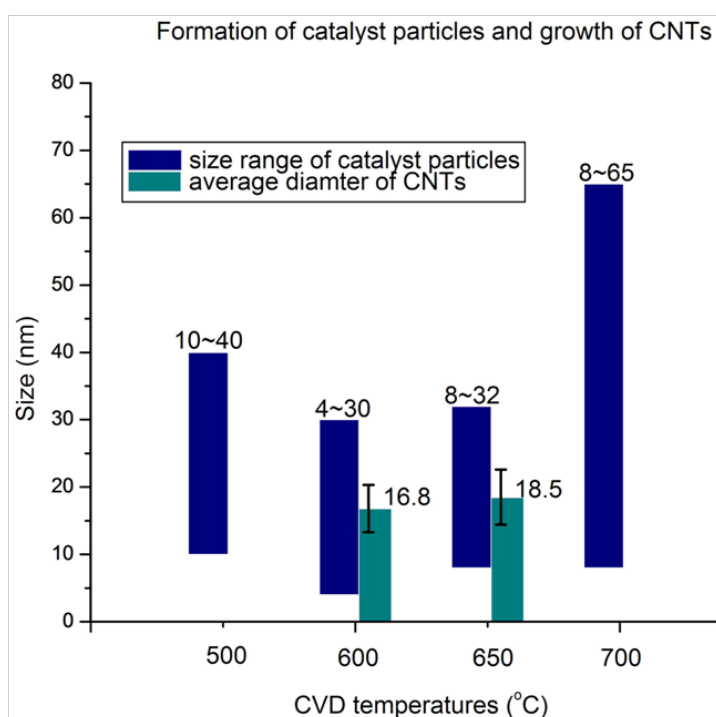


Figure 4.13 – Diagram to show the measured diameter range of catalyst particles and the averaged diameter of CNTs with standard deviation included by using various decomposing temperatures.

The experimental measurements in table 4.2 and figure 4.13 showed that growth of CNTs was only visible when CVD temperatures were at 600 and 650°C. The maximum length of CNTs was observed in figure 4.9 when CVD temperature was at 650°C. The averaged diameter of CNTs shown in figure 4.8 and figure 4.9 were similar, while increasing CVD temperature from 600 to 700°C leads to a broader size distribution of catalyst particles. The diameter of CNTs under the same CVD conditions was distributed in the range of 10 ~ 25 nm, which was not notably affected by the variations of CVD temperatures.

In summary, three parameters during CCVD process have been investigated and were found to be related to catalytic growth of CNTs, namely: the type, concentration of catalyst precursor and cracking temperature of methane. $\text{Co}(\text{NO}_3)_2$ was found to be the only precursor that is effective for catalytic growth of CNTs. While studying the CVD condition for growth of CNTs, the concentration of $\text{Co}(\text{NO}_3)_2$ was varied from 0.001 to 0.3 mol/l, and the cracking temperature of methane was increased from 500°C to 700°C. The size distribution of catalyst particles varied as increasing concentration of $\text{Co}(\text{NO}_3)_2$ and CVD temperature. However, the diameter of CNTs was found most popular on catalyst particles ranged from 10 to 25 nm. It was suggested that the initiation and growth of CNTs were based on continuous absorption of carbon atoms on top surface of catalyst particles, and diffused through the bulk materials into the structure of CNTs at the bottom of catalyst particles. On surface of PAN-based CF, a high yield of CNTs was observed as shown in figure 4.9, when CVD temperature was accomplished at 650°C for 30 minutes, by impregnating $\text{Co}(\text{NO}_3)_2$ with the concentration of 0.3 mol/l.

4.3.3 CNTs growing on PANOX CF block

An alternative source of CF: the CF block that derived from PANOX fibres in 3D structure for friction application was used to testify the in-situ growth of CNTs. As suggested in previous investigations, the sizing materials that introduced during manufacture of PAN-based CFs were found detrimental to uniform impregnation of catalyst particles and catalytic growth of CNTs. The CF block was claimed to have no sizing materials, and therefore, the surface of CFs from inside the CF block was impregnated with $\text{Co}(\text{NO}_3)_2$ without acid treatment.

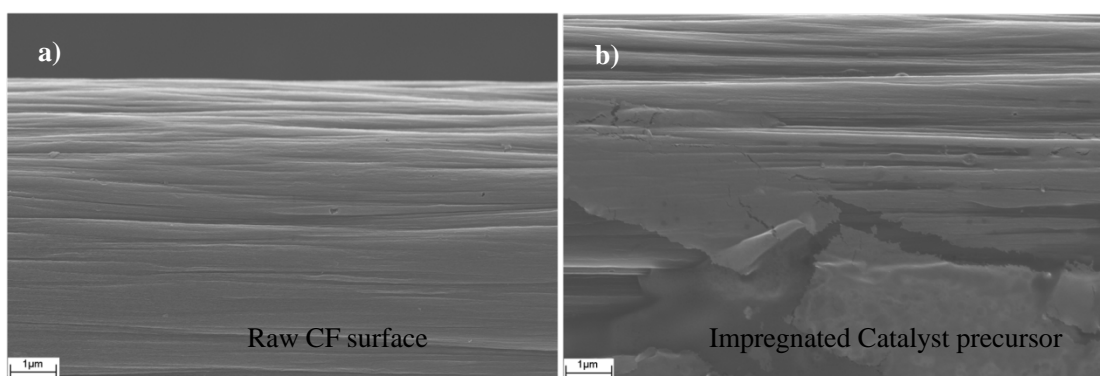


Figure 4.14 – Surface morphologies of CFs from CF block. Precursor solution: 0.05 mol/l $\text{Co}(\text{NO}_3)_2$. a) the raw CF surface; b) after impregnation of $\text{Co}(\text{NO}_3)_2$.

The typical surface feature of the raw CF surface from inside CF block was the groove topography, similar to that of as-treated PAN CF as shown in figure 4.1(d). As suggested in figure 4.14(b), after impregnation of $\text{Co}(\text{NO}_3)_2$, most area on surface of PANOX CF was coated with a layer of dried precursor solution. The CF sample was picked up randomly from inside of the CF block, which implies the precursor solution has wetted all carbon fibres within the

block.

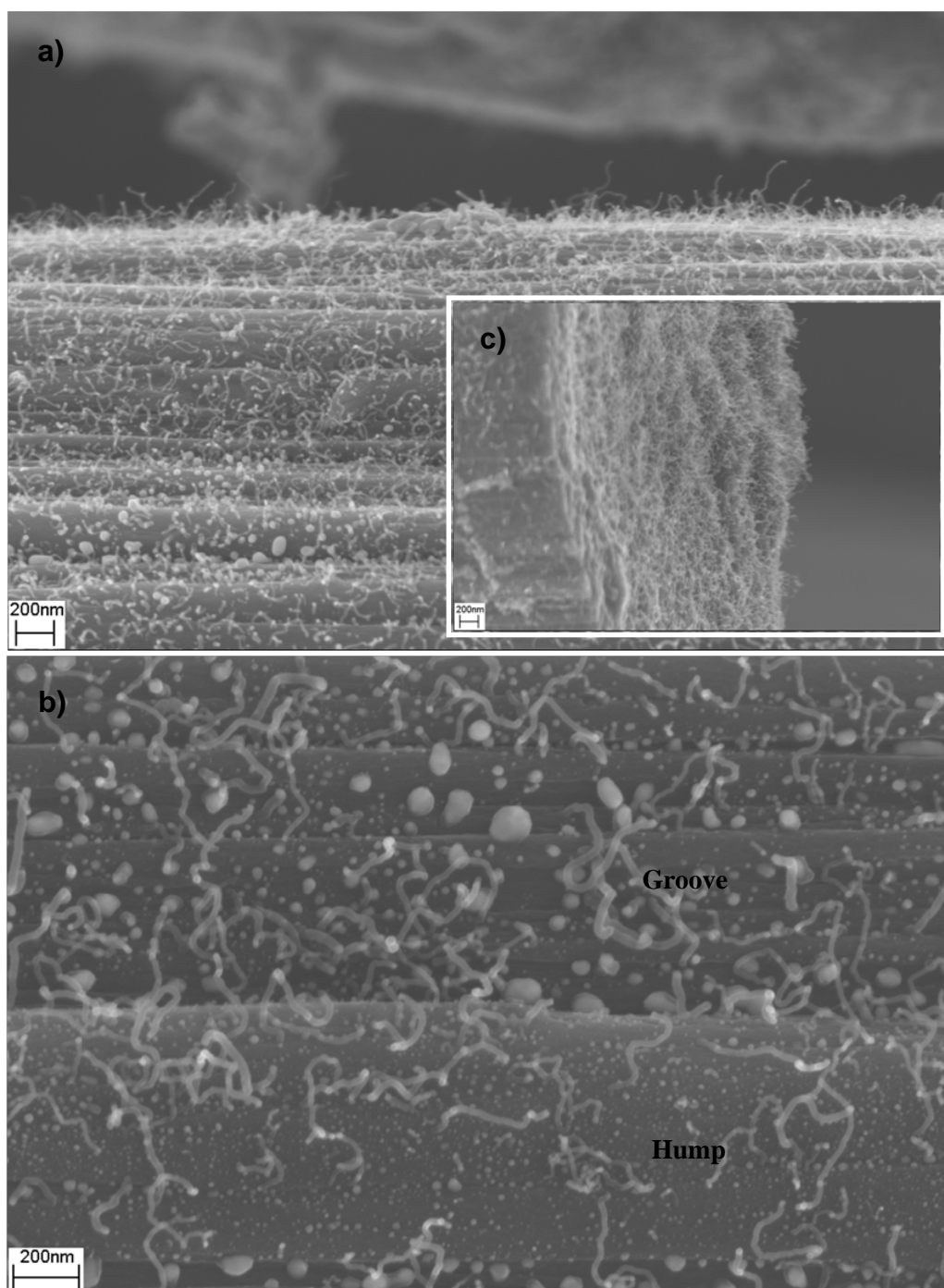


Figure 4.15 – Surface morphology on PANOX carbon fibre with CVD deposition for 60 minutes at 650°C, $\text{Co}(\text{NO}_3)_2$ solution with a concentration of 0.05 mol/l was used. a) overview of CNTs developed on surface of CF, b) appearance of CNT under high magnification, c) CNTs developed on fracture surface of CF.

As shown in figure 4.15, the formation of catalyst particles was not only on the humps but also within the grooves on surface of the PANOX carbon fibre. The size distribution of catalyst particles formed on the two types of surface topographies was also different. The average equivalent diameter of catalyst particles developed on humps was in the range from 5 ~ 30 nm, with an average value of 10.9 nm and a standard deviation of 6.5 nm; while within grooves, the average equivalent diameter of catalyst particles was in a broader range from 5 ~ 120 nm, with an average value of 22.1 nm and a standard deviation of 25.9 nm.

The growth of CNTs was observed on surfaces of humps and within grooves. The measured minimum diameter of the CNT from figure 4.15(b) was about 10 nm, and the maximum about 35 nm; further details on the distribution of the diameter of CNTs will be given in section 4.3.4.1. Compared to that on PAN-based CFs, the measured lower and upper boundary of the diameter of CNTs on PANOX CF had little difference, whilst the catalyst particles was of different size distribution and existing morphology. The measurements and the comparison may imply that the growth of CNTs had a clear selection on the size of catalyst particles.

The yield of CNTs counted on the PANOX-CF shown in figure 4.15(b) was about 55 per $1 \mu\text{m}^2$, significantly more than that on as-treated PAN-CF shown in figure 4.4(c), where only 35 CNTs were observed per $1 \mu\text{m}^2$, under the same CVD condition. The comparison implies the rough surface of CFs could prompt the growth of CNTs. Besides, the growth of CNTs was also developed on

fracture surface of PANOX CFs as suggested in figure 4.15(c).

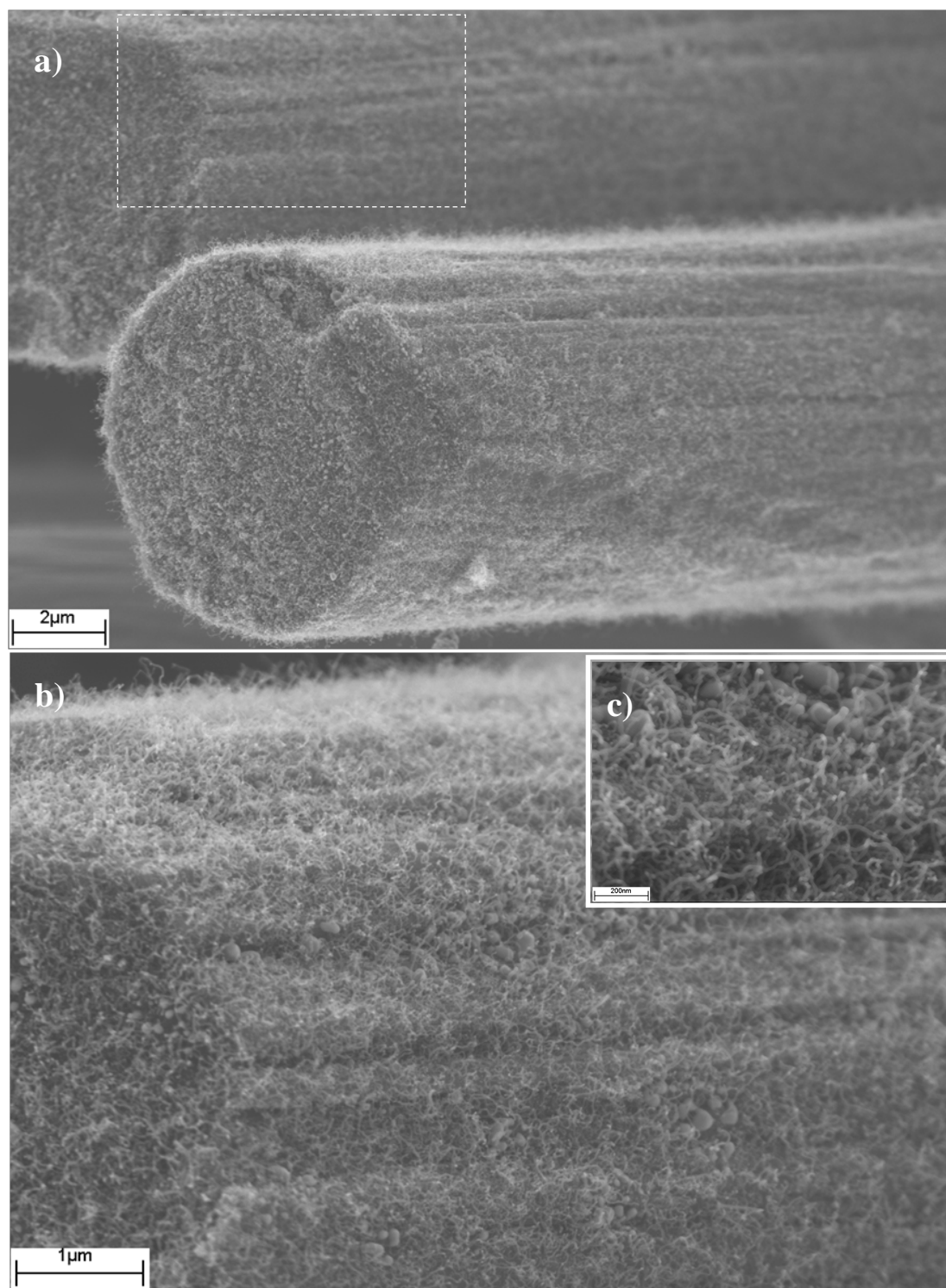


Figure 4.16 – Surface morphology on PANOX carbon fibre, with CVD at 650°C for 60 minutes, and $\text{Co}(\text{NO}_3)_2$ solution concentration: 0.3 mol/l. b) was magnified area in a), and c) was magnified area in b).

After CVD, the CF block was torn up in the middle and observed under SEM as shown in figure 4.16. On surface of PANOX CF, a significant increase of the yield of CNTs was observed compared to that in figure 4.15, the magnified image (c) suggested the yield was about 1000 CNTs per $1 \mu\text{m}^2$, estimated in the software of 'ImageJ 1.42q'. The diameter of CNTs was in the range from about 9 ~ 30 nm, with an average equivalent diameter of 14.3 nm and a standard deviation of 5.4 nm.

The growth of CNTs on surface of PANOX CF was optimised when CVD was accomplished at 650°C and the surface of CF was impregnated with 0.3 mol/l $\text{Co}(\text{NO}_3)_2$, which is the same processing condition as preparing CNTs on surface of PAN-based CF as shown in figure 4.9.

4.3.4 Microstructural analysis of catalyst particles and growth of CNTs

4.3.4.1 Analysis of the size of catalyst particles

Two common features of growth of CNTs on surface of CFs were clearly indicated: 1) catalytic growth of CNTs was on catalyst particles by lifting them up in tips of CNTs, the outer diameter of which was the same as that of catalyst particles, 2) not all catalyst particles have CNTs attached under all CVD conditions. It has been observed that the catalytic growth of CNTs was only popular on catalyst particles in a certain size range from 10 to 30 nm in diameter.

The relationship was studied in terms of the quantification of population of catalyst particles with growth of CNTs within all particles in the selected area for investigation. The population of catalyst particles for catalytic growth of CNTs was studied on a series of CNTs/CF samples prepared at a CVD temperature of 600°C and 650°C. At 600°C, samples were analysed as the concentration of $\text{Co}(\text{NO}_3)_2$ increased from 0.001 to 0.1 mol/l. At 650°C, the PANOX CF block coated with 0.05 mol/l $\text{Co}(\text{NO}_3)_2$ was also analysed.

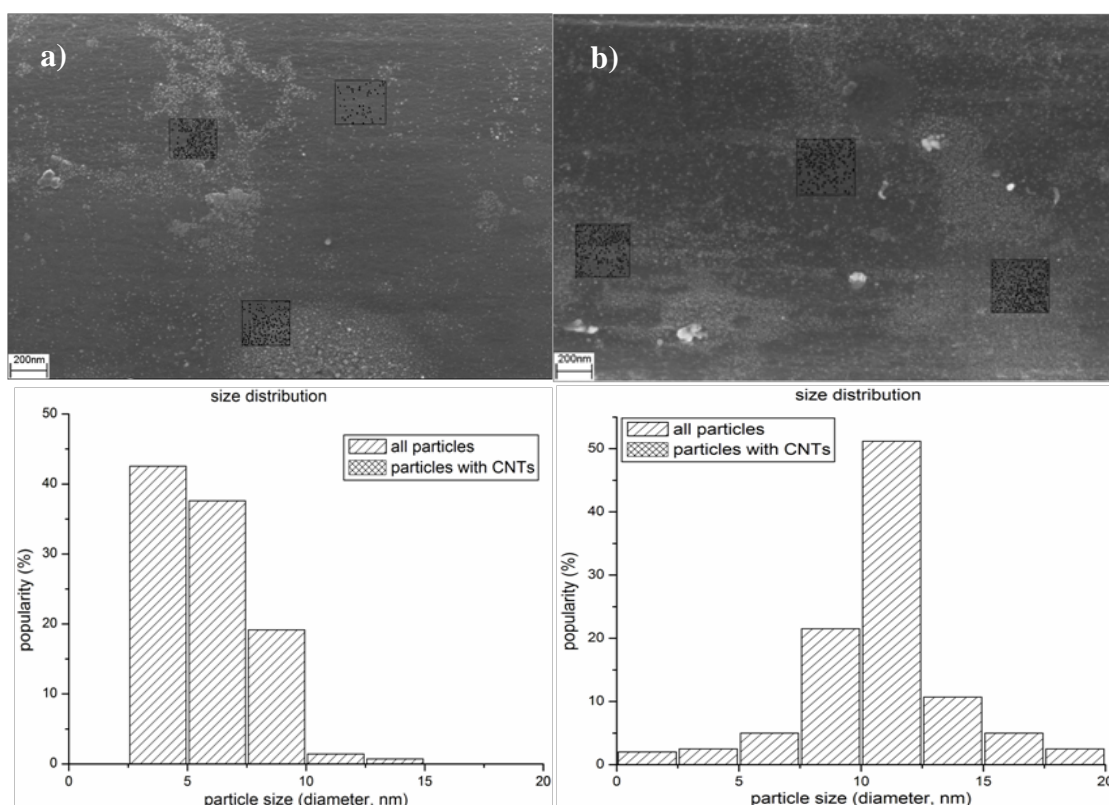


Figure 4.17 – Morphology of catalytic particles on the surface of carbon fibres and the histogram distribution of their size by using $\text{Co}(\text{NO}_3)_2$ solution with different concentrations: (a) 0.001 mol/l, and (b) 0.005 mol/l.

At 0.001 mol/l, as shown in figure 4.17, the size of catalyst particles was distributed in the range from 2.5 to 15 nm. Around 80% of the population was

around 5 nm in diameter. However, there were no visible CNTs on surface of CFs. The catalytic growth of CNTs was started to become visible when the concentration was increased to 0.005 mol/l, while particles were formed between 2.5 and 20 nm, and up to 50% of which were around 10 nm in diameter. As increasing of the concentration of catalyst precursor from 0.001 to 0.005 mol/l, the density of particles (*No. of particles per area*) was increased from 2500 to 3500 per 1 μm^2 .

At 0.05 mol/l, as shown in figure 4.18, the size distribution of catalyst particles was in the range from 2.5 to 40 nm. Catalytic growth of CNTs was clearly visible on CFs. However, the histogram diagram suggested that over 70% of the particles were in the range from 5 to 10 nm, where the growth of CNTs was not observed at all. From 10 to 20 nm, about 20% of the catalyst particles were counted in this range, while up to 55% of which were lifted up by catalytic growth of CNTs.

Figure 4.19 presented the procedures of measuring the size of catalyst particles through which CNTs successfully grew. Images (a) and (b) presented the selection of catalyst particles with growth of CNTs, while images (c) and (d) presented all catalyst particles within the selected area, including those with CNTs attached. The selective catalysation was also found when the concentration was at 0.1 mol/l. The equivalent diameter of catalyst particles was distributed in a broadened range from 2.5 to 60 nm, over 60% of which were between 2.5 and 10 nm. The histogram diagram suggested the majority of CNTs were catalysed by particles between 10 to 25 nm. About 35% of catalyst

particles were in this range, and around 20% of them had successfully catalysed the growth of CNTs.

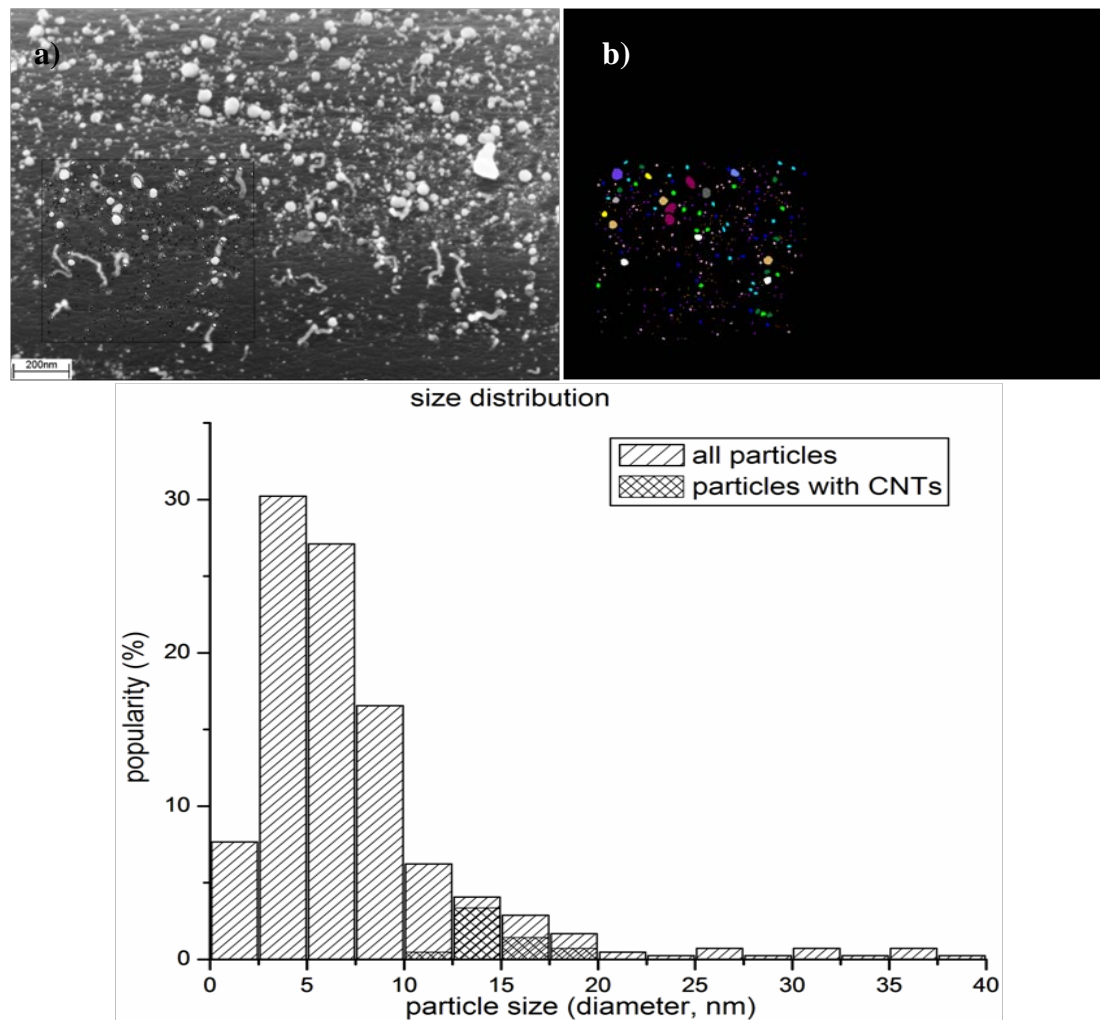


Figure 4.18 – Catalytic particles on the surface of carbon fibres and the histogram distribution of their size by using 0.05 mol/l $\text{Co}(\text{NO}_3)_2$ solution. a) selecting typical area in the SEM image, and b) catalyst particles distinguished by the software of “Image Tool”.

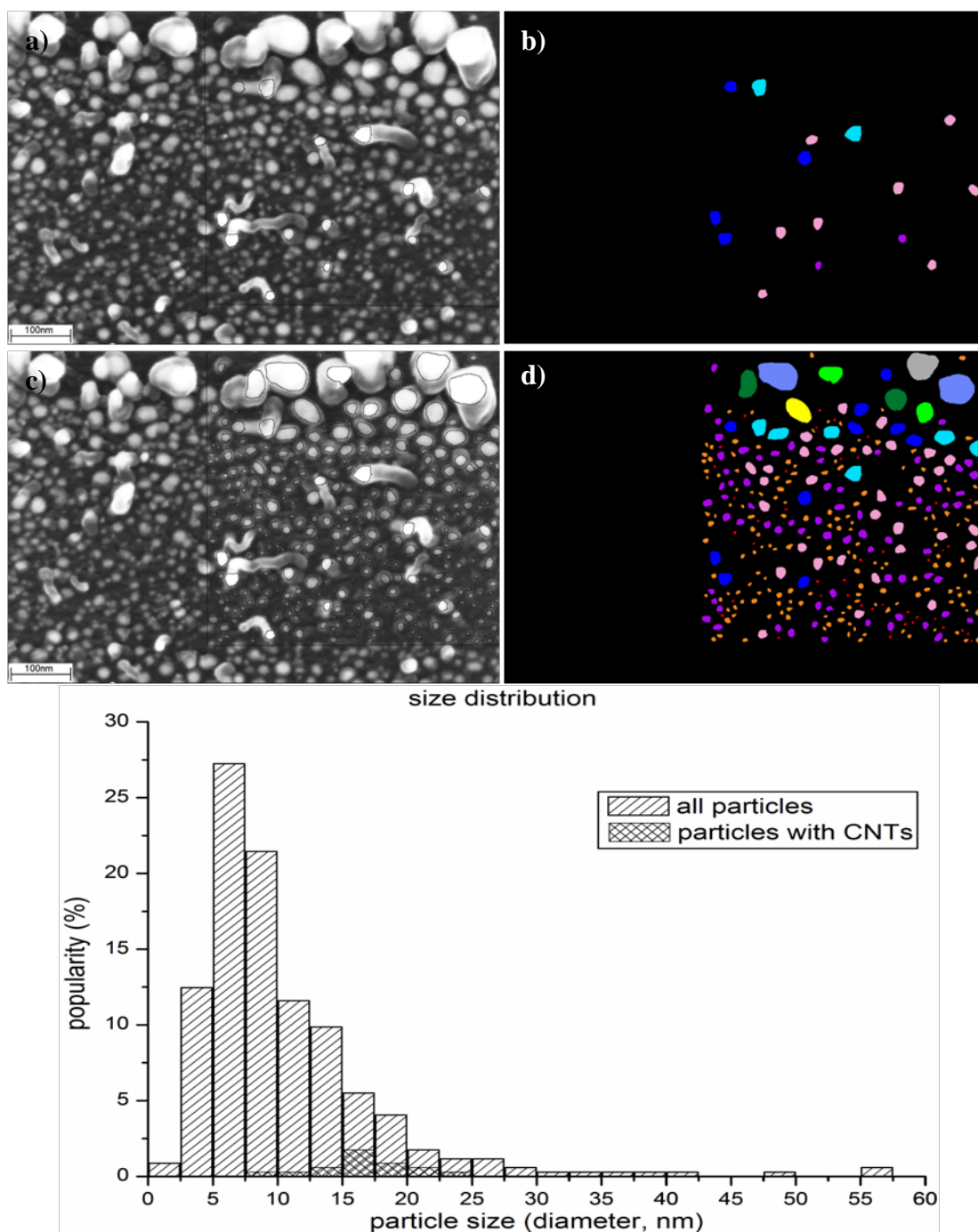


Figure 4.19 – Catalytic particles on the surface of carbon fibres and the histogram distribution of their size by using 0.1 mol/l $\text{Co}(\text{NO}_3)_2$ solution. a) select active catalyst particles and distinguished in b); c) select all catalyst particles and distinguished in d).

The selective growth of CNTs on catalyst particles within a certain size range was universally observed on surface of PAN-CFs under different CVD conditions. Based on previous analysis, the size distribution of catalyst particles

became broader as increasing the concentration of $\text{Co}(\text{NO}_3)_2$ from 0.001 to 0.1 mol/l. Even though the size distribution of catalyst particles varied when the concentration of $\text{Co}(\text{NO}_3)_2$ increased, the catalytic growth of CNTs was seen only on catalyst particles that have a size range of 10 to 25 nm in diameter.

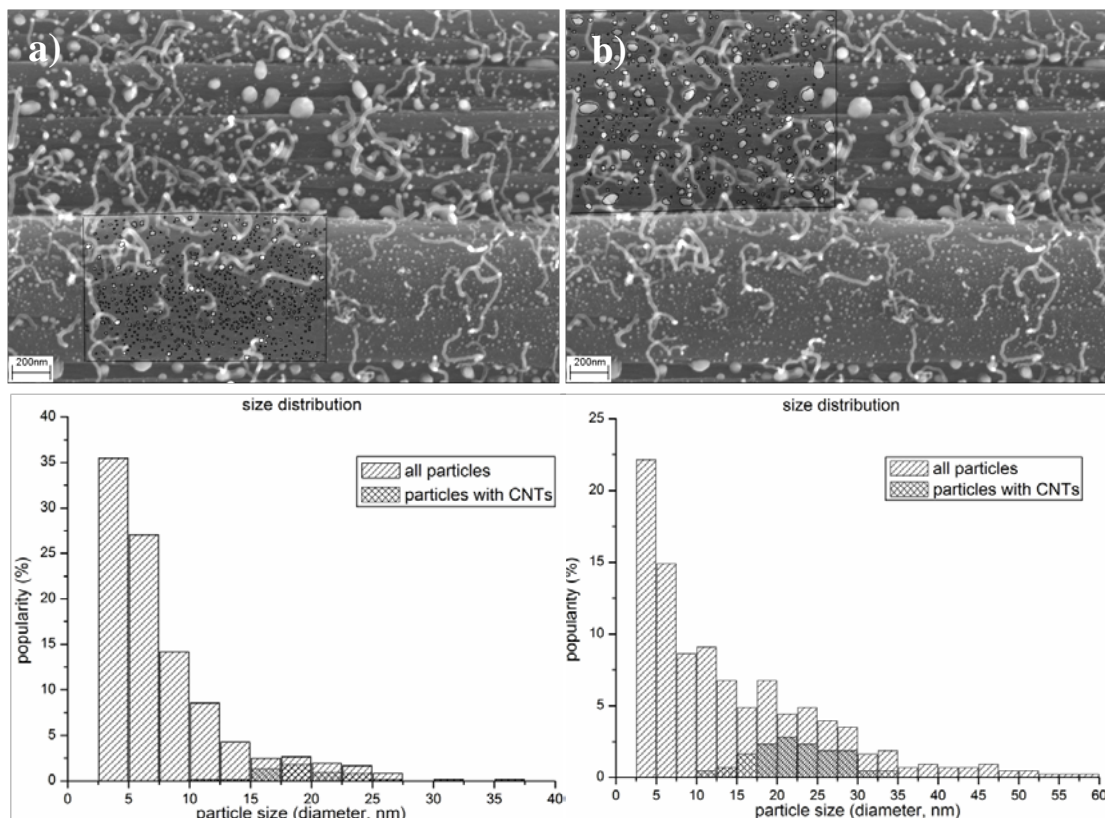


Figure 4.20 – Catalytic particles on the surface of PANOX-CF and the histogram distribution of their size by using 0.05 mol/l $\text{Co}(\text{NO}_3)_2$ solution: (a) on a hump, and (b) within grooves.

The selective catalysation for growth of CNTs was also observed on surface of PANOX-CFs as shown in figure 4.20. Typical surface feature of PANOX CFs was usually consists of humps with smooth surface and grooves. The catalyst particles formed on surface of humps have a narrow size distribution than that within grooves, in the range from 2.5 to 35 nm, where up to 90% of them were

between 2.5 and 15 nm. However, catalytic growth of CNTs was only visible on particles between 15 and 25 nm. About 9% of catalyst particles were in this range, and around 65% of them had successfully catalysed the growth of CNTs. Within grooves, even though particles were distributed in a broadened size range from 2.5 to 60 nm, growth of CNTs was selectively catalysed by particles between 10 and 35 nm. Up to 50% of catalyst particles were in this range, and about 40% of which were catalytic effective for growth of CNTs.

The particle size analysis above suggested three features that were commonly observed in the results: 1) almost all the CNTs were in tip-growth mode, and their diameters were similar to that of catalyst particles, which were lifted up from surface of CFs at the tips of CNTs; 2) catalytic growth of CNTs was found only popular on particles in a certain size range starts from about 10 nm and ends at approximately 35 nm; 3) In the popular size range, not all particles have catalysed the growth of CNTs. Certain amount of particles were still left on surface of CFs after CCVD process, even their size was statistically favourable for catalytic growth of CNTs.

4.3.4.2 TEM analysis of catalyst particles and growth of CNTs

Previous investigations did not answer why some of the catalyst particles were lifted up by growth of CNTs, while others were still left on the substrate, even though they had similar size. It was suspected that the interfacial contact between bottom of the catalyst particles and surface of the substrate might have been the cause.

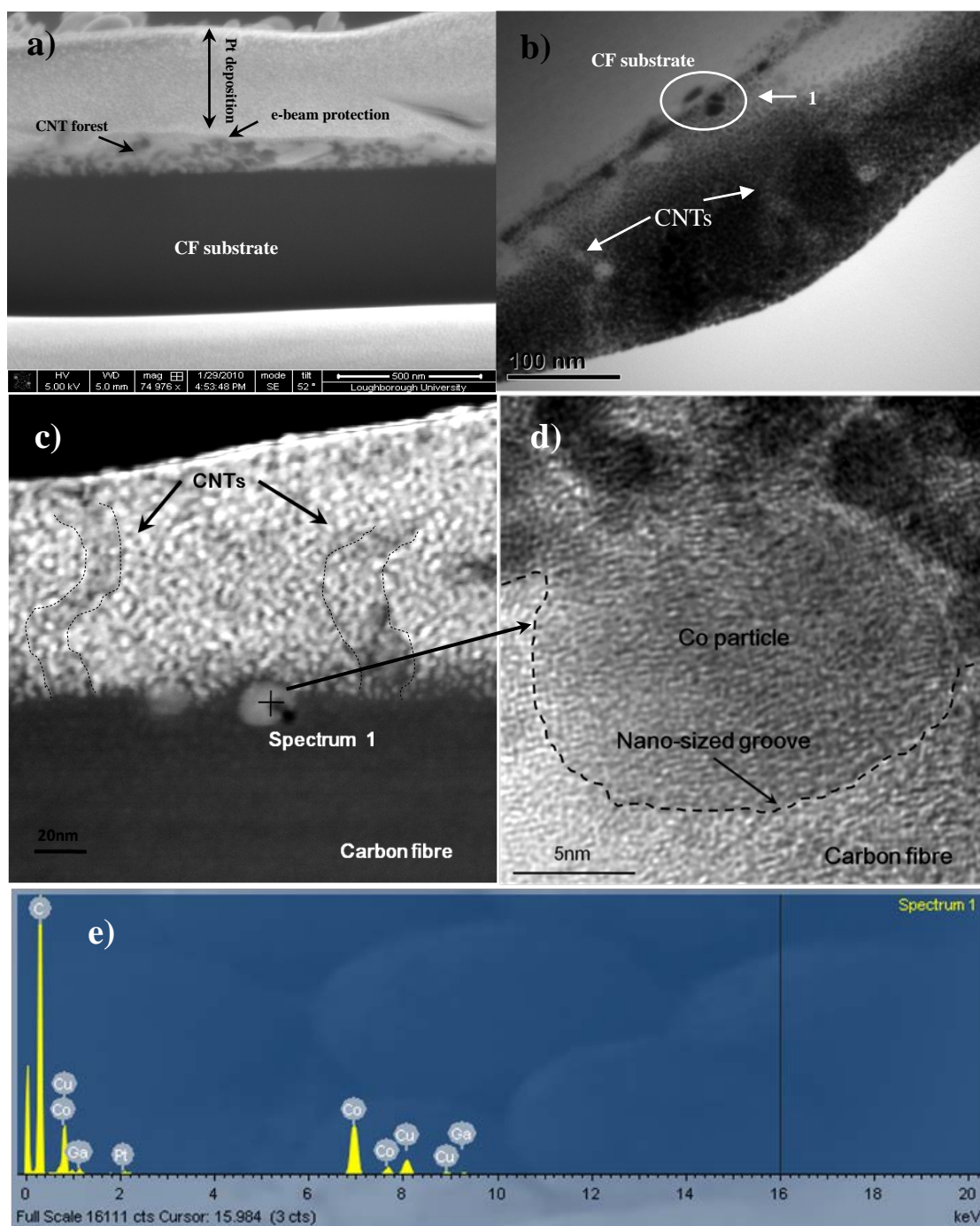


Figure 4.21 – TEM sample preparation and observation of CNTs/CF sample shown in figure 4.9. a) TEM sample preparation by FIB; b) bright field imaging of CNTs on surface of CF; c) and d) same particle imaged under STEM mode and HR-TEM, respectively; e) EDS spectrum of the particle shown in c) and d).

TEM samples were prepared to study the physical contact between the catalyst particles and surface of CFs. Typical catalyst particles were selected with the

diameter between 10 and 30 nm and no visible growth of CNTs.

The CNTs/CF sample (*shown in figure 4.9*) was also used to prepare TEM samples in dualbeam FIB system. The cross-sectional image in figure 4.21(a) suggested the 'forest' of CNTs was well preserved under layers of Pt electron and ion beam deposition. In the bright field TEM imaging mode, the dark regions on surface of CFs were agglomerates of catalyst particles as marked in figure 4.21(b). It was suggested that some of the particles were lifted up from surface of CFs along the growing tracks shown as the white stripes in the dark region of Pt protecting layer. The agglomerated particles on surface of CFs have similar size as that of CNTs. However, the physical contact area for each particle in the agglomerate could be more complex than what the image displayed, considering the contacting context in 3 dimensions. There were also isolated particles which were not catalysed growth of CNTs and left on surface of CFs in figure 4.21(b). These particles were further investigated under TEM observations.

Under STEM imaging mode, two typical particles were located on surface of CFs, close to which catalytic growth of CNTs were also observed in figure 4.21(c). The diameter of particles was similar to that of CNTs, which was around 20 nm. EDS analysis on one of the particles marked as 'Spectrum 1' suggested its chemical composition was cobalt as shown in figure 4.21(e). The particles were isolated from surrounding substances, but did not catalyse for the growth

of CNTs. When taking the particle of 'Spectrum 1' under HR-TEM observation, over 50% of its surface area was embedded within a nano-sized groove on surface of CF, the width of which was about 17 nm as shown in figure 4.21(d). If the formation of a catalyst particle was positioned within a groove as suggested above, extended physical contact was expected, leading to increased interfacial bonding area between catalyst particles and the substrate. At the initiation of a catalytic growth of CNT, more force was required to separate the catalyst particle and the substrate as increasing the interfacial bonding area.

CHAPTER 5 CNTs In-situ Growth on Ceramic Particles

In-situ catalytic growth of CNTs was conducted inside various ceramic powders, including SiC, Al₂O₃ and Y-TZP. Same processing parameters as that used for CNTs/CF preform as shown in figure 4.16: growth for all powders were subjected to a heat treatment in the tube furnace with flowing methane at 650°C for 60minutes. Co(NO₃)₂ solution with concentrations of 0.3 and 0.6 mol/l were set for the trials. Attrition milling was also used on the source powders to change the size of the ceramic particles, when the impact of the size was considered.

5.1 In-situ growth of CNTs on surface of SiC

An overview of the surface after completing the CNT growth, directly on the surface of SiC grits (320#, *equivalent to 46 μm in diameter*) is shown in figure 5.1. Visible CNTs appeared on the surface; catalyst particles were lifted up from

the surface by the CNTs.

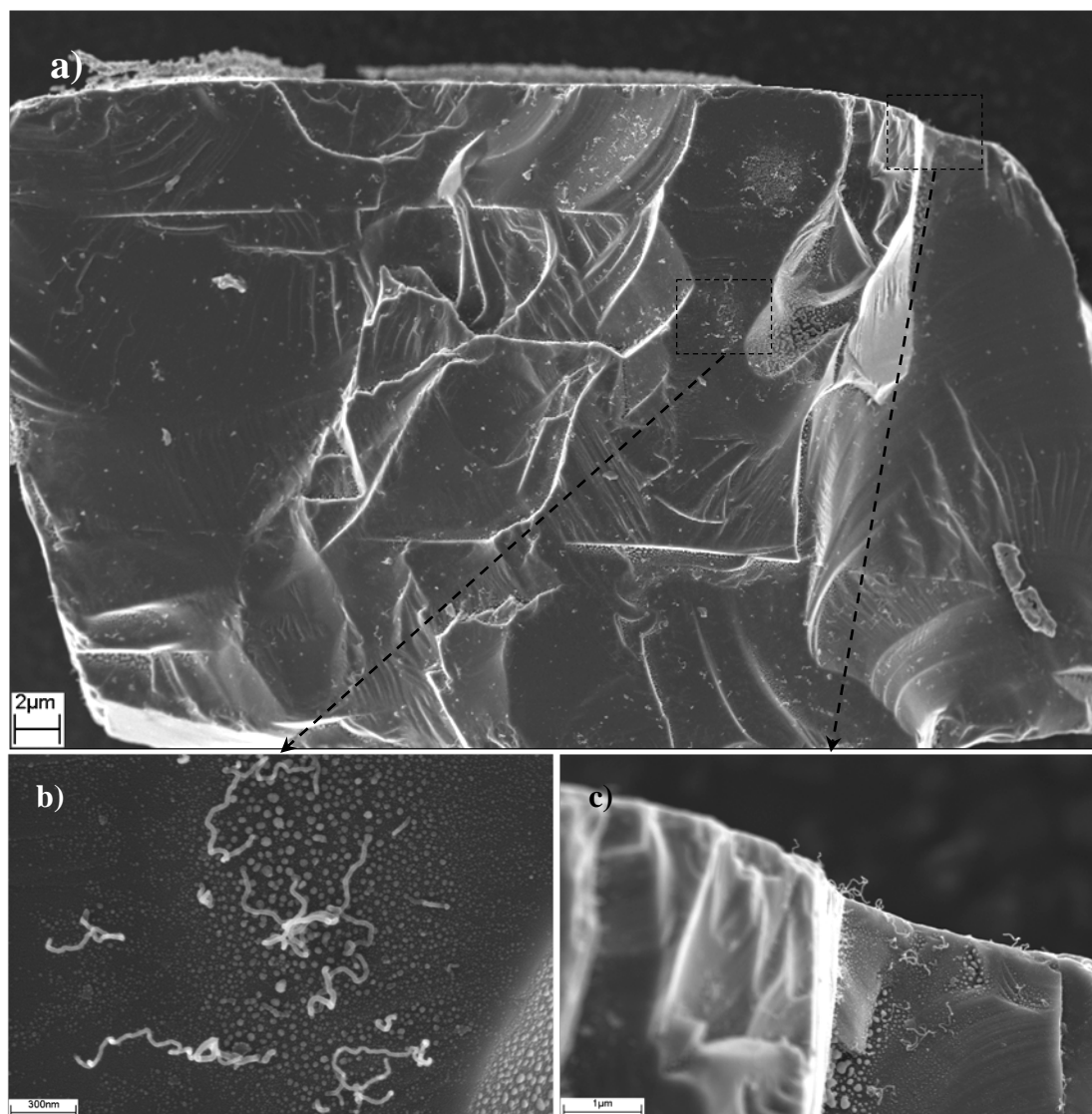


Figure 5.1 – a) An overview of the deposition of catalyst particles and the growth of CNTs on the surface of a SiC grit, concentration of $\text{Co}(\text{NO}_3)_2$ solution was 0.3 mol/l; b) and c) more details on the catalyst particles and CNTs under high magnifications.

As indicated in figure 5.1(b), the size of catalyst particle was measured in the range from about 5 to 50 nm in diameter. However, the growth of CNTs was only on catalyst particles with sizes ranging from 15~25 nm, with an average equivalent diameter of 20.3 nm and a standard deviation of 2.7 nm; this range is

close to the range of 10~30 nm measured on surface of CFs. The coverage of CNTs was not uniform on the substrate, possibly due to the poor coating of $\text{Co}(\text{NO}_3)_2$ as a result of complex surface topography of the SiC particle.

Under the same conditions, the SiC grits were attrition milled at 300 rpm for 4 hours before CVD process. Compared to the source powder, the size of SiC grits was significantly reduced and some typical particles was in the range from 5~10 μm , measured from figure 5.2. The $\text{Co}(\text{NO}_3)_2$ solution with the concentration of 0.6 mol/l was impregnated to attrition milled SiC grits and growth of CNTs was visible shown in figure 5.2.

The equivalent diameter of catalyst particles shown in figure 5.2(a) was in the range from about 8 to 100 nm. However, as indicated in the magnified area in figure 5.2(b), the majority of CNTs were on catalyst particles with equivalent diameter ranged from 15~30 nm, with an average value of 20.9 nm and a standard deviation of 5.7 nm.

It was suggested from figure 5.3 that increasing the concentration of $\text{Co}(\text{NO}_3)_2$ solution leads to the formation of catalyst particles with a much broader size range in diameter. However, the growth of CNTs on surface of milled and un-milled SiC particles was observed on catalyst particles only ranging from 10 to 30 nm. It seems that the particle size of ceramic powder has no visible effect on catalytic growth of CNTs.

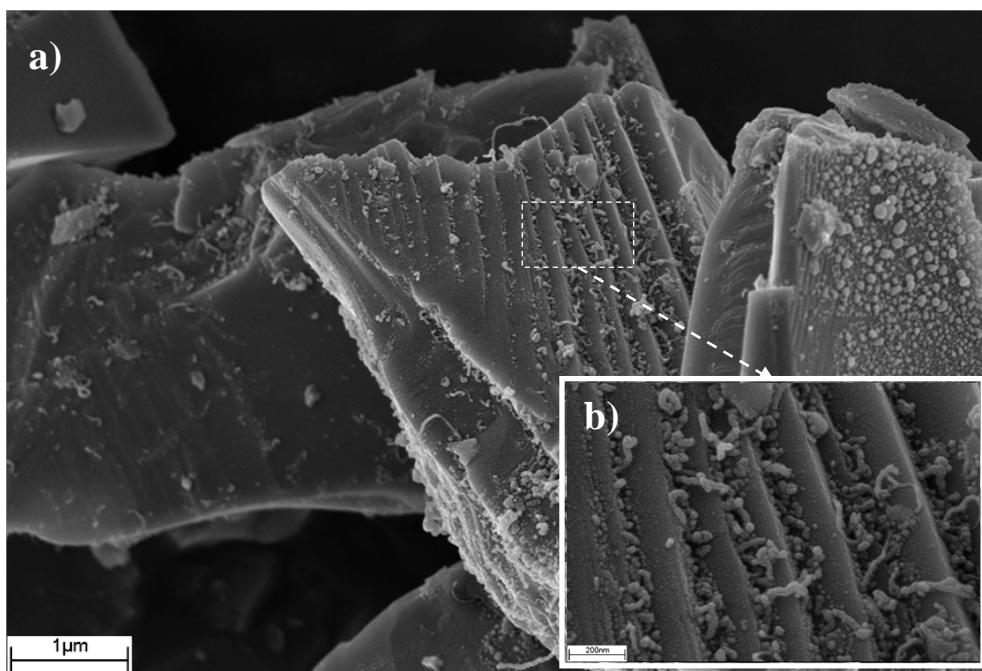


Figure 5.2 – a) An overview deposition of catalyst particles and the growth of CNTs on the surface of attrition milled SiC grits, concentration of $\text{Co}(\text{NO}_3)_2$ solution was 0.6 mol/l; b) more details of CNTs under high magnification.

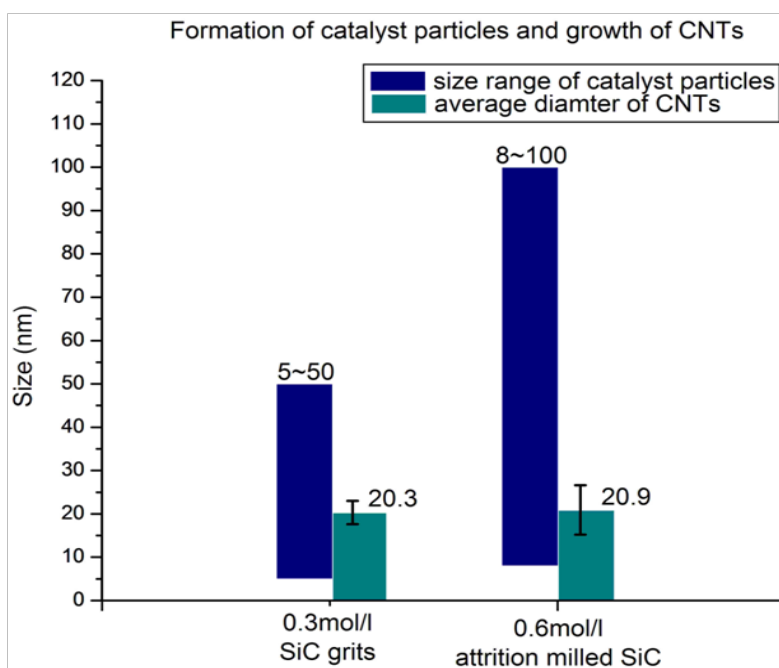


Figure 5.3 – Diagram to show the measured diameter range of catalyst particles and the averaged diameter of CNTs with standard deviation included by using SiC particles with different size distributions and concentrations of catalyst precursor.

5.2 In-situ growth of CNTs on surface of Al₂O₃

Catalytic growth of CNTs was studied for three types of Al₂O₃ powders under two concentrations of Co(NO₃)₂ solution. The CNTs grown on 'AO-micron' alumina powder was shown in figure 5.4. Figure 5.4(a) showed a general picture of some typical 'AO-micron' alumina particles. The scale bar of figure 5.4(a) suggested the particle size was about 10 μm as claimed by the provider (*Sigma-Aldrich, UK*). After CVD process, surface of the Al₂O₃ particle was completely covered by high density of CNTs. Figure 5.4 (a) also suggested not all Al₂O₃ particles were deposited by high density of CNTs.

Figure 5.4 (b) gives details of surface morphology of the Al₂O₃ particle shown in figure 5.4 (a). Some catalyst particles were observed on the edge of the Al₂O₃ particle, while others were lifted up by growth of CNTs at their tips. Diameter of the CNTs measured from figure 5.4(b) was in the range from about 15~30 nm, with the averaged diameter of 20.1 nm and a standard deviation of 4.2 nm. The maximum length of CNTs that can be observed from figure 5.4(b) was up to 3 μm.

Compared to CNTs/ceramic composites prepared through ex-situ method, the CNTs prepared from in-situ method were homogeneously dispersed on surface of Al₂O₃ particles without agglomeration. It has opened a potential application of manufacture of homogeneously reinforced ceramic composites by CNTs.

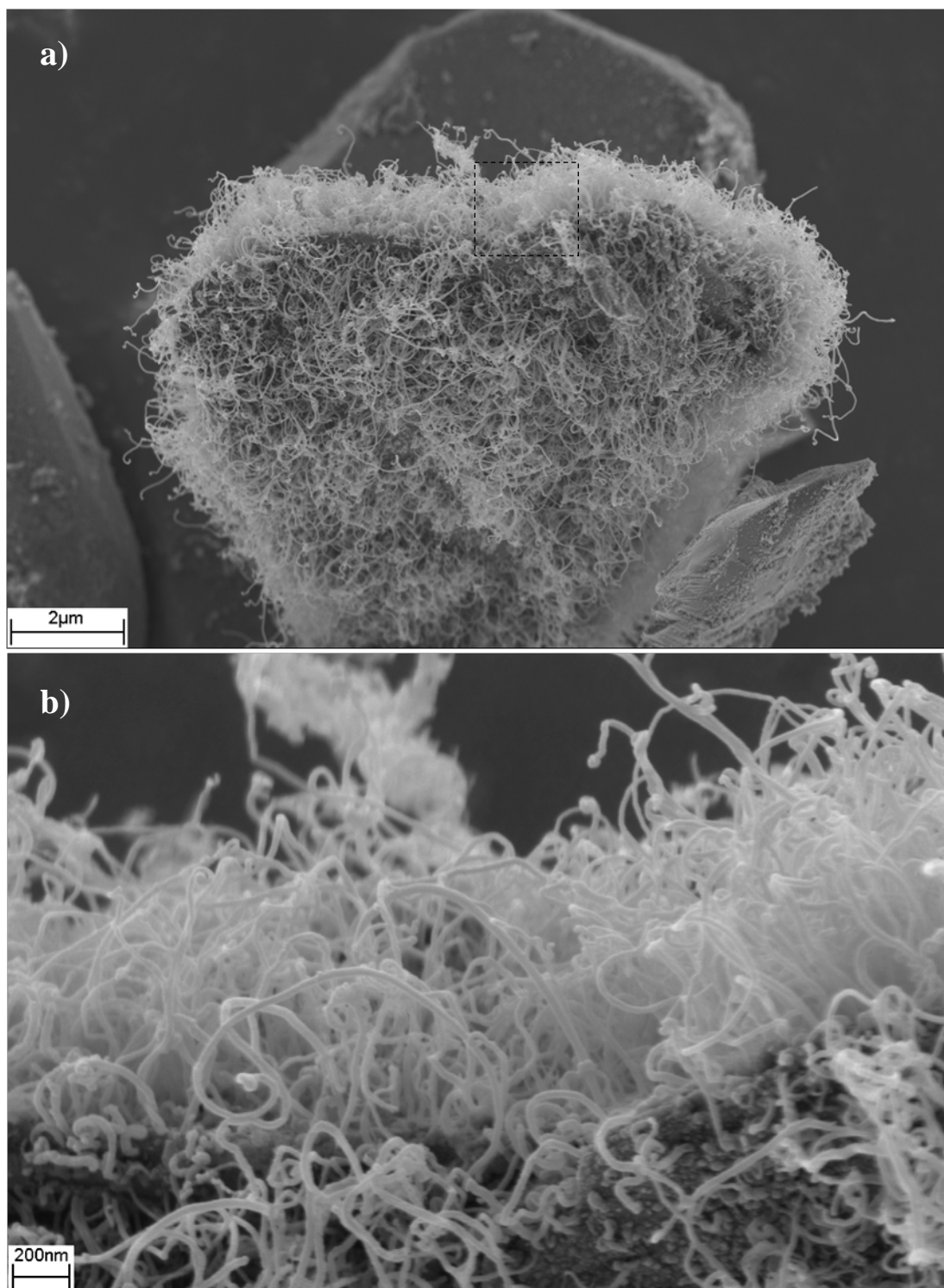


Figure 5.4 – CNTs grown on the surface of Al_2O_3 . a) overview; b) zoom-in view.

When the concentration of $\text{Co}(\text{NO}_3)_2$ solution was increased to 0.6 mol/l, and all the other conditions were maintained the same, growth of CNTs on 'AO-micron' alumina particles was shown in figure 5.5. Figure 5.5(a) showed the general picture of the growth of CNTs, and it suggested CNTs were homogeneously dispersed among Al_2O_3 grits. Almost all Al_2O_3 particles in the microscopic view of figure 5.5(a) had CNTs grown up.

The zoom-in view from figure 5.5(b) & (c) suggested the coverage of CNTs on surface of Al_2O_3 grits was not uniform. Some regions rarely had CNTs and some were covered with high density of CNTs. This heterogeneity of growth might have been related to non-uniform deposition of $\text{Co}(\text{NO}_3)_2$ precursor solution on the surface of Al_2O_3 grits.

Figure 5.5(c) showed a magnified area in figure 5.5(b) covered with high density of CNTs. The diameter of CNTs measured from figure 5.5(c) was between 15 and 35 nm, with the average value of 27.3 nm and a standard deviation of 6.6 nm.

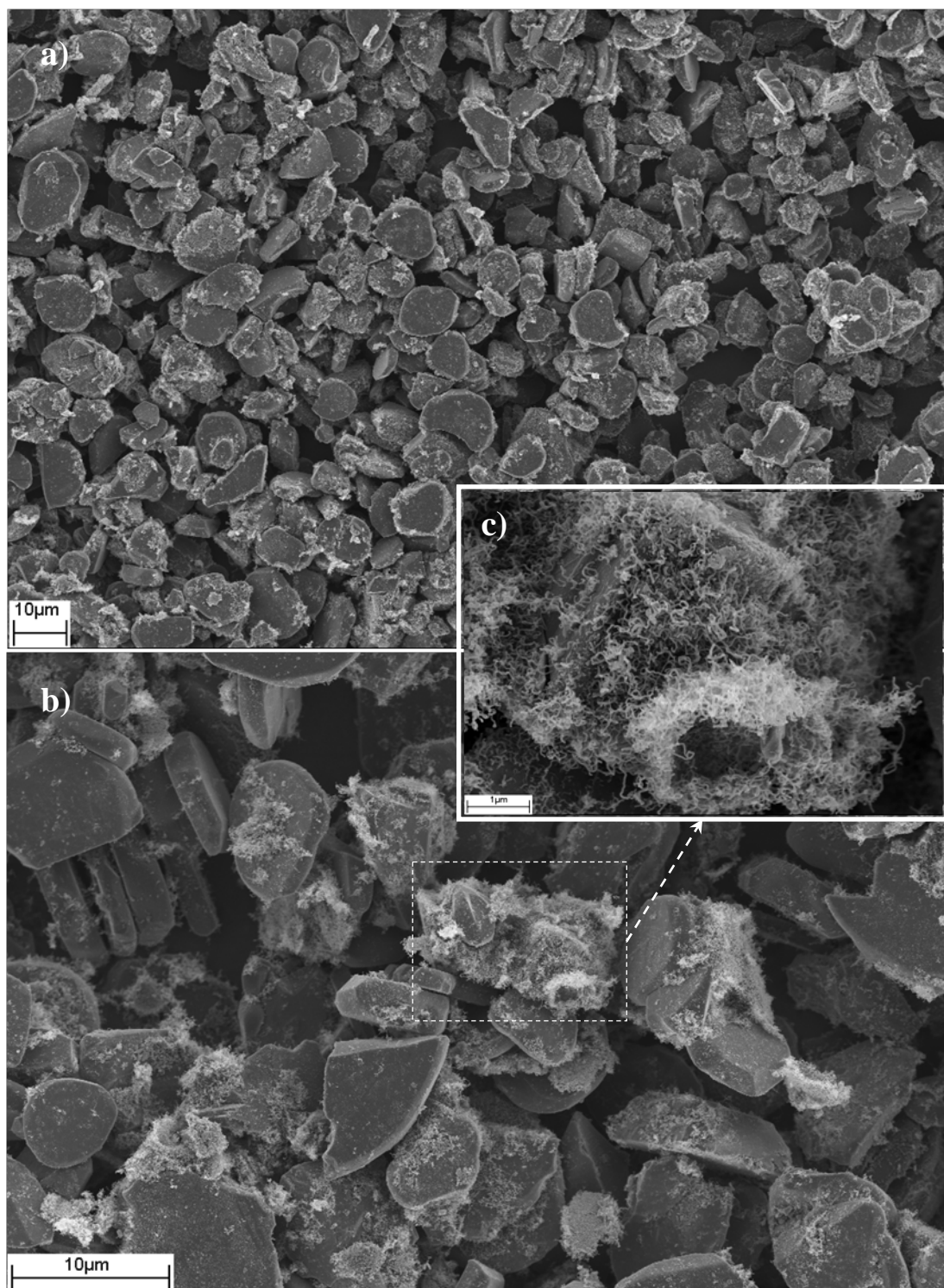


Figure 5.5 – CNTs grown on the surface of Al_2O_3 processed with 0.3 mol/l $\text{Co}(\text{NO}_3)_2$ solution for ‘AO-micron’ alumina. a) overview b) and c) zoom-in view.

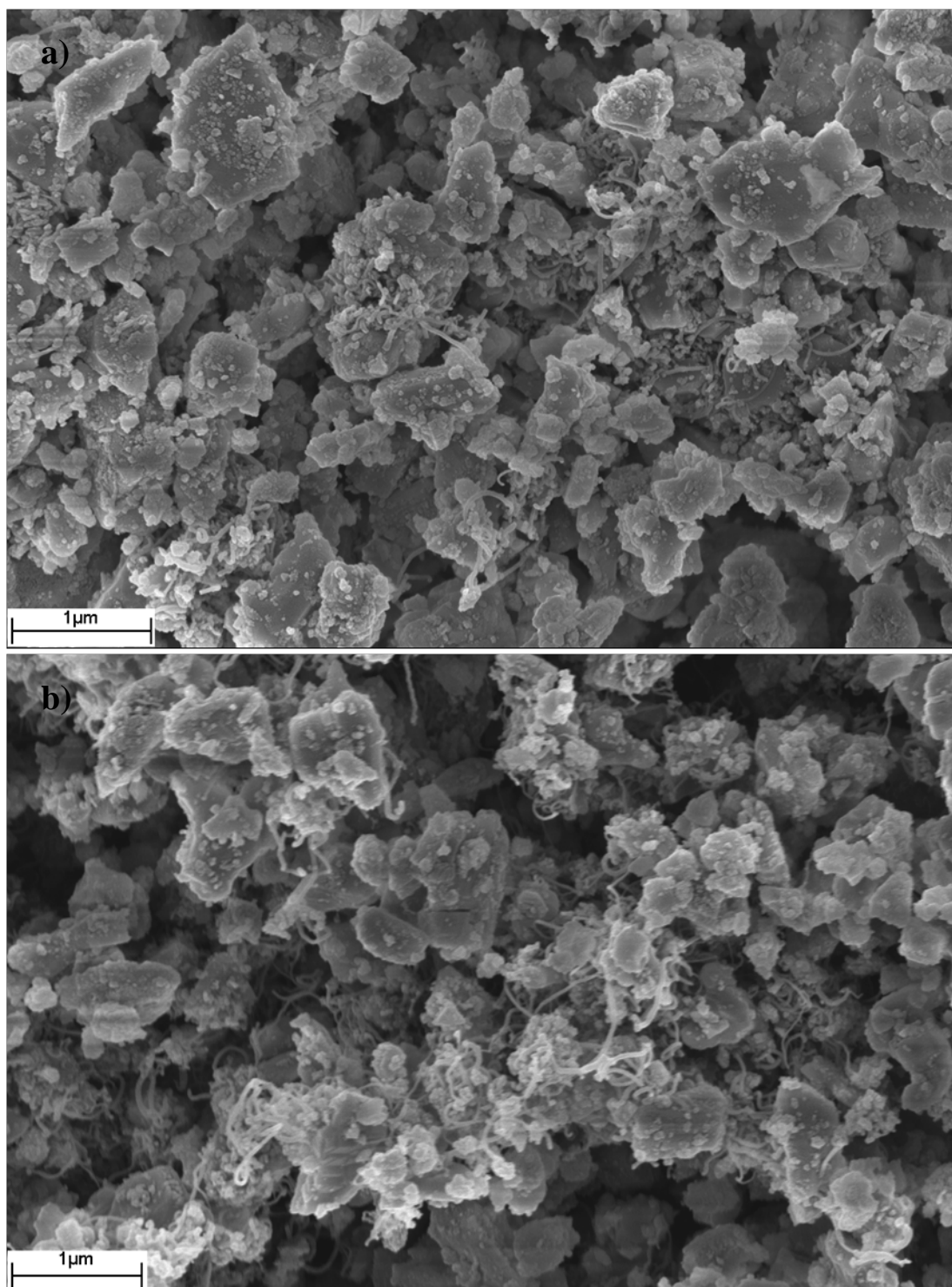


Figure 5.6 – CNTs grown on the surface of Al₂O₃ processed with 0.6 mol/l Co(NO₃)₂ solution. a) CNTs on 'AO-micron+nm' alumina grits, b) CNTs on 'AO-nm' alumina grits.

When the particles size of alumina was reduced to sub-micron and the concentration of $\text{Co}(\text{NO}_3)_2$ solution was remained at 0.6 mol/l, growth of CNTs was tangling among the closely packed Al_2O_3 particles as indicated in figure 5.6.

The measured diameter of CNTs was between 15 and 38 nm, with an averaged diameter of 25.1 nm and a standard deviation of 6.1 nm. While among the 'AO-nm' alumina grits as suggested in figure 5.6(b), the measured diameter of CNTs was between 15 and 35 nm, with an averaged diameter of 25.9 nm and a standard deviation of 7.6 nm.

5.3 In-situ growth of CNTs on Y-TZP powder

When Y-TZP powder was used as the substrate and processed with 0.6 mol/l $\text{Co}(\text{NO}_3)_2$ solution with all the other conditions maintained the same, growth of CNTs was clearly visible among the ZrO_2 particles. The diameter of CNTs measured from figure 5.7(b) was between 15 and 35 nm, with an averaged diameter of 24.4 nm and a standard deviation of 6.2 nm.

As summarised in figure 5.8, the averaged diameter of CNTs was slightly increased as the concentration of $\text{Co}(\text{NO}_3)_2$ solution increased from 0.3 to 0.6 mol/l. By using a precursor concentration of 0.6 mol/l, the averaged diameter on Y-TZP powder was also similar on that of alumina substrates. For the same type of substrate, particle size of the ceramic powders has no obvious influence on the averaged diameter of CNTs.

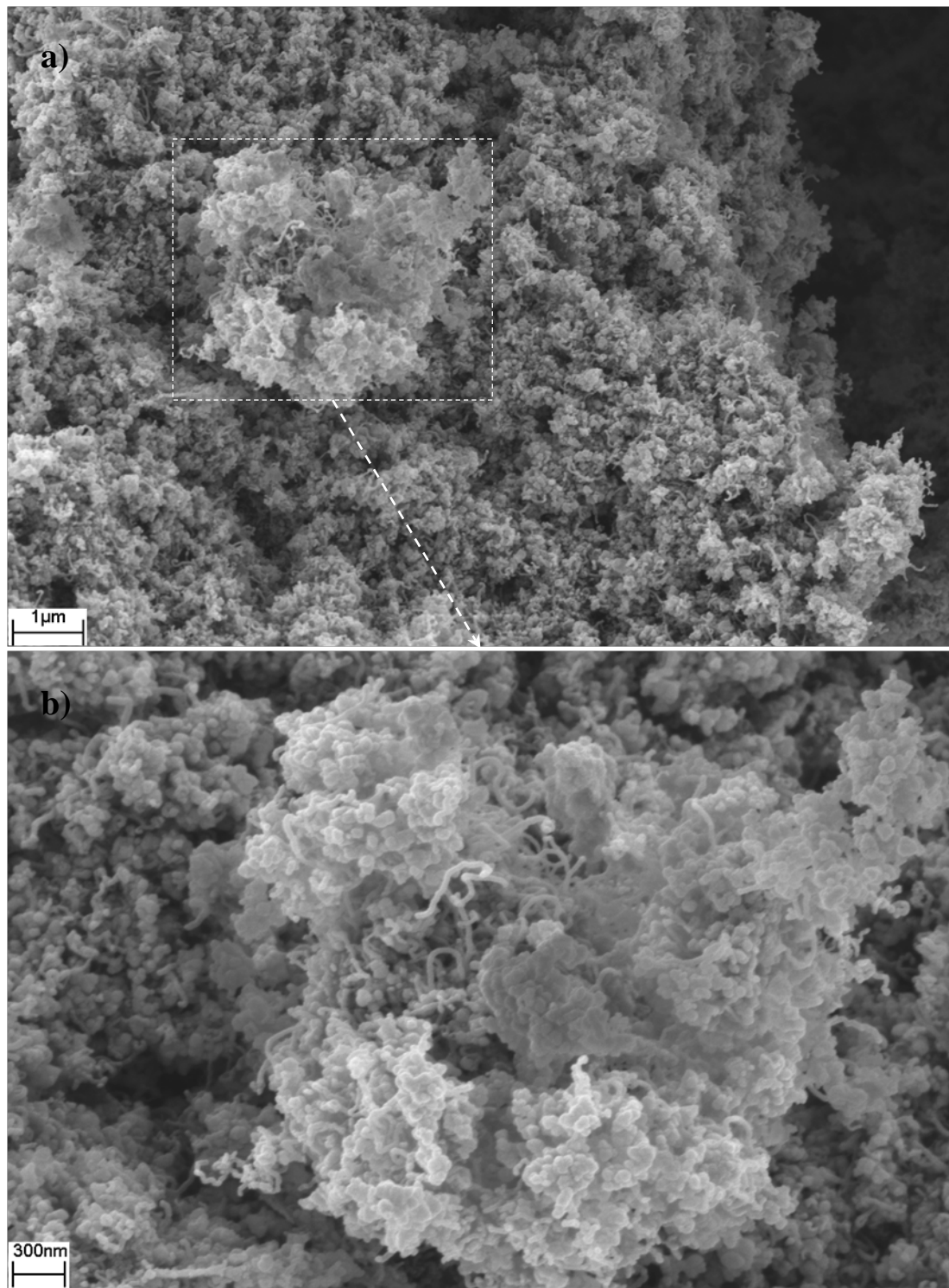


Figure 5.7 – (a) overview of CNTs grown in Y-TZP powder processed with 0.6 mol/l $\text{Co}(\text{NO}_3)_2$ solution. a) overview of the microstructure (b) zoom-in view as marked in a).

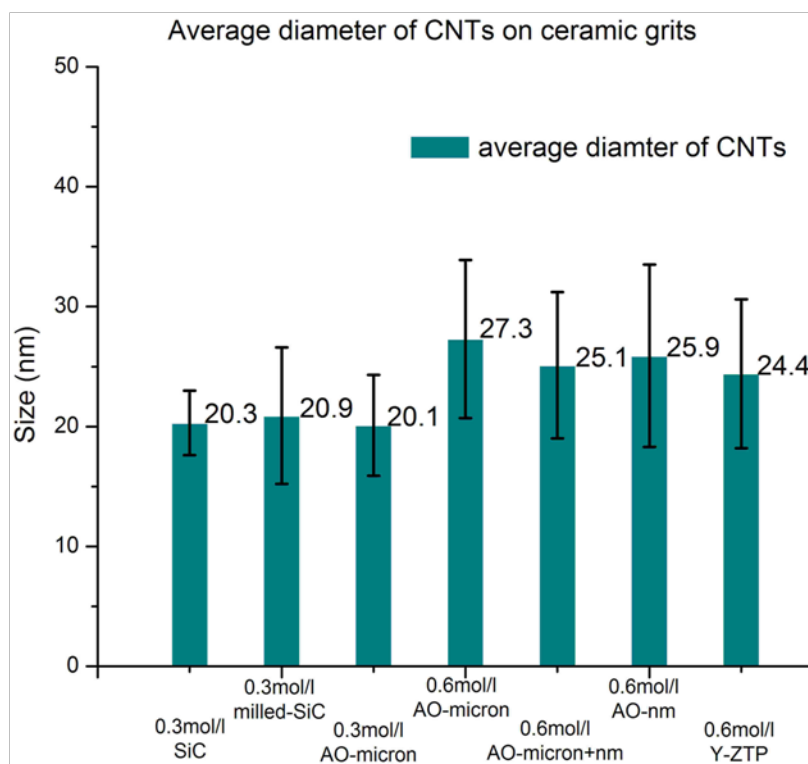


Figure 5.8 – Histogram diagram of the measured averaged diameter of CNTs on surface of different ceramic grits.

In general, the in-situ CCVD method for the growth of CNTs has been applied on substrates with different substances and formats, including long carbon fibres, relative large silicon carbide and alumina grits, Al_2O_3 powder with particle size around sub-micron, and Y-TZP powder with particle size of about 50 nm. The observation of the appearance of the CNTs and their morphology demonstrated the effectiveness of the experimental set-up and chosen processing parameters. The observation results indicated a possibility of more homogeneous dispersion and higher content of CNT in ceramics powders through in-situ growth, comparing to the ex-situ processing methods [73,75].

5.4 TEM analysis of catalytic growth of CNTs on Al₂O₃ particles

In order to study the possible cause that catalyst particles in the popular size range and were not active to deposit CNTs, TEM analysis was used to investigate the interfacial contact between the bottom of catalyst particles and Al₂O₃ substrate. It was suspected the contact situation between catalyst particles and the surface of Al₂O₃ was dominating the catalytic growth of CNTs.

High angle annular dark field imaging mode was chosen to highlight the contrast between CNTs and metallic particles that rooted on the surface of Al₂O₃ grits. The atomic mass contrast gives the metallic particles brighter regions. Two typical catalyst particles were selected for characterisation as marked in figure 5.9: 'particle-1' was a typical catalyst particle that was lifted up from surface of the Al₂O₃ grit by the growth of a carbon nanotube. 'particle-2' was a typical catalyst particle that had no growth of CNTs and still attached to the surface of Al₂O₃ grit after CVD process.

The particle sizes of both 'particle-1' and 'particle-2' were inside the range between 10 and 30 nm, a preferential range for the growth of CNTs on surface of Al₂O₃ as identified in previous sections. HRTEM observation suggested that multi graphene layers had been developed around both particles. As showed in figure 5.11(a), the deposition of graphene layers on top surface of 'particle-1' indicated the catalyst particle was encapsulated at the tip of the tubular structure of CNT.

EDS analysis shown in figure 5.10 suggested that both 'particle-1' and 'particle-2' were Co catalyst particles. The other peaks in EDS spectrums were from copper grid, gold coating, Pt deposition and Al_2O_3 grits.

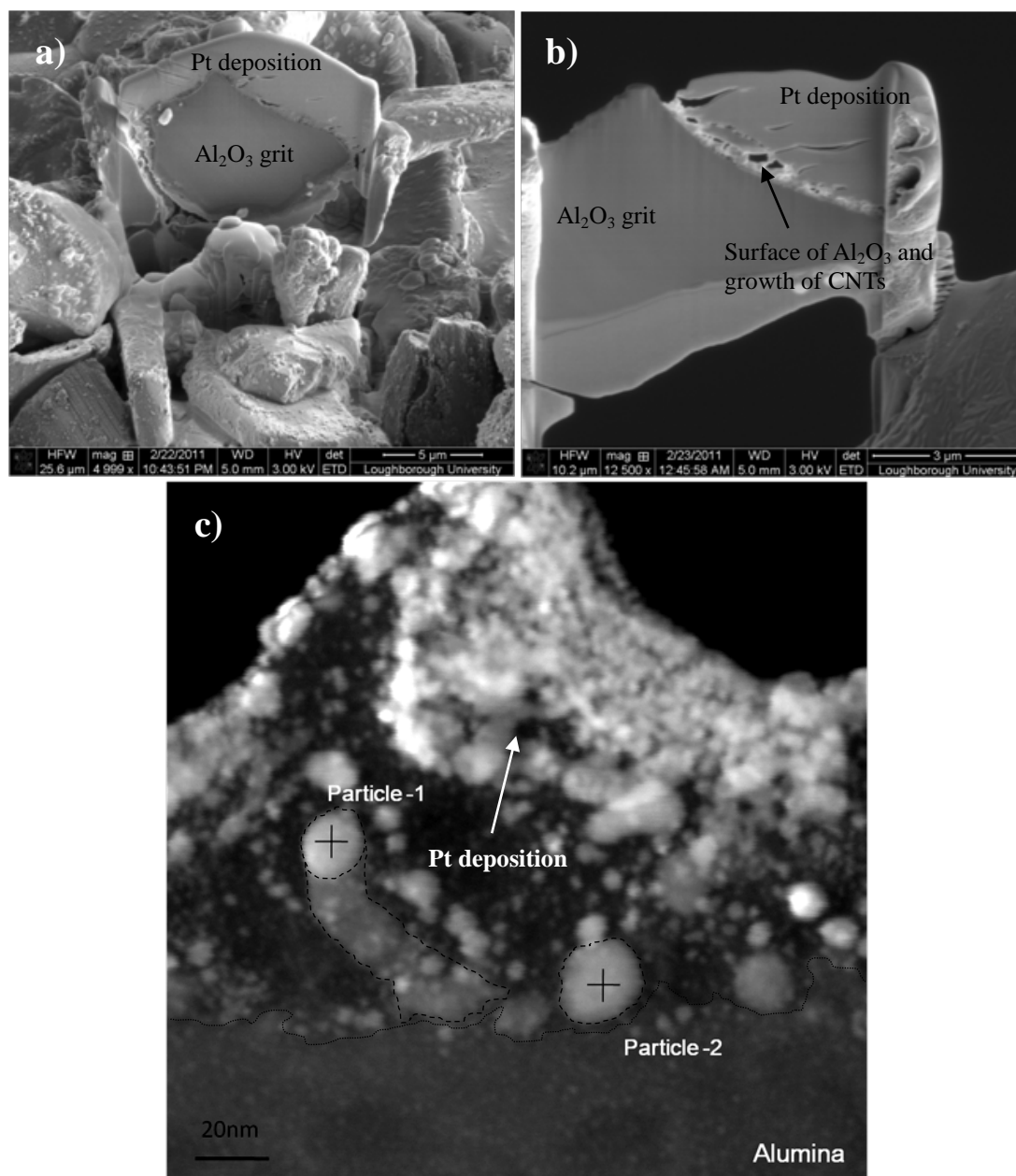


Figure 5.9 – a) cross-sectional view of Al_2O_3 grit with CNTs grown on its surface; b) cross-sectional TEM foil of the Al_2O_3 grit shown in (a); c) cross-sectional view of the surface of Al_2O_3 in high angle annular dark field imaging mode.

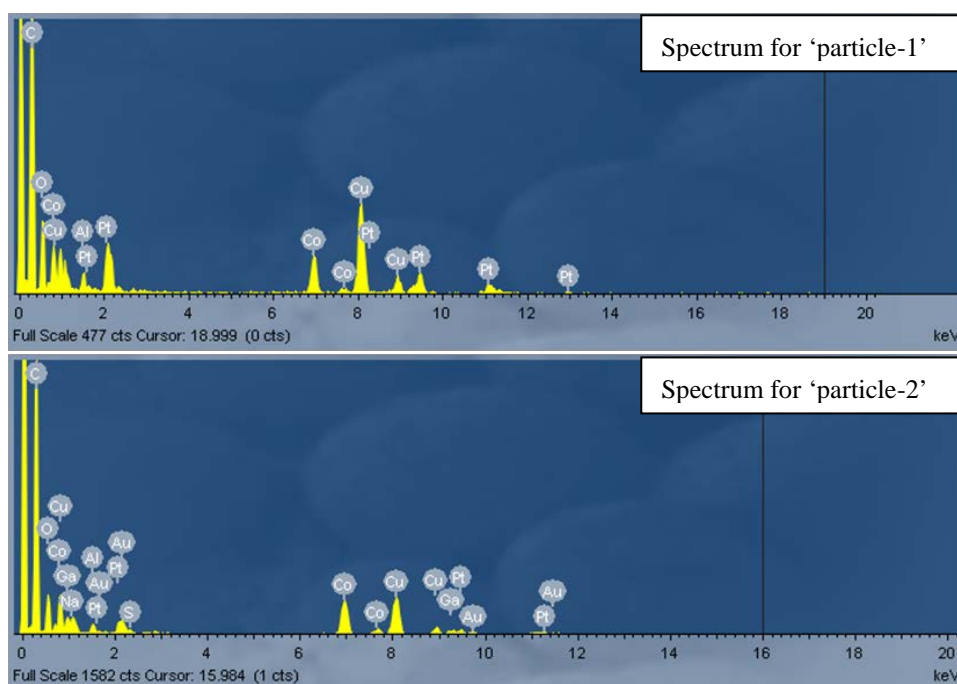


Figure 5.10 – TEM EDS spectrums for both ‘particle-1’ and ‘particle-2’ as indicated in figure 5.9.

In figure 5.11(b) showed the interfacial contact between the bottom of ‘particle-2’ and surface of Al_2O_3 grit after CVD process. The Co ‘particle-2’ was not physically in contact with the Al_2O_3 surface, but was slightly lifted up from the Al_2O_3 substrate with a distance of about 20 layers of graphene. It was assumed that this stage was the initiation of catalytic growth of CNTs, and continuous deposition and formation of graphene layers would eventually lead to the growth of CNT. However, TEM observation showed an extended contact area on the edge of the bottom of Co ‘Particle-2’. This contact situation is similar to Co particles positioned within nano-sized (~17nm in width) grooves on surface of CFs as shown in figure 4.21. The initiation stage of the growth of CNT on ‘particle-2’ was terminated, possibly because the force between Co ‘particle-2’ and Al_2O_3 substrate overcame the growth force of CNT on the opposite direction.

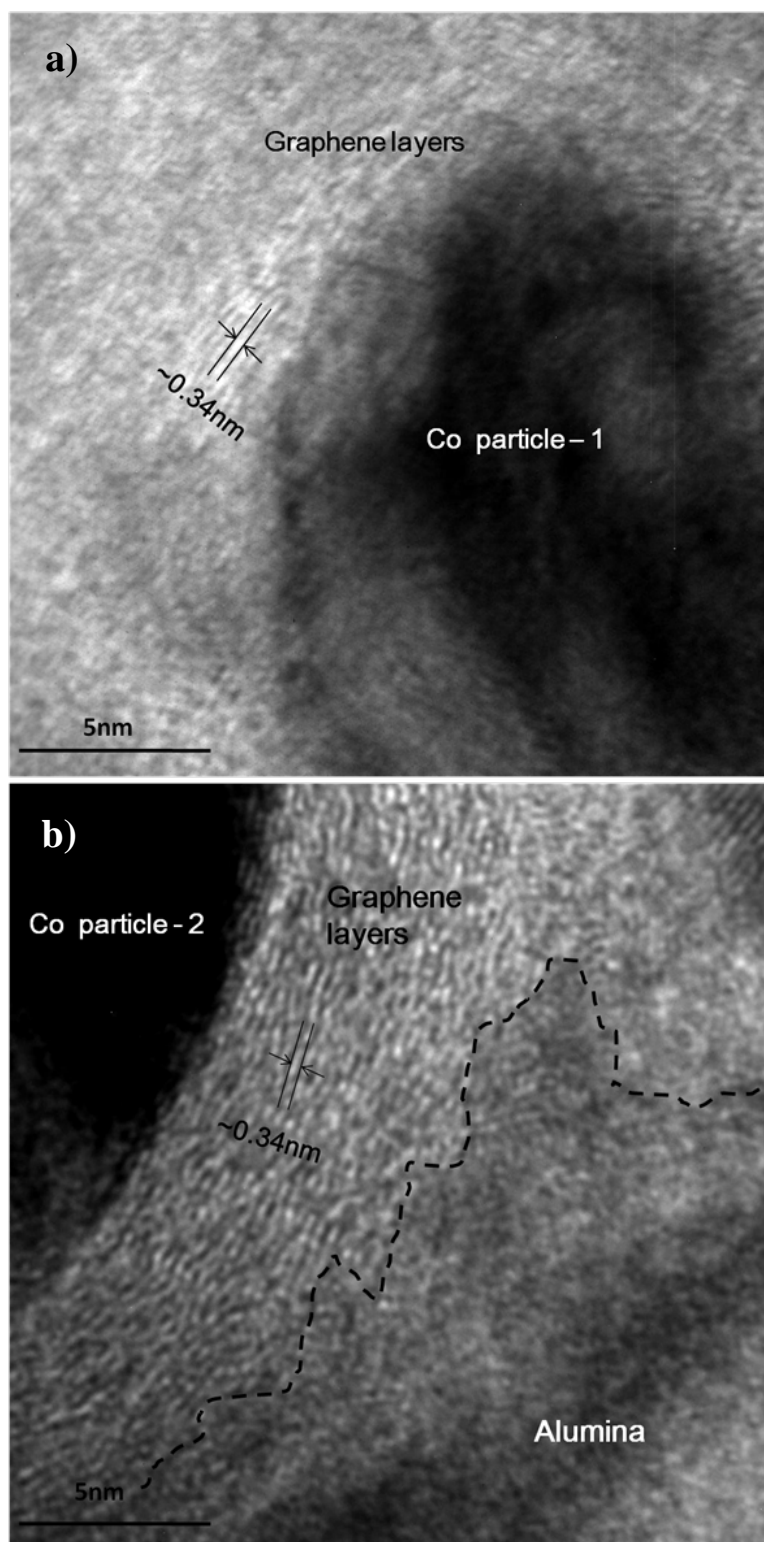


Figure 5.11 – HRTEM images around the Co particles showing the laminated graphite structure. a) Co ‘Particle-1’; b) Co‘Particle-2’.

CHAPTER 6 Preliminary Work in Manufacture of CNT Reinforced Composites

Preliminary work has been done in manufacture of CNTs reinforced composites. Two types of composites have been prepared: 1) CNTs reinforced CF – Carbon composite, and 2) chemically bonded CNTs/Al₂O₃ composite. The former one was achieved through chemical vapour infiltration and the later one was prepared based on chemical method.

6.1 Manufacture of CNTs/CFs reinforced carbon composite

Under polarised lighting condition, the carbon fibre reinforcements can be differentiated from pyrolytic carbon deposited through CVI, as shown in figure 6.1. The averaged diameter of CFs was 6.5 μ m, and the thickness of deposited pyrolytic carbon around 6.5 ~ 6.7 μ m,

Three domains were observed on the cross-sectional area of the pyrolytic carbon matrix, under polarised lighting conditions. Along the vertical direction to the surface of CFs, both the inner and outer domains tend to be dark grey, the extinction angle was 0 degree, suggesting they were isotropic laminar (ISO). The middle domain showed preferred orientation and smooth texture with the extinction angle measured at around 8 ~ 11 degree, suggesting it was smooth laminar (SL). The optical image of the in-plane placed CFs also suggested the SL was associated with ISO. The ISO cannot be graphitised and SL can be partially graphitised [123].

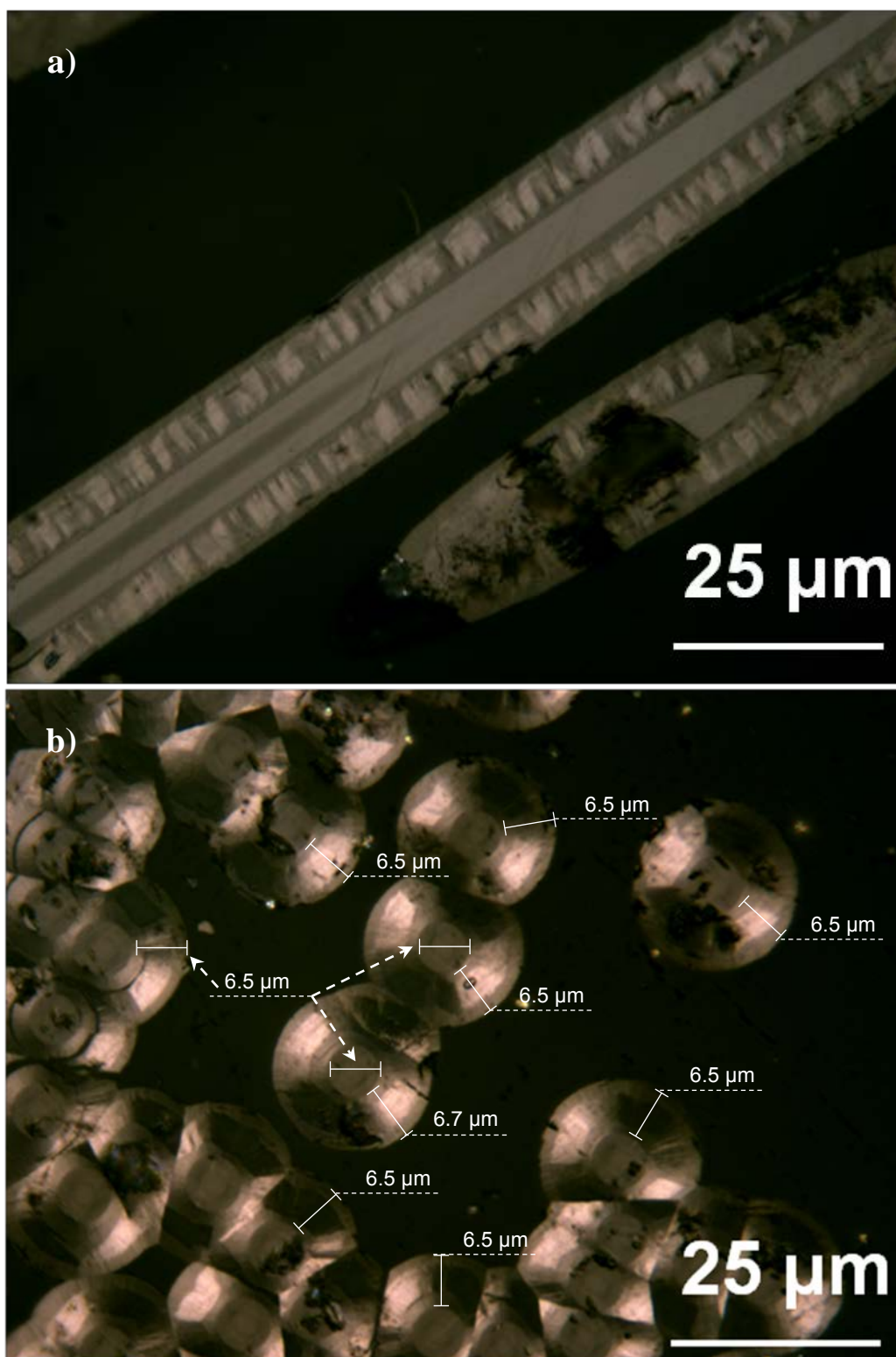


Figure 6.1 – Pyrolytic carbon deposition on surface of CFs. a) in-plane CFs, b) vertical placed CFs.

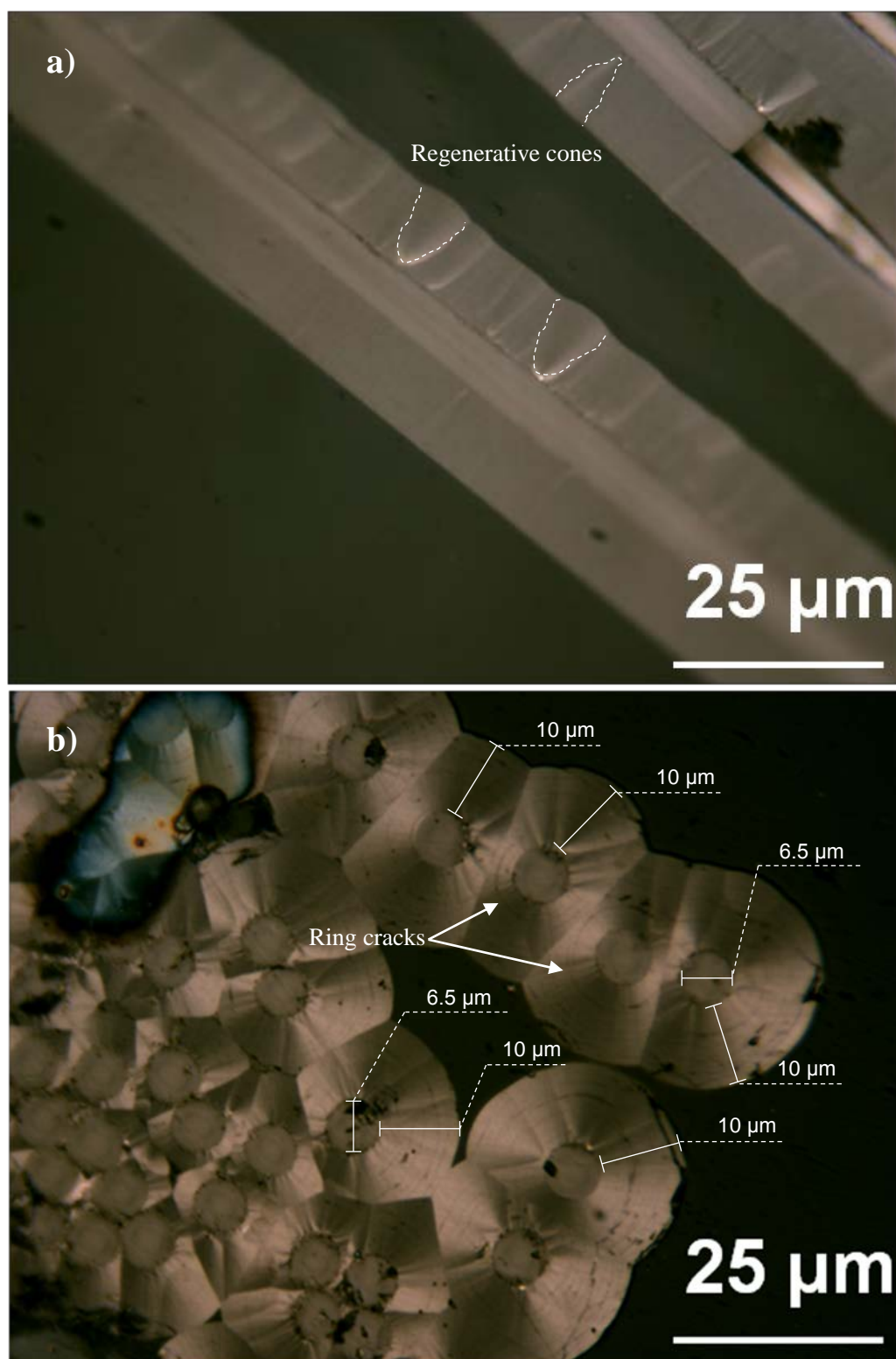


Figure 6.2 – Pyrolytic carbon deposited around CFs with their surface containing CNTs. a) in-plane CFs; b) vertical CFs.

While CNTs/CFs hybrid preform was used, the morphology of pyrocarbon matrix was dramatically changed under same CVI conditions. First, the thickness of the deposited pyrolytic carbon had about 53% increase (from 6.5 μm to about 10 μm), comparing to that containing CF alone. Exemplary measurements are marked in figure 6.2(b). It seems that the existence of CNTs on the surface of CF had promoted the deposition of pyrolytic carbon.

The cross-sectional surface of pyrolytic carbon on in-plane CFs showed flat and smooth texture, compared to the rougher one shown in figure 6.1(a) on CFs without growth of CNTs. Typical feature of pyrolytic carbon deposition known as the 'regenerative cones' was also observed as marked in figure 6.2(a). The 'regenerative cones' was typical feature of regenerative laminar (ReL) in pyrolytic carbon deposition.

The cross-sectional surface of pyrolytic carbon on vertical CFs in figure 6.2(b) showed Maltese-cross with the extinction angle measured at around 10~12 degree, which could support the content of pyrolytic carbon consists of regenerative laminar. On the cross-sectional surface, ring cracks were also observed and marked, indicating the ReL may be also associated with smooth laminar (SL).

Compared to CFs without growth of CNTs, the type of deposited pyrolytic carbon was converted from SL/ISO to SL/ReL. The ReL has the anisotropy as high as rough laminar (RL) and is graphitisable [133].

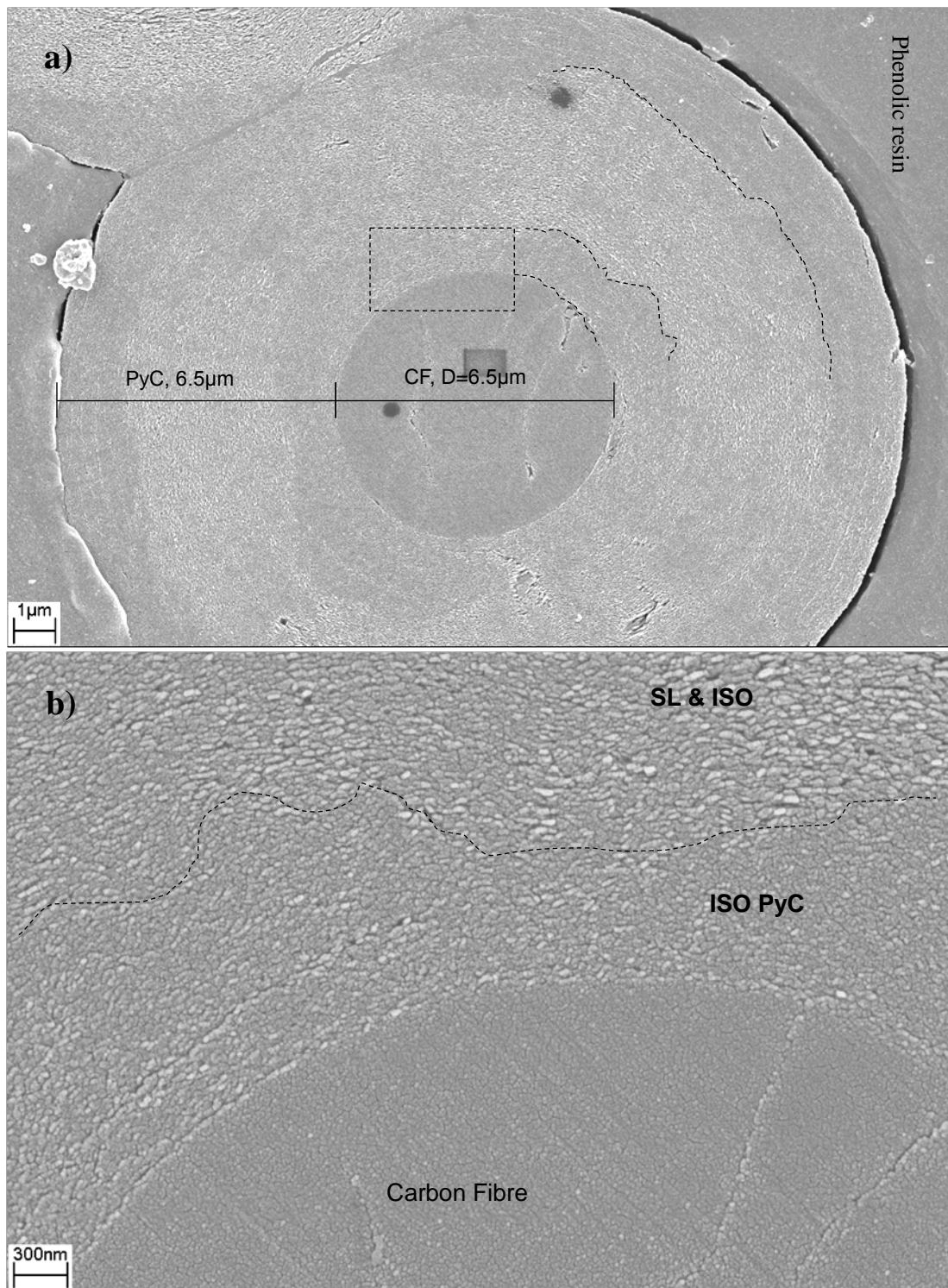


Figure 6.3 – a) SEM image of polished cross section of pyrolytic carbon deposited around CFs; b) more details near the interface marked in (a).

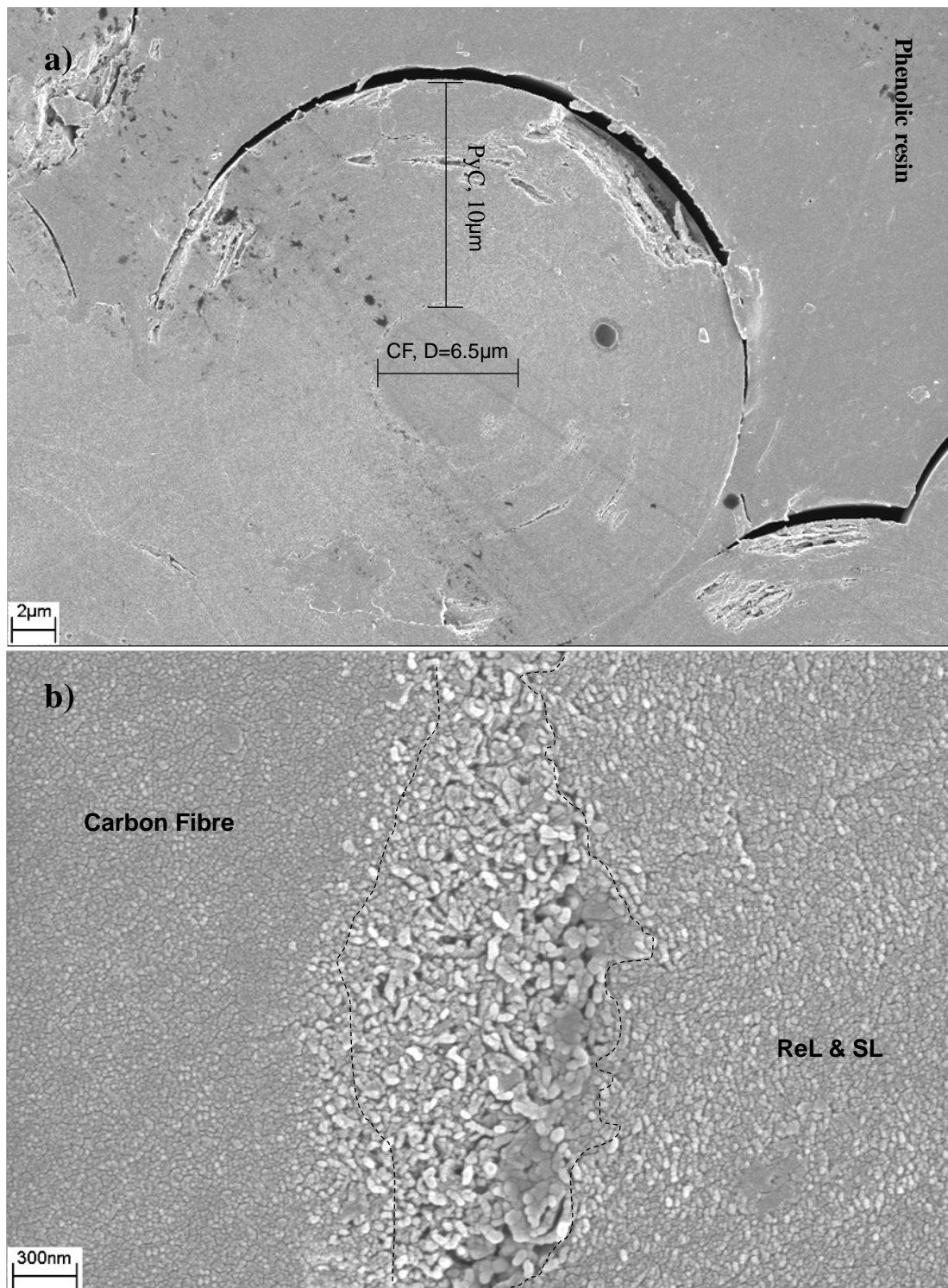


Figure 6.4 – a) SEM image of polished cross section of pyrolytic carbon deposited around CFs with growth of CNTs; b) more details near the interface marked in (a).

For pyrolytic carbon on the surface of CF without CNTs, the three domains were clearly distinguished by surface texture under SEM. As shown in figure 6.3, the ISO has a smooth surface texture, while the SL has the wrinkled laminar. On surface of CF with growth of CNTs as shown in figure 6.4, the SEM observation showed no visible domains in the pyrolytic carbon region. The surface texture of the later one was similar to that of the middle domain shown in figure 6.3(b).

The deposition of pyrolytic carbon on CF without CNTs was directly in contact with the surface of CF as shown in figure 6.3(b). For pyrolytic carbon on the CF with CNTs, an interface between CF and the ReL pyrolytic carbon was observed as shown in figure 6.4(b). It is possible that the deposition of pyrolytic carbon initiated from the interface use CNTs as the nucleating agent during CVI process. Therefore, the CNTs may accelerate the initiating stage of the deposition of pyrolytic carbon around CFs and lead to increase in thickness of the carbon matrix in CFs/CNTs preform, compared to CFs without growth of CNTs for the same processing period during CVI.

6.2 Manufacture of chemically bonded CNTs/Al₂O₃ composites

The composite powder of 'AO-micron' was densified through the 'method a' as introduced in the experimental section, and was slip casted into a mould. As shown in figure 6.5, the particles were not well packed during slip casting, possibly due to large particle size (~10µm) of 'AO-micron' and shrinkage of aluminium phosphate hydrate during dehydration.

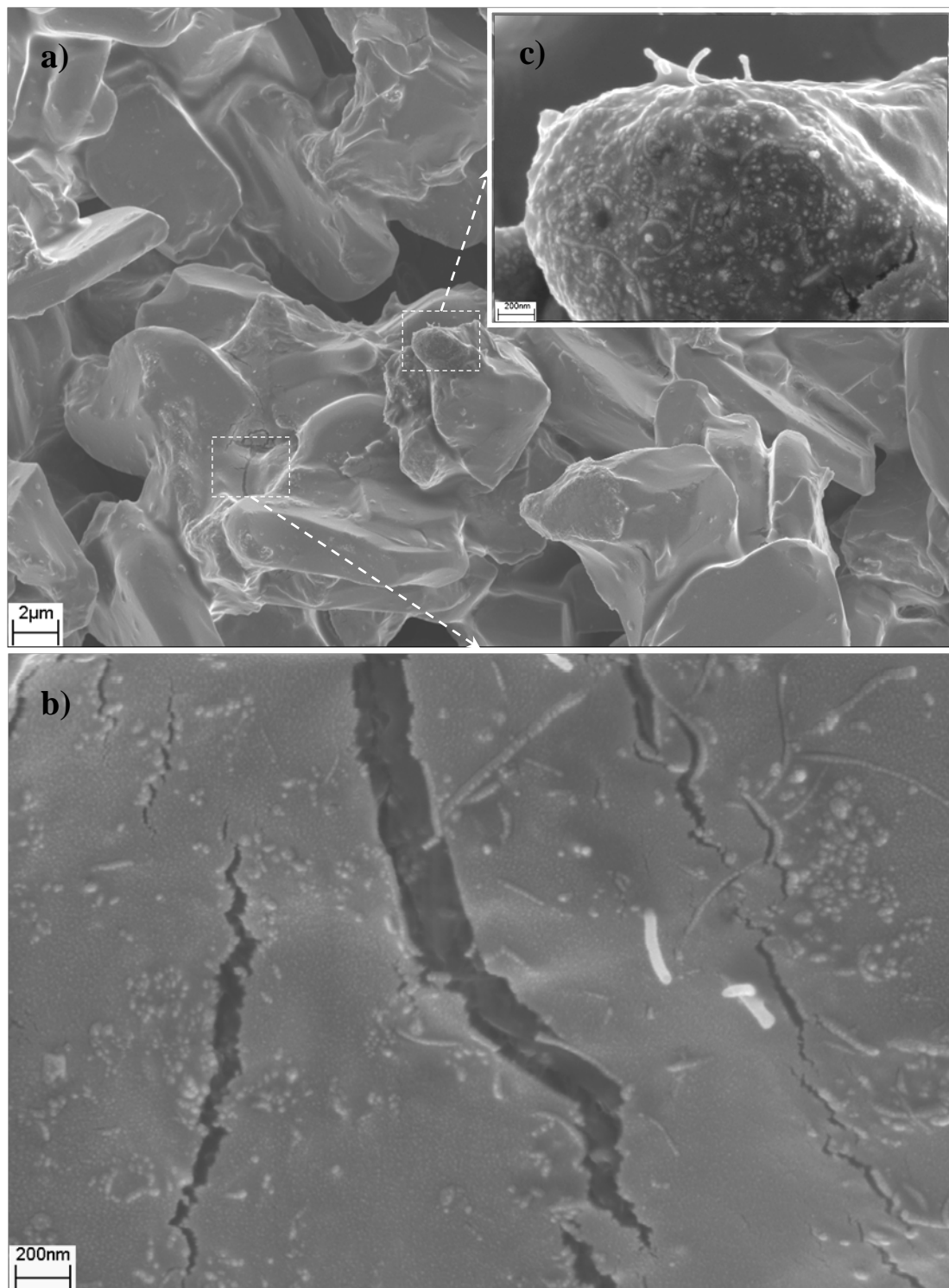


Figure 6.5 – Aluminium phosphate bonded CNTs/alumina composite from as-prepared composite powder of ‘AO-micron’.

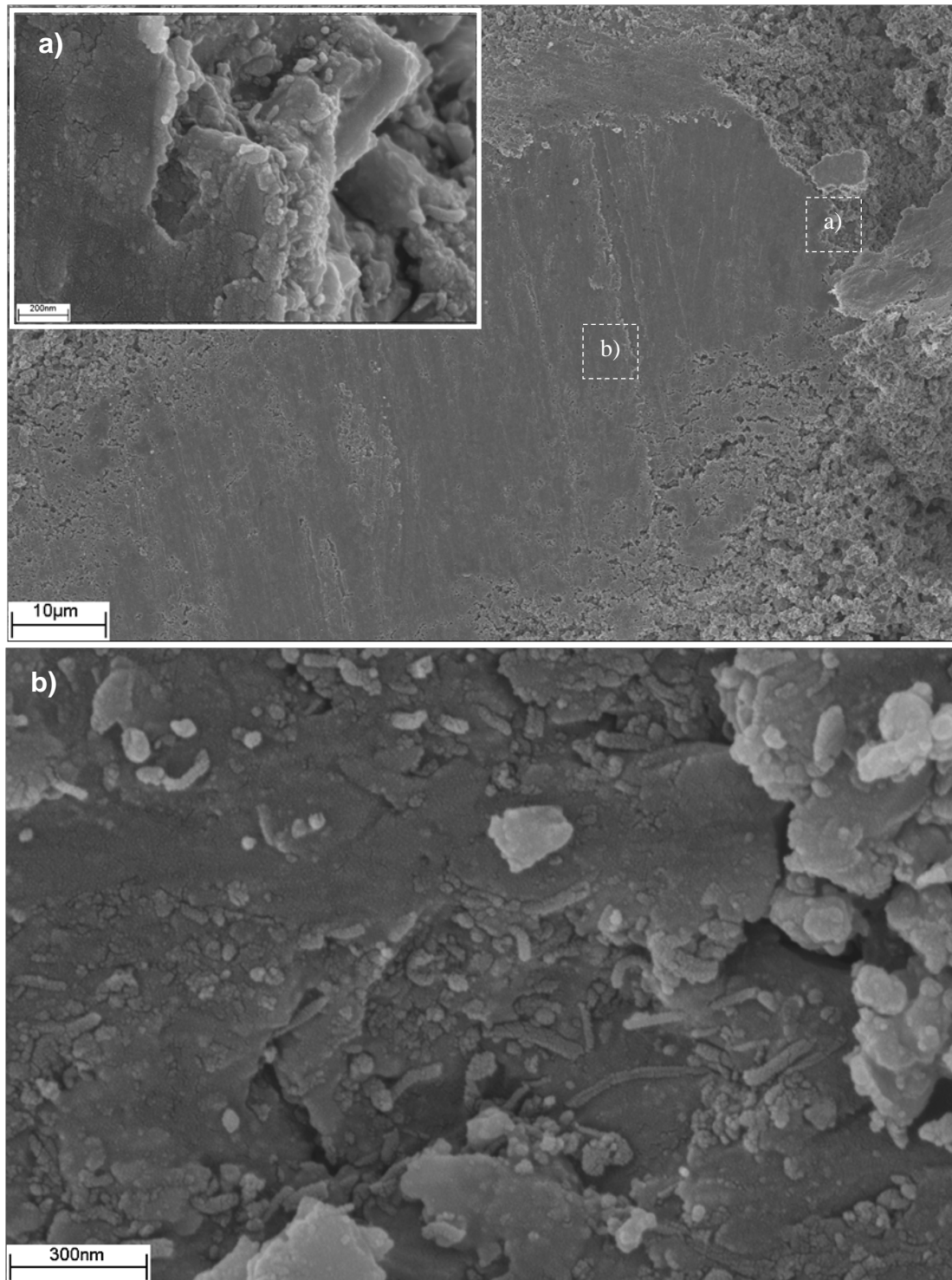


Figure 6.6 – Aluminium phosphate bonded CNTs/alumina composite from as-prepared composite powder of ‘AO-micron+nm’.

The microstructure indicated good wettability of aluminium phosphate to both Al_2O_3 particles and CNTs. As suggested in images b) and c) of figure 6.5, the as-produced chemical bonding (Berlinite) was able to be reinforced by homogeneous dispersion of CNTs, through debonding of CNTs and/or crack deflection, compared to that of traditional CBPCs introduced in the literature.

The composite powder of 'AO-micron+nm' and coated on surface of a $\text{C}_f/\text{C-SiC}$ break disk. The coating material was well bonded to surface of the substrate after curing, possibly due to the bonding agent of aluminium phosphate. The images in figure 6.6 suggested rearrangement of Al_2O_3 particles during coating, and a denser microstructure was produced as the broadened particle size distribution of 'AO-micron+nm' Al_2O_3 powder than that of 'AO-micron' powder. Both areas a) and b) suggested CNTs were homogeneously dispersed and well bonded within the aluminium phosphate matrix.

The $\text{CNTs}/\text{Al}_2\text{O}_3$ composite powder of 'AO-micron+nm' was iso-pressed through 'method b' in order to produce a much denser microstructure of the as-prepared Al_2O_3 ceramic. The fracture surface of the as-pressed pellet before and after introducing of aluminium phosphate was examined under SEM. As shown in figure 6.7(a), before dipping of HF acid, Al_2O_3 particles were well packed together, with the homogeneous dispersion of CNTs. After introducing of aluminium phosphate and cured, no dramatic increasing of particle size of Al_2O_3 was observed, as shown in image b) of figure 6.7. The CNTs were well bonded with aluminium phosphate, and debonding of CNTs was also observed on the fracture surface.

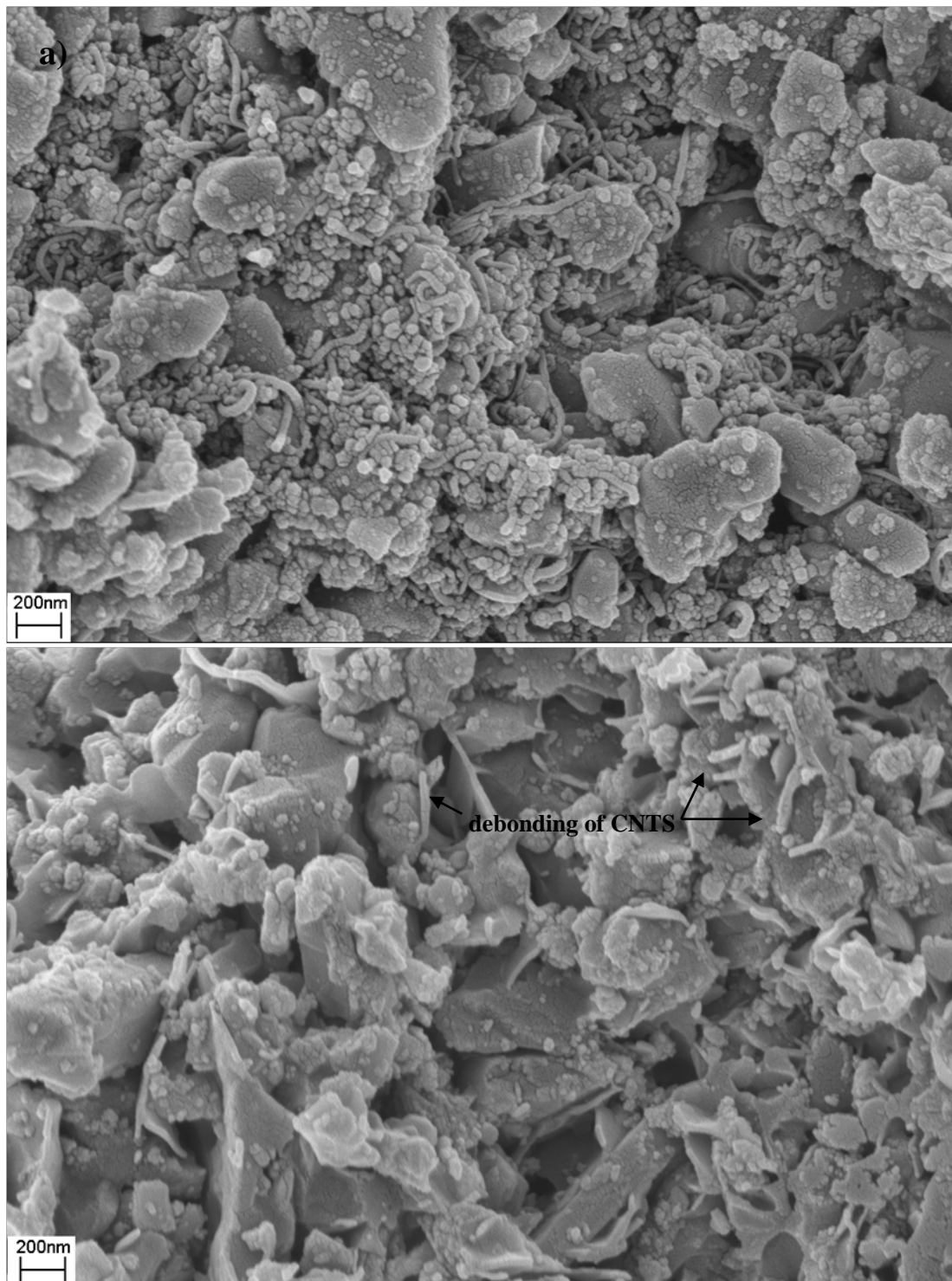


Figure 6.7 – Aluminium phosphate bonded CNTs/alumina composite from as-prepared composite powder of 'AO-micron+nm'.

There were still nano-sized (~ 100nm) pores within the matrix of aluminium phosphate, mostly because of the reaction between HF acid and catalyst particles of cobalt and shrinkage of aluminium phosphate hydrate during curing. However, the microstructure can be further improved in future, e.g. second time of iso-press after dipping of HF acid, before curing.

CHAPTER 7 Growth mechanism of CNTs

7.1 Surface chemistry and roughness of CFs

The surface chemistry of PAN-based CFs is introduced by various techniques during manufacture, including: surface oxidising treatments, sizing and so on. Surface oxidising treatments, such as liquid chemical or electrochemical treatments, commonly undergo oxidation to modify surface of CF with oxygen-containing functional groups [124,125]. It can be used to improve the interfacial adhesive strength between CF and matrix materials (*e.g. epoxy resin*) to promote better mechanical properties of the composites [126,127]. Besides, surface roughness of carbon fibres is also increased through surface oxidising treatments [128]. The sizing material, usually a thin polymeric layer, is often coated on surface of PAN-based CFs to improve its compatibility to the matrix materials and ease of handling (*e.g. weaving or twisting*) during transportation.

While boiling in nitric acid solution, the surface chemistry of PAN-based CFs was changed. Most of the sizing material (*epoxy resin*) on CFs was decomposed and removed by nitric acid, most likely through breakage of C-N

bonds and nitration of benzene rings within the cross-linking structure of epoxy resin [129].

After washing in nitric acid solution, the rough surface of CFs was likely exposed by removal of the sizing material, and H^+ may also be introduced on surface of PAN-based CFs from the nitric acid solution. These H^+ may react chemically with acetone to form $H^+ \cdots O=C$ hydrogen bonds at the surface of CFs. The hydrogen bonds will minimise the surface free energy of the solid-liquid interface in order to improve the wettability of catalyst precursor solution to surface of PAN-based CFs, as schematically shown in figure 7.1.

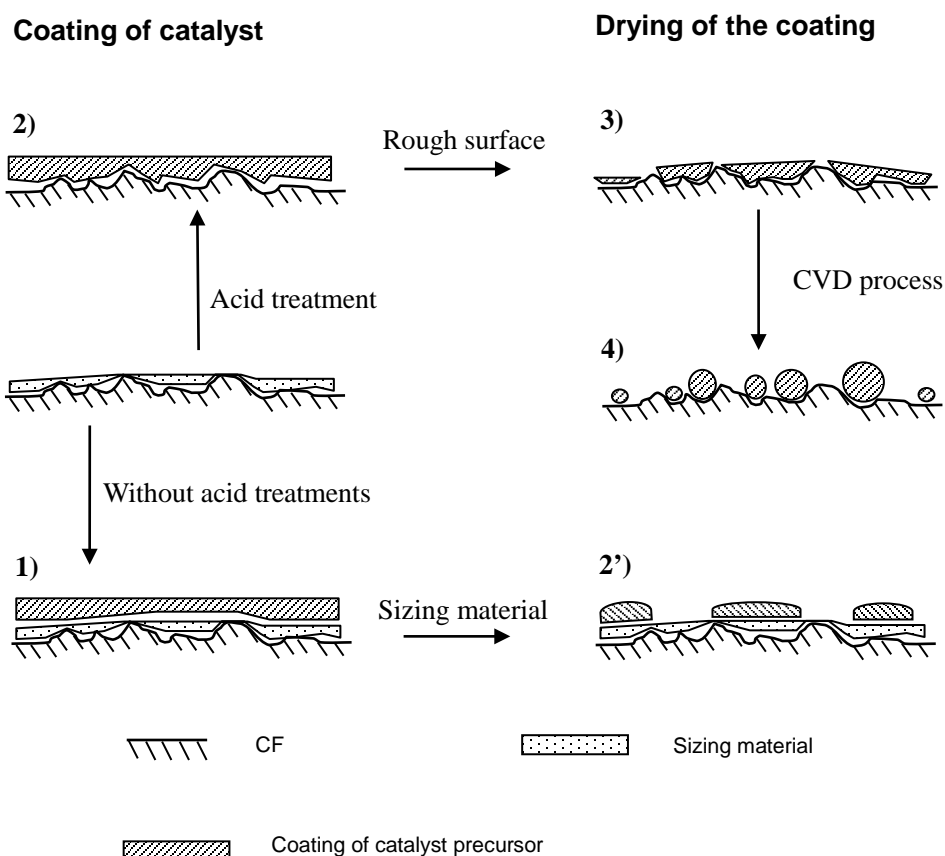


Figure 7.1 – Schematic drawing of surface chemistry and roughness of CFs on coating of catalyst precursor and formation of catalyst particles.

As shown in figure 7.1, the thickness of the coated layer of catalyst precursor was not uniform; on acid washed CFs, the layer of catalyst precursor was partly dictated by the topography of CF surface. When the catalyst precursor was dried during CVD process, the layer of catalyst precursor will be converted into catalyst particles through pyrolysis of the precursor salt and reduction of the metallic oxidants. While on CFs without acid treatment, since the wettability of catalyst precursor solution was not as well as that on acid treated CFs, the coated layer of precursor solution may subsequently accumulated into 'residual' material as indicated in figure 4.1(c).

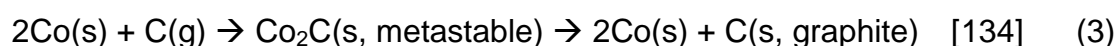
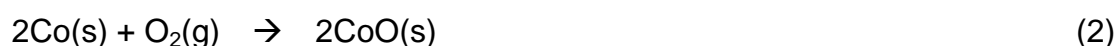
The size of catalyst particles was inside a range from about 2.5 to 60 nm in diameter as observed from results. Since the surface roughness always exists, the thickness of the coated film of catalyst precursor is likely varies with the topography of CFs. The typical surface topography was the groove surface observed on both PANOX-CF and PAN-based CF after surface pre-treatment. The thickness of the coating material tends to be thicker in the groove regions than that on the smooth regions. The effect of surface roughness on the size of catalyst particles was further confirmed in figure 4.20 that the formation of catalyst particles has a broadened size distribution (2.5 ~ 60 nm) on the groove surface, while relatively narrow size distribution (2.5 ~ 35 nm) on the humps.

7.2 Thermodynamic study of in-situ formation of catalyst particles

The formation of catalyst particles is transformed from catalyst precursor during heat treatment in CVD process before cracking methane. The first step is

thermal decomposition of metal nitrides into metal oxides. As for $\text{Co}(\text{NO}_3)_2 \cdot 6\text{H}_2\text{O}$, researches have suggested that in air, $\text{Co}(\text{NO}_3)_2 \cdot 6\text{H}_2\text{O}$ starts to loss H_2O from 150°C and then nitride from about 350°C . Co_3O_4 is the dominate product [130]. In hydrogen atmosphere, the rate of thermal decomposition of $\text{Co}(\text{NO}_3)_2 \cdot 6\text{H}_2\text{O}$ is accelerated; the conversion into Co_3O_4 starts at 130°C , followed by a further reduction into CoO from a temperature of about 350°C [131,132].

The second step is the reduction of cobalt oxides into monolithic Co particles. Cobalt oxides are expected to be reduced into fcc-Co particles by hydrogen at 500°C [133], which is below the CVD temperature of 650°C . The activity of catalyst particles for the growth of CNTs is highly dependent on the formation of monolithic Co particles, and the time period of Co retaining in its format. During catalytic growth of CNTs, the atmosphere condition on top surface of Co particles is complex, including H_2 , O_2 and N_2 . Therefore, the possible reactions are assumed as below:



When a monolithic Co particle is formed, it may be oxidised again by the oxygen content in the reaction tube. Oxygen partial pressure always exists

especially in the reaction tube operated at the ambient pressure. Therefore, there is a possible competition between the oxidation reaction and carbon diffusion into graphite structure of CNTs on surface of the Co particles. If reaction (2) is thermodynamically more favoured than that of reaction (1), then it is more likely the Co particles can be deactivated for continuous carbon diffusion. Thermodynamic calculations of the change of Gibbs free energy of reaction $\Delta_r G$ was used to study whether these reactions can proceed spontaneously at 650°C, based on:

If $\Delta_r G < 0$, the reaction is thermodynamically favoured;

If $\Delta_r G = 0$, the system is in equilibrium state, neither the forward nor the reverse of the reaction is favoured;

If $\Delta_r G > 0$, it is a nonspontaneous reaction.

$$\Delta_r G^\circ = \sum \Delta_f G^\circ (\text{products}) - \sum \Delta_f G^\circ (\text{reactants}) \quad (4)$$

The standard change of Gibbs free energy of reaction $\Delta_r G^\circ$ is given in equation (4), which is the sum of standard Gibbs free energy of formation $\Delta_f G^\circ$ of all products minus that of all reactants. Based on the definition of change of Gibbs free energy shown in equation (5), the change of Gibbs free energy of reaction $\Delta_r G$ at the cracking temperature of methane can be calculated by Gibbs-Helmholtz Equation [135] given by equation (6).

$$\Delta G = \Delta H - T\Delta S \quad (5)$$

The Gibbs-Helmholtz Equation:

$$\left(\frac{\Delta_r G}{T}\right)_{T_2} = \left(\frac{\Delta_r G^\circ}{T}\right)_{T_1} + \Delta_r H^\circ \left(\frac{1}{T_2} - \frac{1}{T_1}\right) \quad (6)$$

where $\Delta_r H^\circ$ is the standard change of enthalpy, and T_1 refers to standard temperature of 25°C, while T_2 is the target temperature. The quantities of both $\Delta_r H^\circ$ and $\Delta_r G^\circ$ for the selected substances in reactions (1) ~ (3) were listed in the table 5.1 [136]. While T_2 increases from room temperature to the cracking temperature of methane at 650°C, the calculated changes of Gibbs free energy of reaction $\Delta_r G$ at the temperature of T_2 for chemical reactions (1), (2) and (3) are shown in figure 7.2.

Table 7.1 – Standard thermodynamic quantities for selected substances.

| | CoO(s) (kJ/mol) | H ₂ (g) (kJ/mol) | Co(s) (kJ/mol) | H ₂ O(g) (kJ/mol) | O ₂ (g) (kJ/mol) | C(g) (kJ/mol) | C(s) (kJ/mol) |
|--------------------|--------------------|--------------------------------|-------------------|---------------------------------|--------------------------------|------------------|------------------|
| $\Delta_r G^\circ$ | -214.2 | 0 | 0 | -228.6 | 0 | 671.3 | 0 |
| $\Delta_r H^\circ$ | -237.9 | 0 | 0 | -241.8 | 0 | 716.7 | 0 |

Therefore, the calculated $\Delta_r H^\circ$ and $\Delta_r G^\circ$ for equations (1) ~ (3) were listed in table 7.2.

Table 7.2 – Calculated $\Delta_r H^\circ$ and $\Delta_r G^\circ$ for reactions (1) ~ (3).

| reactions | (1) (kJ/mol) | (2) (kJ/mol) | (3) (kJ/mol) |
|--------------------|-----------------|-----------------|-----------------|
| $\Delta_r G^\circ$ | -14.4 | -428.4 | -671.3 |
| $\Delta_r H^\circ$ | -3.9 | -475.8 | -716.7 |

Based on the Gibbs-Helmholtz Equation, the changes of Gibbs free energy of reaction $\Delta_r G$ was shown in figure 7.2 as a function of temperature T2 from 25°C to 650°C.

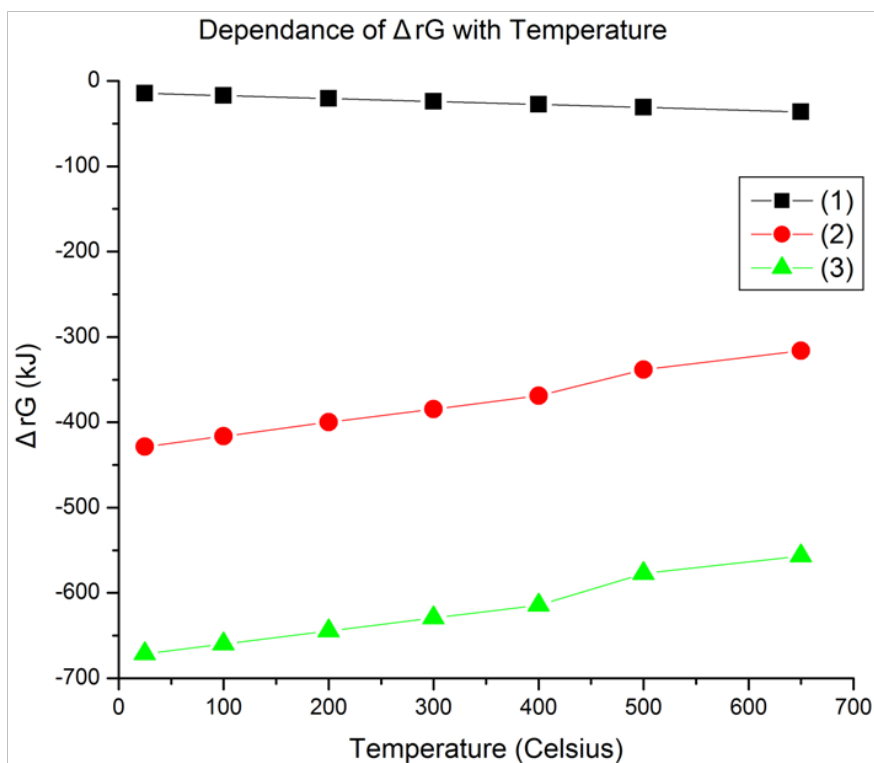


Figure 7.2 – Calculated $\Delta_r G$ as increasing temperatures for chemical reactions (1), (2) and (3).

Figure 7.2 suggests that in the range of temperature from 25°C to 650°C, change of Gibbs free energy of reaction (3) is far less than that of reaction (2). It indicates that during cracking of methane, the chemical reaction (3) was more preferred than chemical reaction (2). The as-reduced monolithic Co particles are thermodynamically more favourable to carbon absorption and diffusion, rather than being oxidised.

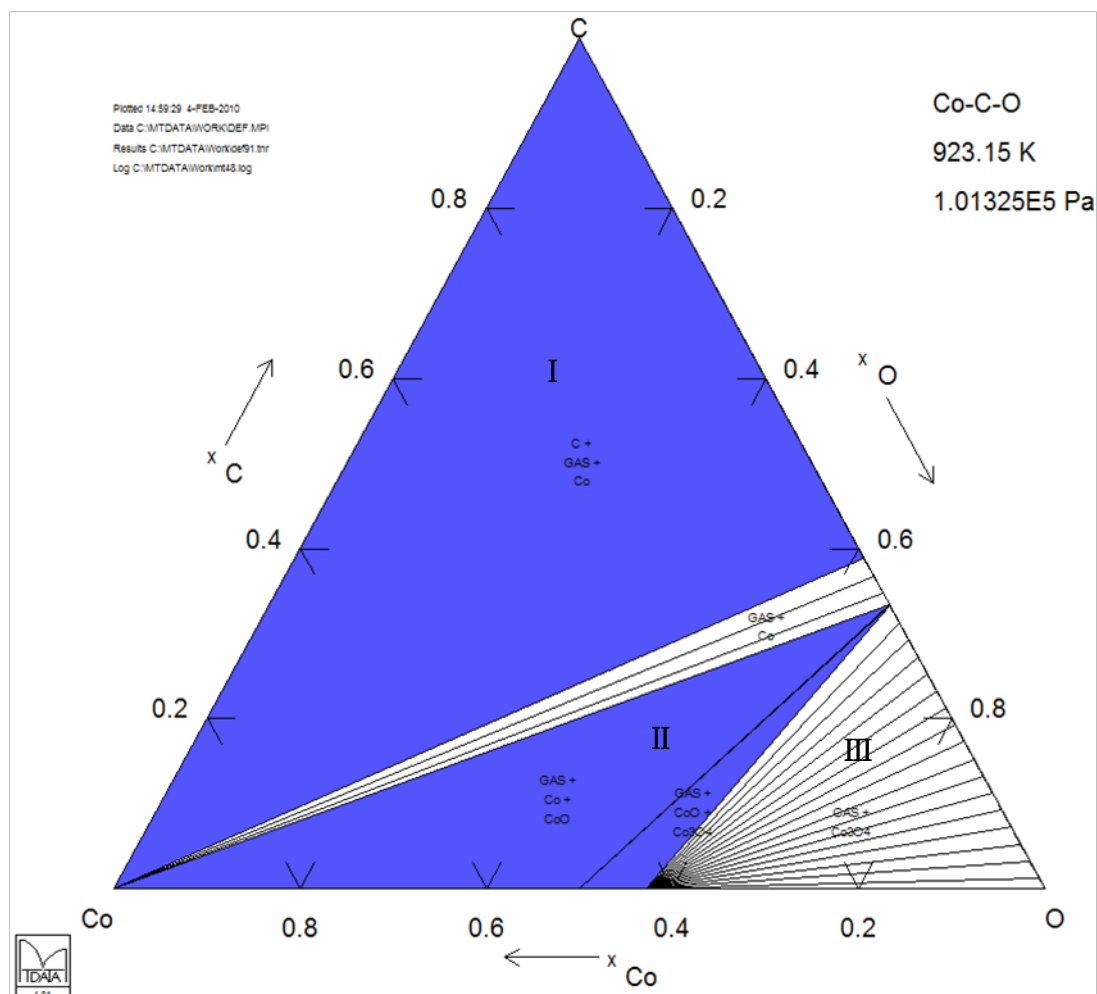


Figure 7.3 – Simulated phase diagram of Co-C-O system at 650°C by using MTDATA.

In order to simulate the competition between the reactions of (2) and (3), the software of 'MTDATA' (*for windows version 4.81*) was used to simulate the ternary diagram of C-Co-O system (*database of 'SUB_SGTE substance database version 11.0-November 2006' was selected*) at 650°C. As shown in figure 7.3, region I indicates even at low concentration of carbon environment down to about 40% of the carbon vapour and oxygen mixture, surface of Co particles is still thermodynamically more favourable for carbon absorption and diffusion, as there is no oxide phase in this region. When the oxygen content is

over 60% within the carbon vapour and oxygen mixture, CoO starts to form gradually and then Co_3O_4 is formed at extreme high oxygen environment as shown in regions II and III. However, for the current experimental set-up of CVD, region I represents the similar scenario to the carbon-rich environment for in-situ growth of CNTs. Therefore, at 650°C of cracking methane, $\text{Co}(\text{NO}_3)_2$ can be easily reduced to monolithic Co particles that are thermodynamically more favourable for carbon absorption and diffusion, rather than reacting with oxygen.

7.3 Understanding of CNTs growth mechanism

However, the thermodynamic analysis cannot explain the selective growth of CNTs in certain size range (10 ~ 30 nm in diameter) of catalyst particles during CVD process, the initiation and termination of catalytic growth of CNTs.

7.3.1 Carbon absorption and diffusion

Based on experimental observations, it was proposed that during CVD process, free carbon atoms decomposed from cracking methane were preferentially absorbed on top surface of catalyst particles, due to larger surface energy compared to that of CFs [137, 138]. As suggested in section 7.2, the chemisorbed free carbon atoms were less likely to react with cobalt in the form of cobalt carbide, but coexist as carbon atoms. For each cobalt particle, the carbon atoms likely diffuse along the concentration gradient of carbon from either the surface of cobalt particle or within the bulk material, to the interface

between CF substrate and the cobalt particle. The carbon atoms accumulated at the interface may precipitate in the form of graphene layers as observed in figure 5.11(b), due to the much lower surface energy of graphene layers ($>120\text{mJm}^{-2}$) [139].

The rates of carbon absorption and diffusion on cobalt particles may also be affected by decomposition temperature, as suggested in section 4.3.2. Both rates were accelerated with increasing the cracking temperature of methane from 500°C to 700°C . However, morphologies of carbon deposition varied as the cracking temperature increased. At 500°C , no visible growth of CNTs or carbon deposition were observed, as the cobalt particles may be oxidised by oxygen content as suggested in figure 4.7, which may hinder the absorption and diffusion of carbon atoms. While at 700°C , the rates of carbon absorption and diffusion were significantly increased that the morphologies of CFs appeared to be cobalt particles embedded within carbon matrix, as suggested in figure 4.12.

When the cracking temperature was at 650°C , the carbon absorption and diffusion on cobalt particles may be balanced to an appropriate state, resulting in optimised yield of CNTs. However, not all catalyst particles have CNTs attached, and it may be related to the diameter of particles as indicated in figure 4.11. It was suggested the total surface energy, expressed by the total surface area (SA) per volume (V), increases significantly when the catalyst particles is down to nanometer size (*2.5~60 nm as examined in SEM analysis*) [140]. Increased total surface energy leads to accelerated carbon absorption rate,

through which the total surface energy can be reduced by chemisorbing carbon atoms onto surface of cobalt particles. As for the 'particle 4' shown in figure 4.11 with a large SA/V, rapid carbon absorption may lead to fast encapsulation of cobalt particles, compared to that of 'particle 3'.

7.3.2 Theory of carbon diffusion and growth of CNTs

7.3.2.1 Contact of Co–substrate interface and theory of carbon diffusion

TEM observations have suggested that the interfacial contact between Co particles and the substrate was versatile, not only depending on the surface topography of substrates, but also the geometry of the catalyst particles. Based on the SEM observation shown in figure 4.11, morphologies of Co particles can be generally divided into three categories: sphere, reversed-pear and semi-sphere. When catalyst particles with different geometries were deposited on the surface of substrate, the contact situation between the two could be very complex.

A possible theory for carbon diffusion on catalyst particles of different interfacial contact with the substrate has been proposed in figure 7.4. The direction of carbon diffusion was from top surface of the Co particle and gradually accumulated at the bottom through carbon concentration gradient in the bulk material of cobalt. Therefore, the growth of a CNT was likely initiated from the bottom surface of the catalyst particle. The zone formed between the bottom surface of a catalyst particle and the surface of the substrate could be the 'Key

Zone' for catalytic growth of CNTs as marked in figure 7.4(a).

Based on the model proposed in figure 7.4, the angle of the 'Key Zone' varies depending on the geometry of the catalyst particle and surface topography of the substrate. For catalyst particles with the geometry of sphere or reversed-pear on a flat surface as shown in figure 7.4(a), the angle of the 'Key Zone', is normally less than 90° . During continuous graphitisation of carbon, a growing force that is along the direction of perpendicular upwards to the substrate is applied on the bottom surface of the Co particle. The growing force will be interpreted in more details in the next section of 7.3.2.2. The Co particle will be eventually detached from surface of the substrate by the growing force. However, if the geometry of the Co particle is semi-sphere as shown in figure 7.4(a), there will be no growing force from its bottom surface. Alternatively, graphene layers are more likely to be formed on this type of catalyst particles, by encapsulating the surface and eventually deactivating the catalyst particles, as suggested in figure 4.11.

The second scenario of the theory was shown in figure 7.4(b). If the catalyst particles are not isolated, but agglomerated on surface of CFs, the interactions among catalyst particles are likely to be strong enough to overcome the growing force. The Co particles may be stuck on surface of the substrate during CVD process, and be deactivated by encapsulated in carbon deposition as suggested in figure 4.10(b).

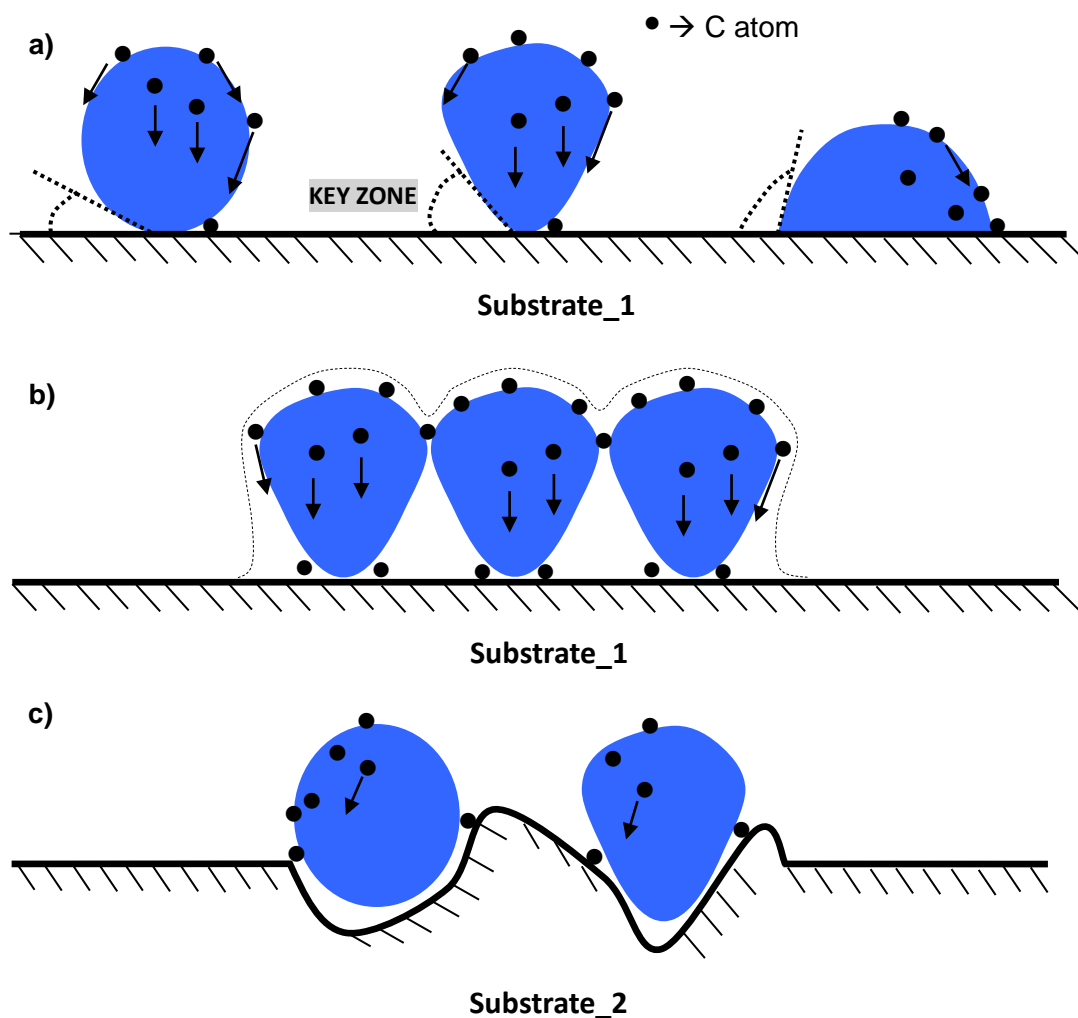


Figure 7.4 – Proposed interfacial contact between Co particles and surface of substrate and carbon diffusion within the bulk material of cobalt. a) flat surface with Co particles of different geometries, b) flat surface with agglomerated Co particles, and c) Co particles with spherical and reversed-pear geometries embedded in groove substrate.

The third scenario of the theory was shown in figure 7.4(c). When Co particles with spherical and reversed-pear geometries are embedded in grooves of the substrate, the contact area of the interface will be extended. Therefore, more force is needed to separate Co particles and the substrates, which is also detrimental to catalytic growth of CNTs as suggested in figure 6.11(d).

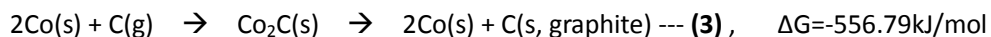
7.3.2.2 Initiation of the growth of CNTs

At the initiation of a growing CNT, assume a gas is confined in the 'Key Zone', by boundaries including: 1) surface of the substrate, 2) bottom surface of the Co particle, and 3) walls of the CNT. The confined ideal gas was undergoing isobaric process during CVD. From the energy point of view, during isobaric process, the energy absorbed by the ideal gas was partially used to increase its internal energy, and partially used to apply work externally, according to the first law of thermodynamics [141]. The applied work is related to volume expansion of the ideal gas, as shown in the equations:

$$Q_p = \Delta E + W_p \quad (7)$$

$$W_p = \int_{V_1}^{V_2} p dV \quad (8)$$

where Q_p is absorbed energy by the ideal gas from the chemical reaction of (3), ΔE is the increment of energy of the confined ideal gas, which may be released in forms of heat, light, etc. W_p is applied work externally by the ideal gas, p is pressure of the ideal gas, which is atmospheric pressure during CVD process, and dV is volume expansion of the ideal gas, presume the amount of the confined ideal gas inside the tube was constant.



Atmospheric pressure:

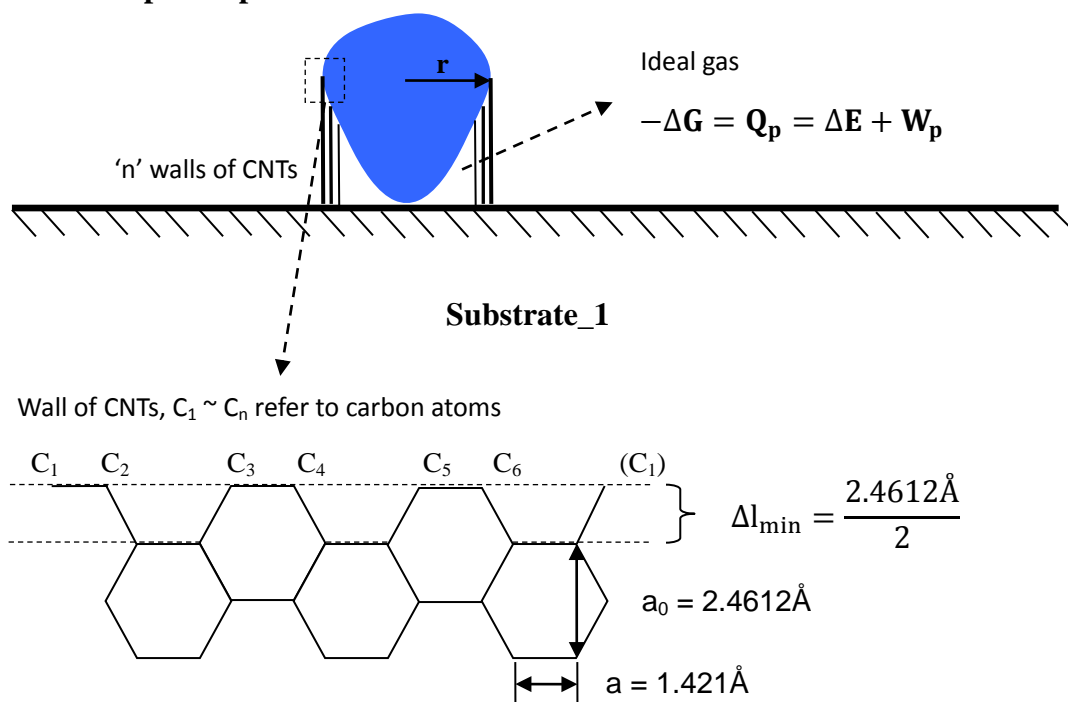


Figure 7.5 – Initiation of a growing CNT, and schematic drawing of the increased number of carbon atoms associated with volume expansion of the ideal gas.

In chemical reaction of (3), assume $X\%$ ($0 < X < 100$) of the Gibbs free energy of formation (556.79kJ/mol) was absorbed by the ideal gas in the 'Key Zone', i.e. $Q_p = X\% \times (\Delta G) \times (\text{mole number of carbon})$. During isobaric process, part of the energy was used to increase internal energy of the ideal gas, and the other part of the energy was applied on bottom surface of the Co particle by pushing it upwards from surface of the substrate, through volume expansion of the ideal gas.

As shown in figure 7.5, the minimum spacing (Δl_{\min}) that the Co particle has to

be lifted up by $\frac{a_0}{2}$. For each wall of a CNT, the number of carbon atoms required for a Δl_{\min} increasing in length is $\frac{C}{3a} \times 2$, where C is the perimeter of the CNT at this wall. Since the interplanar spacing between walls of a CNT is approximately 3.4Å, close to graphene layers in graphite, the total number of carbon atoms required for a Δl_{\min} increasing in length of a n-wall CNT is given by:

$$\sum_1^n \left[\frac{C}{3a} \times 2 \right] = \sum_1^n \left\{ \frac{2\pi[r-(n-1) \times 3.4\text{\AA}]}{3a} \times 2 \right\} \quad (9)$$

Since there are 6.02×10^{23} carbon atoms in 1mol C, the mole number required for a Δl_{\min} increasing in length of a n-wall CNT is given by:

$$\frac{\sum_1^n \left\{ \frac{2\pi[r-(n-1) \times 3.4\text{\AA}]}{3a} \times 2 \right\}}{6.02 \times 10^{23}} \quad (10)$$

According to chemical reaction of (3), the total energy released by a Δl_{\min} increasing in length of a n-wall CNT can be calculated by:

$$\frac{\sum_1^n \left\{ \frac{2\pi[r-(n-1) \times 3.4\text{\AA}]}{3a} \times 2 \right\}}{6.02 \times 10^{23}} \times (-\Delta G) \quad (11)$$

Taking (11) into equation (7), given,

$$\frac{\sum_1^n \left\{ \frac{2\pi[r - (n-1) \times 3.4\text{\AA}]}{3a} \times 2 \right\}}{6.02 \times 10^{23}} \times (-\Delta G) \times X\% = \Delta E + \int_{V_1}^{V_2} p dV$$

$$= \Delta E + \int_{l_1}^{l_2} p \pi [r - (n-1) \times 3.4\text{\AA}]^2 dl$$
(12)

In order to initiate the catalytic growth of a CNT, the minimum distance of the Co particle has to be popped up from surface of the substrate is: Δl_{\min} , therefore,

$$\frac{4\pi \times (-\Delta G) \times X\%}{3a \times 6.02 \times 10^{23}} \times \sum_1^n [r - (n-1) \times 3.4\text{\AA}] \geq \Delta E + p \pi [r - (n-1) \times 3.4\text{\AA}]^2 \times \Delta l_{\min}$$
(13)

Since $0 < X\% < 1$, therefore,

$$\frac{4\pi \times (-\Delta G)}{3a \times 6.02 \times 10^{23}} \times \sum_1^n [r - (n-1) \times 3.4\text{\AA}] > \Delta E + p \pi [r - (n-1) \times 3.4\text{\AA}]^2 \times \Delta l_{\min}$$

Taking $(-\Delta G) = 5.5679 \times 10^5$ J/mol, $p = 1.01 \times 10^5$ Pa, $d_{(001)}$ of graphite = $3.4\text{\AA} = 3.4 \times 10^{-10}$ m, and $\Delta l_{\min} = 1.2306 \times 10^{-10}$ m, into (13), therefore,

$$3.9027 \times 10^{-5} r^2 - [2.6538 \times 10^{-14} (n-1) + 2.7250 \times 10^{-8} n] r + \Delta E + 4.5115$$

$$\times 10^{-24} (n-1)^2 + 4.6325 \times 10^{-18} (n^2 - n) < 0$$
(14)

While in (14), $a=3.9027 \times 10^{-5}$, $b=-[2.6538 \times 10^{-14}(n-1)+2.7250 \times 10^{-8}n]$,
 $c=\Delta E+4.5115 \times 10^{-24}(n-1)^2+4.6325 \times 10^{-18}(n^2-n)$, therefore,

$$r_1 > \frac{-b - \sqrt{b^2 - 4a \times [\Delta E + 4.5115 \times 10^{-24}(n-1)^2 + 4.6325 \times 10^{-18}(n^2-n)]}}{2a} \quad (15)$$

$$r_2 < \frac{-b + \sqrt{b^2 - 4a \times [\Delta E + 4.5115 \times 10^{-24}(n-1)^2 + 4.6325 \times 10^{-18}(n^2-n)]}}{2a} \quad (16)$$

In the expression of $r_{1,2}$, ΔE is increase of energy of the confined ideal gas. If the energy was released in the form of heat, then the value of ΔE is related to the increment of temperature of the ideal gas at the peak temperature during CVD process, which is difficult to identify. However, the value of ΔE must have meet the condition that $\Delta E > 0$, which is as a function of the increment of temperature and heat capacity of the ideal gas.

The expression of r has indicated that there exists a minimum value of r_1 , less than which the catalytic growth of CNTs cannot be initiated. As increasing of the number of walls of CNTs, the value of r_1 can be estimated as below:

When $n=1$, $r_1^* > 0.17$ nm, $d^* > 0.34$ nm;

$n=5$, $r_1^* > 0.67$ nm, $d^* > 1.34$ nm;

$n=10$, $r_1^* > 1.53$ nm, $d^* > 3.06$ nm;

$n=15, r_1^* > 2.38 \text{ nm}, d^* > 4.76 \text{ nm};$

$n=20, r_1^* > 3.23 \text{ nm}, d^* > 6.46 \text{ nm}.$

.....

Where * means the value were not the critical value, but should further increased when considering the positive value of ΔE .

When growth of CNTs was initiated and catalyst particles was popped up from the surface of substrate, the minimum value of r_1 should also satisfy the condition that $r > (n-1) \times 3.4 \text{ \AA}$, based on the electron microscopic observation of tip-growing CNTs, giving:

When $n=1, r_1' > 0 \text{ nm}, d' > 0 \text{ nm};$

$n=5, r_1' > 1.36 \text{ nm}, d' > 2.72 \text{ nm};$

$n=10, r_1' > 3.06 \text{ nm}, d' > 6.12 \text{ nm};$

$n=15, r_1' > 4.76 \text{ nm}, d' > 9.52 \text{ nm};$

$n=20, r_1' > 6.46 \text{ nm}, d' > 12.92 \text{ nm}.$

.....

The calculations above suggest that the size of catalyst particles should larger than a critical value of diameter in order to initiate the tip-growth of CNTs. The model is based on thermodynamic point of view; there are also other factors that may affect the minimum value of r , such as adhesion force between catalyst particles and surface of substrates, gravity force, etc. However, the current calculations indicate the initiation of catalytic growth of CNTs should on catalyst particles, the diameter of which is larger than a critical value.

This model explained why the catalytic growth of CNTs was only effective on catalyst particles with a certain size range. Theoretically, when the surface of substrate was perfectly flat and the contact situation between bottom of catalyst particles and the substrate was fitted well to the scenario that shown in figure 7.4(a), all catalyst particles with the diameter larger than the calculated critical value (*and smaller than about 50nm in diameter*) should be catalytic effective for growth of CNTs. The diameter of CNTs was dominated by that of catalyst particles, and the length of CNTs can be controlled by processing condition of CVD.

CHAPTER 8 Conclusions and Further work

8.1 Conclusions

The growth of CNT reinforcements was carried out on various substrates, including carbon fibre, silicon carbide and alumina grits, as well as Y-TZP powder. The experimental results demonstrated possible techniques to anchor CNTs onto substrates through an in-situ catalytic chemical vapour deposition process. Fairly systematic studies were conducted to seek and optimise the processing conditions for the successful growth of CNTs, including surface pre-treatment, type of catalyst, catalyst deposition, and heat treatment. The processing condition for in-situ CVD was investigated first on surface of carbon fibre, and then applied on ceramic powders. The morphology of catalyst particles and CNTs grown on various substrates were analysed by electron microscopy. The diameters of catalyst particles and CNTs were quantitatively measured, and the results demonstrated that the growth of CNTs has a strong tendency to occur on a specific range of sizes of the catalyst particles. The key points drawn from the research are summarised as followings:

(1) In-situ CCVD growth of CNTs on carbon fibres

- (a) Under the current setup for the growth of CNTs, Co particles provided a clear catalytic effect for the successful growth on all surfaces of the studied ceramic constituents. However, neither Fe nor Ni particle was approved successful. The growth of CNTs mainly followed tip-growing

mode.

- (b) For commercially available carbon fibres, the sizing materials on the surface had no any beneficial to promote the impregnation of catalytic precursor. By boiling in nitric acid solution at 60°C for 30 minutes, much better impregnation was achieved when carbon fibres were dipped into precursor solution.
- (c) The following processing conditions was approved success for the growth of CNTs on all surfaces of studied ceramic constituents and carbon fibre: temperature of CVD was 650°C with a dwelling period of 60 minutes; and catalyst precursor was $\text{Co}(\text{NO}_3)_2$ in a solution concentration of 0.3 mol/l.
- (d) As the concentration of precursor solution was increased from 0.001 to 0.1 mol/l, the size range of the achieved catalyst particles became broader in diameter. However, at a concentration of 0.3 mol/l, the range became the same as that at 0.05 mol/l, i.e. 4 to 30 nm.
- (e) At temperatures of 500 to 600°C, the range of equivalent diameter of catalyst particles became narrow, and was from 8 to 32 nm at 650°C; at 700°C, the upper limit increased to 65 nm and no change for the lower limit.
- (f) The growth of CNTs was visible at 600°C, while concentration of

$\text{Co}(\text{NO}_3)_2$ solution was from 0.005 to 0.3 mol/l. At 650°C, growth of CNTs on surface of carbon fibres was optimised, while concentration of $\text{Co}(\text{NO}_3)_2$ was adjusted at 0.3 mol/l.

(g) Statistically, the analysis suggested that the size of developed catalyst particles ranged from about 2.5 to 60 nm in diameter, but CNTs grew from catalyst particles with a size ranging from 10 to 30 nm. Beyond this size range, CNTs were rarely observed on catalyst particles.

(2) In-situ CCVD growth of CNTs on ceramic substrates

(a) The optimised in-situ CCVD processing conditions on surface of carbon fibres has been successfully conducted on the surface of other ceramic substrates, including silicon carbide, alumina and Y-TZP.

(b) Similar selective catalysation was observed on surface of ceramic particles. Catalyst particles with a diameter of 15 to 35 nm were most likely popular ones to promote the growth of CNTs.

(c) When the concentration of $\text{Co}(\text{NO}_3)_2$ was changed from 0.3 to 0.6 mol/l, the average diameter of CNTs was slightly increased from about 20 to 27 nm, whilst the range of the diameter of CNTs was the same between 15 and 35 nm.

(d) There was no obvious change in the averaged diameter of CNTs as

the changes in size of ceramic constituents; the diameter of CNTs was still in the range between 15 and 35 nm.

(3) Characterisation of CNTs on various substrates

- (a) The growth of CNTs was mostly in a tip-growing mode. The catalyst particles were detached from surface of the substrate and lifted up by the CNTs.
- (b) The maximum length of CNTs observed on surface of carbon fibres was about half-micron for 1 hour of CVD process at 650°C, while up to 3 µm on surface of Al₂O₃ grit for 1 hour of CVD process at 650°C.

(4) Mechanism of catalytic growth of CNTs

- (a) Chemical reactions of the transformation of monolithic cobalt particles from Co(NO₃)₂ were validated from thermodynamic point of view. The Gibbs free energy of reaction was calculated for each chemical reaction as the variation of temperature from 25°C to 650°C. The calculations suggested at 650°C, Co particle is thermodynamically more favourable for carbon absorption and diffusion, i.e. as a catalyst, rather than reacting with oxygen. The analysis was also supported by MTDATA simulation in the C-Co-O phase diagram.
- (b) The initiation of growth of CNTs on Co particles was proposed by a

model based on First Law of thermodynamics. At the bottom of a typical catalyst particle deposited on a smooth surface, a gas was assumed to be confined by bottom surface of the catalyst particle, surface of substrate and walls of CNTs. During the isobaric process of CVD, the force required to initiate the growth of CNTs was calculated based on the energy absorbed by the ideal gas from deposition of carbon in the form of graphene layers, associated by the volume expansion of the ideal gas. The calculated diameter of cobalt particles suggested the value has to be larger than a critical value in order to initiate the growth of CNTs, which was universally observed in the experimental results.

8.2 Further work

- Manufacture of CFs reinforced carbon composite, through chemical vapour infiltration process by using the CFs/CNTs hybrid preform, in comparison with that without in-situ growth of CNTs. Apply various mechanical properties testing, such as 3-point bending, on the as-produced CNTs/CF carbon composite in order to study the effect of reinforcement of CNTs, in associated with the microstructural analysis.
- Manufacture of Al_2O_3 composite, through chemical methods by using the Al_2O_3 /CNTs composite powders, in comparison with that without in-situ growth of CNTs. Apply various mechanical properties testing, such as Vick's indentation, on the as-produced Al_2O_3 /CNTs composite (*aluminium*

phosphate as bonding agent) in order to study the effect of reinforcement of CNTs, in associated with the microstructural analysis.

- The CNTs may be further converted to Si-NTs by infiltrating Si vapour into the forest of CNTs. The composite with unique microstructure can be potentially used in lots of application, such as friction materials in automotive, train and aerospace areas.
- Further applying the processing condition for growth of CNTs on other systems, for example, the area of geopolymers, in order to promote its potential application as the replacement of other composites.

CHAPTER 9 References

- [1] S. Iijima, *Nature*, 1991 Vol. 354, 56
- [2] A. Allaoui, S. Bai, H.M. Cheng and J.B. Bai, *Compos. Sci. Technology*, 2002, Vol. 62, 1993–1998
- [3] K.T. Kim, S. Il Cha, S.H. Hong and S.H. Hong, *Mater. Sci. Eng*, 2006, Vol. 430, 27–33
- [4] T. Laha, A. Agarwal, T. McKechnie and S. Seal, *Mater. Sci. Eng*, 2004, Vol. 381 249–258
- [5] M. Yu, O. Lourie, M.J. Dyer, K. Moloni, T. F. Kelly and R. S. Ruoff, *Science*, 2000, Vol. 287 (5453), 637-640
- [6] S. Bellucci. *Physica status solidi (c)*, 2005, Vol. 2, Issue.1, 34-47
- [7] J.M. Makar, J.J. Beaudoin, 1st International Symposium on Nanotechnology in Construction, Paisley, Scotland, 2003, 331-341
- [8] R.H. Baughman, A.A. Zakhidov, W.A. de Heer, *Science*, 2002, Vol. 297, 787
- [9] M.Mcyyappan, *Nanotechnology Aerospace Applications*, 2006, 7-1~ 7-2
- [10] M. Endo, T. Hayashi, Y. A. Kim, and H. Muramatsu, *Jpn. J. Appl. Phys (JJSP)*, 2006, Vol. 45, No. 6A, 4883-4892
- [11] Y. Ando and S. Iijima, *Jpn. J. Appl. Phys (JJSP)*, 1993, Vol. 32, L107.
- [12] B. I. Yakobson and R.E. Smalley, *American Scientist*, 1997, Vol. 324, 85
- [13] G. Che, B. B. Lakshmi, C. R. Martin, E. R. Fisher and R. S. Ruoff, *Chem. Mater*, 1998, Vol. 10, 260-267
- [14] M. Daenen, R.D. de Fouw, B. Hamers, P.G.A. Janssen, K. Schouteden and M.A.J. Veld, Eindhoven University of Technology, Netherlands, Multi Disciplinary project, 2003, 9
- [15] A. Oberlin, M. Endo and T. Koyama, *Journal of Crystal Growth*, 1976, Vol. 32, 335-349
- [16] A. Gorbunov, O. Jost, W. Pompe and A. Graff, *Carbon*, 2002, Vol. 40 113–118
- [17] S.B. Sinnott, R. Andrews, D. Qian, A.M. Rao, Z. Mao, E.C. Dickey, F. Derbyshire,

Chemical Physics Letters, 1999, Vol. 315, 25-30

[18] L. Vaisman, H. D. Wagner, G. Marom, *Advances in Colloid and Interface Science*, 2006, Vol. 128, 37–46

[19] A. Peigney, C. Laurent, F. Dobigeon and A. Rousset, *J. Mater. Res*, 1997, Vol. 12, 613–615

[20] E. Flahaut, A. Peigney, C. Laurent, C. Marliere, F. Chastel and A. Rousset, *Acta Mater*, 2000, Vol. 48, 3803–3812

[21] A. Peigney, E. Flahaut, C. Laurent, F. Chastel and A. Rousset, *Chem. Phys. Lett.*, 2002, Vol. 352, 20–25

[22] A. Oberlin, M. Endo, and T. Koyama, *Carbon*, 1976, Vol. 14, 133-135

[23] P. M. Ajayan, S. Iijima and T. Ichihashi, *Phys. Rev. B*, 1993, Vol. 47, 6859-6862

[24] D. S. Bethune *et al.*, *Nature*, 1993, Vol. 363 605–607

[25] E. T. Thostenson, Z. Ren, T. Chou, *Composites Science and Technology*, 2001, Vol. 61, 1899–1912

[26] Australian Stainless Steel Development Association (ASSDA) - Properties of Stainless Steel

[27] P. G. Collins, P. Avouris, *Scientific American*, 2000, Vol. 283 (6), 67-69

[28] W. Tang, M.H. Santare and S.G. Advani, *Carbon*, 2003, Vol. 41, 2779-2785

[29] A. Peigney, C. Laurent, E. Flahaut, R. R. Bacsa, and A. Rousset, *Carbon*, 2001, Vol. 39, 507-514

[30] X. Lu and Z. Chen. *Chem. Rev.*, 2005, Vol. 105 (10), 3643–3696

[31] C. S. Rul, A. Laurent, A. R. Peigney, *Journal of the European Ceramic Society*, 2003, Vol. 23, 1233–1241

[32] A.R. Harutyunyan, B.K Pradham, G.U. Sumanasekera, E. Yu. Korobko and A.A. Kuznetsov, *European Cells and Materials*, 2002, Vol. 3, 84-87

[33] T. Guo, P. Nikolaev, A. Thess, D.T. Colbert and R.E. Smalley, *Chem. Phys. Lett.*, 1995, Vol. 243, 49-54

[34] S. M. Irving and P. L. Walker, *Carbon*, 1967, Vol. 5, 399-402

-
- [35] F.J. Derbyshire, A.E.B. Presland and D.L. Trimm, *Carbon*, 1975, Vol. 13, 111-113.
- [36] R.T.K. Baker and P.S. Harris, *Chemistry and Physics of Carbon*, 1978, Vol. 14, 83-165
- [37] R.T.K. Baker, *Carbon*, 1989, Vol. 27 (3), 315-323
- [38] M. Endo, T. Hayashi, Y. A. Kim and H. Muramatsu, *Jpn. J. Appl. Phys (JJSP)*, 2006, Vol. 45(6A), 4883–4892
- [39] H. Dai, A. G. Rinzler, *et al.*, *Chemical Physics Letters*, 1996, Vol. 260, 471-475.
- [40] S. Helveg *et al.*, *Nature*, 2004, Vol. 427, 426-429
- [41] Guozhong Cao, *Nanostructures & Nanomaterials Synthesis, Properties & Applications*, published by World Scientific, Imperial College Press, 2003, 127.
- [42] M. Daenen, R.D. de Fouw, B. Hamers, P.G.A. Janssen, K. Schouteden and M.A.J. Veld, *Eindhoven University of Technology, Netherlands, Multi Disciplinary project*, 2003, 9
- [43] T. W. Ebbesen and P. M. Ajayan, *Nature*, 1992, Vol. 358, 220-222
- [44] S. Farhar, M. L. La Chapelle, A. Loiseau, C. D. Scott, S. Lefrant, C. Journet, and P. Bernier, *Journal of Chemical Physics*, 2001, Vol. 115 (14), 6752-6759
- [45] C. Journet, and P. Bernier, *Applied Physics A-Materials Science & Processing*, 1998, Vol. 67(1), 1-9
- [46] S. H. Jung, M. R. Kim, S. H. Jeong, S. U. Kim, O. J. Lee, K. H. Lee, J. H. Suh and C. K. Park, *Applied Physics A-Materials Science & Processing*, 2003, Vol. 76 (2), 285-286
- [47] T. Guo, P. Nikolaev, A. Thess, D.T. Colbert and R.E. Smalley, *Chemical Physics Letters*, 1995, Vol. 243, 49-54
- [48] W. K. Maser, E. Munoz, A. M. Benito, M. T. Martinez, G.F. de la Fuente, Y. Maniette, E. Anglaret and J. L. Sauvajol, *Chemical Physics Letters*, 1998, Vol. 292, 587–593
- [49] E.F. Kukovitsky, S.G. L'vov and N.A. Sainov, *Chemical physics letters*, 2000, Vol. 317, 65-70
- [50] W. Li, D. Wang, S. Yang, J. Wen and Z. Ren. *Chemical Physics Letters*, 2001, Vol. 335, 141-149

-
- [51] Z. Ren, Z. Huang, D. Wang *et al.*, Applied Physics Letters, 1999, Vol. 75 (8), 1086–1088
- [52] T. Schauer, L. Weber, J. Hafner, O. Kus, E. V. Pechen, A. V. Varlashkin, T. Kaiser and K. F. Renk. Supercond. Sci. Technol., 1998, Vol. 11, 270-272
- [53] S. Proyer, E. Stangl, M. Borz, B. Hellebrand and D. Bäuerle, Physica C, 1996, Vol. 257, 1
- [54] M. Daenen, R.D. de Fouw, B. Hamers, P.G.A. Janssen, K. Schouteden and M.A.J. Veld, Eindhoven University of Technology, Netherlands, Multi Disciplinary project, 2003, 18
- [55] M. Endo, Chemtech, 1998, Vol. 18, 568-576
- [56] M. Endo, T. Hayashi, Y. A. Kim and H. Muramatsu. Jpn. J. Appl. Phys (JJSP), Vol. 45 (6A), 4883–4892
- [57] A. Larsen, R. Whetstone, J. Liang. Worcester Polytechnic Institute, US, project number: MQP-JNL-CNT9. 2010.
- [58] Atomic Physics, Göteborg University, Image comes from web address:
http://www.physics.gu.se/forskning/atomic_and_molecular/atomfysik/forskning/nanotubes/experimental_facilities/
- [59] J. Dijon, P. D. Szkutnik, A. Fournier *et al.*, Carbon 2010, Vol. 48, 3953-3963.
- [60] H. Neumayer and R. Haubner, Diamond and Related Materials, 2004, Vol. 13, Issues 4-8, 1191-1197
- [61] K. Otsuka, H. Ogihara, S. Takenaka, Carbon, 2003, Vol. 41, 223-233
- [62] H. Neumayer and R. Haubner, Diamond and Related Materials, 2004, Vol. 13, Issues 4-8, 1191-1197, fig. 2
- [63] G. G. Tibbetts, C. A. Bernardo, D. W. Gorkiewicz and R. L. Alig, Carbon, 1994, Vol. 32, 569-576
- [64] I. Martin-Gullon, J. Vera, J. A. Conesa, J. L. González and C. Merino, Carbon, 2006, Vol. 44, Issue 8, 1572-1580
- [65] C. M. Veziri, G. Pilatos, G. N. Karanikolos, A. Labropoulos *et al.*, Microporous and Mesoporous Materials, 2008, Vol. 110, Issue 1, 41-50

-
- [66] A. Moisala, A. G. Nasibulin, D. P. Brown, H. Jiang, L. Khriachtchev and E. I. Kauppinen, *Chemical Engineering Science*, 2006, Vol. 61, Issue 13, 4394-4395
- [67] M. S. P. Shaffer and A. H. Windle, *Adv. Mater.*, 1999, Vol. 11, 937–941
- [68] D. Qian, E. C. Dickey, R. Andrews, T. Rantell. *Applied Physics Letters*, 2000, Vol. 76(20), 2868–2870
- [69] P. J. F. Harris, *International Materials Reviews*, 2004 Vol. 49 No. 1, 31-43
- [70] K. T. Kim, S. Il Cha, Seong Hyeon Hong and Soon Hyung Hong, *Materials Science and Engineering A*, 2006, Vol. 430, 27–33
- [71] T. Kuzumaki, K. Miyazawa, H. Ichinose and K. Ito, *J. Mater. Res.*, 1998, Vol. 13, 2445–2449
- [72] K. Ahmad and W. Pan, *Composites Science and Technology*, 2008, Vol. 68 1321–1327
- [73] J. Fan, D. Zhuang, D. Zhao *et al.*, *Applied Physics Letters*, 2006, Vol. 89, 121910
- [74] G. Yamamoto, M. Omori, T. Hashida and H. Kimura, *Nanotechnology*, 2008, Vol. 19, 315708 (7pp)
- [75] O. Smiljanic, T. Dellerio, A. Serventi, G. Lebrun, B. L. Stansfield, J.P. Dodelet, M. Trudeau, S. Desilets. *Chemical Physics Letters*, 2001, Vol. 342 503-509
- [76] X. Sun, B. Stansfield, J. P. Dodelet, S. Desilets. *Chemical Physics Letters*, 2002, Vol. 363, 415–421
- [77] X. Sun, R. Li, B. Stansfield, J. Dodelet, G. Ménard and S. Désilets, *Carbon*, 2007, Vol. 45, 732-737
- [78] J. Zhao, L. Liu, Q. Guo, J. Shi, G. Zhai, J. Song and Z. Liu, *Carbon*, 2008, Vol. 46, 365-389
- [79] United States Patent 5271917, 'Activation of carbon fiber surfaces by means of catalytic oxidation'
- [80] C.C. Luhrs, D. Garcia, M. Tehrani *et al.* *Carbon*, 2009, Vol. 47, 3071–3078
- [81] Y. Xia, L. Zeng, W. Wang, J. Liang *et al.*, *Applied Surface Science*, 2007, Vol. 253, Issue 16, 6807-6810
- [82] T. Bordjiba, M. Mohamedi and L. H. Dao, *Nanotechnology*, 2007, Vol. 18, 035202 (5pp)

-
- [83] M.F. De Riccardis, D. Carbone, T. D. Makris, R. Giorgi, N. Lisi, E. Salernitano. Carbon, 2006, Vol. 44, 671–674
- [84] J. Zhao, Q. Guo, J. Shi *et al.*, Carbon, 2009, Vol. 47, 1747–1751
- [85] M. P Manning, J. E. Garmirian, R. C. Reid, Ind. Eng. Chem. Process Des. Dev., 1982, Vol. 21, 404
- [86] S. Zhu, C. Su, S.L. Lehoczky, I. Muntele, D. Ila. Diamond and Related Materials, 2003, Vol. 12, 1825–1828
- [87] Z. P. Huang, D. Z. Wang, J. G. Wen, M. Sennett, H. Gibson, Z. F. Ren, Appl. Phys. A, 2002, Vol. 74, 387–391
- [88] M. J. O’Connell, Taylor & Francis Group, California, USA, 2006.
- [89] O .Smiljanic, T. Dellerio, A. Serventi, G. Lebrun, B. L. Stansfield, J.P. Dodelet, M. Trudeau, S. Desilets. Chemical Physics Letters, 2001, Vol. 342 503-509
- [90] X. Sun, B. Stansfield, J.P. Dodelet, S. Desilets, Chemical Physics Letters, 2002, Vol. 363, 415–421
- [91] N. S. M. Ohshita, A. Nijubu, H. Nishikawa, H. Yanase, J. Hayashi, T. Chiba. Carbon, 2006, Vol. 44, Issue 9, 1754-1761
- [92] R. B. Mathur, S. Chatterjee, B. P. Singh, Composites Science and Technology, 2008, Vol. 68, 1608–1615
- [93] S. Zhu, C. Su, S. L. Lehoczky, I. Muntele, D. Ila. Diamond and Related Materials, 2003, Vol. 12, 1825–1828
- [94] N. S. M. Ohshita, A. Nijubu, H. Nishikawa, H. Yanase, J. Hayashi, T. Chiba. Carbon, 2006, Vol. 44, Issue 9, 1754-1761
- [95] Q. Gong, H. Li, X. Wang, Q. Fu, Z. Wang, K. Li. Composites Science and Technology, 2007, Vol. 67, 2986–2989
- [96] L. Ci, Z. Rao, Z. Zhou, D. Tang, X. Yan, Y. Liang *et al.*, Chem Phys Lett, 2002, Vol. 359, 63-67
- [97] N. S. M. Ohshita, A. Nijubu, H. Nishikawa, H. Yanase, J. Hayashi, T. Chiba. Carbon, 2006, Vol. 44, Issue 9, 1758, fig.7

-
- [98] A. Govindaraj, E. Flahaut, Ch. Laurent, A. Peigney, and A. Rousset, C. N. R. Rao, J. Mater. Res., 1999, Vol. 14, No. 6, 2567-2576
- [99] A. Peigney, Ch. Laurent, E. Flahaut and A. Rousset, Ceramics International, 2000, Vol. 26, 677-683
- [100] M. H. A. Kudus, H. Md. Akil, H. Mohamad, L. E. Loon. Journal of Alloys and Compounds, 2011, Vol. 509, 2784–2788
- [101] J. W. An, D. H. You and D. S. Lim, Wear, 2003, Vol. 255, 677–681
- [102] K. J. Probst, T. M. Besmann, D. P. Stinton, R. A. Lowden, T. J. Anderson, T. L. Starr, Surface and Coatings Technology, 1999, Vol. 120–121, 253, fig.2
- [103] B. Wirlage, A.G. Odeshi, H. Mucha, H. Lang and R. Buschbeck. Journal of Materials Processing Technology, 2003, Vol. 132, 313-322
- [104] K. J. Probst, T. M. Besmann, D. P. S., R. A. Lowden, T. J. Anderson and T. L. Starr, Surface and Coatings Technology, 1999, Vol. 120–121, 250–258.
- [105] R. Morrell, Comprehensive Composite Materials, Elsevier Science, 2004, Vol. 4, 1-24
- [106] W. Kowbel, H. L. Liu and H. T. Tsou, Metallurgical and Materials Transactions A, 1992, Vol. 23, No. 4, 1051-1062
- [107] W. Kowbel, P. S. Chen and H. Yenchang. Ultramicroscopy, 1989, Vol. 29 89-109
- [108] M. Y. He and J. W. Hutchinson, Int. J. Sol. Str., 1989, Vol. 25, 1053-1067
- [109] B. D. Agarwal, L. J. Broutman and K. Chandrashekhara, Analysis and performance of fiber composites. 3rd Edition, Published by John Wiley and Sons, 2006, 342
- [110] A. R. Bhatti and P. M. Farries, Comprehensive Composite Materials, Elsevier Science, 2004, Vol. 4, 14
- [111] S. Rul, F. Lefevre-schlick, E. Capria, Ch. Laurent, A. Peigney. Acta Materialia, 2004, Vol. 52, 1061–1067
- [112] J. W. An, D. H. You, D. S. Lim. Wear, 2003, Vol. 255, 677–681
- [113] G. D. Zhan, J. D. Kuntz, J. Wan and A. K. Mukherjee, Nat. Mater., 2003, Vol. 2, 38-42
- [114] A. Peigney, S. Rul, F. Lefevre-Schlick, C. Laurent. Journal of the European Ceramic Society, 2007, Vol. 27, 2183-2193

-
- [115] R. Kamalakaran, F. Lupo, N. Grobert, D. Lozano-Castello, N.Y. Jin-Phillipp, M. Rühle. Carbon, 2003, Vol. 41, 2737–2741
- [116] A. S. Wagh and S. Y. Jeong, J. Am. Ceram. Soc., 2003, Vol. 86, 1838–1844
- [117] A. S. Wagh and S. Y. Jeong, J. Am. Ceram. Soc., 2003, Vol. 86, 1845–1849
- [118] A. S. Wagh and S. Y. Jeong, J. Am. Ceram. Soc., 2003, Vol. 86, 1850–1855
- [119] The composite materials handbook, Vol. 1, ASTM Stock Number: MIL17V102, p. 3-3.
- [120] U. Zielke, K.J. Hüttinger and W.P. Hoffman, Carbon, 1996, Vol. 34, Issue 8, 999-1005.
- [121] A. B. Strong, Practical Aspects of Carbon Fiber Surface Treatment and Sizing, Composites Manufacturing, 2003
- [122] K. J. Probst, T. M. Besmann, D. P. Stinton, R. A. Lowden, T. J. Anderson and T. L. Starr, Surface and Coatings Technology, 1999, Vol. 120–121, 250–258
- [123] X. Bourrat, J. Lavenac, F. Langlais and R. Naslain, Carbon, 2001, Vol. 39, 2376-2380
- [124] A. Proctor and P. M. A. Sherwood, J Electron Spec and Rel Phen, 1982, Vol. 27, 39
- [125] A. Proctor and P. M. A. Sherwood, Carbon, 1983 Vol. 21, 53
- [126] F. Zhao and Y. Huang, Materials Letters, 2010, Vol. 64, Issue24, 2742-2744
- [127] J. Li and Y. H. Su, Surface and Interface Analysis, 2009, Vol. 41, Issue4, 333-337
- [128] P. A. Zhdan, M. Bors and J. E. Castle, Comp Sci and Technol, 1998, Vol. 58, 559-570
- [129] W. Dang, M. Kubouchi, S. Yamamoto, H. Sembokuya and K. Tsuda, Polymer, 2002, Vol. 43, 2953-2958
- [130] W. M. Keely and H. W. Maynor, J. Chem. Eng. Data, 2002, Vol. 8 (3), 297-300
- [131] J. M. Jabłoński, J. Okal, D. Potoczna-Petru and L. Krajczyk, Journal of Catalysis, 2003, Vol. 220, 146-160
- [132] S. Yuvaraj, F. Lin, T. Chang and C. Yeh, J. Phys. Chem. B, 2003, Vol. 107, 1044-1047
- [133] Y. Du and G. Xu, Atomic Energy Science and Technology, 1999, Vol. 33, 360-363
- [134] R. S. Iskhakov, S. V. Stolyar, L. A. Chekanova, E. M. Artem'ev, V. S. Zhigalov, JETP Letters, 2000, Vol. 72, No.6, 316-319
- [135] D. K. Kondepudi, Introduction to modern thermodynamics, Publisher: Wiley, 2008,

Chapter 5

[136] N. J. Tro and R. S. Boikess, Chemistry 2nd Edition: A molecular approach, Publisher: Prentice Hall. Appendix II: Useful Data.

[137] S. Wang, Y, Zhang, N. Abidi and L. Cabrales, Langmuir, 2009, Vol. 25, 11078-11081

[138] T. A. Roth, Materials Science and Engineering, 1975, Vol. 18, 183-192

[139] P. E. Vickers, J. F. Watts, C. Peruchot and M. M. chehimi, Carbon, 2000, Vol. 38, 675-689

[140] G. Cao, Nanostructures and nanomaterials, Publisher: Imperial College Press, 2004,

Chapter 2

[141] D. K. Kondepudi, Introduction to modern thermodynamics, Publisher: Wiley, 2008,

Chapter 2